



Dipl.-Ing. Paul Maierhofer, BSc

# **The Miniaturization of a Particulate Matter Sensor**

## **DISSERTATION**

zur Erlangung des akademischen Grades

Doktor der technischen Wissenschaften

eingereicht an der

**Technischen Universität Graz**

Betreuer

Univ.-Prof. Mag. Dr. Alexander Bergmann

Institut für Elektrische Messtechnik und Sensorik



## EIDESSTATTLICHE ERKLÄRUNG

### ***AFFIDAVIT***

Ich erkläre an Eides statt, dass ich die vorliegende Arbeit selbstständig verfasst, andere als die angegebenen Quellen/Hilfsmittel nicht benutzt, und die den benutzten Quellen wörtlich und inhaltlich entnommenen Stellen als solche kenntlich gemacht habe. Das in TUGRAZonline hochgeladene Textdokument ist mit der vorliegenden Masterarbeit/Diplomarbeit/Dissertation identisch.

*I declare that I have authored this thesis independently, that I have not used other than the declared sources/resources, and that I have explicitly indicated all material which has been quoted either literally or by content from the sources used. The text document uploaded to TUGRAZonline is identical to the present master's thesis/diploma thesis/doctoral dissertation.*

---

Datum / Date

---

Unterschrift / Signature





# Abstract

Small particles in the air like PM<sub>2.5</sub> - colloquially referred to as fine dust - pose a serious threat to life and limb. In the EU alone, more than 400,000 premature deaths are associated with these particles each year. Increasing public awareness and stricter regulations also place greater demands on the measurement and monitoring of air quality in terms of particle concentration. Close and comprehensive monitoring has so far failed due to the size, complexity and cost of currently available sensors. This dissertation develops the fundamentals for a highly integrated, cost-effective, maintenance-free and easy-to-use particle sensor suitable for mobile applications. By means of statistical methods, the inherent uncertainty of the measurement is estimated. This uncertainty is caused by measuring small volumes and consequently a small number of particles. In this context the limits of the reasonability of miniaturising sensors for particulate matter are discussed.

A literature research on the current state of the art is presented with attention to the possibility of miniaturisation of the measuring principles. Selected approaches are considered by analytical methods and experimental validation in the aerosol laboratory. Particularly promising are optical measuring principles such as the aethalometer, light scattering, evanescent field particle sensing and interference-based methods. Against this background, a design for a sensor is shown in a highly integrated manner. Here, methods from the semiconductor industry are used such as functional packaging.

The work includes an intensive examination of different measurement principles, the selection of a suitable metric, the theoretical and experimental consideration of the selected measurement principles, conception and implementation as a first prototype, as well as a validation of the sensor. A correlation to reference equipment for PM<sub>2.5</sub> is shown.



# Zusammenfassung

Kleine und kleinste Partikel in der Luft wie PM<sub>2.5</sub> – umgangssprachlich als Feinstaub bezeichnet – stellen eine ernstzunehmende Gefährdung für Leib und Leben dar. Allein in der EU werden jährlich über 400.000 vorzeitige Todesfälle mit diesen Partikeln in Verbindung gebracht. Steigendes Bewusstsein in der Bevölkerung und strengere Regulierungen ziehen auch höhere Anforderung an die Messung und Überwachung der Luftqualität bezüglich Partikelkonzentration mit sich. Eine engmaschige und flächendeckende Überwachung scheitert bisher an der Größe, der Komplexität und der Kosten der aktuell verfügbaren Sensoren. Die vorliegende Dissertation erarbeitet Grundlagen für einen hochintegrierten, kostengünstigen, wartungsfreien und einfach zu bedienenden Partikelsensor u.a. für mobile Anwendungen. Mittels statistischer Methoden wird die inhärente Messunsicherheit bedingt durch das Messen kleiner Volumina bzw. einer kleinen Anzahl an Partikeln abgeschätzt und Grenzen der Sinnhaftigkeit kleiner Sensoren diskutiert.

Es wird eine Literatur- und Patentrecherche zum aktuellen Stand der Technik dargelegt mit Augenmerk auf die Miniaturisierbarkeit verschiedener Messprinzipien. Ausgewählte Ansätze werden mittels analytischer Methode und experimenteller Validierung im Aerosollabor betrachtet. Als besonders vielversprechend stellen sich optische Messprinzipien wie das Aethalometerprinzip, Streulicht, Detektion unter Ausnutzung evaneszenter Wellen und Interferenz-basierte Methoden dar. Vor diesem Hintergrund wird ein Design für einen Sensor in hochintegrierter Weise gezeigt. Hierbei werden Methoden aus der Halbleiterindustrie zum Einsatz gebracht wie das funktionale Packaging.

Die Arbeit umfasst eine intensive Betrachtung verschiedener Messprinzipien, die Auswahl einer geeigneten Metrik, die theoretische und experimentelle Betrachtung ausgewählter Messprinzipien, Konzeptionierung und Umsetzung in Form eines ersten Prototyps, sowie eine Validierung des Sensors. Es wird die Korrelation zu PM<sub>2.5</sub> Referenzgeräten gezeigt.



# Acknowledgement

This work was funded by FFG (Austrian Research Promotion Agency) Grant # 86197.

Besonders möchte ich meinem Betreuer und Vorgesetzten Alexander Bergmann danken, der trotz der Vielzahl an Dissertantinnen und Dissertanten, Projekten und Verpflichtungen, stets ein offenes Ohr für mich hatte. Der Erfolg dieser Arbeit ist maßgeblich seinem Einsatz und seiner Führung geschuldet.

Weiters möchte ich dem gesamten Team am Institut für Elektrische Messtechnik und Sensorik danken. Der starke Zusammenhalt und die Kollegialität haben die vergangenen Jahre sehr positiv geprägt.

Von Seiten ams AG möchte ich vor allem Georg Röhner und Gernot Fasching meinen Dank für die sehr gute und konstruktive Zusammenarbeit aussprechen. Seitens SAL bedanke ich mich bei Jaka Pribošek und Martin Kraft für die sehr gute Zusammenarbeit und die wertvollen Diskussionen.

Neben meinem Kollegen Markus Bainschab, möchte ich mich bei meinen Studienkollegen Christian Platzner, Michael Rumetshofer, Alexander Schiffmann, Alexander Schossmann, Ralf Meyer, Leo Treiber, Fabian Huber, Michael Draxler und Alexander Betzler für die prägende Zeit bedanken. Diese Gemeinschaft möchte ich nicht missen!

Besonderer Dank gilt meiner Mutter Veronika Maierhofer, ohne deren bedingungslose Unterstützung in allen Lebenslagen ich nicht an diesem freudigen Punkt stehen würde.

Auch mein Vater Franz Maierhofer hat Anteil an diesem Erfolg. Der Hunger nach Bildung wurde maßgeblich von ihm in mir ausgelöst.

Mein Bruder Florian darf an dieser Stelle keinesfalls unerwähnt bleiben. Danke für deine Unterstützung!

Auch meiner großen Familie möchte ich an dieser Stelle danken, die stets zu mir und hinter mir gestanden ist.

Großer Dank gebührt Theresa, die eventuelle Dissertations-induzierte Launen mit einem Lächeln im Gesicht entschärft hat und mich mutig werden lässt.



# Table of contents

<b>1</b>	<b>Introduction</b>	<b>1</b>
1.1	Problem Statement . . . . .	1
1.2	Commercially available low-cost sensors . . . . .	2
1.3	Overview of academic approaches to low-cost miniaturised particle sensors	2
1.4	Structure of the thesis . . . . .	3
<b>2</b>	<b>Particulate Matter Metrics and Health Effects</b>	<b>5</b>
2.1	Particulate Matter Metrics . . . . .	5
2.1.1	Particle number concentration - PN . . . . .	5
2.1.2	Lung deposited surface area - LDSA . . . . .	6
2.1.3	Particle mass concentration - PM10, PM2.5 and PM1 . . . . .	6
2.1.4	Black Carbon - BC . . . . .	6
2.2	Health Effects . . . . .	7
2.3	Regulatory measures in the EU . . . . .	8
2.4	Discussion and choice of target metric for the miniaturised sensor . . . . .	9
<b>3</b>	<b>Inherent uncertainty of measurement</b>	<b>11</b>
3.1	On the Inherent Variability of Particulate Matter Concentrations on Small Scales and the Consequences for Miniaturized Particle Sensors . . . . .	11
<b>4</b>	<b>Sensor effects and applicability with regard to miniaturisation</b>	<b>23</b>
4.1	Requirements for miniaturisation and the consumer market . . . . .	23
4.2	Gravimetric measurement . . . . .	24
4.2.1	Filter-based gravimetric measurement . . . . .	25
4.2.2	Related gravimetric techniques . . . . .	25
4.3	Beta-Attenuation Monitor . . . . .	26
4.4	Photoacoustics . . . . .	26

4.5	Charge based techniques - Diffusion charging and direct photoelectron emission charging . . . . .	27
4.6	Capacitive particle sensor . . . . .	27
4.6.1	Characterization of a Capacitive Sensor for Particulate Matter - publication in MDPI proceedings . . . . .	29
4.7	Optical sensors . . . . .	34
4.7.1	Light Scattering . . . . .	34
4.7.2	Waveguide based evanescent field sensing . . . . .	36
4.7.3	Aethalometer . . . . .	37
4.7.4	Interferometric Particle Detection . . . . .	43
4.8	Discussion and choice of target sensor effect . . . . .	57
<b>5</b>	<b>Concept and Realisation</b>	<b>59</b>
5.1	Overview of targeted specifications and constraints . . . . .	59
5.2	Design concept and overview . . . . .	60
5.3	Inlet and Outlet . . . . .	62
5.4	Particle Size Separation: Impactor . . . . .	62
5.5	Optical Sensing Element . . . . .	64
5.6	Filter . . . . .	65
5.7	Micro Pump . . . . .	66
5.8	Electronics . . . . .	67
5.9	Assembly . . . . .	67
<b>6</b>	<b>Experimental Evaluation</b>	<b>69</b>
6.1	Fluidic tests . . . . .	69
6.2	Stray light . . . . .	70
6.3	Validation . . . . .	71
6.3.1	Reference Aerosol . . . . .	71
6.3.2	Estimator for PN and PM2.5 . . . . .	77
6.3.3	Ambient Aerosol . . . . .	79
<b>7</b>	<b>Summary and Outlook</b>	<b>91</b>
<b>8</b>	<b>List of Publications</b>	<b>95</b>
	<b>References</b>	<b>101</b>



---

<b>Appendix A</b>	<b>107</b>
A.1 Patent Application WO 2019/115690 A1: INTEGRATED FILTER-BASED PARTICULATE MATTER SENSORS . . . . .	107
A.2 Patent Application EP 3 499 215 A1: PARTICLE DENSITY SENSOR USING EVANESCENT WAVE OF WAVEGUIDE . . . . .	156
A.3 Patent Application EP19211018.7: APPARATUS AND METHOD FOR DETECTING OBJECTS . . . . .	167



# Chapter 1

## Introduction

### 1.1 Problem Statement

Particles in the air we breath cause a serious threat to human health in various ways. Health risks range from cardiovascular and cardiopulmonary diseases to Alzheimer's disease and damages to the unborn life. Preliminary deaths caused by air pollution in general and in specific particles are estimated to be in the hundred thousands per year in the EU alone. In order to better assess particle related risks and to regulate particle concentrations and emissions, a close-meshed monitoring is necessary. Not only are the few high-end instruments that are placed at points of interest insufficient to capture the variability of particle concentrations, they lack in information on the personal exposure to particle pollution. Especially indoor concentrations are insufficiently monitored. There is a need for highly-integrated, easy-to-use, cost-efficient and maintenance-free particle sensors which could be installed in mobile devices like phones or watches to monitor the personal particulate matter exposure. The benefits of such an approach reach from a vast amount of data for future research and regulation, to benefits for the individual by enabling a user to react to and change its environment.

State of the art low-cost particle sensors are approximately palm sized and cost around 10 \$ to 300 \$, which is still too bulky and evidently too expensive for a broader public. The goal of this thesis and the overall project is to develop a sensor in the size range of  $12 \times 10 \times 3 \text{ mm}^3$  which is roughly the size of two one-cent coins stacked. The small size enables mobile integration of the sensor and will lead together with the targeted large volume production to a significantly lower cost compared to available devices.

Since the overall complexity of a miniaturised particle sensor is similar to their handheld-sized counterparts, the project poses a significant complexity with respect to aerosol physics, physics of sensor effects, micro-fluidics, micro-packaging and assembly, and calibration and testing. The overall complexity and challenge is caused by the interaction of those fields and

makes an interdisciplinary approach necessary.

## 1.2 Commercially available low-cost sensors

As shown in detail in chapter 4, there exists a plurality of sensor principles to quantify air quality with respect to air quality. These principles include mainly gravimetric, charge-based, capacitive, photo-acoustic, beta-radiation and optical methods. While all of these methods have certain benefits and drawbacks, only a few show the potential for a cost-effective miniaturisation. In fact available low-cost (<300 \$) sensors all operate on a light scattering basis (for details see chapter 4). Evaluations and reviews of the most used commercially available sensors are shown for example in [1]–[3].

One promising product has been launched by Sensirion which will be shortly presented representative for all available sensors. The Sensirion SPS30<sup>1</sup> works on a light scattering principle and targets mass concentrations PM1, PM2.5, PM4 and PM10 as well as number concentrations in the respective size bins plus an additional bin for particles smaller than 0.5  $\mu\text{m}$ . The lower limit of detection with respect to particle diameter is 0.3  $\mu\text{m}$ , which is typical for light scattering based instruments. It features a size of 40.6 x 40.6 x 12.2 mm<sup>3</sup> with a mass concentration accuracy of  $\pm 10 \mu\text{g m}^{-3}$  and costs of approximately 30\$. The overall stats make it one of the most reasonable low-cost PM sensors available. Still the size of the sensor does not allow mobile integration.

Other available low-cost sensors include but are not limited to Alphasense OPC-N3, Plantower PMS 7003 and PMS 5003, Novafitness SD018 and SD021, Shinyei PPD42NS, Samyoun DSM501A and Sharp GP2Y1010AU0F. All of these sensors work on a light scattering principle and are in a similar regime with respect to size.

Up to now, no commercial solution for a miniaturised particulate matter sensor for integration in mobile devices exists in the sense of the thesis.

## 1.3 Overview of academic approaches to low-cost miniaturised particle sensors

There exists a plurality of approaches for miniaturised particle sensors for personal monitoring which are under research in academia. The sensor effects in use include light scattering [4], [5], solidly mounted resonators [6], [7], film bulk acoustic resonators (FBAR) [8], [9] as well

<sup>1</sup><https://www.sensirion.com/de/umweltsensoren/feinstaubsensoren-pm25/>. Last accessed 07.04.2020

as a capacitive measurement scheme [10]–[12] and a charge based approach [13].

Within the thesis there is a difference in the meaning of sensor and sensor system. The sensor refers to the sensor effect and the realisation in a sensor element. The sensor system consists of not only the sensor element but also of additional parts such as an integrated pump and the package. Most publications only focus on the sensor effect and show realisations of sensor elements in that sense. For example Dong et al. [5] show a light scattering based sensor with dimensions of only  $15 \times 10 \times 1 \text{ mm}^3$  including a virtual impactor realised by silicon microfabrication and wafer-level packaging. While this is still impressive, the necessary flow rate for the device is  $6.5 \text{ mL min}^{-1}$  which is provided by an external pump. For an integration in a mobile device, the functionality of a pump must necessarily be integrated into the device, which the publication provides no solution for.

A fully functional MEMS based system is shown by Fahimi et al. [9] which utilises a FBAR sensing element, a virtual impactor for particle size separation, thermophoretic particle deposition onto the sensing element and an integrated pump with a nominal flow rate of  $9.5 \text{ mL min}^{-1}$ . The pump is not specified in the publication, although in earlier publications the flow was achieved by a stack of commercially available miniature fans [8]. The overall size of the system is  $27 \times 14 \times 2 \text{ mm}^3$ . A drawback of the system is that lifetime of the sensor is approximately half a year of regular use according to the the publication. The incorporation of multiple resonators might expand the lifetime although a sufficient lifetime for mobile integration seems to be under question.

Overall there is ongoing research activity for particle sensors. The research seems to mostly target the physical sensor effect and the sensor element rather than the overall system.

Up to now no publication has shown a fully functional particle sensor system that might reasonably be integrated into mobile devices. In particular, most publications lack in solutions for the active flow and rely on a flow rate which can not be achieved using available technologies at reasonable dimensions.

## 1.4 Structure of the thesis

In addition to the introduction, the present thesis covers a chapter on particulate matter metrics and health effects, see chap. 2. The most common metrics for particles are discussed in the context of health effects. Rationale for the choice of the targeted particle metric is presented and the authors opinion on currently used metrics is expressed.

In chapter 3 the inherent uncertainty of the measurement due to small sample volumes and therefore a low number of particles is presented. The implications for miniaturised sensors are discussed. The chapter consists of a peer reviewed Journal article which is directly

incorporated in the thesis. The chapter answers the question whether it makes sense to miniaturise a particle sensor and at which point a potentially small sample size prohibits a useful measurement a priori.

Chapter 4 addresses relevant sensor effects. The discussed sensor effects cover both state of the art approaches, as well as novel effects that were investigated in the thesis. A capacitive sensor approach has been investigated experimentally in close cooperation with and based on the work of the group of Univ.-Prof. Marco Sampietro at Politecnico di Milano, Dipartimento di Elettronica, Informazione e Bioingegneria. Two novel sensor effects have been investigated. The author contributed to the concepts for an evanescent field based sensor and has driven the concepts and evaluations of an interferometric approach. Those two novel and promising sensor effects may be used in future generations of particle sensors. The chapter addresses the question which sensor effects can reasonably be used in the context of sensor miniaturisation. The rationale for the choice of light scattering as the target sensor effect for the present project is presented.

Chapter 5 presents the concept and the realisation of the miniaturised particle sensor. Necessary functional parts and components are discussed and the prototyping and assembly is briefly covered. Both concept and realisation have been a joint task of the project partners TU Graz, SAL GmbH, and ams AG. In addition to the author, Georg Röhrer, Jaka Pribošek, Harald Etschmaier, Hubert Enichlmair, Anderson Singulani, Jožef Pulko, Gernot Fasching, Martin Kraft and Alexander Bergmann have contributed in various ways. The author contributed substantially to the concept and the detailed design. The impactor has been developed by the author. The author contributed to the choice of the manufacturing technologies and the assembly process.

The experimental evaluation of the prototypes and the results are shown in chap. 6. The prototypes rely on a flow rate substantially lower than the reference equipment, which poses a challenge to the experimental setup. A novel setup has been realised which addresses this challenge. Within the thesis an experimental setup has been proposed and realised, and a calibration procedure for the sensor has been found.

A summary of the thesis and the results as well as an outlook is given in chap.7.

The thesis is structured as a monograph, whereas two relevant publications are directly incorporated in the text.

## Chapter 2

# Particulate Matter Metrics and Health Effects

The term aerosol defines a suspension of particles within a matrix of gas [14]. These particles are discrete objects in a size range of 1 nm to well above 10  $\mu\text{m}$ . Particles in the air differ by size, morphology, chemical composition, phase and state of charge [15]. Typically there are no two particles which are exactly the same and so is their impact on the human body. Since it is not feasible to determine all properties of each and every particle in the air, simplifying metrics have to be used to estimate overall health effects or environmental relevant parameters. Depending on the application there are benefits and drawbacks in any of them and none is qualified to fully describe the environment. Concerning health effects, the exact mechanisms of how particles can damage the human body are not yet fully understood and are subject to ongoing research, see section 2.2. The metrics used for regulatory purposes, which are mainly driven by knowledge about adverse health effects, are therefore likely to change within the next years or decades.

The metric has severe implications for the design of the sensor as the sensor effect has to map the target metric. An overview of particle health effects is given and the currently most used metrics are briefly introduced in the following.

## 2.1 Particulate Matter Metrics

### 2.1.1 Particle number concentration - PN

PN refers to the particle number concentration per unit volume. This metric neglects all properties of single particles and is proportional to  $d^0$  whereas  $d$  denotes the particles diameter. Since health effects depend largely on the size, chemical composition and morphology of

the particles, this metric is rather simplified and may not be ideally suited as an indicator for health effects.

### **2.1.2 Lung deposited surface area - LDSA**

LDSA refers to the lung deposited surface area <sup>1</sup>, which is the particle surface distribution per unit volume weighted by the probability of deposition in the lung. The contribution of each single particle is roughly proportional to  $d^{1.1}$ . Although there is not a consensus over whether there is a stronger correlation to health effects compared to other metrics, it seems reasonable that the particles surface area reacts with organs like the lung. For example Schmid et al. [16] state that the surface area is the most relevant metric for lung toxicity. Although LDSA is not part of any regulatory approaches and is largely unknown to the public, it might be a promising and reasonable approach for future activities.

### **2.1.3 Particle mass concentration - PM10, PM2.5 and PM1**

The currently most used metrics PM10, PM2.5 and PM1 measure the particle mass per unit volume, whereas only particles with diameters generally lower than 10 µm, 2.5 µm and 1 µm respectively are taken into account. A more strict definition for PM10 and PM2.5 can be found in DIN EN 16450:2017-07 which defines the metrics via a sampling system with a cyclone impactor operated at a transmission efficiency of 50% at 10 µm and 2.5 µm respectively, and a gravimetric filter-based measurement.

Since the mass of a particle is proportional to the particles volume ( $d^3$ ), these metrics tend to overestimate the influence of large particles which are not frequently observed and in general penetrate less deep into the lung compared to smaller ones. Mass concentration metrics are the most used metrics for regulatory and monitoring purposes and there is solid epidemiological evidence that there is a correlation to health effects, see section 2.2.

### **2.1.4 Black Carbon - BC**

This metric refers to black carbon particles suspended in the air in mass per unit volume, neglecting all other particles. There are indications that BC, which mostly stems from combustion processes, is especially harmful to the human body and the estimated effect for daily mortality is an order of magnitude higher for BC than it is for PM10 and PM2.5 [17]. Also there are indications that BC can act as a carrier of a variety of constituents damaging the body [18]. In addition to enhanced health effects, BC also has a substantial climate force

---

<sup>1</sup><https://www.naneos.ch/pdf/LDSA.pdf>. last accessed 07.04.2020.



potential [19]. BC is not well described by metrics like PM<sub>2.5</sub> and PM<sub>10</sub> since BC is only a relatively small fraction of the total particle mass.

More information on metrics can be found in the database of the EU FP7 project AirMonTech<sup>2</sup>

## 2.2 Health Effects

There exists a vast amount of studies concerning health effects of particulate matter, both epidemiological and toxicological approaches are taken and both mean effects and specific health damaging mechanisms are found [20]–[26]. These studies all show that in principle an increased PM<sub>2.5</sub> pollution increases the probability for cardiovascular and cardiopulmonary diseases and that the all-cause mortality correlates to higher particle exposure. To quote Pope et al [23] : *"Each 10 µg m<sup>-3</sup> elevation in fine particulate air pollution was associated with approximately a 4%, 6%, and 8% increased risk of all-cause, cardiopulmonary, and lung cancer mortality, respectively."* Brook et al. [27] state that short term (hours or weeks) PM<sub>2.5</sub> exposure can already increase the risk for cardiovascular mortality significantly. The effect of long term exposure over years is even more drastic and leads to a reduction in life expectancy of highly exposed individuals of several months to years. The WHO [28] concludes that the adverse health effects caused by particulate matter are well documented and that there is no threshold level of exposure which can be considered to cause no health effects, this is also supported by [27]. In addition the concentration-response function between particle concentration and mortality is non-linear over wider ranges of concentrations [29]. The response to an incremental increase in concentration has a larger effect the lower the concentration is. This function also shows that the response is almost constant at relatively high concentrations. These findings indicate that even in relatively clean environments there is a benefit in further reducing air pollution with respect to particles. The effect may be even elevated in relatively clean environments due to the concentration-response function. In addition to an increased mortality, central nervous system diseases like Alzheimer's disease are also associated with PM<sub>2.5</sub> exposure [30]. There are a variety of pathways in which PM<sub>2.5</sub> can damage the nervous system and specifically the brain. Possible pathways include but are not limited to a damage to the blood brain barrier or a direct path through the olfactory nerve and subsequent deposition of the particles, which leads to an increased probability of inflammation symptoms damaging the nervous system.

In addition PM<sub>2.5</sub> poses a threat to the unborn life. There is evidence that maternal exposure to PM induces pulmonary diseases in the fetus [31]. Basu et al. [32] state that PM<sub>2.5</sub> is

---

<sup>2</sup><https://db-airmontech.jrc.ec.europa.eu/search.aspx> . Last accessed 10.06.2020

associated with preterm delivery.

In summary there is a vast amount of evidence that air pollution with respect to particles poses a serious threat to human health in general. A further regulation and reduction of exposure to particle pollution is not only beneficial for highly polluted areas but also for relatively clean environments. This further underlines the relevance and the impact a miniaturised low-cost sensor would have.

## 2.3 Regulatory measures in the EU

The EU regulates on the one handside emission and on the other handside immission, which is ultimately the health relevant parameter. Concerning particle immission PM10 and PM2.5 is regulated. Directive 2008/50/EC regulates annual and daily average immission values which are listed in table 2.1.

Table 2.1 EU limits for 24h and annual PM10 and PM2.5 averages

Pollutant	Annual average $\mu\text{g m}^{-3}$	24h Average $\mu\text{g m}^{-3}$	Permitted exceedences p.a.
PM10	50	40	25
PM2.5	n.a.	25	35

The Clean Air for Europe (CAFE) Directive 2008/50/EC has introduced additional PM2.5 targets to limit the exposure of the population starting 2020. These targets are not uniform across the EU but are set at national level by taking into the account an initial 3 year average before 2020 of selected measurement stations in highly populated areas. The reduction depends on this background level and ranges between 0% for an initial level of below  $8.5 \mu\text{g m}^{-3}$  to 20% for initial levels of above  $18 \mu\text{g m}^{-3}$ . Regardless of the individual reduction, all measures have to be taken to reduce PM2.5 levels to a maximum of  $18 \mu\text{g m}^{-3}$  by 2020.

There are indications that especially nanosized-particles with diameters of 100 nm and below pose a significant health risk [21] and are insufficiently regulated by PM10 and PM2.5 limits. Therefore, it seems reasonable that additional regulatory measures with respect to nanosized-particles will be introduced in the future, especially since these particles often stem from anthropogenic sources.

## 2.4 Discussion and choice of target metric for the miniaturised sensor

The author concludes that mechanisms which damage the human body are not yet fully understood. There is epidemiological evidence that in general PM<sub>2.5</sub> is related to an increased mortality and increases the probability for a number of diseases including cardiovascular and cardiopulmonary diseases. Still it might be oversimplified to take into account only the mass of particles and neglect the size distribution, morphology and chemical composition.

There are simple examples where PM<sub>2.5</sub> is misleading. For example there is an increased PM<sub>2.5</sub> concentration near coasts as sea salt is emitted in the air. A sensor measuring PM<sub>2.5</sub> would suggest that the air quality is poor despite the fact that sea salt is not classified as a hazardous compound.

Another example is asbestos where a small number of particles is sufficient to severely damage human lungs because of the unfortunate fibrous morphology of the particles which get permanently stuck in the lung. A PM<sub>2.5</sub> sensor is unable to quantify this hazard correctly. When we try to evaluate nutrition and food we take into account the calories we eat, think about various kinds of fats and carbohydrates, micro-nutrients, vitamins, and even more parameters. There might well be at least a weak correlation between body weight and food intake in terms of mass per day, as there is a correlation between PM<sub>2.5</sub> exposure and mortality. There is most likely a consensus that it is insufficient to only quantify food intake in terms of total mass regarding health. Yet this is the main approach we take in order to quantify the particulates we are exposed to and ultimately inhale. In the authors opinion PM<sub>2.5</sub> might not be the ultimately best metric to quantify particulate matter with respect to health effects but it is the most plausible at the moment. PM<sub>2.5</sub> gives a reasonable indication for air quality in most cases although it still requires knowledge on the ambient particle sources to better understand the implications. The user of a PM sensor should not fully rely on only the measurement value.

Also regulatory measures tackle PM<sub>10</sub> and PM<sub>2.5</sub> and therefor public awareness is mostly related to PM<sub>2.5</sub>. It seems unlikely that a novel low-cost sensor utilising a largely unknown metric is well received. This reasoning led to the decision that PM<sub>2.5</sub> is targeted as the main metric of the project and the thesis.

In the authors opinion the most reasonable metric at the moment is BC. BC is clearly related to enhanced health effects and can most often be linked to anthropogenic sources [33] such as combustion processes. The sources of PM<sub>2.5</sub> are more diverse and are also not equally well attributed to anthropogenic origin. This makes BC on the one hand side a well-suited metric concerning health effects and on the other hand side regulatory measures

are more likely to succeed in reducing the BC concentration as they are in reducing PM<sub>2.5</sub> concentrations. Overall the author concludes that PM<sub>2.5</sub> will be a discontinued metric. The author suggests to target BC for future research concerning particle sensors. This is supported by the conclusions found in the EU FP7 project AirMonTech.<sup>3</sup>

---

<sup>3</sup><https://cordis.europa.eu/project/id/265116/reporting>. Last accessed 10.06.2020

## **Chapter 3**

### **Inherent uncertainty of measurement**

A miniaturised sensor will typically use a relatively small sample volume in order to estimate the ambient particle concentration. This leads to an increased uncertainty of the measurement since a small sample may be insufficient for the estimation of a complex environmental parameter such as PM<sub>2.5</sub>. The following paper [34] is published in the Journal of Aerosol and Air Quality Research and deals with this aspect analytically and answers the question up to what point it even makes sense to miniaturise a PM sensor in general.

The main findings are that the inherent variability of the particle mass per volume rises drastically when volumes on the order of a few mL are investigated since the number of particles within the sample becomes low at typical ambient concentrations.

As a consequence of the findings, an active flow element such as a pump or a fan, is to be considered necessary for a particulate matter sensor in order to have a sufficiently large sample for a reasonable measurement uncertainty.

#### **3.1 On the Inherent Variability of Particulate Matter Concentrations on Small Scales and the Consequences for Miniaturized Particle Sensors**

*Aerosol and Air Quality Research*, 20: 271–280, 2020  
Copyright © Taiwan Association for Aerosol Research  
ISSN: 1680-8584 print / 2071-1409 online  
doi: 10.4209/aaqr.2019.01.0048



## On the Inherent Variability of Particulate Matter Concentrations on Small Scales and the Consequences for Miniaturized Particle Sensors

Paul Maierhofer<sup>1\*</sup>, Georg Röhrer<sup>2</sup>, Markus Bainschab<sup>1</sup>, Alexander Bergmann<sup>1</sup>

<sup>1</sup> Institute of Electronic Sensor Systems, Graz University of Technology, 8010 Graz, Austria

<sup>2</sup> ams AG, 8141 Premstätten, Austria

### ABSTRACT

Despite all the evident benefits of miniaturized particulate matter (PM) sensors, an inherent drawback exists in the uncertainty and validity of the measurement, which is closely related to the discrete nature of particulates suspended in air. The miniaturization of these devices not only leads to a smaller footprint for the devices themselves but also to a smaller volume of air being sampled. Even if a perfect measurement system is assumed, an uncertainty lies in assigning a supposedly representative particle concentration value to an environment due to the inherent variability of PM concentrations on small scales. This stems from the fact that particles are stochastically distributed in the air, leading to a non-uniform concentration for arbitrarily small volumes. Consequently, an uncertainty exists according to counting statistics, as the number of investigated particles in a small air sample is also low. Depending on the metric, the uncertainty may be augmented, as a small number of particles cannot accurately capture the distribution of particle sizes, especially since the size distribution extends over several orders of magnitude. This distribution related uncertainty is relevant for surface and mass related metrics in addition to the uncertainty resulting from counting statistics. We detected a minor impact from the distribution of the particle mass density, which contributes to the uncertainty for mass-related metrics, such as  $PM_1$ ,  $PM_{2.5}$  and  $PM_{10}$ . We investigated the expected measurement uncertainty by analytical means and concluded that the distribution of particle sizes, the sample size and the ambient particle concentration significantly affect the measurement uncertainty for the range of conditions considered. To the best of our knowledge, this uncertainty has not been discussed in the current literature.

**Keywords:** Aerosol sampling; Measurement uncertainty; Miniaturized sensors.

### INTRODUCTION

Serious adverse health effects of particulate matter (PM) on the human body (Ranft *et al.*, 2009; Kioumourtzoglou *et al.*, 2016) raise a public desire for highly integrated, cost-effective and easy-to-use PM sensors. As the chase for smaller and smaller PM sensors is currently at an all-time high (Paprotny *et al.*, 2013; Li *et al.*, 2014; Ciccarella *et al.*, 2016; Bao *et al.*, 2018; Hapidin *et al.*, 2019), it is not only fruitful but also necessary to have a closer look at limitations we encounter. The miniaturization of microfluidic devices, such as miniaturized PM sensors, yields lower flow rates compared to available macroscopic devices, e.g., Papronty *et al.* (2013) report a flow rate of only  $6 \text{ mL min}^{-1}$ . Therefore, the sample size of PM sensors is typically decreasing for a given integration time as they get smaller.

As the sampled volume gets smaller, also the number of particles analyzed and consequently used to estimate ambient PM concentrations gets lower.

The target of this work is to evaluate the impact of miniaturization on the validity of the measurements, neglecting all possible imperfections of a sensor. The uncertainty of the estimated ambient particle concentration given the measurement of a sensor is equal to the inherent variability of PM on the scale of the sample volume. We find three separate contributions to the total uncertainty: One stems from counting statistics, the second one is caused by the broad distribution of particle sizes in the ambient environment, which plays a role for metrics such as surface concentration and mass concentration, and a third contribution to the total measurement uncertainty comes from the distribution of particle mass densities. A small number of particles does not represent this complex situation ideally. The smaller the sample gets, the higher the variability between measurements within the same ambient conditions will be. This uncertainty is also dependent on the metric used, which can depend on the sensor effect in use.

The discussed uncertainty is not covered by the current

\* Corresponding author.

Tel.: 0043-316-873-3350

E-mail address: paul.maierhofer@tugraz.at

literature to the best of our knowledge.

## METHODS

We state the analytical expressions of three investigated metrics in terms of the relevant particle properties as shown in Eq. (1). We use these analytical expressions to find the expectation value and the variance of the metrics on small volumes.

We can write the particulate concentrations within a sample volume as PN, PS and PM<sub>x</sub>, as in Eq. (1). PN is the particle number concentration. PS corresponds to the total particle surface area per volume. PM<sub>x</sub> is a placeholder for the most used mass metrics, such as PM<sub>1</sub>, PM<sub>2.5</sub> or PM<sub>10</sub>. These metrics count the total mass of particles up to a diameter indicated after “PM” in units of μm. For example, PM<sub>1</sub> corresponds to the total mass of particles less than 1 μm in diameter per cubic meter.

$$PN = \frac{1}{V_{\text{Sample}}} \sum_{n=1}^N \frac{N}{V_{\text{Sample}}} \quad (1)$$

$$PS = \frac{1}{V_{\text{Sample}}} \sum_{n=1}^N S_n$$

$$PM_x = \frac{1}{V_{\text{Sample}}} \sum_{n=1}^N V_n \rho_n$$

where N is the total number of particles within the sample, and S<sub>n</sub>, V<sub>n</sub> and ρ<sub>n</sub> are the surface, volume and the mass density of the n<sup>th</sup> particle, respectively. V<sub>Sample</sub> denotes the sampled volume of air. Mathematically speaking, N is a random positive integer number, and S<sub>n</sub>, V<sub>n</sub> and ρ<sub>n</sub> are each independent and identically distributed random variables, which means that, e.g., all V<sub>n</sub> have the same probability distribution, with finite expectation value and variance.

For the particle number concentration, only the number of particles per volume is relevant, whereas for the surface concentration, the individual surfaces of the single particles are summed up and for mass concentrations, their masses. This concentration will, especially for small sample volumes, vary from the mean ambient particle concentration since the suspended particles are discrete objects. In an extreme case, we could think of a situation where only one particle is suspended in a known volume of air. We can assume a sensor, which would need a large number (m) of measurements to analyze the whole air in the total volume. This sensor would report in m – 1 measurements a concentration of 0 and in one measurement, a concentration of m times the mean concentration in said volume. Clearly, this sensor would not be able to capture the situation with only one measurement—not because of imperfections of the sensor itself but because of the high variability in the particle concentration. Another effect stems from the size distribution and the mass density distribution of particles, which complicates the situation for surface concentration and mass concentration metrics.

A sensor will use the measurement value of the sampled volume to estimate the particle concentration on a larger

scale. Therefore, we are interested in the expectation value, < >, and the variance, Var(), for each of the investigated metrics, which we calculate using Wald’s equation as well as Blackwell-Girshick’s equation (Klenke, 2013) and the assumption that the number of particles (N), the surface (S), the volume (V) and the density (ρ) are uncorrelated.

$$\langle PN \rangle = \langle N \rangle \frac{1}{V_{\text{Sample}}} \quad (2)$$

$$\langle PS \rangle = \langle N \rangle \langle S \rangle \frac{1}{V_{\text{Sample}}}$$

$$\langle PM_x \rangle = \langle N \rangle \langle V \rangle \langle \rho \rangle \frac{1}{V_{\text{Sample}}}$$

$$\text{Var}(PN) = \text{Var}(N) \times \left( \frac{1}{V_{\text{Sample}}} \right)^2 \quad (3)$$

$$\text{Var}(PS) = \left( \text{Var}(N) \langle S \rangle^2 + \text{Var}(S) \langle N \rangle \right) \times \left( \frac{1}{V_{\text{Sample}}} \right)^2$$

$$\text{Var}(PM_x) = \left( \langle V \rangle^2 \langle \rho \rangle^2 \text{Var}(N) + \langle \rho \rangle^2 \langle N \rangle \text{Var}(V) + \langle V \rangle^2 \langle N \rangle \text{Var}(\rho) \right) \times \left( \frac{1}{V_{\text{Sample}}} \right)^2$$

Eq. (3) shows the total variance of each metric’s value. For PN, the situation is straightforward since only the counting uncertainty plays a role. The surface concentration has an additional term including the variance of a single particle’s surface. PM<sub>x</sub> has a term proportional to the variance of a single particle’s volume, Var(V), as well as a term with the variance of the mass density, Var(ρ). Var(V) and Var(S) are functions of the particle-size distribution. This distribution typically ranges in terms of diameter over decades, from nanometers up to micrometers, and is not ideally captured by a small number of particles; therefore, it is obvious that the size distribution has an influence on the total uncertainty. In order to evaluate the variances, a discussion of the distributions of the number of particles (N), the surface and the volume of particles (S and V) and the particle density (ρ) is necessary. Since both surface and volume distribution of the particles are functions of the size distribution, we can discuss the more frequently used particle size distribution.

## Particle Size Distribution

The size distribution of particles is frequently assumed to be lognormal (Hinds, 1999) in diameter, D, but can, in principle, have any shape. In order for Eqs. (2)–(3) to be valid, the variances of S and V must be finite, which is the case for any realistic distribution since diameter, surface and volume of particles are always finite. Since the size distribution of particles is not constant in the ambient air but depends on season, weather, nearby emissions and a

variety of other environmental parameters (e.g., Väkevä *et al.*, 2000), it is not possible to assume one size distribution that is representative for all cases.

Given the size distribution,  $p(D)$ , as a function of the particles' diameter,  $D$ , we can write the expectation value and the variance of a variable being dependent on  $D$ , such as the surface ( $S$ ) and the volume ( $V$ ), as in Eqs. (4)–(5), where  $V$  is used as an example.

$$\langle V \rangle = \int_0^{\infty} p(D) V(D) dD \quad (4)$$

$$\text{Var}(V) = \int_0^{\infty} p(D) (V(D) - \langle V \rangle)^2 dD \quad (5)$$

Eqs. (4)–(5) show the expectation value,  $\langle V \rangle$ , and the variance,  $\text{Var}(V)$ , of a single particle's volume, which is only dependent on the distribution  $p(D)$ . Since the variance of  $S$  and  $V$  is a function of this distribution, we can see that the distribution indeed affects the variability of the mass and the surface concentration of particulate matter directly. In order to evaluate Eqs. (4)–(5), a particle shape has to be assumed in order to find surface and volume as a function of diameter. The model is valid for any particle shape. Without any loss of generality, we choose spherical particle shapes for further evaluations for the sake of simplicity.

#### Distribution of Particle Mass Density

The distribution of the mass density,  $\rho$ , is—similar to the size distribution—dependent on various factors, such as the type of particle sources near the measurement. Measurement principles that do not directly determine mass—such as light scattering—need an assumption for the mean mass density to determine  $\text{PM}_x$ . An incorrect assumption of  $\langle \rho \rangle$  directly affects the measured mass concentration, causing a systematic error. For the estimation of the total variability, we assume the mass density to be Gaussian distributed with a mean of  $\langle \rho \rangle$  and a variance of  $\text{Var}(\rho)$ . If these cannot be experimentally evaluated, the parameters have to be estimated by using prior knowledge, such as knowledge of the nearby aerosol sources. Aerosol particles, in principle, may consist of any material, which implies a broad range of mass densities theoretically possible, ranging from a few hundred  $\text{kg m}^{-3}$  up to over 19,000  $\text{kg m}^{-3}$  for metallic particles. However, for realistic ambient cases, we can typically narrow down dominant particle densities. For example, Hand and Kreidenweis (2002) report a mass density of  $1850 \pm 140 \text{ kg m}^{-3}$  for  $\text{PM}_{2.5}$  measured in the southwest of Texas in the U.S.

#### Particle Number

For consistency, we require that  $\langle \text{PN} \rangle = c_{\text{PN}}$ ,  $\langle \text{PS} \rangle = c_{\text{PS}}$  and  $\langle \text{PM}_x \rangle = c_{\text{PM}_x}$ , which means that the expectation value of each metric is equal to the respective ambient particle concentration on a large scale. We can use Eq. (2) to express the expectation value of the number of particles counted,  $\langle N \rangle$ , as stated in Eq. (6). While all three equations are valid, it makes sense to use only the equation with the

corresponding ambient concentration of each metric for further evaluations.

$$\langle N \rangle = c_{\text{PN}} V_{\text{Sample}} \quad (6)$$

$$\langle N \rangle = \frac{c_{\text{PS}}}{\langle S \rangle} V_{\text{Sample}}$$

$$\langle N \rangle = \frac{c_{\text{PM}_x}}{\langle \rho \rangle \langle V \rangle} V_{\text{Sample}}$$

We further assume uncorrelated particle positions, leading to uniformly distributed particles in space. Therefore, the total number of particles in a given volume will be Poisson distributed (Badger, 1946; Hinds, 1999). Although the assumption that particle positions are uncorrelated is under debate (Damit *et al.*, 2014; Larsen, 2006), we draw the conclusion that the Poisson assumption is a valid starting point and neglect any possible correlations of particle positions, such as a clustering of particles of the same size or a complete avoidance of such clusters. In other words, we assume completely uniformly distributed particle positions. According to Larsen (2006), assuming that particles are randomly distributed in a volume, the Poisson distribution describes the number of particles within any subvolume.

Since we assume the number of particles within a sample is Poisson distributed, Eq. (7) expresses the variance of  $N$ , as the variance of the Poisson distribution is equal to its expectation value.

$$\text{Var}(N) = \langle N \rangle \quad (7)$$

#### Coefficient of Variation

In order to compare the uncertainties of the metrics, we use the coefficient of variation, which is the standard deviation divided by the expectation value and therefore shows the relative variability. The standard deviation of  $\text{PN}$ ,  $\text{PS}$  and  $\text{PM}_x$  is given by the square root of the respective variance, as given in Eq. (3). This is the inherent variability of particle concentrations on an arbitrary scale and is therefore independent of the type of PM sensor, e.g., whether the sensor will analyze single particles and add them up, or take a cumulative measurement. The type of sensor used will, of course, influence the metric of the measurement and vice versa. The coefficient of variation of the measurement can be written as stated in Eq. (8) by using Eqs. (2), (3) and (7).

$$\begin{aligned} \sigma_{\text{PN},\text{rel}} &= \frac{\sqrt{\text{Var}(\text{PN})}}{\langle \text{PN} \rangle} = \frac{1}{\sqrt{\langle N \rangle}} \\ \sigma_{\text{PS},\text{rel}} &= \frac{\sqrt{\text{Var}(\text{PS})}}{\langle \text{PS} \rangle} = \frac{1}{\sqrt{\langle N \rangle}} \sqrt{1 + \frac{\text{Var}(S)}{\langle S \rangle^2}} \\ \sigma_{\text{PM}_x,\text{rel}} &= \frac{\sqrt{\text{Var}(\text{PM}_x)}}{\text{PM}_x} = \frac{1}{\sqrt{\langle N \rangle}} \sqrt{1 + \frac{\text{Var}(V)}{\langle V \rangle^2} + \frac{\text{Var}(\rho)}{\langle \rho \rangle^2}} \end{aligned} \quad (8)$$



In Eq. (8), we can clearly see that the coefficient of variation of each metric considered drops as the sample size increases with a typical  $1/\sqrt{N}$  behaviour. As stated in Eq. (6),  $\langle N \rangle$  is directly proportional to the sample volume,  $V_{\text{sample}}$ , and the mean ambient particle concentration in either metric. Therefore, the variability decreases for increasing sample volumes and higher concentrations, which both lead to better statistics. Another contribution to the variability of the measurement stems from the distribution of the particle surface for PS and the volume for  $PM_x$ , which are both directly related to the particle size distribution. In addition, the distribution of the mass density affects the variability of mass related metrics ( $PM_x$ ).

The formalism can easily be adapted to metrics such as  $PM_{10}$ ,  $PM_{2.5}$  or  $PM_1$ . The upper bound of the metric influences the expectation value and variance of the volume of single particles  $\langle V \rangle$  and  $\text{Var}(V)$ . For example, the variance of particle sizes of  $PM_1$  is typically lower than for  $PM_{10}$  because the particles of interest expand over one more decade in diameter for  $PM_{10}$ , as  $1 \mu\text{m}$  is the limit for  $PM_1$  and  $10 \mu\text{m}$  for  $PM_{10}$ . Since the volume is proportional to the diameter cubed, the variance in volume is significantly affected by the particle sizes that are taken into account. Also, the majority of particles is typically below  $1 \mu\text{m}$  in diameter, which means that the Poisson counting uncertainty is not greatly affected by lowering the upper bound of the metric to  $1 \mu\text{m}$ . For example, Klejnowski *et al.* (2013) report that during a measurement campaign in Zabrze in Poland, 99% of all particles by number concentration are below  $1 \mu\text{m}$  in diameter. Given a distribution,  $p(D)$ , the variance for the metric of interest can be calculated by a normalization of  $p(D)$  within the size window of interest. The probability outside this window is set to 0. Then again, Eqs. (4) and (5) can be used to calculate expectation value and variance of a single particle's volume, respectively. Note that the ambient concentration, which is used to calculate the expectation value of the number of particles,  $\langle N \rangle$ , must therefore match the metric of interest.

## RESULTS AND DISCUSSION

We begin our discussion with the uncertainty of particle number concentration measurements. This uncertainty is straightforward to calculate and to estimate for a measurement, as for a PN measurement, the number of particles counted has to be known obviously. Eq. (8) can be evaluated, which gives the uncertainty. The uncertainty of the measurement can be lowered by prolonging the measurement until a relative uncertainty is reached that is acceptable for the user.

For the particle surface concentration, the situation is already more complex, as can be seen in Eq. (8). There, the expectation value and the variance of a single particle's surface, which is a function of the particle size distribution, play a role. Depending on the measurement technique, the size distribution can be known or unknown. If there is no information on the particle size distribution, the exact uncertainty cannot be determined. Since the situation for mass concentrations, such as  $PM_x$ , is similar, and these

metrics are the most common metrics for low-cost sensors, we focus the discussion on mass metrics.

As shown in Eq. (8) and Fig. 1, the coefficient of variation of the measured  $PM_{2.5}$  value is strongly dependent on the size distribution of particles. For this evaluation, we assume the particle diameter,  $D$ , to be lognormally distributed and set  $\rho$  to  $1850 \pm 140 \text{ kg m}^{-3}$  according to Hand and Kreidenweis (2002). For narrow particle size distributions, the variability is dominated by the Poisson contribution and the contribution from the mass density distribution. If we assume monodisperse particles, the geometric standard deviation (GSD) is 1, and  $\text{Var}(V)$  is 0. In this case, we are left with the Poisson uncertainty and the small contribution due to the mass density distribution. At broader particle size distributions with higher GSD, the size distribution related contribution dominates. Note that the standard deviations stemming from different sources do not add up, but the variances do, as shown in Eq. (3). The total coefficient of variation for the investigated case for  $PM_{2.5}$  ranges from roughly 4% to over 30% depending solely on the parameters of the size distribution. This major influence of the underlying particle size distribution makes the estimation of confidence intervals for a real measurement tricky. In a real case, users are forced to use the measured  $PM_x$  value as an estimate for the ambient concentration. This is reasonable since the expectation value of the measurement equals the ambient concentration when there are no systematic errors in the measurement. If the measurement technique counts and sizes particles such as, for example, a light scattering device does, then Eq. (8) can be used to estimate the uncertainty. In this case, a mean mass density for the particles has to be assumed as well as a variance of the mass density. However, if the measurement technique does not provide information on the particle number and the size distribution, there is no estimate for the uncertainty of the measured  $PM_x$  value as the coefficient of variation as stated in Eq. (8) cannot be evaluated. This is, for example, the case for gravimetric measurements. Also, the evaluation of Eq. (8) for a real measurement case will not lead to the exact uncertainty, as the information on the mean ambient concentration and the size distribution is not exact for finite sample sizes. In this work, we have all the information of the ambient situation and use it to find the variability of the particle concentrations. In a real case, there is little to no information on the mean ambient particle concentration, the size distribution and the mass density distribution of particles.

Mathematically speaking, the influence of the particle size distribution and the influence of the mass density distribution are equal. Nevertheless, we can state that for cases that are to be expected in the ambient air, the size distribution of particles dominates. This is reasonable since the particle size distribution ranges over more than three decades from nanometers to micrometers, while the mass density distribution can safely be assumed to extend over less than one decade. Therefore, the term  $\text{Var}(\rho)/\langle \rho \rangle^2$  is, in general, small compared to  $\text{Var}(V)/\langle V \rangle^2$ .

Fig. 2 shows the uncertainty of  $PM_1$ ,  $PM_{2.5}$  and  $PM_{10}$  for lognormally distributed particles with an exemplary geometric mean (GM) of  $0.3 \mu\text{m}$  as a function of the

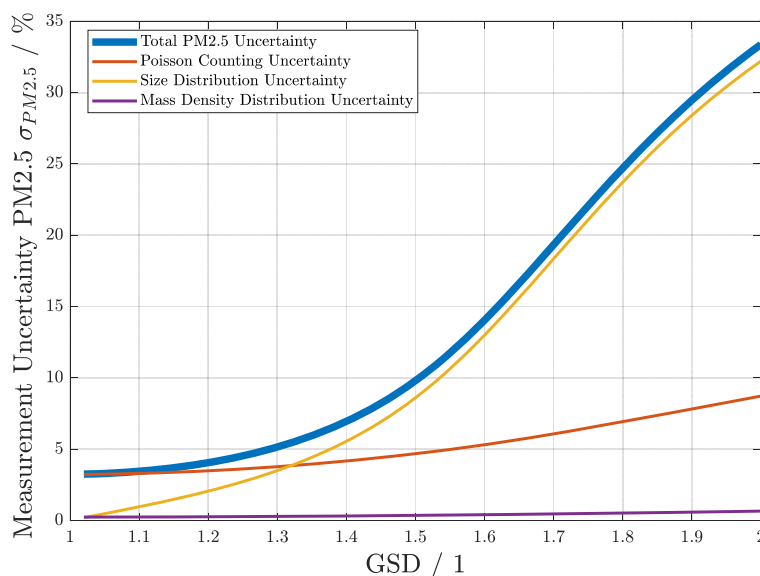


**Fig. 1.** Coefficient of variation as a function of the geometric standard deviation of the particle sizes for  $PM_{2.5}$ . GSD corresponds to the width of the distribution. The calculation is done at an exemplary geometric mean of 300 nm. For the calculation, only particles with diameters lower than  $2.5 \mu m$  are taken into account in order to show the uncertainty for  $PM_{2.5}$ . The calculation is shown for a constant ambient  $PM_{2.5}$  concentration of  $25 \mu g m^{-3}$ , a particle mass density  $\langle \rho \rangle$  of  $1850 kg m^{-3}$  with a variance  $Var(\rho)$  of  $(140 kg m^{-3})^2$  and a sample volume of 1 mL. Although the ambient  $PM_{2.5}$  concentration is held constant, and therefore, the total mass that is sampled is also constant, the total uncertainty ranges over tens of percent. For realistic cases, the uncertainty stemming from the particle size distribution dominates. The Poisson contribution also rises as GSD rises since the number of particles at a constant ambient concentration gets lower as the variance of the size distribution rises.

geometric standard deviation (GSD) of the size distribution. The ambient mass concentration is set to  $25 \mu g m^{-3}$  in each of the metrics. The relative uncertainty in general rises as GSD, and therefore the width of the particle size distribution, rises. At GSD values approximately lower than 1.5, the relative uncertainties of the metrics are equal, as the metrics do not differ from each other as long as all particles are below  $1 \mu m$  in diameter. For higher GSD values, the size distribution relevant to each of the metrics begins to differ, leading to a higher uncertainty of  $PM_{10}$  compared to  $PM_{2.5}$  and  $PM_1$ . We can state that for the investigated parameters, the estimation of a mass concentration based on a small sample yields results that are more robust the lower the upper cutoff is. Since only a small number of particles typically has a diameter of greater than  $2.5 \mu m$  but their total volume is still of relevance,  $PM_{10}$  is especially prone to a high uncertainty.

Fig. 3 shows the measurement uncertainty of PN, PS and  $PM_{2.5}$  as a function of the sample volume. We assumed lognormally distributed particles with an exemplary GM of  $0.3 \mu m$  and a GSD of 1.7. The particle density,  $\rho$ , is set to  $1850 \pm 140 kg m^{-3}$  according to Hand and Kreidenweis (2002). We only took particles with diameters below  $2.5 \mu m$  into account for this evaluation. In general, the relative uncertainty drops as the sample volume increases. The uncertainty of  $PM_{2.5}$  is the highest, followed by the

uncertainty of the total particle surface (PS). The particle number concentration, PN, has the lowest uncertainty, which is immediately evident in Eq. (8), as for the uncertainty of  $PM_x$  and PS, more terms are added. For lognormally distributed spherical particles, the relative uncertainty of the particle surface concentration is necessarily lower than the uncertainty of the volume concentration. The reason is that the surface is proportional to the square of the diameter of the particle, whereas the volume is proportional to the diameter cubed. This makes the mass metrics more prone to a relatively high uncertainty due to a small number of large particles. For the investigated parameters, a sample volume of 1 mL yields a relative uncertainty of 6% for PN, 11% for PS and 19% for  $PM_{2.5}$ . Especially for  $PM_{2.5}$ , this might be a high uncertainty, bearing in mind that it is only the inherent uncertainty of the measurement when the sensor's imperfections are yet to be considered. For a sample volume of 1 L, the uncertainty below 1% for each metric is most likely overshadowed by the sensor's imperfections in a realistic case, which is why this uncertainty has never been observed using high-end laboratory equipment providing high flow rates and therefore has not been discussed in literature yet.

In Figs. 4 and 5, we show the relative uncertainty for  $PM_{2.5}$  as a function of the total mass that is sampled. As the uncertainty depends on the total number of particles that

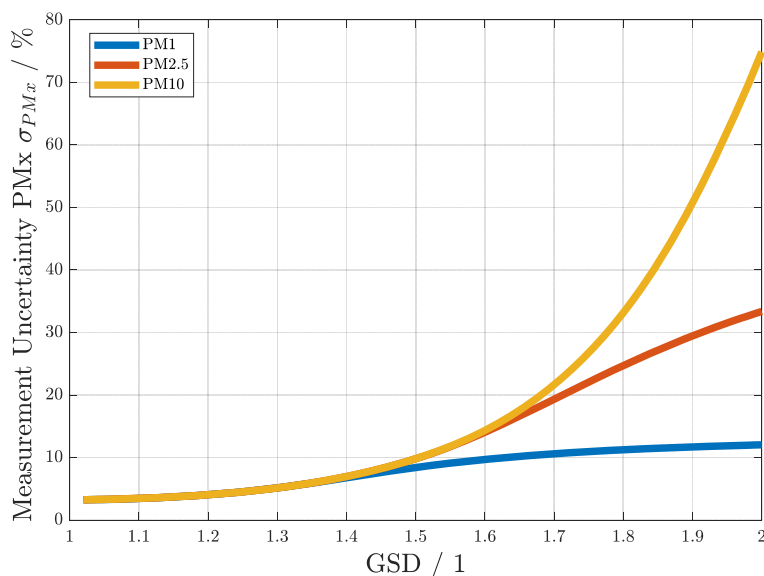


**Fig. 2.** Coefficient of variation as a function of the geometric standard deviation of the particle sizes for PM<sub>1</sub>, PM<sub>2.5</sub> and PM<sub>10</sub>. GSD corresponds to the width of the distribution. The calculation is done at an exemplary geometric mean of 0.3 μm. The calculation is shown for an ambient particle mass concentration of 25 μg m<sup>-3</sup> in both metrics, a particle mass density <ρ> of 1850 kg m<sup>-3</sup> with a variance Var(ρ) of (140 kg m<sup>-3</sup>)<sup>2</sup> and a sample volume of 1 mL. Although the ambient particle mass concentration is held constant in each metric, and therefore, the total mass that is sampled is also constant, the total uncertainty ranges over tens of percent and is a function of the upper cutoff of the relevant particle sizes. We can clearly see that at a GSD lower than ~1.5, the uncertainties are almost equal, as there are almost no particles that have a diameter above 1 μm, which makes the metrics' output equal. At higher GSDs, the metrics begin to differ, and so do the uncertainties. The lower the upper cutoff of the metric is, the lower the Var(V) of the relevant size window is. We can see that for equal distributions and similar mass concentrations, the relative uncertainties of PM<sub>1</sub>, PM<sub>2.5</sub> and PM<sub>10</sub> differ, although all of them take the mass into account.

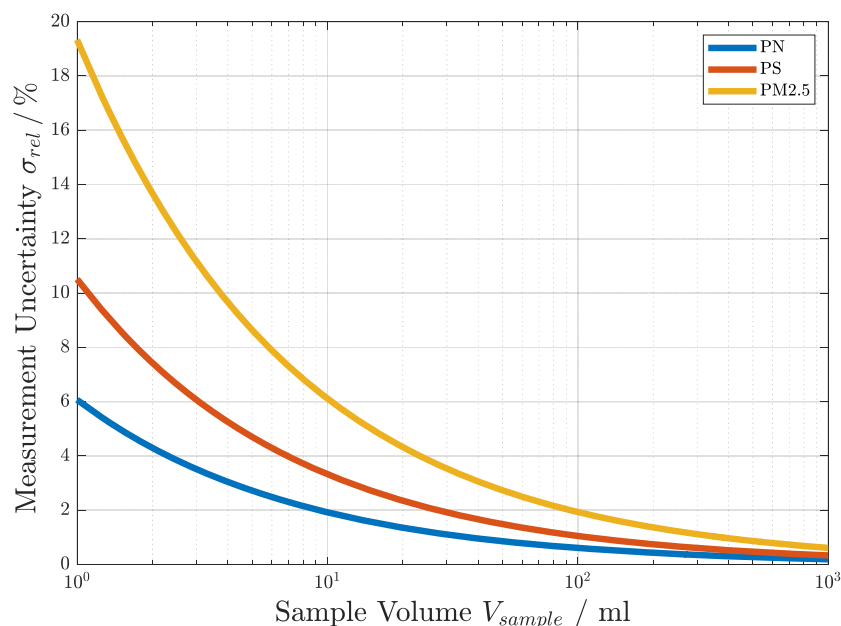
are sampled, which is proportional to the sample volume times the ambient mass concentration, the total mass sampled by the sensor is a reasonable parameter. In Fig. 4, the uncertainty of PM<sub>2.5</sub> is shown for lognormally distributed particles with a GM of 0.3 μm and various GSD values. The particle density, ρ, is set to 1850 ± 140 kg m<sup>-3</sup> according to Hand and Kreidenweis (2002). In Fig. 5, the same is shown for a fixed GSD value of 1.5 and various values of GM. The relative uncertainty declines when higher total masses are sampled, which can be due to either a high sample volume, a high ambient particle mass concentration, or both. In general, the uncertainty rises for higher GSD values, as the size distribution becomes broader and therefore, the variance of the particles volume becomes higher. The uncertainty is also dependent on the geometric mean of the size distribution. The lower the GM, the more particles are necessary to have a fixed mass concentration.

Fig. 6 shows the relative uncertainty of PM<sub>1</sub>, PM<sub>2.5</sub> and PM<sub>10</sub> as a function of the total mass that is sampled at an exemplary lognormal particle size distribution with a GM of 0.3 μm and a GSD of 1.7. The particle density, ρ, is set to 1850 ± 140 kg m<sup>-3</sup> according to Hand and Kreidenweis (2002). PM<sub>1</sub> has the lowest cutoff and therefore the lowest relative uncertainty at equal masses that are sampled,

whereas PM<sub>10</sub> has the highest of the three.

As a rule of thumb, we propose that for PM<sub>2.5</sub> and PM<sub>10</sub>, a minimum total mass of 100 pg should be sampled, which yields a measurement uncertainty for PM<sub>2.5</sub> of ~10%, as can be seen in Figs. 4 and 6. This assumes lognormally distributed particles with a geometric mean of 0.3 μm, a GSD of 1.7 and a particle density (ρ) of 1850 ± 140 kg m<sup>-3</sup>. We consider this a realistic worst-case scenario. At a PM<sub>2.5</sub> mass concentration of 25 μg m<sup>-3</sup>, this would mean that approximately 4 mL of air have to be sampled; at 10 μg m<sup>-3</sup>, 10 mL would be necessary to stay below the 10% measurement uncertainty. For PM<sub>1</sub>, we propose a minimum of 30 pg be sampled in order to have a relative uncertainty below 10%. We would like to emphasize that this is not valid for arbitrary particle size distributions and mass density distributions. In order to evaluate the exact uncertainty, Eq. (8) has to be utilized.

For particle number measurements, the rule of thumb we propose is to count at least 100 particles, which yields a relative uncertainty of 10%. Keeping in mind that imperfections of the measurement system itself come on top of this inherent uncertainty, a 10% inherent uncertainty may well be low compared to the uncertainties coming from technological boundaries.



**Fig. 3.** The plot shows the measurement uncertainty as a function of the sample volume. The particle size distribution is assumed to be lognormal with an exemplary GM of  $0.3 \mu\text{m}$  and a GSD of 1.7. The ambient  $\text{PM}_{2.5}$  concentration is set to  $25 \mu\text{g m}^{-3}$  and the particle density,  $\rho$ , to  $1850 \pm 140 \text{ kg m}^{-3}$  according to Hand and Kreidenweis (2002).  $\sigma_{rel}$  drops as the sample volume increases for each of the metrics. Particles with diameters higher than  $2.5 \mu\text{m}$  are neglected for each metric. The relative uncertainty of PN is the lowest, followed by PS, and  $\text{PM}_{2.5}$  has the highest uncertainty.

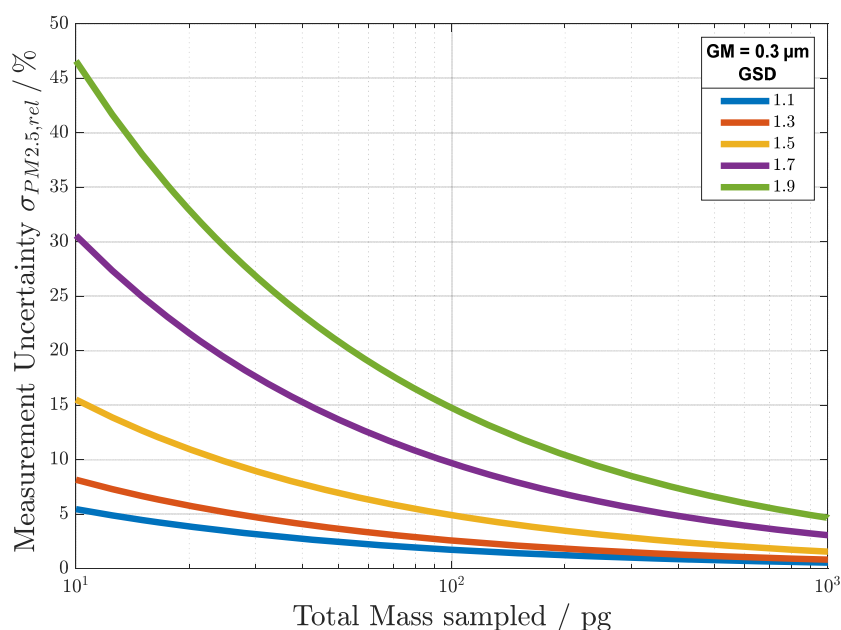


**Fig. 4.** The plot shows the relative uncertainty of  $\text{PM}_{2.5}$  as a function of the total mass that is sampled. A lognormal particle size distribution with an exemplary GM of  $0.3 \mu\text{m}$  is assumed. The results for various GSD values are shown. Assuming a  $\text{PM}_{2.5}$  concentration of  $25 \mu\text{g m}^{-3}$ , a volume of 4 mL is typically necessary in order to sample a total mass of 100 pg. Depending on the GSD of the particle size distribution, the relative uncertainty of  $\text{PM}_{2.5}$  can differ significantly.

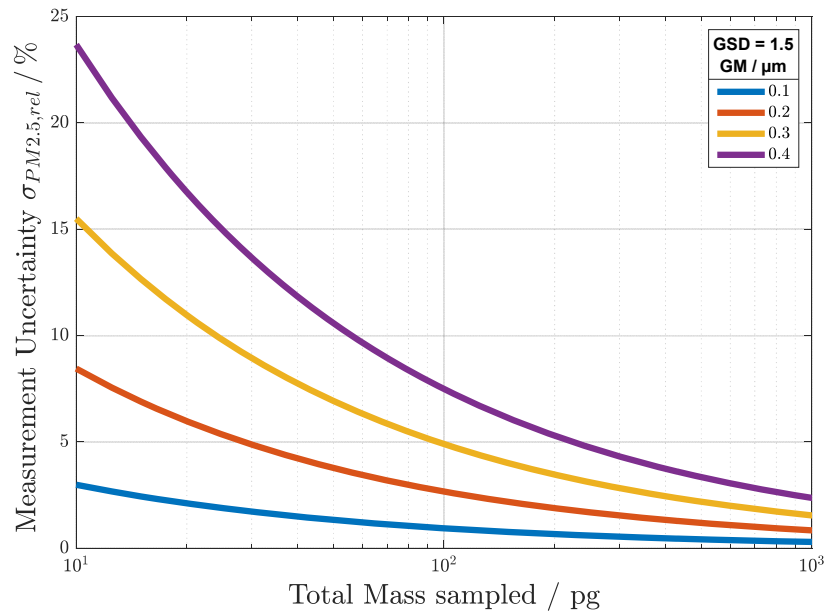


**Fig. 5.** The plot shows the relative uncertainty of  $PM_{2.5}$  as a function of the total mass that is sampled. A lognormal particle size distribution with a GSD of 1.5 is assumed. The results for various GM values are shown. Depending on the GM, the relative uncertainty of  $PM_{2.5}$  can differ significantly. This is reasonable since at lower GM values, a greater number of particles is necessary to have the same mass concentration as for higher GM values. The greater number of particles lowers the relative uncertainty.

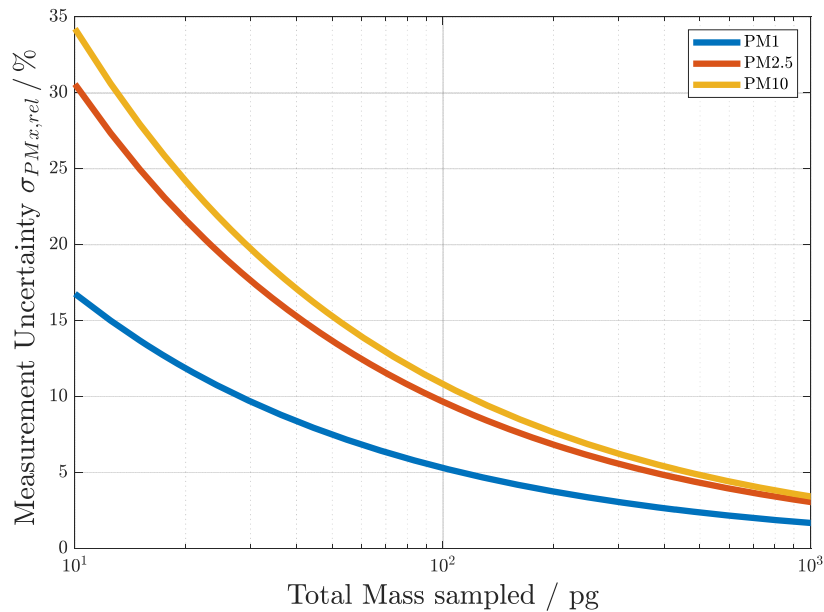


**Fig. 6.** The plot shows the relative uncertainty of  $PM_1$ ,  $PM_{2.5}$  and  $PM_{10}$  as a function of the total mass that is sampled. For each of the metrics, the same lognormal particle size distribution with a GM of  $0.3 \mu m$  and a GSD of 1.7 is assumed. The relative uncertainties of  $PM_1$ ,  $PM_{2.5}$  and  $PM_{10}$  differ due to the upper cutoff in particle size that is considered. With a total sampled mass of 100 pg, the uncertainty is 5% for  $PM_1$ , 10% for  $PM_{2.5}$  and 11% for  $PM_{10}$ . For  $PM_1$ , 30 pg are sufficient for the assumed parameters to have a relative uncertainty below 10%.

## CONCLUSIONS

We have established a model for estimating the local variability of particulate matter concentrations on arbitrarily small scales and evaluated it using various parameters. The model addresses the uncertainty in the particle number concentration and the surface concentration as well as the mass concentration for metrics such as  $PM_{10}$ ,  $PM_{2.5}$  and  $PM_{10}$ . The variability is due to the small number of particles within a small sample, which is used to represent a rather complex distribution of particle sizes and mass densities. Although we assume that variability on a small scale has no influence on human health, it does have a major impact on the validity of miniaturized PM sensor measurements. We find that even a sensor without any imperfections is barely able to assign a reliable particle concentration to the ambient environment when the sample volume is on the order of milliliters. Depending on the metric used, the uncertainty depends on the distributions of the influencing parameters. The overall uncertainty for the particle number concentration depends on the total particle concentration and the sample volume; additionally, the particle surface concentration is dependent on the size distribution, and for mass-related metrics such as  $PM_{10}$ ,  $PM_{2.5}$  and  $PM_{10}$ , also the mass density distribution has to be taken into account. These values, aside from the sample volume, may remain unknown with low-cost sensors and low sample volumes, effectively preventing the estimation of the uncertainty in the measurement. The total uncertainty is on the order of 10% for realistic cases and a sample volume of a few milliliters.

We have shown that for the same ambient conditions, the relative uncertainty in the particle number is lower than that in the surface concentration, which is lower than the relative uncertainty in the mass concentration. A small sample volume is therefore better suited to estimating number or surface concentrations than ambient mass concentrations. When mass metrics are used, the uncertainty is typically lower for estimating  $PM_{10}$  than  $PM_{2.5}$ . The highest relative uncertainty is generally associated with  $PM_{10}$ , as the range of measured particle sizes expands to include the largest diameters.

Miniaturized sensors with small footprints can overcome these limitations only by allowing relatively long measurement times or providing high flow rates. These measures, however, are incompatible with miniaturization since both features increase energy consumption and a high flow rate usually requires a large footprint. On top of these inherent limitations, sensor imperfections must be taken into account. As a rule of thumb for  $PM_{2.5}$  and  $PM_{10}$ , we propose a minimum total sample mass of 100 pg—typically 4 mL of sampled air at an ambient mass concentration of  $25 \mu\text{g m}^{-3}$ —in order to cap the relative uncertainty at approximately 10% for cases we consider to be realistic for ambient measurements; to obtain a ~10% uncertainty for  $PM_{10}$ , a minimum total sample mass of 30 pg is required. The miniaturization of particle sensors may hit a boundary once sample volumes reach ~1 mL due to the inherent statistical variability of particle concentrations on such

small volumes. In the opinion of the authors, a sample volume of less than 1 mL at realistic ambient particle concentrations may be insufficient for providing any reliable results. This handicap is especially severe when measuring mass-related metrics, such as  $PM_{10}$ ,  $PM_{2.5}$  and  $PM_{10}$ .

## ACKNOWLEDGMENTS

This work was funded by FFG (Austrian Research Promotion Agency) Grant #86197 and ams AG.

Supported by TU Graz Open Access Publishing Fund.

## SUPPLEMENTARY MATERIAL

Supplementary data associated with this article can be found in the online version at <http://www.aaqr.org>.

## REFERENCES

- Badger, E.H.M. (1946). Particle counts in the ultramicroscope. *Nature* 157: 480.
- Bao, Y., Cai, S., Yu, H., Xu, T., Xu, P. and Li, X. (2018). A resonant cantilever based particle sensor with particle-size selection function. *J. Micromech. Microeng.* 28: 085019.
- Ciccarella, P., Carminati, M., Sampietro, M. and Ferrari, G. (2016). Multichannel 65zF RMS resolution CMOS monolithic capacitive sensor for counting single micrometer-sized airborne particles on chip. *IEEE J. Solid-State Circuits* 51: 2545–2553.
- Damit, B., Wu, C. and Cheng, M. (2014). On the validity of the poisson assumption in sampling nanometer-sized aerosols. *Aerosol Sci. Technol.* 48: 562–570.
- Hand, J.L. and Kreidenweis, S.M. (2002). A new method for retrieving particle refractive index and effective density from aerosol size distribution data. *Aerosol Sci. Technol.* 36: 1012–1026.
- Hapidin, D. A., Saputra, C., Maulana, D. S., Munir, M. M., and Khairurrijal, K. (2019). Aerosol chamber characterization for commercial particulate matter (PM) sensor evaluation. *Aerosol Air Qual. Res.* 19: 181–194.
- Hinds, W.C. (1999). *Aerosol technology: Properties, behavior, and measurement of airborne particles*. Wiley, New York, USA.
- Kiountourtzoglou, E., Schwartz, J.D., Weisskopf, M.G., Melly, S. J., Wang, Y., Dominici, F. and Zanobetti, A. (2016). Long-term  $PM_{2.5}$  exposure and neurological hospital admissions in the northeastern United States. *Environ. Health Perspect.* 124: 23–29.
- Klenke, A. (2013). *Wahrscheinlichkeitstheorie. 3. Auflage*. Springer Spektrum, Berlin-Heidelberg, Germany, pp. 103–109.
- Larsen, M.L. (2007). Spatial distributions of aerosol particles: Investigation of the Poisson assumption. *J. Aerosol Sci.* 38: 807–822.
- Li, X., Iervolino, E., Santagata, F., Wei, J., Yuan, C.A., Sarro, P.M. and Zhang, G.Q. (2014). Miniaturized particulate matter sensor for portable air quality monitoring devices. *IEEE Sensors 2014 - Valencia*

- Conference Centre, Valencia, Spain, pp. 2151–2154.
- Linden, W., Dose, V. and Toussaint, U. (2014). *Bayesian probability theory: Applications in the physical sciences*. Cambridge University Press, Cambridge, UK.
- Paprotny, I., Doering, F., Solomon, P.A., White, R.M. and Gundel, L.A. (2013). Microfabricated air-microfluidic sensor for personal monitoring of airborne particulate matter: Design, fabrication, and experimental results. *Sens. Actuators, A* 201: 506–516.
- Ranft, U., Schikowski, T., Sugiri, D., Krutmann, J. and Krämer, U. (2009). Long-term exposure to traffic-related particulate matter impairs cognitive function in the elderly. *Environ. Res.* 109: 1004–1011.
- Väkevä, M., Hämeri, K., Puhakka, T., Nilsson, E.D., Hohti, H. and Mäkelä, J.M. (2000). Effects of meteorological processes on aerosol particle size distribution in an urban background area. *J. Geophys. Res.* 105: 9807–9821.

*Received for review, January 30, 2019*

*Revised, May 9, 2019*

*Accepted, May 11, 2019*





# **Chapter 4**

## **Sensor effects and applicability with regard to miniaturisation**

Before an overview of currently used sensor principles is given, a discussion of the requirements for miniaturisation and the suitability for volume production and the consumer market is necessary. Since the ultimate goal of the current project is to end up with a sensor that can be used in smartphones and wearable mobile devices, not only technical suitability and a possible realisation in high-volume production is necessary but also applicability to the consumer market.

An overview of sensor effects relevant for the thesis is given and the relevant literature is discussed. Significant benefits and drawbacks with respect to the overall goal of the project are highlighted. Rationale for the choice of the targeted sensor principle is presented.

### **4.1 Requirements for miniaturisation and the consumer market**

The overall goal of the project and the thesis within is to end up with a PM sensor system that is not only able to measure particulate matter concentration with reasonable accuracy, but to have a system design that will bring a benefit to a broader public by enabling the monitoring of the personal environment. The technical implementation is in general not straight forward on the targeted scale of the sensor and is further complicated by requirements resulting from the latter aspects. The choice of the sensor effect to be realised is therefore not only affected by the targeted metric and the size constraints, but also by aspects concerning the production and safety of the user.

**Imperative requirements for the sensor effect include:**

- Principle must work on the target scale
- Correlation to PM<sub>2.5</sub> must be at least clearly conceivable
- Limit of detection well below 50% of the 24h EU limit of 25  $\mu\text{g m}^{-3}$
- No maintenance or recalibration necessary
- No radioactive source
- No high voltage
- No UV light due to eye safety and to avoid O<sub>3</sub> generation
- Low power consumption, preferably below 100 mW
- Realisation must be possible in high volume production
- No extensive calibration of single sensors necessary

**Potential complications which might be overcome include:**

- Sample preconditioning required (charge, size distribution)
- Deposition of particles required
- Sensor lifetime under question
- Correlation to PM<sub>2.5</sub> not yet evident

## 4.2 Gravimetric measurement

Gravimetric measurement techniques are the only way to directly measure mass concentrations. The spectrum of techniques ranges from filter-based sampling in combination with conventional micro-balances, to related techniques such as the utilisation of quartz-crystal-microbalance, film-bulk acoustic resonators (FBAR) and tapered element oscillating microbalances (TEOM).

### 4.2.1 Filter-based gravimetric measurement

The most used gravimetric method relies on a filter which is weighted before a known volume of air is drawn through said filter. Particles stuck in the filter increase the overall weight which can be measured after loading [15, p. 217 ff.]. The filter weighting needs to be done very carefully at specified humidity and temperature conditions. Also the sample needs to be pre-conditioned in a sense that only the particle fraction of interest must be stuck at the filter. The volumes of air drawn through the filter are typically on the order of cubic meters since the practical sensitivity of the weighting is on the order of  $\mu\text{g}$ . Gravimetric measurements define PM2.5 and are therefore best-suited to measure PM2.5. Despite that, these methods can not be included in an integrated device.

### 4.2.2 Related gravimetric techniques

TEOM, the quartz-crystal micro-balance as well as FBAR are able to measure the mass of particles collected at a surface of the sensor. The deposited particles cause a shift in the resonance frequency of an oscillating element which is proportional to the mass increase. The most promising, and with respect to miniaturised particle measurements, most advanced technique is FBAR [8], [9]. There is also a patent filed on this system [35]. Fahimi et al. [9] have recently reported a FBAR based MEMS PM2.5 sensor with a footprint of  $27\text{ mm} \times 14\text{ mm} \times 2\text{ mm}$ . The system features a size separator realised as a virtual impactor, thermophoretic deposition is then used to deposit the PM2.5 fraction of particles on the FBAR. The sensitivity of the device is  $7\text{ }\mu\text{g m}^{-3}$  at a flowrate of  $9.5\text{ mL min}^{-1}$ . An integrated pump is mentioned, although no details are shown in the publication.

Fahimi et al. claim that they have estimated a lifetime of the sensor of approximately half a year assuming "regular use". The lifetime might be expanded by the implementation of multiple resonators.

Advantages of the method include the direct relation of the signal to PM2.5 and the compatibility of the design with semiconductor processes. The thermophoretic deposition might be a problem in terms of power consumption. Fahimi et al. [9] report a heating power between 30 and 42 mW which is relatively high for deposition only, although they claim to end up with an overall power consumption including an external fan of only about 150 . The lifetime of the sensor is still under question whereas the estimated half year of lifetime is to be considered insufficient for the integration in mobile devices.

### 4.3 Beta-Attenuation Monitor

Also for this principle particles are drawn through a filter. A beta-radiation source and a detector are used to measure the transmittance of the filter as a function of particle loading [36]. Particles in the filter will scatter the beta radiation leading to a decreasing signal.

This method is often used to measure 1h average values of PM<sub>2.5</sub> in environmental measurement stations. The system is often combined with a filter based gravimetric measurement for calibration.

This principle is inherently unsuitable for miniaturisation due to the necessary radioactive source. Other drawbacks include the necessity for sample preconditioning and the necessity of a filter change leading to an unclear lifetime without maintenance.

### 4.4 Photoacoustics

Photoacoustic techniques are widely spread for environmental measurements, specifically for gas concentration measurements [37]. The system utilises a pulsed light source which transfers energy to the investigated species. This leads to a local increase of temperature and pressure modulated with the frequency of the light source. The resulting acoustic signal is detected whereas its intensity is proportional to the respective concentration. The detection can be realised by utilising an acoustic resonator and a microphone or for example with a quartz tuning fork. Typically a lock-in amplifier is used to filter the photoacoustic signal. An essential parameter of the setup is the Q factor of the resonator used. There are commercially available products for measuring soot (e.g. Micro Soot Sensor, AVL List GmbH), still a correlation to PM<sub>2.5</sub> has not been shown yet. Also the targeted limit of detection might not be reached using such a system [38], especially since the sample volume is significantly smaller compared to table-top devices. Key problems include

- typically high laser power required
- acoustic resonator can hardly be scaled to the designated size range
- stray light affects the measurement especially with tuning forks
- ambient acoustic noise needs to be blocked
- single particles can not be detected, thus a large sample volume is needed

## 4.5 Charge based techniques - Diffusion charging and direct photoelectron emission charging

Particles can be charged using various techniques such as direct photoelectron emission charging or diffusion charging. Charged particles can subsequently be easier manipulated and information on the aerosol can be retrieved, see [14, p. 350 ff.] and [15, p. 324 ff.]. Direct photoelectron emission charging directly ionises the aerosol particles using photons with an energy above the photoemission threshold of the particle. The amount of charges per particle is proportional to  $d^2$ . Since UV light has to be used in order to have reasonable ionisation efficiencies, the method is often referred to as direct UV charging. For diffusion charging an ionised gas species is generated using for example a corona discharge. The charged gas molecules are then mixed with the aerosol and attach to the aerosol particles due to Brownian motion. The amount of charges on the aerosol particles is typically proportional to the particle diameter  $d^1$  [39] or proportional to in between the diameter  $d^1$  and the particle surface  $d^2$  [40]. Excess gas molecules are removed by an electric field in an ion trap. The overall charge of the aerosol can then be measured using a Faraday cage electrometer.

Direct UV charging is not suitable for miniaturisation since UV light cannot be used due to eyesafety regulations and the potential generation of  $O_3$ . Diffusion charging cannot be used since high voltages should be avoided. Also the sensitivity of the sensor depends on the sensitivity of the electrometer. Usually diffusion charging based devices have a resolution of approximately fA which is even for tabletop devices not an easy task. A miniaturised sensor with a lower flowrate (approximately a factor  $10^3$  smaller) and therefore a proportionally lower signal would have to have an proportionally better resolution. Given the limited space, this seems highly unlikely. Another drawback is that sample preconditioning is required and that a correlation of the signal to PM2.5 is unclear.

Lim et al [13] have shown a compact corona charging based prototype in MEMS technology with a footprint of  $75 \times 55 \text{ mm}^2$ . The device relies on an external pump and a flow rate of  $330 \text{ mL min}^{-1}$  which is beyond the definition of a miniaturised system in the sense of the present thesis.

## 4.6 Capacitive particle sensor

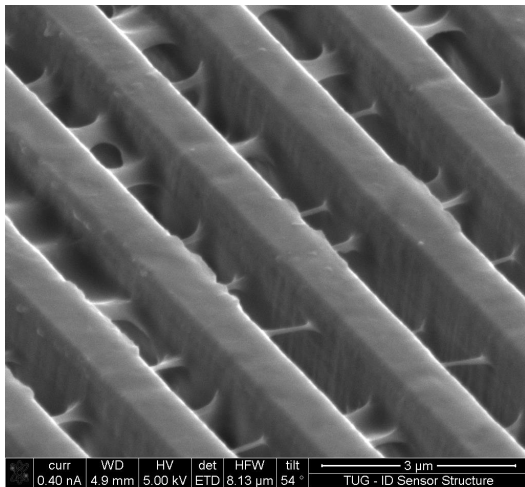
The significant difference in the dielectric constant of air and particles can be exploited by means of a capacitive measurement. Ciccarella et al [41] have shown a monolithic capacitive sensor in CMOS technology. The chip features an active area of  $1.15 \text{ mm}^2$  with 32 channels of interdigitated differential microelectrodes. The width, height and spacing of the

electrodes is 1  $\mu\text{m}$ . Due to the close proximity of the charge-preamplifier of each channel the resolution of the system is approximately 65 zF whereas the simulated effect of 1  $\mu\text{m}$  PSL particles according to their publication is 700 zF. Since the sensor is already realised in CMOS technology, the principle is a promising candidate for the project.

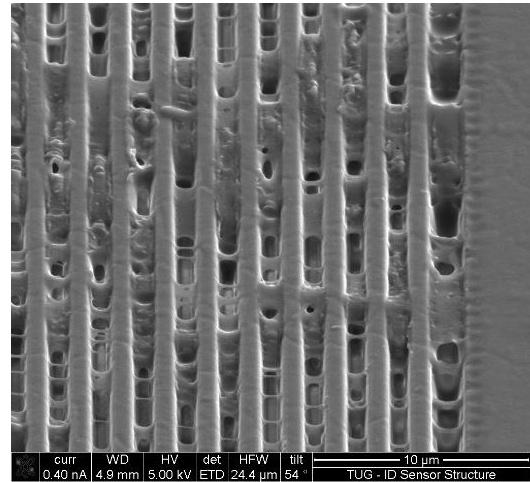
During a cooperation with the group of Prof. Sampietro from Polytechnico di Milano [11], [41], the capacitive sensor was further tested and evaluated, see sec. 4.6.1. An aerosol setup for controlled deposition of reference aerosol particles has been designed, realised and tested. A data evaluation algorithm has been implemented in Matlab and the experimental results have been compared to numerical simulations. A FIB cross section of the sensor has been done at TU Graz FELMI-ZFE. Major parts of this evaluation work have been done at TU Graz by the author of the thesis, whereas the numerical simulations have been done by Marco Carminati, Giorgio Ferrari and Marco Sampietro.

In conclusion the sizing capabilities of the sensor turned out to be insufficient for the measurement of PM<sub>2.5</sub>. During the experiments no significant difference in signal could be observed for PSL particle diameters of 0.5, 1 and 2  $\mu\text{m}$ . The observed signals are approximately  $2\text{aF} \pm 2\text{aF}$  for either of the PSL particle sizes used. This observation is most likely caused by the geometry of the interdigitated electrodes which leads to significantly different sensor responses dependent on the particles position relative to it. It seems reasonable that this effect overshadows the difference in signal due to different particle sizes. Further drawbacks include the necessity for an active particle deposition, an unclear correlation to PM<sub>2.5</sub> in general as well as a potential sensitivity to water and humidity compromising the sensor effect. In addition the process chosen for fabrication of the sensor is not ideally suited to form the targeted structure in sufficient quality. The etch step in AMS 0.35  $\mu\text{m}$  C35B4 process is typically used to form pads without significant structure. The FIB analysis of the sensor showed a high density of defects which compromise the sensors functionality. SEM images from the FIB analysis are shown in fig. 4.1. The sensor cannot be used for the measurement of PM<sub>2.5</sub> in the current state. A redesign of the sensor with a focus on an improvement of the sizing capabilities of the system is necessary and a better suited fabrication process has to be identified. Further research needs to be done on the influence of the particle material and morphology on the signal.

The capacitive sensor unit has been excluded from further investigation within this project.



(a) The interdigitated structures show connections which should not be present.



(b) Flowmarks caused by an unsuited etch step for this structure.

Fig. 4.1 SEM images of the capacitive sensor surface done by FELMI-ZFE. A number of defects can be observed which are likely to cause unclear signals when particles are deposited.

#### 4.6.1 Characterization of a Capacitive Sensor for Particulate Matter - publication in MDPI proceedings



## Characterization of a Capacitive Sensor for Particulate Matter <sup>†</sup>

Paul Maierhofer <sup>1,\*</sup>, Marco Carminati <sup>2</sup>, Giorgio Ferrari <sup>2</sup>, Georg Röhrer <sup>3</sup>, Marco Sampietro <sup>2</sup> and Alexander Bergmann <sup>1</sup>

<sup>1</sup> Institute of Electronic Sensor Systems, Graz University of Technology, 8010 Graz, Austria;

alexander.bergmann@tugraz.at

<sup>2</sup> Dipartimento di Elettronica, Informazione e Bioingegneria, Politecnico di Milano, 20133 Milano, Italy;

marco1.carminati@polimi.it (M.C.); giorgio.ferrari@polimi.it (G.F.); marco.sampietro@polimi.it (M.S.)

<sup>3</sup> ams AG, 8141 Premstätten, Austria; Georg.Roehrer@ams.com

\* Correspondence: paul.maierhofer@tugraz.at; Tel.: +43-316-873-3350

<sup>†</sup> Presented at the Eurosensors 2018 Conference, Graz, Austria, 9–12 September 2018.

Published: 17 December 2018

**Abstract:** We characterize a novel micro-sensor with pairs of interdigitated combs of microelectrodes designed to detect particles in air. We evaluate the sensor's response to 1  $\mu\text{m}$  Polystyrene Latex (PSL) particles experimentally and crosscheck the results with simulations. Experiment and simulation show good consistency. Based on the promising results we propose a redesign of the capacitive particle sensor with respect to PM2.5.

**Keywords:** particle sensor; capacitive sensing; particle deposition

### 1. Introduction

Small and very small particles in the ambient air, such as PM2.5—commonly known as fine dust—and PM1 represent a serious threat to life and limb [1]. Increasing awareness among the population and stricter regulations on the part of the legislation also lead to greater demands on the measurement and monitoring of air quality with respect to particle concentration. A close-meshed and wide-area monitoring has up to now failed due to the size, complexity and cost of the currently available systems. The aim of this work is to explore the possibility to use a novel capacitive sensor as a PM2.5 sensor. Since the sensor is already processed using a standard CMOS technology, a major advantage is the cost efficiency and relatively easy scalability which both are premises for a dense sensor network. The detection principle relies on interdigitated pairs of electrodes which are arranged on a surface [2,3]. Particles induce a sudden change in capacitance when deposited on this surface, see Figure 1. Width, height and spacing of the electrodes is 1  $\mu\text{m}$  which allows 1  $\mu\text{m}$  particles to be deposited both onto the electrodes as well as in between them. The capacitive change depends on size, shape, dielectric constant, and the exact position of the particles. Since the dispersed particles are uniform within an experiment, the only influence left is the position of the particles relative to the surface structure of the sensor.



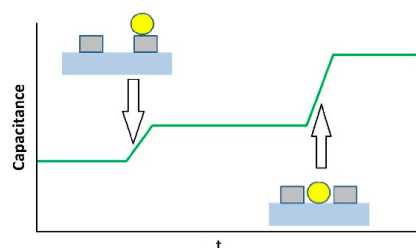


**Figure 1.** Detection principle of the capacitive sensor. The grey rectangles indicate micro-electrodes on top of the blue SiO<sub>2</sub>. Yellow spheres indicate particles deposited on top of the electrodes, which then cause the capacitance to change abruptly.

## 2. Materials and Methods

We have built a setup for selective deposition of well-defined spherical particles in order to evaluate the performance of the capacitive microsensor, see Figure 2. The deposition setup consists of an atomizer (Topas ATM221) in combination with a diffusion dryer (Topas DDU 570), which disperses PSL particles in air. Said particles are then neutralized (TSI Aerosol Neutralizer 3077) in order to minimize charge effects. A nozzle is used to accelerate the particles towards the sensor in order to use impaction as a means of depositing. The sensor is placed underneath the nozzle in a distance of a few millimeters where the particles are then deposited. A needle valve in parallel to the nozzle allows for steady control of the flow rate through the nozzle. We are able to assign detected events of the sensor to deposited particles with a digital microscope (Keyence VHX and VHZ-250R), see Figure 1. Deposited particles are detected both optically using a digital microscope, see Figure 3, and utilizing the described sensor effect. The experiment is further simulated using Comsol, results see Figure 5.

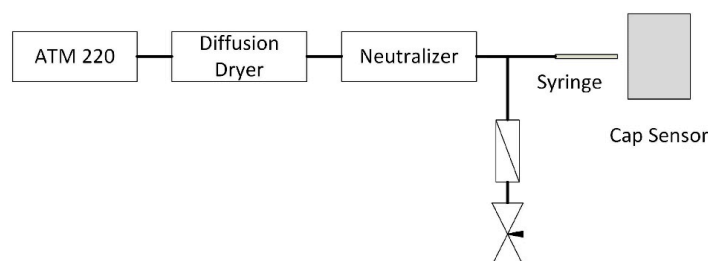


**Figure 2.** Setup for deposition of 1  $\mu\text{m}$  PSL spheres onto the surface of the investigated capacitive sensor.

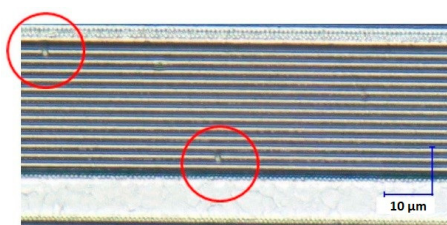


**Figure 3.** Image of deposited 1  $\mu\text{m}$  spheres on top of the sensor's surface. Spheres are in the middle of the red circles. The horizontal lines are the microelectrodes, which form the sensor.

### 3. Results

We are able to show that the sensor is able to correctly count deposited particles on the surface, which is confirmed using the microscope to count deposited particles optically. The number of detected capacitive steps matches the number of deposited particles.

The response of the sensor to a particle is an abrupt change of the capacitance with step heights of roughly 0.5 aF up to 10 aF for the investigated particles, results see Figure 4. The relatively broad distribution of capacitive steps caused by monodisperse 1  $\mu\text{m}$  particles stems from the distribution of positions of the particles relative to the microelectrodes. A particle on top of the electrodes will lead to a weaker signal compared to a particle in between the combs, results see Figure 4. Since the electrodes protrude above the  $\text{SiO}_2$ , particles are more likely to be deposited onto the electrodes rather than in between them leading to a weaker signal. Experimentally a small number of larger capacitance steps than predicted by simulation are observed, which is most likely due to inhomogeneities of the sensor's surface. Overall, the experimental results match the simulation reasonably well.

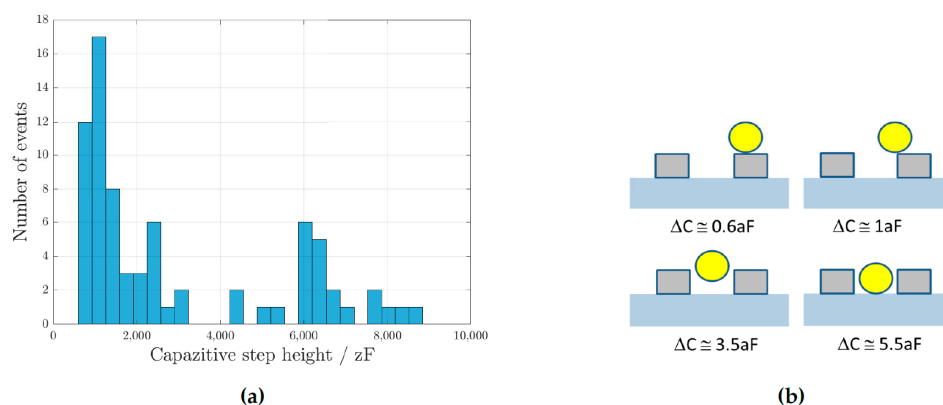


**Figure 4.** (a) Histogram of the observed capacitive changes caused by monodisperse 1  $\mu\text{m}$  PSL particles. (b) Simulation of the sensor's response to the monodisperse 1  $\mu\text{m}$  PSL particles. The position of the particles relative to the electrodes has a significant impact on the signal.

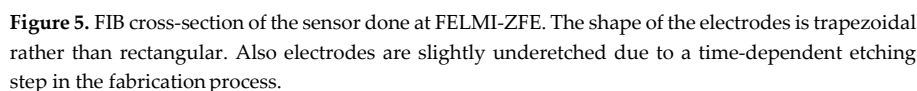
As particles of larger diameters than the distance between two electrodes cannot fall between the electrodes, the sensor can operate in two regimes: large particles are detected on top of the electrodes, smaller ones which would induce a low capacitance change on top of the electrodes are detected in between them. This finding can be utilized to redesign the capacitive microsensor with a focus on the detection of PM2.5.

### 4. Conclusions and Outlook

The setup for the dispersion and deposition of 1  $\mu\text{m}$  PSL particles works and allows a systematic investigation of various sensors where particle deposition is necessary.

We have shown that the investigated sensor is able to count monodisperse PSL particles with a diameter of 1  $\mu\text{m}$  correctly. Simulation and experimental results regarding the response of the sensor agree reasonably well for the investigated particles. We have shown that the sensor can work in two regimes. Particles larger than the pitch are detected on top of the electrodes whereas smaller ones can be detected in between them. This effect is to be used for a redesign of the sensor with respect to PM2.5 by reducing the pitch to roughly 0.5  $\mu\text{m}$  in order to push the lower limit of detectable particles to lower diameters. Recent findings from a Focused Ion Beam (FIB) and Scanning Electron Microscope (SEM) investigation are to be taken into account for the simulations, see Figure 5. This regards the trapezoidal shape of the electrodes as well as the depth of the gaps between the electrodes. The electrodes are

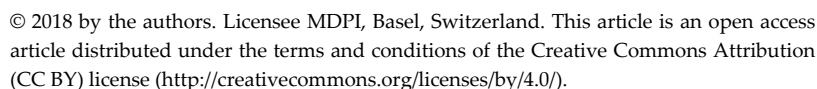
Further research is necessary to determine the exact limit of detectable particles in terms of size and concentration and to explore the possibility to discriminate different particle sizes by the signal. In conclusion the capacitive sensor is a promising candidate for a cost-efficient and integrated sensor.



**Funding:** This work was funded by FFG grant 86197, Fondazione Cariplo through the projects MINUTE (No. 2011-2018) and ESCHIO (No. 2013-1760), and ams AG.

## References

1. Kioumourtzoglou, M.A.; Schwartz, J.D.; Weisskopf, M.G.; Melly, S.J.; Wang, Y.; Dominici, F.; Zanobetti, A. Long-term PM(2.5) Exposure and Neurological Hospital Admissions in the Northeastern United States. *Environ. Health Perspect.* **2016**, *124*, 23–29, doi:10.1289/ehp.1408973.
2. Ciccarella, P.; Carminati, M.; Sampietro, M.; Ferrari, G. Multichannel 65 zF rms Resolution CMOS Monolithic Capacitive Sensor for Counting Single Micrometer-Sized Airborne Particles on Chip. *IEEE J. Solid-State Circ.* **2016**, *51*, 2545–2553, doi:10.1109/jssc.2016.2607338.
3. Carminati, M.; Pedalà, L.; Bianchi, E.; Nason, F.; Dubini, G.; Cortelezzi, L.; Ferrari, G.; Sampietro, M. Capacitive detection of micrometric airborne particulate matter for solid-state personal air quality monitors. *Sens. Actuators A Phys.* **2014**, *219*, 80–87, doi:10.1016/j.sna.2014.09.003.



## 4.7 Optical sensors

Especially in the field of low-cost sensors, optical measurement techniques are dominating. Due to the refractive index of particles which is different from the surrounding gas, there is a significant interaction of light with particles. In general light is absorbed and scattered. The most common technique is light scattering where light hits single particles and the scattered light in a specified solid angle is detected. Another technique is realised in the aethalometer, where particles are trapped in a filter and the optical transmission of the filter is measured - similar to a beta-attenuation monitor but with optical radiation instead of beta-radiation. In addition to the classical light scattering approach and the aethalometer, two novel ideas have been found and investigated. The first one being the utilisation of optical waveguides and the interaction of the particle with the surrounding evanescent field, which has not been utilised for particle measurements before. The second one is an interferometric approach where the extincted light as well as the phase shift of the forward scattered light are exploited.

### 4.7.1 Light Scattering

When light interacts with a particle, a fraction of the incoming light will be absorbed and another fraction is scattered. The scattering is dependent on the wavelength of the incoming light, as well as on the particle size, refractive index, and morphology. For spherical particles, the interaction is fully described by Mie theory, which provides the solution to Maxwell's equations for a plane wave interacting with a spherical object, in detail described in [42]–[44].

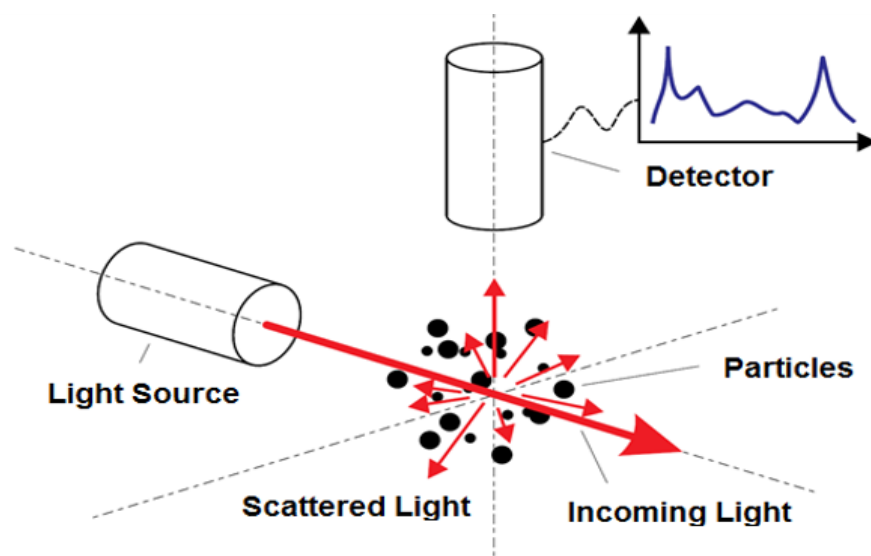


Fig. 4.2 Light scattering principle. Image reproduced from [44]

A photodetector is placed at an angle relative to the incoming light, which detects the scattered light in the geometrically covered solid angle. The number of peaks detected by the detector is then proportional to the number of particles passing the light beam, whereas the peak height is a non-trivial function of the particle size and the solid angle of measured scattered light by the detector, described by Mie theory. The amount of scattered light is generally low. For example we assume a spherical particle with a refractive index  $n$  of  $1.5 + 0i$  a wavelength of 808 nm and an optical input power of 1 mW. The spot is assumed to have a diameter of 300  $\mu\text{m}$ . The photodiode is assumed to have a size of 1  $\text{mm}^2$  in a distance of 650  $\mu\text{m}$  centered at an angle of  $90^\circ$  relative to the incoming light. A particle with a diameter of 300 nm scatters in this setup a power of approximately  $10^{-10}$  W towards the detector. Due to the generally low amount of scattered light, care has to be taken that the stray light reaching the photodiode without present particles is minimised. The detector can therefore not be placed in forward scattered direction. A light trap has to be used which is crucial for the limit of detection with respect to particle size. The quality of the light trap can be compromised by limited space, which is the only penalty of this effect for miniaturisation. The interaction of the light with the particle is identical to larger devices and the signal at the detector caused by single particles is not inherently smaller. Due to limited space, refractive optical elements may not be incorporated in the sensor which makes the design more delicate. Currently all state of the art low-cost PM2.5 sensors are based on a light scattering principle, which is a benefit in terms of acceptance of the technique both in the scientific community and the consumer market.

Significant advantages include that no particle preconditioning is necessary as PM2.5 can be estimated by excluding the signal from particles larger than 2.5  $\mu\text{m}$  from the estimation. Nevertheless, it is beneficial to prevent large objects and particles larger than approximately 10  $\mu\text{m}$  in diameter from entering and contaminating the sensor. As for the estimation of the particle concentration the volume of aerosol passing the sensor has to be known, there may be a need for a flow sensing element if the flow rate can not be assumed constant. In the case of light scattering there may be an indication of the flow rate in the signal as the temporal peak width caused by single particles passing the light beam is proportional to the velocity of the particle and the flow rate. Another significant benefit of the principle is that the theoretical background can be considered solid and no additional research with respect to the sensor effect is necessary. Standard simulation packages (e.g MiePlot by Philip Laven <sup>1</sup>) can be utilized to estimate the signal.

Disadvantages include that for the estimation of PM2.5, an average particle mass density has to be assumed, which is on the other hand necessary for every sensor effect except the

---

<sup>1</sup><http://www.philiplaven.com/mieplot.htm>

gravitational techniques. Also a constant index of refraction must be assumed as well as a spherical particle shape.

Another disadvantage is that light scattering devices typically cannot detect particles smaller than approximately 300 nm in diameter. While this is not a significant drawback for the estimation of PM<sub>2.5</sub>, it lacks in information on nanosized particles and BC. A potential shift of the legislation and public awareness towards metrics targeting smaller particles, could therefore render light scattering devices redundant.

#### **4.7.2 Waveguide based evanescent field sensing**

A small fraction of light will protrude in the optical less dense medium when light undergoes total internal reflection. This part of the wave decays rather quickly after the boundary of reflection and is referred to as evanescent field. Evanescent fields along the surface of optical fibers or waveguides can then interact with species in close vicinity, whereas light can be absorbed or scattered, thus influencing the transmission of light through the fiber or waveguide. This technique is implemented in various chemical and bio-chemical sensors for optical-spectroscopic analysis [45]. While the effect is well established for the measurement of gaseous compounds, it has not been extensively used specifically for the detection of aerosol particles. Kulkarni et al. [46] investigated the influence of black carbon on the evanescent field of a fiber, highlighting the high potential for aerosol measurement. Although this potentially exploitable effect is known, there has been no comprehensive understanding of the physical basics of the type of interaction between the evanescent field and one or several particles on the surface, and the resulting changes in the signal transmitted through the waveguide. The correlation of the effect to PM<sub>2.5</sub> is under question although it seems highly likely that there is a correlation.

We have recently shown a single particle detector based on a single nitride waveguide where PSL spheres down to a diameter of 200 nm were detected [47]. The results were supported by numerical simulations which agree reasonably well in terms of signal. A design for a miniaturised sensor based on this approach in combination with a through-silicon-via to expose the active waveguides to the aerosol, has been filed for patent as shown in Appendix A.2 whereas the author of the present thesis is one of the inventors. In addition to the filed patent, a project proposal titled "Evaneszenz-Feld Partikel-Sensoren - EFiPaS" has been submitted in collaboration with ams AG and CTR to the Austrian Research Promotion Agency (FFG). The author has written major parts of the proposal. The proposal has been accepted under grant number 864341 and the project is ongoing from May 2018 to May 2020 whereas Anton Buchberger is working as a PhD student on the topic at TU Graz Institute of Electronic Sensor Systems. The author is involved in parts of the ongoing research and

co-authored parts of the publications such as [47].

Since the proposal including the detailed workplan is not under disclosure, it can not be provided in this thesis.

The proposed technique is promising and scientifically challenging but was not yet ready to be implemented in a sensor system. The present project and the thesis within do not focus on this topic beyond the patent application and the project proposal.

### 4.7.3 Aethalometer

Similar to a beta-attenuation monitor and gravitational filter-based measurements, the aerosol is drawn through a filter where the particles are trapped. An optical light source and a detector are used to measure the optical transmission through the filter as a function of loading time [48], [49], see fig.4.3. The attenuation is proportional to the amount of particles on the filter since particles extinct a fraction of the incoming light. There may be a reference filter which remains unloaded, as indicated in fig. 4.3, in order to quantify the absolute increase in attenuation and to account for a drift of the system. This reference filter spot can be dismissed and a differential measurement scheme can be applied thus decreasing the overall system complexity. The attenuation effect is dominated by highly absorbing particles such as black carbon, which is why aethalometers are mainly used to quantify BC. Despite the dominating effect of the BC content of PM<sub>2.5</sub>, a correlation of the signal to PM<sub>2.5</sub> seems reasonable as well but has not been shown in literature. The signal evaluation is not straight forward as filter loading effects and humidity affect the attenuation as well and are taken into account. There are products commercially available, e.g. by the companies Magee Scientific<sup>2</sup> and Aethlab<sup>3</sup>. The available products range from table-top devices to hand-held devices and are targeting the measurement of BC. There is no miniaturised low-cost PM<sub>2.5</sub> sensor based on an aethalometer available.

A central question regarding the aethalometer is whether the number of possible measurements in a miniaturised system are sufficient. The number of possible measurements has been estimated in the following.

---

<sup>2</sup>[www.mageesci.com](http://www.mageesci.com). Last accessed 07.04.2020

<sup>3</sup>[www.aethlabs.com/microaeth](http://www.aethlabs.com/microaeth). Last accessed 07.04.2020

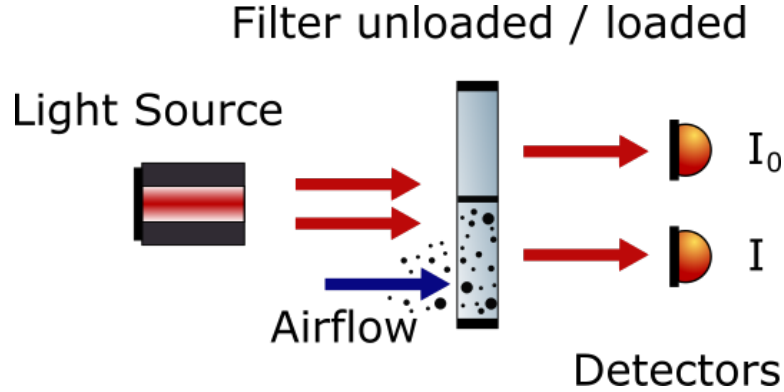


Fig. 4.3 Aethalometer measurement principle

The following estimations are based on Weingartner et al. [50] The text is an excerpt from their publication.

Fig.4.3 shows the aethalometer measurement principle where a light source shines light on two filter spots, one of which is exposed to the investigated airflow. Loading of this filter spot with particles leads to an attenuation of the light which is used to calculate the concentration of particles in the air.

The absorption coefficient is defined via Beer-Lambert's law:

$$I = I_0 e^{-b_{abs}d} \quad (4.1)$$

$I_0$  is the intensity of the incoming light and  $I$  the intensity of the light after the sample with thickness  $d$ . The attenuation is then defined as in eq. 4.2.

$$ATN = -\ln\left(\frac{I}{I_0}\right) \quad (4.2)$$

By measuring the intensity after an unloaded filter, the optical properties of the filter itself are not taken into account in the calculation. Also a drift in the intensity of the light source can be monitored this way.

The aerosol absorption coefficient  $b_{ATN}$  is then defined as:

$$b_{ATN} = \frac{A \cdot \Delta ATN}{Q \cdot \Delta t} \quad (4.3)$$

$A$  is the area of the filter spot,  $Q$  is the volumetric flow rate through the filter,  $\Delta ATN$  is the change in attenuation during the time  $\Delta t$ .

$b_{ATN}$  can differ from the true aerosol absorption coefficient  $b_{abs}$ , therefore correction factors are introduced. The correction factors take into account loading effects of the filter



as well as multiple scattering effects. The corrections are empirical or semi-empirical. For further information see [50] [51].

For the following simplified estimations the correction factors are set to unity which leads to  $b_{ATN} = b_{abs}$ .

The aerosol concentration  $M$  can then be estimated by eq.4.4:

$$M = \frac{b_{abs}}{\sigma_{abs}} \quad (4.4)$$

Where  $\sigma_{abs}$  is the mass specific absorption cross section which depends on the type of particles and the wavelength used. Weingartner et al. [50] report values for  $\sigma_{abs}$  for black carbon ranging from 5 to 20 m<sup>2</sup> g<sup>-1</sup>. Chou et al. [52] have collected PM<sub>2.5</sub> samples in Taipei (Taiwan) and have measured the mass specific cross section of the sample. They assume that only the carbonaceous fraction of PM<sub>2.5</sub> contributes to absorption and derive the mass specific absorption cross section of elemental carbon, which seems unreasonable. Nevertheless, they report values for  $\sigma_{abs}$  for their PM<sub>2.5</sub> samples of roughly 1 m<sup>2</sup> g<sup>-1</sup>.

### Sensitivity Estimation

In order to estimate the sensitivity of the detector necessary for resolving typical particle concentrations in air in reasonable time, equations 4.2, 4.3 and 4.4 are used.

$$\Delta ATN = \frac{Q\Delta t}{A} \cdot M \cdot \sigma_{abs} \quad (4.5)$$

For an initial attenuation of 0 and an attenuation  $ATN_1$  of  $\Delta ATN_1$  after an integration time of  $\Delta t$

$$\frac{I}{I_0} = e^{ATN_1} = e^{-\frac{Q\Delta t}{A} \cdot M \cdot \sigma_{abs}} \quad (4.6)$$

Assuming  $\sigma_{abs} = 1 \frac{m^2}{g}$  [52],  $M = 25 \mu g m^{-3}$ ,  $A = (300 \mu m)^2$ ,  $Q = 3 mL min^{-1} = \frac{3}{60} \cdot 10^{-6} \frac{m^3}{s}$  and an integration time of  $\Delta t = 10s$  leads to  $1 - \frac{I}{I_0} \approx 10^{-4}$ . For the assumed values, the detector needs to resolve a relative change in intensity of  $10^{-4}$ . In other words, the detector needs to have a sensitivity of better than  $10^{-4}$  with respect to  $I_0$  in order to be able to detect a mass concentration  $M$  of  $25 \mu g m^{-3}$  with a mass specific absorption cross section of  $\sigma_{abs} = 1 \frac{m^2}{g}$  in 10s filter loading time, assuming a volumetric flow rate  $Q$  of  $3 mL min^{-1}$  on a filter spot size  $A$  of  $(300 \mu m)^2$  and an initially unloaded filter. As the sensor is most sensitive when the filter is unloaded (the slope of the Beer-Lambert law is decreasing for higher  $b_{abs}$ ) the sensitivity of the detector should in general be better than  $10^{-4}$  or else the integration time needs to be adjusted. For further evaluations a sensitivity  $S$  of  $10^{-5}$  is assumed.

The value for  $\sigma_{abs} = 1 \frac{m^2}{g}$  is just a rough initial estimation. It can be tuned by the choice of the wavelength and it has to be carefully evaluated experimentally in order to show a correlation of the aethalometer measurement to PM2.5.

### Estimation of the number of possible measurements

Again the starting point is Beer-Lambert's law for this case where  $\frac{QM\sigma}{A}$  is set constant according to the values assumed in the sensitivity estimation.

$$I = I_0 e^{-\frac{QM\sigma}{A}t} = I_0 e^{-\alpha t} \quad (4.7)$$

$$\frac{QM\sigma}{A} = const. = \alpha \quad (4.8)$$

The idea is to define a constant  $\Delta I$  instead of a fixed single measurement time  $\Delta t$ . Also a maximum single measurement time  $\Delta t_{max}$  needs to be defined after which the measurement stops. By defining this parameters, the number of measurements possible with one filter, can be estimated.

$$\Delta I = const. = SI_0 \quad (4.9)$$

$$\Delta I = SI_0 = I_0(\exp(-\alpha t) - \exp(-\alpha(t + \Delta t)))$$

$$S \cdot \exp(\alpha t) = 1 - \exp(-\alpha \Delta t)$$

$$\Delta t = -\frac{\ln(1 - S \cdot \exp(\alpha t))}{\alpha} \quad (4.10)$$

Eq.4.10 shows the dependence of the single measurement time of the total integrated measurement time  $t$  of the filter. As expected the single measurement time increases with increasing integrated measurement time.

The calculation assumes not only a constant volume flow,  $\sigma$  and filter spot area but also a constant mass concentration of particles in the air.

The maximum single measurement time  $\Delta t_{max}$  can be used to calculate the maximum loading time  $t_{max}$  after which the filter is unusable.

$$t_{max} = \frac{1}{\alpha} \cdot \ln \left( \frac{1 - \exp(-\alpha \Delta t_{max})}{S} \right) \quad (4.11)$$

As expected the maximum integrated measurement time increases with increasing maximum single measurement time.

$t_{max}$  corresponds to a minimum intensity  $I_{min}$  from whereon the change in  $I$  is insufficient to measure the concentration in a reasonable time  $\Delta t_{max}$ .

$$I_{min} = I_0 \cdot \exp(-\alpha t_{max})$$

$$I_{min} = I_0 \cdot \frac{S}{1 - \exp(-\alpha \Delta t_{max})} \quad (4.12)$$

The number of measurements  $N_{meas.}$  can be calculated using eq.4.9 and 4.12

$$N_{meas.} = \frac{I_0 - I_{min}}{\Delta I} = \frac{1}{S} - \frac{1}{1 - \exp(-\alpha \Delta t_{max})} \quad (4.13)$$

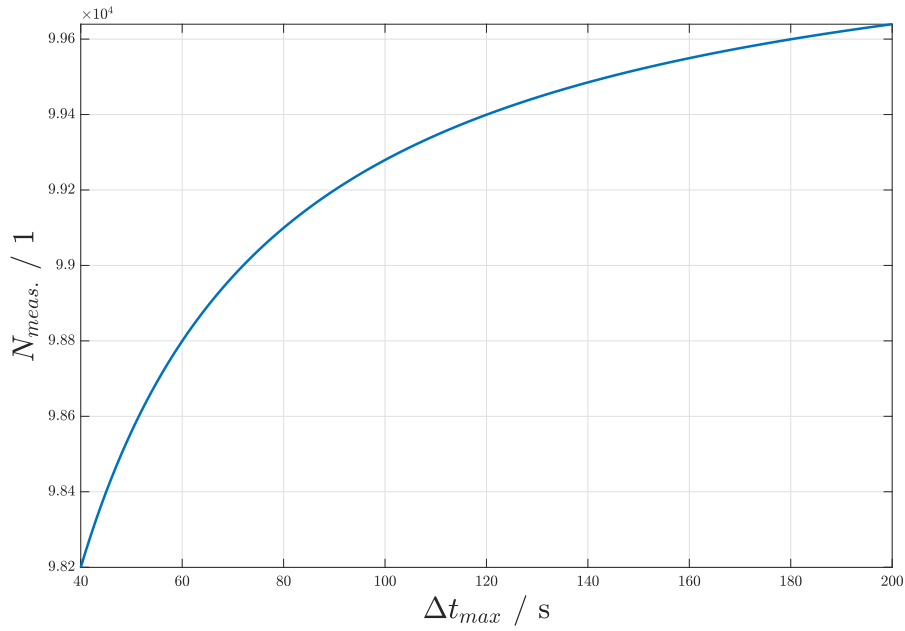


Fig. 4.4 Number of measurements possible before the change in signal is too weak to resolve the concentration in reasonable time as a function of the maximum single measurement time  $\Delta t_{max}$ . Assuming  $\sigma_{abs} = 1 \frac{m^2}{g}$  [52],  $M=25 \mu g m^{-3}$ ,  $A = (300 \mu m)^2$ ,  $Q = 3 mL min^{-1}$

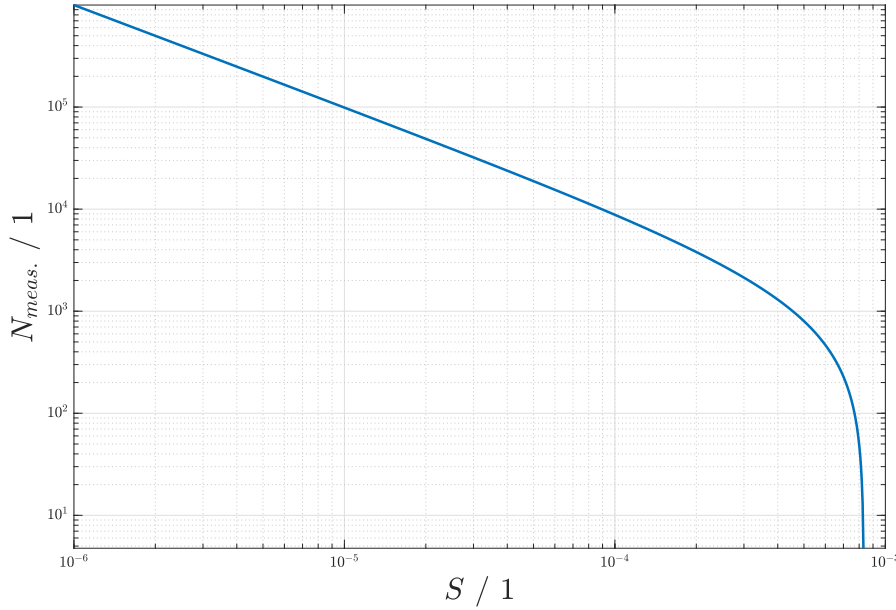


Fig. 4.5 Number of measurements possible before the change in signal is too weak to resolve the concentration in reasonable time, as a function of  $S (= \Delta I/I_0)$ . Assuming  $\sigma_{abs} = 1 \frac{m^2}{g}$  [52],  $M=25 \mu g m^{-3}$ ,  $A = (300 \mu m)^2$ ,  $Q = 3 mL min^{-1}$

Eq.4.13 shows that the number of measurements possible is determined by  $\alpha$  (see eq.4.8), the sensitivity  $S$  of the detector and the maximum single measurement time  $\Delta t_{max}$ . The dominating parameter is the sensitivity of the detector. The number of possible measurements is mostly determined by the term  $S^{-1}$ . For a filter spot size of  $4 \cdot 10^{-3} m^2$ , a flow rate of  $1 cm^3/min$ . and a mass specific absorption cross section of  $1 m^2/g$ , a sensitivity of  $10^{-5}$  and a maximum single measurement time of 60 s, the number of measurements possible is approximately  $10^5$ .

The total time the filter is loaded is in this case approximately 5000 min according to eq. 4.11, which corresponds to a total sampled volume of  $0.015 m^3$  given the flow rate  $Q$  of  $3 mL min^{-1}$ . Assuming a concentration of  $25 \mu g m^{-3}$ , the total mass on the filter is  $0.38 \mu g$ . Assuming a mean density of the particles of  $1200 kg m^{-3}$  and a filter spot size of  $(300 \mu m)^2$ , the height of the captured particles on the filter is  $3.5 \mu m$  if they are assumed to be close packed. The total mass of the captured particles seems to be insufficient to clog the filter with respect to the flow although this point should be evaluated experimentally.

As stated by Maierhofer et al. [34] a minimum mass of 100 pg of PM2.5 particles is recommended for a single measurement in order to ensure an inherent measurement uncertainty of below 10%. This aspect is not accounted for in the above estimations. Under this aspect it is

beneficial to choose the filter size and the size of the light beam in a way that a loading of 100 pg leads to exactly the minimum decrease in intensity the photodiode is able to resolve.

## Conclusion

What can be seen from the estimations is that typical aerosol concentrations can be resolved in reasonable time by an integrated miniaturised aethalometer. The system can be tuned by the choice of wavelength which will affect the mass specific absorption cross section of the aerosol. Other tunable parameters are the filter spot size and the volumetric flow rate.

The number of possible measurements is determined by eq. 4.13 and is dominated by the sensitivity of the photodiode.

Assuming a lifetime of an integrated device of 5 years, the number of possible measurements with the assumed parameters is 54 per day, which seems to be sufficient in average.

Disadvantages of the technique include the necessity of a sample pre-conditioning with respect to the targeted metric and that the correlation of the sensor effect to PM<sub>2.5</sub> has not yet been shown, although this correlation appears to be very likely.

One major advantage of the aethalometer is that it is inherently sensitive to carbonaceous particles such as BC. Due to the enhanced health effects of BC (see sec. 2.2) this can be considered beneficial.

Another advantage is that the flow through the filter does not have to be constant as the average effect is measured. Depending on the type of pump or fan used, the flow may show oscillations which are hard to control.

Typically the functionality of a sensor can be compromised by deposited particles. In this case the sensor fouling is the sensor effect that is measured.

Due to the very promising outlook of the aethalometer, the ideas and a design of an integrated aethalometer particle sensor has been filed for patent, whereas the author of the present thesis is one of the inventors. [53] The patent application can be found in the Appendix A.1.

### 4.7.4 Interferometric Particle Detection

We show a concept and experimental proof of principle for a particle detector utilising optical interference effects in a Fabry-Perot cavity. Due to the difference in refractive index of the particle relative to the gas, light will be scattered and absorbed when it interacts with a particle. The extincted light as well as the forward scattered light which has a phase shift relative to the incident beam, influence the transmission function of the interferometer. The operating point of the interferometer is chosen in a way that without particles present in the interferometer the signal at the detector is at a minimum. We show experimental proof that

by monitoring the reflected power of a Fabry Perot cavity, particles can be counted. We show that the signal is proportional to the particle size within a simplified mathematical model. The proposed measurement technique is complementary to light scattering regarding signal since the total extinction and the phase shift in forward direction contribute to the measured effect. Additionally the proposed technique shows potential for a low-cost miniaturised realisation and might be an alternative to light scattering in future applications.

Batchelder et al. [54] have shown a coherent detection technique where the light scattered by single particles is coherently overlapped with a reference laser beam thus being sensitive to the phase shift caused by particles. Potenza et al. [55] have shown an overview of this and related techniques which rely on interference effects. These methods are capable of counting particles and there is a size information in the signal [55]. Pettit et al. [56] have shown a Coherent Optical Particle Spectrometer which works on a similar basis utilising a Mach-Zehnder interferometer. One arm of the interferometer is used as a reference whereas the second arm is exposed to particles. Light is scattered and absorbed by the particles leading to a signal modulation by coherent overlapping the signal in the reference arm with the measurement arm. All of the methods mentioned have been realised using discrete optical parts and fall in the category high-end equipment. The method we propose is related to this work. We propose to use coherent detection and exploit interference effects and extinction of light by utilising a Fabry-Perot interferometer. Due to the multiple reflections of the light in the Fabry-Perot cavity and the sensitive transmission function, this setup might be more sensitive than the ones covered by the current literature. Additionally this approach shows the potential for miniaturisation and may be used as an alternative to the standard light-scattering techniques for low-cost sensors.

## Measurement Principle

The principle utilizes a Fabry-Perot interferometer as shown in fig.4.6 consisting of a light source on one side of a cavity formed by two parallel highly reflecting mirrors and a detector. The transmission through the cavity and thus the signal at the detector is a function of the wavelength, the pathlength and the refractive index of the medium in the cavity. This behaviour is ultimately caused by interference effects of the incident light. Since a particle typically has a refractive index significantly higher than the gas, the effective optical pathlength is increased when a particle enters the cavity as the forward scattered light will have a phase shift relative to the incident light. Also the extincted light influences the signal. These two effects lead to a sudden change in the signal which can be used to count particles. The system requires a forced airflow since it is unable to measure absolute particle numbers in the cavity but sudden changes in the transmission. By applying an airflow, slow changes

in the signal relate to a change in the ambient conditions such as temperature and humidity, whereas rapid changes in the signal can be assigned to particles in the air entering and leaving the cavity.

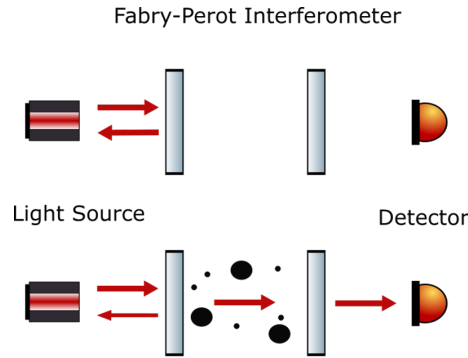


Fig. 4.6 Sketch of operational principle. Particles entering the cavity change the optical pathlength and shift the transmission characteristics of the cavity. Thus a drastic increase in signal at the detector is emerging when particles are present in the cavity.

The transmission through a cavity without particles being present is described by an Airy-Function, see [57]. The ideal operating point for this application depends on where the detector is placed. The signal without particles should be lowest possible and should show a strong enhancement when particles are present. Fig.4.7 shows the relative transmitted power as a function of the parameter  $\alpha$  which is discussed in the theory section. The minimum transmitted power is a function of the reflectivity of the mirrors used and is non-zero. The maximum transmission is independently of the mirrors reflectivity 100% which makes the reflected power zero for an ideal system. This leads to the conclusion that in order for the signal at the detector to be lowest possible without particles in the cavity, the detector should be configured to detect the reflected light of the cavity. This can be realised by introducing a beam splitter as shown in fig.4.9. [54] state that a dark field configuration of an Michelson interferometer, which shows similarities to the proposed technique, would fail due to mechanical instability. While this might be true for table-top systems, integrated and rigid devices do not suffer from this drawback. It is crucial to have a stable and rigid setup which is to a great extent immune against vibrations. Preliminary tests with table-top optical setups have shown that even modest vibrations cause a change in the pathlength and therefore in the signal. This signal can not be discriminated from a signal due to particles.

Due to the dependency of the effective path-lengths on ambient parameters, the operating point is not at a single fixed wavelength of light and a constant distance between the mirrors. Feasible solutions include:

- Differential measurement, neglecting slow changes. In this case the advantage of a low signal at the detector without particles being present cannot be exploited fully.
- Adaptive change of cavity size e.g. by means of a piezo-controller. This would add much complexity.
- Active adapting of the wavelength to the operating point. The light source must be tunable in this case.
- Use a broadband light source and a spectrometer to determine the transmission function of the cavity as a function of wavelength. This would yield additional spectral information and adds reasonable complexity.

The system can either be built in a discrete setup or could also be realised with a pigtailed light source, an etched Fabry-Perot cavity within a single-mode fiber and a detector or spectrometer. Also a chip-integrated FP cavity is an option which could be formed by utilising a waveguide on a substrate and a through silicon via.

### General Concepts and Simplified Estimations

$$I_t = I_0 \frac{1}{1 + F \sin^2(\alpha/2)} \quad (4.14)$$

$$\alpha = \frac{4\pi nd}{\lambda}$$

$I_t$  describes the transmitted intensity through the Fabry-Perot cavity. Whereas  $F$  is the finesse,  $R$  is the reflectivity of the two mirrors which is assumed to be identical,  $\lambda$  is the wavelength of light,  $\alpha$  the phase,  $n$  is the refractive index within the cavity, and  $d$  is the length of the cavity itself.

### Mathematical Description

A simplified mathematical description of the system will be provided. The discussion of the principle is introduced by showing the description of the standard Fabry Perot interferometer without particles in the cavity.



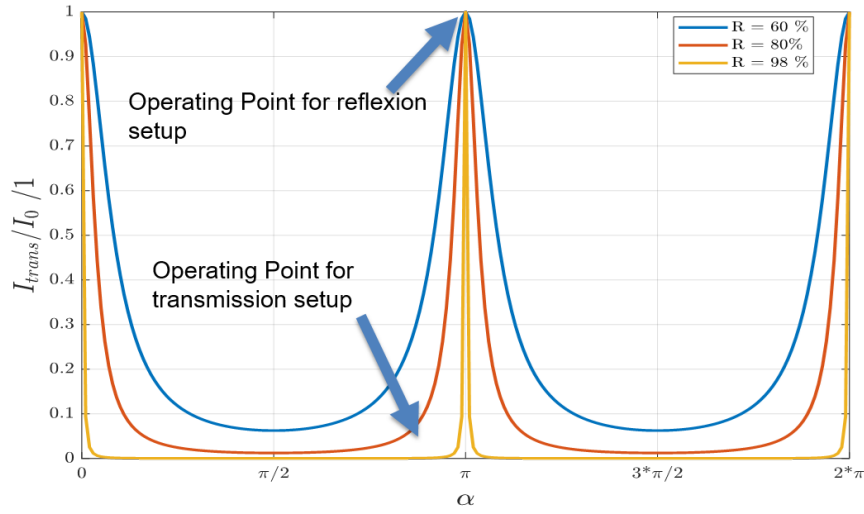


Fig. 4.7 Transmitted intensity as a function of the phase  $\alpha$  as defined in eq.4.14 for different mirror reflectivities  $R$ . The higher the reflectivity the sharper is the response and the lower is the transmitted intensity out of resonance. The ideal operating point or region is indicated with a blue arrow.

### Fabry Perot interferometer without particles

The transmitted electric field  $E_{trans}$  can be described as in eq.4.15. The overall transmitted field is the sum of all fields leaving the cavity after  $m$  round trips in the cavity. Each round trip causes a phase of  $2 \cdot \phi_{FP}$ , a number  $2 \cdot m$  reflections, and in each round trip a fraction of the electric field will leave the cavity. In order to simplify the expression we can use the geometric series and get rid of the sum. Eq.4.16 shows the reflected electric field  $E_{refl}$  which is derived in a similar fashion. The number of reflections is  $2 \cdot m + 1$ .

$$\begin{aligned}
 E_{trans} &= E_0 \cdot (1 - R) \sum_{m=1}^{\infty} R^m \cdot \exp(-2i \cdot \phi_{FP} \cdot m) \\
 &= \frac{E_0 \cdot (1 - R)}{1 - R \cdot \exp(-2i \cdot \phi_{FP})}
 \end{aligned} \tag{4.15}$$

$$\begin{aligned}
 E_{refl} &= E_0 \cdot R^{1/2} \cdot \exp(-i \cdot \pi) + E_0 \cdot (1 - R) \sum_{m=1}^{\infty} R^{m+1/2} \cdot \exp(-2i \cdot \phi_{FP} \cdot (m + 1)) \\
 &= E_0 \cdot R^{1/2} \cdot \exp(-i \cdot \pi) + \frac{E_0 \cdot (1 - R) \cdot R^{1/2} \cdot \exp(-2i \cdot \phi_{FP})}{1 - R \cdot \exp(-2i \cdot \phi_{FP})}
 \end{aligned} \tag{4.16}$$

In order to calculate intensities we use eq.4.17

$$I = E \dot{E}^* \quad (4.17)$$

For this case conservation of energy leads to eq.4.18 whereas  $I_0$  is the incident intensity,  $I_{trans}$  and  $I_{refl}$  are the transmitted and reflected intensity respectively.

$$I_0 = I_{refl} + I_{trans} \quad (4.18)$$

### Fabry Perot with Particle

Pettit and Peterson [56] argue that due to the Cittert-Zerninke theorem light scattered from small particles can be made coherent if gathered at the focal point of a lens thus the incident beam can be described as a Gaussian beam. While this coherence condition is not rigorously shown analytically for the interaction of a plane wave with the scattered wave, we assume that there is coherence. This is motivated by the fact that the well established inline holography methods (see for example [58], [59]) implicitly rely on said coherence. We use the formulae shown in sec.4.7.4 and add terms which describe the influence of particles in the cavity.

Particles cause a phase shift proportional to their size and refractive index, which can be assumed to be in first approximation proportional to their diameter [56]:

$$\phi_{particle} = \frac{\Delta n \cdot d}{\lambda} \cdot 2\pi \quad (4.19)$$

We assume that a particle extincts a fraction  $S_{ext}$  of light which can be expressed as eq.4.20.  $c_{ext}$  denotes the total extinction cross section which can be calculated by using Mie theory.  $A_{Laser}$  is the area of the laser cross section.

$$S_{ext} = \frac{c_{ext}}{A_{Laser}} \quad (4.20)$$

The optical theorem connects the total extinction cross section to the forward scattered amplitude as shown in eq.4.21

$$c_{ext} = \frac{4\pi}{k^2} \cdot Re\{S(0)\} \quad (4.21)$$

Light scattered in the solid angle  $\Omega$  centred in forward direction will interfere with the non-interacting light. This solid angle can be estimated by geometric considerations taking into account the size of the mirrors and the cavity length. The cross section for scattering in forward direction can then be calculated by eq. 4.22, cf. [42].

$$c_{phase} = \frac{\Omega}{k^2} \cdot \text{Re}\{S(0)\} \quad (4.22)$$

The forward scattered fraction of light  $S_{phase}$  will have an additional phase shift of  $\phi_{particle}$ , whereas  $S_{phase}$  is defined as in eq.4.23

$$S_{phase} = \frac{c_{phase}}{A_{Laser}} \quad (4.23)$$

Whereas  $0 \leq S_{phase} < S_{ext} \leq 1$ .

We can therefore write the transmitted E-field as stated in eq.4.24

$$\begin{aligned} E_{trans} &= E_0 \cdot (1 - R) \sum_{m=1}^{\infty} R^m \cdot \exp(-2i \cdot \phi_{FP} \cdot m) \\ &\quad \cdot ((1 - S_{ext}) + S_{phase} \cdot \exp(-i \cdot 2 \cdot \phi_{particle}))^{\frac{2 \cdot m + 1}{2}} \\ &= \frac{E_0 \cdot (1 - R) \cdot ((1 - S_{ext}) + S_{phase} \cdot \exp(-i \cdot \phi_{particle}))^{1/2}}{1 - R \cdot \exp(-2i \cdot \phi_{FP}) \cdot ((1 - S_{ext}) + S_{phase} \cdot \exp(-i \cdot 2 \cdot \phi_{particle}))} \end{aligned} \quad (4.24)$$

Whereas in every round trip there is an additional damping due to  $S_{ext}$ ,  $1 - S_{ext}$  is the fraction which does not get extinct. Analogous to the transmitted E-field, the reflected E-field can be expressed as:

$$\begin{aligned} E_{refl} &= E_0 \cdot R^{1/2} \cdot \exp(-i \cdot \pi) + E_0 \cdot (1 - R) \sum_{m=1}^{\infty} R^{m+1/2} \exp(-2i \cdot \phi_{FP} \cdot (m + 1)) \\ &\quad \cdot ((1 - S_{ext}) + S_{phase} \cdot \exp(-i \cdot 2 \cdot \phi_{particle}))^{\frac{2 \cdot m + 2}{2}} \\ &= E_0 \cdot R^{1/2} \cdot \exp(-i \cdot \pi) \\ &\quad + \frac{E_0 \cdot (1 - R) \cdot R^{1/2} \cdot \exp(-2i \cdot \phi_{particle}) \cdot ((1 - S_{ext}) + S_{phase} \cdot \exp(-i \cdot \phi_{particle}))}{1 - R \cdot \exp(-2i \cdot \phi_{FP}) \cdot ((1 - S_{ext}) + S_{phase} \cdot \exp(-i \cdot 2 \cdot \phi_{particle}))} \end{aligned} \quad (4.25)$$

Again eq.4.17 can be used to calculate intensities. Conservation of energy reads in this case as in eq.4.26 as there is an additional term  $I_{ext}$  which accounts for the extinction.

$$I_0 = I_{refl} + I_{trans} + I_{ext} \quad (4.26)$$

For the further evaluation we assume a laser wavelength of 532 nm, a particle refractive index of  $n = 1.55 + 0.55i$  and a beam size of  $(200 \mu m)^2$ . We further use Mie theory implemented in MiePlot by Philip Laven<sup>4</sup> to calculate extinction cross sections for various particle sizes. We set  $\phi_{FP} = \pi$  which leads to a total transmission of the incident intensity as indicated in fig.4.7. The reflected intensity is therefore zero when no particles are present in the cavity. Fig.4.8 shows the reflected intensity as a function of the particle diameter for the aforementioned parameters.

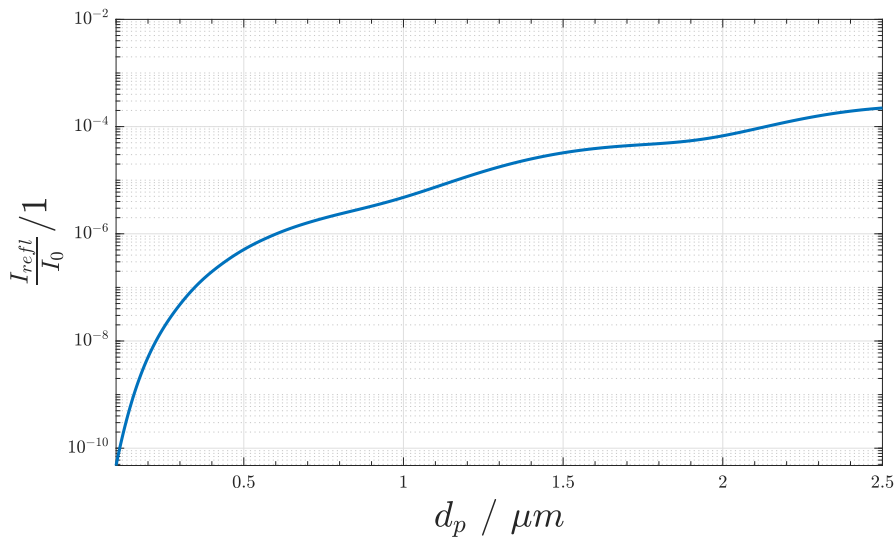


Fig. 4.8 Theoretical relative reflected intensity of an exemplary FP cavity as a function of the particle diameter, according to the proposed model. The signal shows a clear dependence on the particle size.

## Experimental

A similar system is commercially available as an optical membrane-free microphone from Xarion<sup>5</sup> [60], [61], [62] which we have utilized in the particle experiments. The microphone consists of a tunable laser with a central wavelength of 1500 nm as a light source, a discrete fabry perot cavity which is rigidly connected and integrated into a fiber and a photodetector configured to detect the reflected light using a beam splitter, see fig.4.9. An acoustic pressure wave modulates the effective path length in the cavity and therefore the reflected intensity at the detector. This signal can be used to retrieve the acoustic signal. A particle entering the cavity is in that sense similar to an acoustic wave as it also changes the effective path length in

<sup>4</sup>The Program “MiePlot v4.6” is available at [www.philiplaven.com](http://www.philiplaven.com). Last accessed 22 November 2019

<sup>5</sup><https://xarion.com/>

the cavity. Additionally the extinction of light caused by a particle also influences the signal. The reflected signal caused by a particle is in first approximation described by eq.4.25. Since the time resolution necessary to detect particles can be tuned by the flow velocity which is in general lower than the speed of sound, we conclude that the time resolution of the system is sufficient to detect particles. Also the signal change caused by a particle entering the cavity is theoretically higher than for a sound wave since the change in refractive index due to a pressure wave is low compared to the mean change in the index of refraction a micro-metric particle induces in the cavity. The effect of extinction is also negligible for sound waves. We conclude that the microphone should theoretically be suited to detect particles in the cavity. The operating point for the function as a microphone is at the quadrature of the transmission curve where the second derivative with respect to  $\alpha$  is zero. This is reasonable for a microphone since the refractive index can also get lower due to a pressure valley of an acoustic wave. Also the response is linear around this operating point. Since a particle typically has a refractive index higher than the surrounding gas, the ideal operating point for a Fabry Perot interferometer configured to detect particles is at maximum transmission as discussed above. When used as a microphone the use in reflection mode is most likely due to the fact that the device can be built in a more compact way. In the particle case the reflection is more beneficial since the signal at the detector can be near zero in the destructive mode which could potentially even lower the limit of detection with respect to size. Another difference of the microphone to the proposed setup is that the laser is in this case tune-able in order to stabilise the system at the operating point. As mentioned above this could also be done for a particle sensor although other approaches such as the use of a broadband light source and a spectrometer instead of the detector seem promising and might be simpler to implement. For a proof of principle and a feasibility study the microphone is still well suited and is used for in the further context. Due to limited information on the exact properties of the microphone such as mirror reflectivity and the design of the data acquisition and the conversion of the output voltage to light power, we are unable to compare absolute signal heights to our theoretical model but can qualitatively state the feasibility of the proposed principle for particle measurements.

### Experimental Setup

The experimental evaluations of the setup have been conducted within a master thesis [63] supervised by Univ.-Prof. Alexander Bergmann and co-supervised by the author of the present thesis. As shown in fig. 4.10, we have utilised an atomizer to generate NaCl particles. Consequently we have used a dilution bridge to change the particle concentration accordingly. A condensation particle magnifier as used in a regular condensation particle counter (CPC)

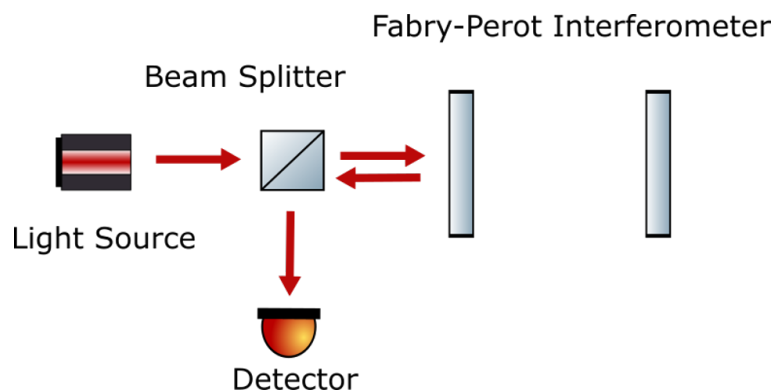


Fig. 4.9 Optical setup of Xarions optical microphone. The microphone consists roughly of a tunable laser source, a beam splitter, the fabry perot cavity as well as a detector which is configured to measure the reflected power.

but without the optics is used in order to have particles with a diameter of roughly  $5\text{ }\mu\text{m}$ . The regular counting optics are exchanged with a custom cavity holder for the microphone head, as shown in fig.4.11. As a reference a regular CPC (TSI3775) including the regular counting optics is used.

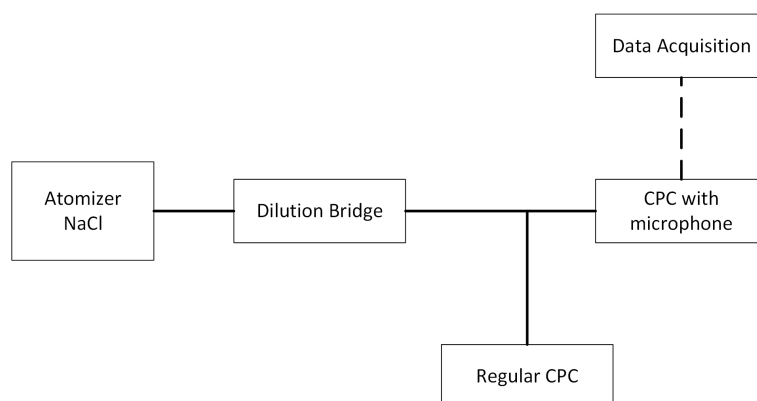


Fig. 4.10 Aerosol Setup for experiments using a regular CPC and a CPC unit with the microphone instead of the regular counting optics.

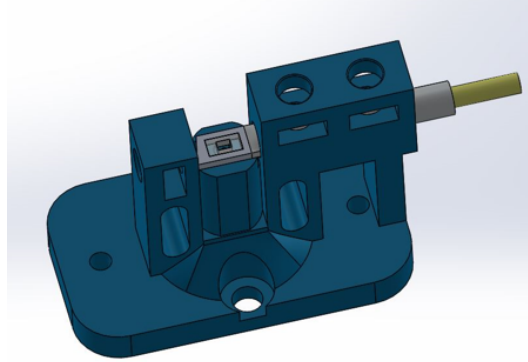


Fig. 4.11 CAD model of the cavity holder. The fiber is indicated on the right hand side which is attached to the laser and detector unit. This is used as the optical counting unit of a CPC in order to count the number of magnified particles. Image reproduced from [63]

## Results

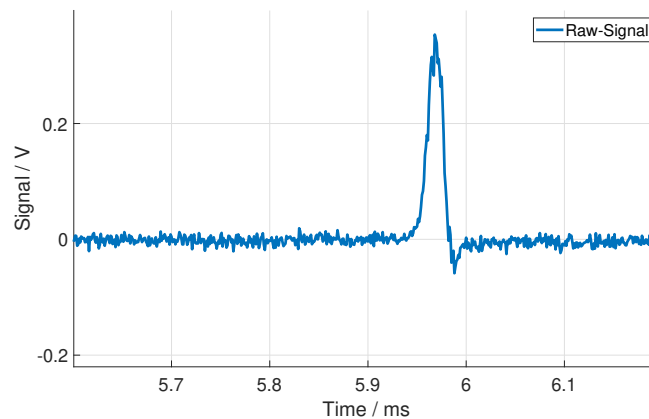


Fig. 4.12 Exemplary signal from the microphone due to a particle. The signal up to approximately 5.9 ms results from ambient noise whereas the protruding peak stems from a particle going through the cavity. The pulse width is approximately  $25 \mu s$  which fits the estimated width of  $22.5 \mu s$ , considering the beam width and the flow velocity, reasonably well. Using a HEPA filter to block particles in the flow, no such peaks have been observed. Image reproduced from [63]

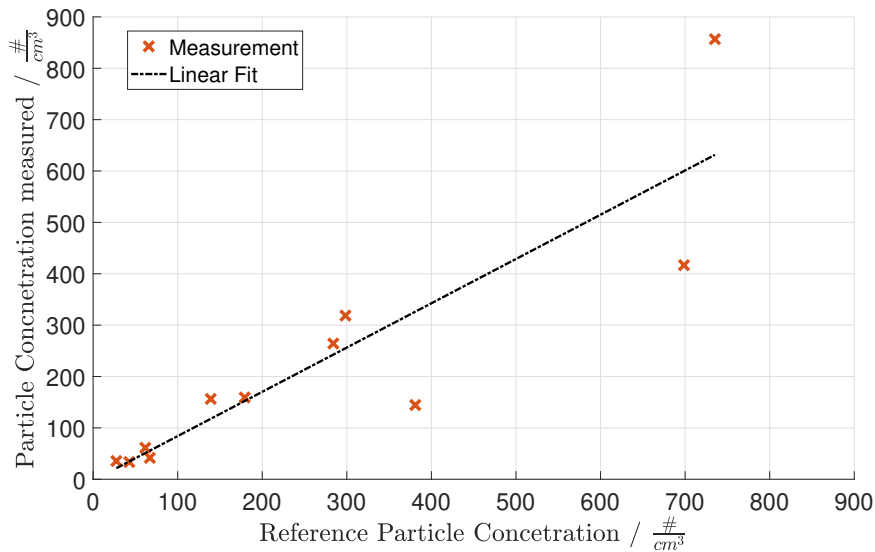


Fig. 4.13 Measured particle concentration with the microphone vs. the nominal concentration. The correlation is clearly visible. The slope of the linear fit is 0.86. Especially at high particle concentrations there is a deviation of the measurement from the reference CPC. This might be due to coincidences which lead to a lower count rate and therefore also lead to a slope lower than 1.  $R^2$  of the fit is 0.79. Image reproduced from [63]

A particle entering the optical cavity of the microphone drastically changes the transmission and consequently the signal, as shown in fig.4.12. The noise in the figure is the acoustic background in the laboratory which gives an indication that the influence of a particle is substantially greater compared to background noise.

As shown in fig.4.13 the particle count rate of the microphone and consequently the measured particle concentration fits the reference reasonably well, especially for lower concentrations. We can state that the microphone is able to count particles with a diameter of approximately  $5\ \mu\text{m}$  reasonably well.

Additionally, we have utilised monodisperse NaCl particles which we have sized using a differential mobility analyser (TSI 3082 and TSI 3081) as a classifier in order to challenge the microphone. The results have not been fully conclusive as no clear correlation between signal height and particle size did occur. We believe that this is due to an inhomogeneous intensity profile of the beam. These suspected inhomogeneities do not compromise the abilities of the setup to work as a microphone as acoustic waves expand over the whole cavity and therefore only an average signal can be seen. Particles on the other hand might be small enough to resolve these inhomogeneity. We have seen that  $400\ \text{nm}$  particles can clearly be distinguished from the background noise whereas further experiments should be done on this.

Since the microphone is not optimised for particle measurements but for its function to a



microphone, the results obtained using it for particle measurements should be seen as a proof of principle rather than a fully conclusive setup evaluation. Our findings show that the proposed system works in principle.

### **Simulation approaches**

Since the experimental results could not be compared to the analytical model, we approached the proposed effect and setup with simulation tools. Unfortunately no approach has been found which is able to describe the system reasonably well.

The complexity of the system stems from the combination of interference effects in an optical cavity and the interaction of light with particles. These effects take place simultaneously and one influences the behaviour of the other.

A ray tracing simulation is not feasible since the interaction of the light with the particle is not fully described by ray tracing simulations. A drawback arises from the fact that in ray tracing simulations the rays only interact with the geometrically specified object in the simulation and show no diffraction. This leads to a localised energy loss of the incoming light on the particle which leads to a hole in its intensity distribution. Ray tracing can model optical cavities and even the scattering at the particle can be implemented as a mean effect but said geometric effect compromises the results severely. Zemax OpticsStudio has been used for preliminary tests.

The most reliable option would be to model the setup in a full wave-optical simulation. This simulation is in principle able to model the light-particle interaction in the optical cavity fully. The computational effort is in this case immensely high as the full cavity needs to be modelled also in wave-optics. Assuming a total volume of  $27 \text{ mm}^3$  to be modelled, a wavelength  $\lambda$  of 532 nm and a cell length of  $\lambda/10$ , the total number of cells necessary is  $1.8 \cdot 10^{14}$ . Within the thesis no solution to this has been found. Further research should be done on this.

### **Concept for the measurement of the refractive index of single particles**

For the concepts described above, a mean refractive index applicable to all particles has to be assumed. The light scattering technique suffers from the same drawback, which is not critical for the assessment of PM2.5. Especially for the investigation of the climate force potential of aerosols, the measurement of the refractive index of single particles is crucial and remains a challenge. We propose a measurement scheme which might be able to measure the refractive index of single particles. The setup is shown in fig.4.14. Similar to the aerodynamic particle sizer [64] (APS) from TSI Inc., a nozzle is used to accelerate particles. The final velocity of

the particle depends on its aerodynamic diameter. By a measurement of the time a particle takes to travel a fixed distance, the velocity can be calculated. The velocity can then be used to estimate the aerodynamic diameter of the particle. In the APS this velocity measurement is realised by two light sheets and two photodetectors. We propose a similar setup with at least one interferometric particle detection unit as described above. The velocity of the particle and the aerodynamic particle diameter can again be estimated by using the time difference between the two consecutive measurements. The signal at the interferometric measurement unit can then be used to estimate the refractive index of the particle based on the considerations shown before. The proposed system has not been evaluated experimentally. Due to the high potential of the measurement, the proposed setup is incorporated in the patent application shown in the appendix A.3.

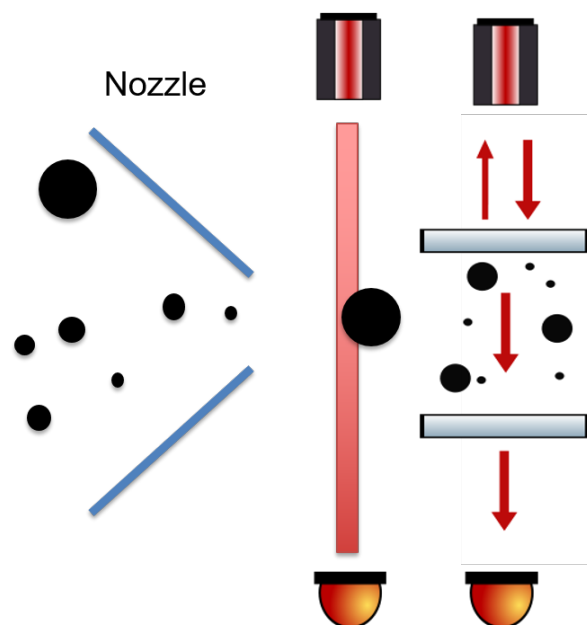


Fig. 4.14 Proposed setup for the measurement of the refractive index of single particles.

## Conclusions

We propose a setup for optical particle detection and sizing utilising an interferometric effect exploited by a Fabry-Perot interferometer. By applying a flow through the cavity and operating the cavity in a dark-field configuration, the change in the transmitted as well as the reflected signal is theoretically proportional to the particle size and via the extinction cross section and Mie theory, proportional to the index of refraction. The setup shows potential for miniaturisation as it can be realised as a waveguide using established silicon-photonics

processes. The setup might be an alternative for future miniaturised and low-cost sensors. We have shown a proof of principle by utilising an optical microphone which is working on a similar basis as the proposed setup. We have shown that the signal correlates to particles and the system is able to count the number of particles with a diameter of  $5\text{ }\mu\text{m}$  drawn through the cavity with reasonable accuracy. Due to limited information on the exact design of the microphone we were unable to quantitatively compare the results to the mathematical model. The setup has not been accessible for numerical simulations up to now.

We conclude that the proposed setup is in principle feasible. More research is to be done on the sizing capabilities of the proposed setup. Further optimisation with respect to particles should be done.

Due to the promising first experimental results and the novelty of the proposed setup, the ideas have been filed as a patent application, see A.3. The patent application incorporates in addition to the proposed measurement scheme, potential realisations using waveguides, a setup including evanescent waves on waveguides, and an additional setup for the measurement of the refractive index of single particles as described above based on the interferometric setup.

## 4.8 Discussion and choice of target sensor effect

The review of relevant sensor effects and principles for particle measurements with a focus on the potential towards miniaturisation, has revealed that only a few principles are relevant for the cause.

The aethalometer and light scattering have been identified as the most promising principles. All other principles either show drastic drawbacks with respect to the requirements defined in sec.4.1, or they are scientifically or technically not advanced enough to be incorporated in a highly-integrated design.

After evaluation of potential risks and benefits, the main focus of the project is put on the light scattering principle. One of the main reasons is that there is an accepted correlation of the measurement to PM<sub>2.5</sub>. The aethalometer shows a vast potential but is not in the focus of the realisation at this point.

The following chapter 5 will deal with the overall sensor system with an incorporated light scattering sensor part. It should be emphasised that the overall sensor system can in principle be used with other sensor effects as light scattering, since main parts of the system such as the package and a pump are necessary for a particle sensor in general.



# Chapter 5

## Concept and Realisation

### 5.1 Overview of targeted specifications and constraints

The reasoning from chapters 3 and 4 as well as currently available packaging and assembly technologies, form the framework for the design of the sensor.

Targeted specifications of the overall sensor system are shown in tab. 5.1. As a sensor effect the classical light scattering technique is chosen. Since light scattering devices can not detect arbitrarily small particles but have a limit of detection of typically 300 nm, the minimum detectable particle size is targeted to be at least 300 nm. As the overall goal is to have a sensor small enough to be incorporated in mobile devices, the severe size constraints on the sensor are of significant importance. The targeted maximum size is  $12 \times 10 \times 3 \text{ mm}^3$ . Especially the height of 3 mm is considered to be a crucial dimension.

Due to the estimations of the inherent uncertainty due to insufficient small sample sizes in chapter 3, there must be an active flow element incorporated, such as a pump or a fan. The targeted flow rate is  $3 \text{ mL min}^{-1}$ .

Obligatory functional parts of the integrated particle sensor include an aerosol inlet, outlet and a general flow path for the aerosol. An impactor as a protection from large objects must be installed to protect the optical sensing element from damage. A light scattering based sensing element must be realised and an active flow element such as a pump must be incorporated in the system. Additionally, electronic components have to be fit into the design.

For a proof of principle, the electronics as well as the pump will be attached externally. The design of the sensor must be compatible with common packaging and assembly technologies. The final package of the sensor is to be injection moulded which puts constraints on the system design. The minimum feature size of standard moulded parts as used from ams

Table 5.1 Targeted specifications of the sensor system

Dimension	Target
Metric	PM2.5 / $\mu\text{g m}^{-3}$
Sensor Effect	Light scattering
Particle size	$\leq 300 \text{ nm} - 2.5 \mu\text{m}$
Measurement time per single measurement	60 s - 120 s
Flow rate	$3 \text{ mL min}^{-1}$
Height	$\leq 3 \text{ mm}$
Lateral dimensions	$\leq 12 \text{ mm} \cdot 10 \text{ mm}$

AG is approximately  $300 \mu\text{m}$ . A complication arises from the fact that injection moulding cannot be used for prototyping due to the high cost of the tools. The package of the prototype is a milled part consisting of aluminium, whereas the features used must also be mouldable. Innerbichler GmbH<sup>1</sup>, has produced the milled part.

Components which require electrical contact, should ideally be mounted on the same substrate in one plane to minimise assembly efforts. The system complexity can a priori be considered relatively high due to the high number and complexity of the functional parts and the severe size constraints. It is all the more important to make the design as complex as necessary but as simple as possible.

The concepts applied in the following sections have been filed as a patent application [65] by ams AG and TU Graz. The author of the present thesis is not part of the inventors of this application. Still the author contributed substantially to the implementation in close cooperation with ams AG and SAL GmbH.

## 5.2 Design concept and overview

Resulting from the specification and constraints outlined in section 5.1 the design principle is as follows, see fig.5.1

<sup>1</sup><https://www.innerbichler.co.at>

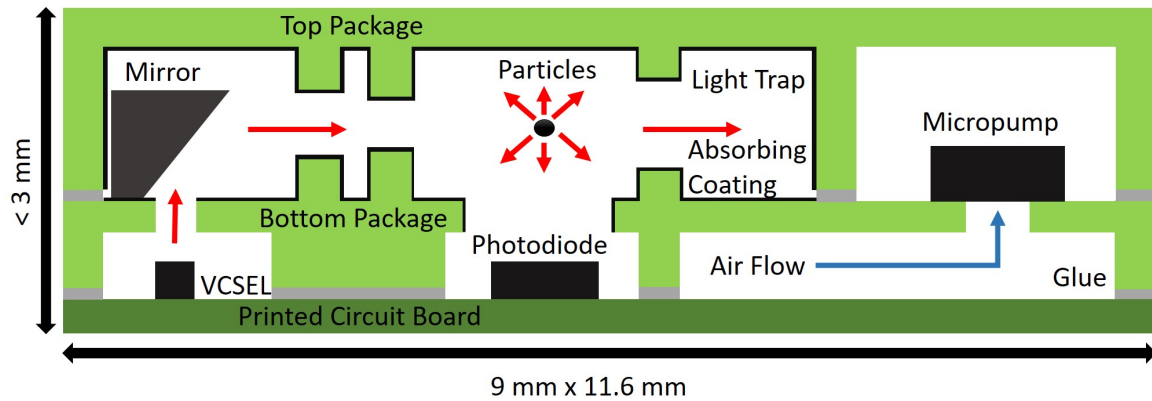


Fig. 5.1 Concept of the sensor design

Due to the size constraints on the sensor system, the package must not only provide basic functionalities like mechanical stability and protection from external influences, but has to provide integral properties of the sensor system. In the context of functional packaging, the package provides the flow path for the aerosol including the impactor, defines the apertures for the optical sensor element, provides a functional framework for the integrated pump and the overall system.

The package consists of three main parts, namely a common PCB as a substrate, a bottom package, and a top package. The light source as well as the photodiode are mounted at the PCB on top of which the bottom package will be assembled. Inlet, outlet as well as the impactor and parts of the flow path are formed by the PCB and the bottom part. On the bottom package are a mirror as well as the incorporated micro-pump mounted.

At the end of the assembly steps, the top package is mounted on the bottom package. Beam guiding apertures as well as parts of the flow path are formed by the bottom part and the top part. The aerosol enters the light-particle interaction volume perpendicular to the sketch shown in fig.5.1.

A more detailed plan of the PM sensor system is shown in fig.5.2. The inlet is located in the PCB after which the impactor is formed by the bottom part and the PCB, details see sec.5.4. The aerosol is then guided towards the optical sensor where a funnel-like structure is formed to bring the particles to the spot where the light-particle interaction takes place.

A second funnel-like structure is formed to guide the particles out of the sensing element towards the pump. Before the pump a filter is installed to capture the particles and avoid a damaging of the pump. The air is then pushed out of the sensor system via the outlet which is again located in the PCB. Necessary electronics are placed onto the PCB where a recess is provided in the bottom part.

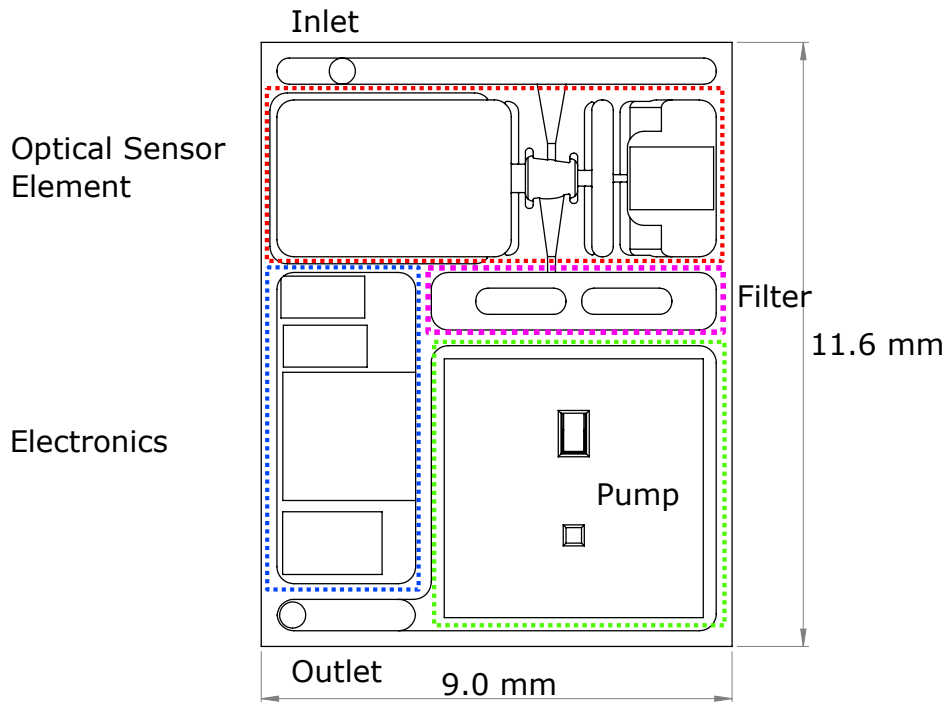


Fig. 5.2 Bottom part of the PM sensor system

### 5.3 Inlet and Outlet

Both inlet and outlet are situated in the PCB in form of a via on the non-sensor side of the PCB. The PCB features a pad around the via where tubing can be soldered on for fluidic connection to reference equipment.

### 5.4 Particle Size Separation: Impactor

Depending on the sensor effect in use, it might be necessary to adjust the aerosol to the metric, which is targeted. For example gravimetric methods can not differentiate in particle size concerning single particles. Therefore, particles with a diameter of greater than  $2.5\ \mu\text{m}$  must be removed from the aerosol in order to estimate PM<sub>2.5</sub>. Since the light scattering technique estimates the diameter of the particles, this aspect is less critical. Particles irrelevant for the metric can simply be ignored when PM<sub>2.5</sub> estimated. Another more important aspect for the present sensor system is that especially large particles may damage the sensor severely if deposited on critical sites such as optical components. It is therefore beneficial to prevent large particles which are irrelevant for PM<sub>2.5</sub> from entering the optical sensor.

In principle there are a plurality of techniques that can be utilised to separate particles accord-



ing to their size. The separation mechanisms include size dependent filters, virtual impactors, impactor, thermophoretic deposition as well as charge based deposition, in detail described in [15]. Due to the limited fluid flow the virtual impactor cannot be realised. Thermophoretic and charge based effects increase overall complexity and power consumption and are therefore unsuited.

The minimal dimension of  $300\text{ }\mu\text{m}$  of the package due to the prototyping as well as the overall packaging technology, led to an impactor design which is shown in fig.5.3.

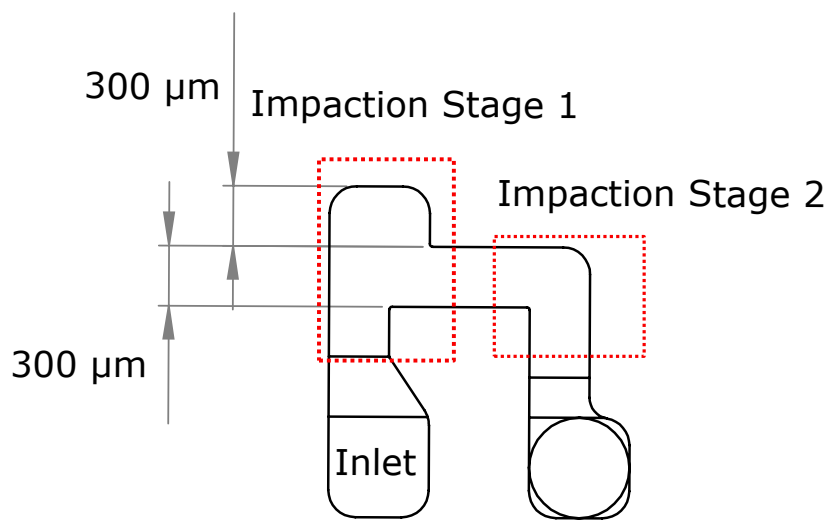


Fig. 5.3 Design of the two-stage impactor. Particles enter sensor through the inlet perpendicular to the sketch and are then transported in upward direction. Impaction stage 1 features a pocket which increases the potential loading volume before clogging and in which large objects get trapped. Impaction stage 2 does not feature the pocket in order to have a smaller cutoff with respect to particle diameter. The impactor prevents the sensor from large objects and particles but does not affect the particles within PM<sub>2.5</sub>.

The main idea is to guide the aerosol around a sharp angle. Especially large particles can not follow the streamlines sufficiently and will therefore impact in the wall. The impactor consists of two stages, the first impaction stage after the inlet has an additional pocket after the sharp turn in order to trap potential large objects and to avoid a clogging of the sensor due to overloading of the impactor. The second impaction stage does not feature such a pocket leading to a smaller cutoff point with respect to particle diameter. The cascade of the impaction stages leads to a satisfying size separation and a sufficient protection of the more delicate optical sensor element. The impactor has been simulated with Comsol Multiphysics 5.2 using computational fluid dynamics and particle tracing. The first impaction stage has a 50% transmission probability at particle diameters of  $11\text{ }\mu\text{m}$  and no significant losses below

6  $\mu\text{m}$ , whereas the second impaction stage has 50% transmission probability at a particle diameter of 6  $\mu\text{m}$  and no significant losses below 5  $\mu\text{m}$ . The overall probability for particles with diameters above 10  $\mu\text{m}$  is below 1% and can be neglected. Particles relevant for the targeted metric are not affected by the impactor, the measurement is not distorted. After the impactor, particles are guided towards the optical sensing element.

## 5.5 Optical Sensing Element

A cut of the optical sensing element is shown in fig.5.4. For assembly reasons it is beneficial to have all elements which need to be electrically bonded to be placed at the same surface. Therefore the light source and the photodiode are mounted on the same PCB as shown in fig. 5.1.

A VCSEL is used as a light source. The designated VCSEL has a wavelength of 808 nm with a divergence of below  $2.5^\circ$  in CW mode with an optical output power of 1mW - 15 mW. The photodiode is designed and processed in-house at ams AG. It features a  $1 \times 1 \text{ mm}^2$  active area and a time resolution of 29.6  $\mu\text{s}$ . The resolution of the photodiode is 0.56 pA which corresponds to a power of 1.6 pW. The maximum power is approximately 18 nW. The photodiode is reverse biased and features a two stage analog to digital converter.

The part of the sensor system is placed on top of the PCB. In order to realise  $90^\circ$  light scattering, the light is redirected by a mirror towards the particle inlet above the photodiode. For assembly reasons the mirror is shaped as a prism as indicated in fig.5.1. This shape allows a handling with regular pick and place tools and supports the alignment of the mirror. The emitted light beam is shaped by three apertures leading to a sufficiently small and homogeneous light intensity distribution over the light-particle interaction volume. The first aperture is formed by a circular hole in the bottom part, two further apertures are formed by both the bottom and the top part of the package. The scattered light is then detected by the photodiode which is configured to detect light with a central angle of  $90^\circ$  with respect to the incoming beam. The incident light is attenuated in the following beam trap. Since the available space is insufficient for regular approaches for the light trap, top part and bottom part are coated with Magic Black<sup>2</sup> by ACM Coatings GmbH. The hemispherical reflectivity at 808 nm is below 1% leading to a stray light suppression ratio of  $2 \cdot 10^7$  according to the simulations. Overall the system is designed to detect particles with a diameter of at least 300 nm. The relevant geometry for the optical sensing element has been optimised by CTR (now SAL) using Zemax OpticStudio. A number of minor features has been implemented in

<sup>2</sup><https://www.acm-coatings.de/produkt/magic-black/>. Last accessed 10.06.2020

the design to minimise stray light, cross-talk of the VCSEL to the photodiode via the PCB, as well as ambient light. The particle inlet into the optical sensing element has been optimised with respect to a minimum of deposited particles on critical elements such as the photodiode and to avoid particle circulation in the sensing element. Flow simulation and optimisations have been done by CTR (now SAL) using Ansys.

As the optical sensor element is especially prone to malfunction due to deposited particles on critical surfaces, a number of fouling experiments has been conducted with a prototype consisting of an uncoated bottom and top part and the PCB. The prototype has been challenged with ambient air at a concentration of  $6 \mu\text{g m}^{-3}$  for 7 days continuously. No contamination of the optical sensor element has been observed. Consequently the sensor has been challenged with soot particles from a Jing Ltd. miniCast Series6200 with a total mass loading of  $100 \mu\text{g}$  which is significantly more than can be expected during the lifetime of the sensor. Again no significant particle deposition was found, especially in the sensor element. The sensor element can be considered robust against fouling due to particle contamination.

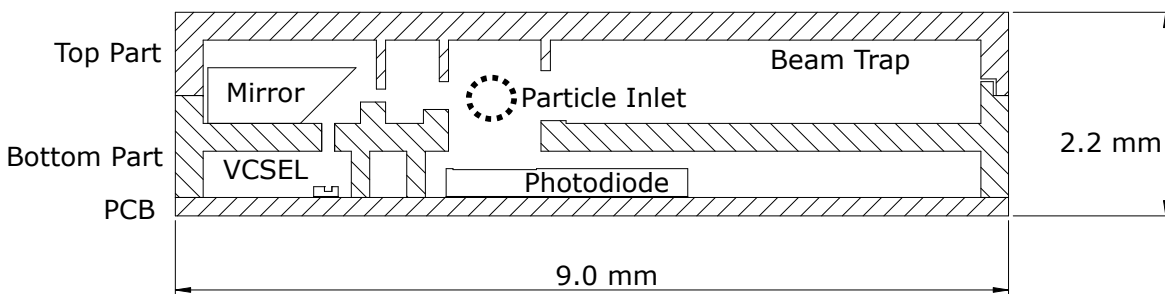


Fig. 5.4 Cross section of the optical sensing element. Particles enter the sensing element perpendicular to the cross section.

## 5.6 Filter

In order to prevent the pump from particle contamination as well as to provide a pressure drop in between the pump and the sensing element, a filter is installed. The filter features a size of  $3 \text{ mm}^2$ . Since humidity in the air might clog the filter, a hydrophobic filter material is to be used. A supported PTFE membrane filter with pore sizes of  $2 \mu\text{m}$  is used ((Pall Life Sciences, Zefluor,  $2 \mu\text{m}$ )). The pressure drop over the filter at the targeted flow rate of  $3 \text{ mL min}^{-1}$  is approximately 250 Pa.

Novick et al. [66] have shown an experimental investigation of the increase in pressure drop due to particle mass loading. The results show that significant increases of the pressure drop over the filter are not to be expected for the proposed filter geometry and flow rate. Assuming a total mass of  $25 \mu\text{g}$  which equals the sampling of  $1 \text{ m}^3$  of air at the EU limit of PM<sub>2.5</sub>

of  $25 \mu\text{g m}^{-3}$ , the mass loading of the filter is  $8 \text{ g m}^{-3}$ . The experimental results stated by Novick et al. [66] indicate an increase in the pressure drop over the filter of roughly 500 Pa, which can be handled by pump. Note that the filter used in the experiments is a fiber filter which might have a higher mass loading capacity within the filter volume compared to a membrane filter.

## 5.7 Micro Pump

An active flow element has to be incorporated into the sensor system for reliable measurements. Especially in this case the severe space limitations exclude most available solutions. A very promising approach has been shown by Fraunhofer EMFT. Richter et al. [67] show a MEMS silicon membrane micropump<sup>3</sup> with dimensions of only  $5 \times 5 \times 0.6 \text{ mm}^3$  with a flow rate of  $0.6 \text{ mL min}^{-1}$ . The pump features a piezo membrane and two silicon valves. The piezo is typically actuated by a rectangular or smoothed rectangular signal with a difference in high to low level of 100 V with a frequency of 1 kHz. The Richter group from Fraunhofer EMFT working on this pump has agreed to redesign the pump for application in the PM sensor system. The redesign led to a flow rate of approximately  $3 \text{ mL min}^{-1}$  which fits the target specifications of the overall sensor system. A set of 27 pump prototypes has been tested within the thesis. The maximum back pressure is 13 kPa whereas the maximum suction pressure is  $-12 \text{ kPa}$ . The mean power during operation is approximately 20 mW. The pumps have been tested in long term operation (24h) and under constant temperatures between  $-20^\circ\text{C}$  and  $80^\circ\text{C}$  in short term operation. The pumps were then stressed with 1000 temperature cycles in the same temperature range and were then stored at  $85^\circ\text{C}$  and 85% humidity for 1000 h. The pumps have shown no significant degradation during and after the tests and are qualified for use in the sensor system.

Since the pump inherently generates a pulsating flow due to its principle of operation, a smoothing of the flow is necessary in order to enable stable operation of the optical sensing element. This smoothing is achieved by maximising the buffer volume in between the pump and the filter and by tuning the pressure drop over the filter. The recess intended for the electronics is fluidically connected to the pump inlet, thus maximising the buffer volume. The pressure drop over the filter is designed to be 250 Pa leading to a flow in the optical sensing element which can be considered constant according to computational fluid dynamics simulations.

---

<sup>3</sup>[www.emft.fraunhofer.de/content/dam/emft/en/documents/Infosheets/21\\_E\\_Smartpump\\_public.pdf](http://www.emft.fraunhofer.de/content/dam/emft/en/documents/Infosheets/21_E_Smartpump_public.pdf). Last accessed 07.04.2020.

## 5.8 Electronics

The overall sensor must provide a driver for the VCSEL which is driven in CW mode with a constant current of 10 mA-15 mA. In addition a driver for the pump must be incorporated. The pump is driven with an rectangular or smoothed rectangular signal with a difference in voltage of high to low level of 100 V. As the sensor should be supplied with either 3.3 V or 5 V, a charge pump will be incorporated to provide the necessary voltage. Additionally the readout for the photodiode as well as a data processing unit is necessary.

According to specialists at ams AG, these components can be incorporated in the overall system with reasonable effort. For the proof of principle, validation and the evaluation of the design, these components are provided externally.

## 5.9 Assembly

The assembly of the sensor is a crucial step towards the functional prototype. A potential misalignment of elements within the optical sensing element leads to an increased level of stray light compromising the sensors sizing capability and overall performance. In addition, with the exception of the inlet and the outlet, the sensor must necessarily be airtight in order to ensure reliable operation. The requirements for the adhesive bonding are therefore both strict with respect to the thickness of the adhesive and to the quality of the bonds in terms of airtightness. Acceptable alignment tolerances are on the order of 10  $\mu\text{m}$  typically whereas especially the alignment of the VCSEL to the circular aperture in the bottom part is to be considered critical. The assembly is done at SAL in Villach, Austria mainly by Jaka Pribošek and is described in detail by Pribošek et al. [68], whereas the author of the present thesis is among the co-authors.

At this point the assembly is not yet fully under control which manifests in an increased level of stray light compared to the simulations, see sec.6.3. The assembly of the top part is done without adhesive as no solution for the application of the adhesive at the relevant interface has been found yet. Preliminary experiments showed that the milled bottom and top part do not show internal leakages when properly aligned. Therefore, the sensor is sealed from the outside once the top part is in position using silicon glue.

The improvement of the assembly process is subject to ongoing research activity.



# Chapter 6

## Experimental Evaluation

The prototype has been tested in the aerosol reference laboratory for basic functionality and has been challenged with test aerosols to validate the design especially in terms of sizing capability and counting efficiency. In addition, the prototype has been tested against PM<sub>2.5</sub> reference equipment using ambient aerosol. The present generation of the prototypes is supplied with an external pump and a mass flow controller (MFC) to provide the target flow rate of  $3 \text{ mL min}^{-1}$  as well as an external driver for the VCSEL and an additional external PCB for the readout of the photodiode signal. This external equipment will be included in future generations of prototypes which is beyond the scope of the present thesis. The data evaluation has been done using Matlab.

Before the prototype can be challenged with particles, the system is checked for basic functionality. This includes fluidic tests to exclude leakages, and the evaluation of the background level of stray light without particles being present.

### 6.1 Fluidic tests

The prototype has been tested for functionality in terms of airtightness which was part of a feedback loop with the assembly, leading to a functional assembly process. In particular the joints between the PCB and bottom part are prone to leakage which severely compromises the sensors functionality. The setup is shown in fig.6.1. An external pump is used to provide a flow. A MFC (mass flow controller, Vögtlin Instruments AG, GSC-A9TA-BB21) is used to provide a defined flow rate of  $3 \text{ mL min}^{-1}$  through the sensor. A high efficiency particle filter (HEPA filter) is used to filter any particles in order to prevent the MFC from damage. A MFM (mass flow meter, Vögtlin Instruments AG, GSM-A9TA-BB00) used to measure the flow into the sensor prototype which should be equal to the flow through the outlet if the

prototype is sufficiently airtight. Again a HEPA filter is used to protect the MFM. Ambient air is used for these tests.

Preliminary assembly tests have shown major leakages which manifested in a flow rate through the inlet of below 20% of the targeted flow defined through the outlet of the prototype. The leakage has been identified to be caused by the joint of the PCB and the bottom part of the package. Minor adaptations in the design of the PCB and an improved assembly process led to a sufficiently airtight system and a flow rate of >98% at the inlet relative to the target flow defined at the output. This behaviour is sufficient for the final sensor system.

Pressure decay tests have not been done in order to prevent the small number of functional samples from potential damage.

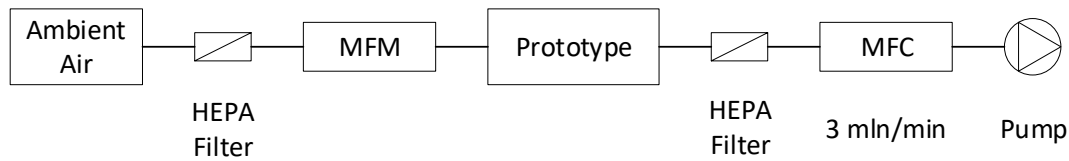


Fig. 6.1 Setup for the fluidic tests of the prototype.

## 6.2 Stray light

The VCSEL is driven by a 15 mA constant current provided by a laser driver (Thorlabs ITC4001). This leads to an optical output power of 15 mW and a power of 1.5 mW in the optical interaction volume according to simulations. The mean level of stray light at the photodiode in this configuration is approximately 7.8 nA which is 44 % of the saturation current. An exemplary signal is shown in fig.6.4. The standard deviation of the signal is 8.7 pA in this configuration and seems to be mainly caused by the absolute level of stray light rather than by external influences. The stray light is a factor 65 higher than anticipated and therefore the noise on the signal is a factor of 8 higher due to properties of the photodiode. The simulated signal for 300 nm PSL particles is approximately 13 pA. As the signal increase is in this case within a 2- $\sigma$  range with respect to the background, the prototype is unable to detect 300 nm PSL particles without mayor misclassifications of the noise. The lower limit of detection with respect to particle diameter is found experimentally.

The level of stray light can be caused by the glue which was not modelled by the simulations. An other reason might be a possible deviation in the reflectivity of the black coating with respect to the specification. Also alignment issues might cause the increased stray light. This



level of stray light might be decreased by further improvements of the assembly. A less reflective glue might suppress the level of stray light.

## 6.3 Validation

The validation of the sensor system with respect to aerosol measurements consists of two mayor steps.

In a first step the prototype is challenged with reference aerosol, namely monodisperse PSL (polystyrene latex) particles (Polysciences, Inc., Polybead standard monodisperse polystyrene microspheres), in order to evaluate the response of the sensor to particles of various sizes. Reference equipment is used in order to assure a monodisperse particle distribution and to evaluate the counting efficiency of the prototype relative to the reference.

Having evaluated the size response and the counting efficiency of the sensor, an estimate for PM<sub>2.5</sub> for arbitrary particle size distributions can be found by assuming spherical particles with equal mass density and a constant index of refraction.

In the second step the prototype is challenged with ambient air in parallel to reference equipment for PM<sub>2.5</sub>. The estimator on the basis of the information found during the experiments utilising PSL spheres, is used to estimate ambient PM<sub>2.5</sub> values. The results obtained with the prototype are compared to the reference equipment and the correlation statistics are evaluated.

### 6.3.1 Reference Aerosol

Monodisperse polystyrene latex spheres are used as reference particles in order to evaluate the response of the sensor to various particle diameters. Particle diameters of 300 nm, 500 nm, 750 nm, 1  $\mu$ m, 2  $\mu$ m and 3  $\mu$ m are used sequentially. For particle diameters up to 750 nm the setup as shown in fig.6.2 is used where a differential mobility analyser (DMA) is used as a classifier and a condensation particle counter (CPC) is used as a reference order to find the counting efficiency of the prototype. Particles larger than 750 nm can not be classified with the DMA. For those particles a setup as shown in fig.6.3 is used where an aerodynamic particle sizer (TSI APS3321) is used as a reference.

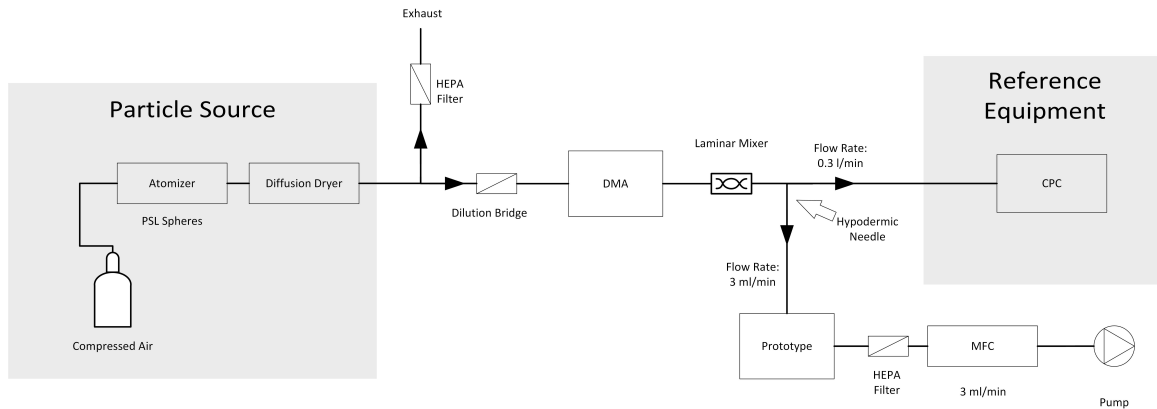


Fig. 6.2 Validation setup for the prototype for particle diameters up to 750 nm

As shown in Fig.6.2, the aerosol setup consists of a particle source which is a atomizer (Topas ATM 221) used to generate a monodisperse PSL particle distribution. The PSL particles (Polybead Microspheres Polysciences Inc.) are in a ultra-pure water solution and are dispersed by high pressure through a nozzle. A diffusion dryer (Topas DDU 570) is used to get rid of the water vapor. A dilution bridge is used to tune the concentration of particles. We utilise a DMA (TSI 3082 and TSI 3081) as a classifier in order to make sure that no particles other than the PSL spheres can distort the measurement. The DMA separates the pre-charged particles based on their electrical mobility by applying an electrical field. A laminar mixer is utilised to guarantee a homogeneous concentration of particles over the cross-section of the tube [69]. A CPC (TSI3775) is used as a reference in order to ensure that particles are present and to be able to compare the measured concentrations of the prototype to the reference. A medical-grade hypodermic needle is used to take the sample for the prototype. The inner diameter of the hypodermic needle is chosen such as to ensure iso-kinetic sampling [15] in order not to distort the sample. Additionally, the hypodermic needle is electrically conductive to minimise particle losses. To provide the correct flow rate, a mass flow controller is used at the outlet of the prototype. The mass flow controller is protected by a high-efficiency-particulate-air (HEPA) filter and is followed by a suction pump.

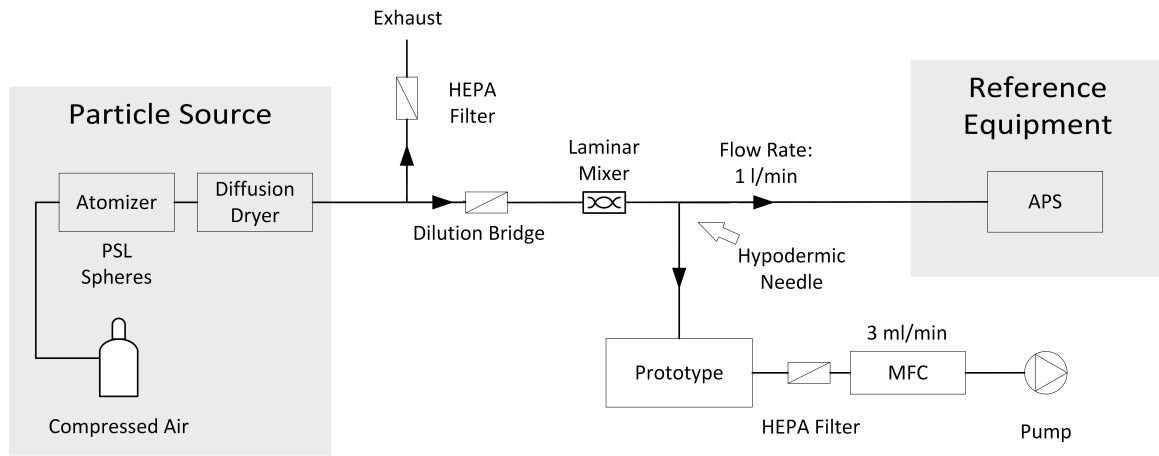


Fig. 6.3 Validation setup for the prototype for particle diameters greater than 750 nm

The setup for reference PSL particles greater than 750 nm in diameter is shown in fig.6.3. The setup is similar to the setup for particles up to 750 nm in diameter as shown in fig.6.2. Since the DMA can not be used for particles greater than 750 nm in diameter, the aerosol can not be classified. Potentially particles different from the PSL spheres may be present. Previous experiments have shown that a mode around 100 nm is present in the aerosol generated by the atomizer. This mode is most likely caused by residuals in the ultra-pure water in which the PSL spheres are suspended. Those particles do not influence the behaviour of the prototype but are detected by the CPC. The CPC can not be used in this setup due to the previous reasoning. Instead of the CPC, an aerodynamic particle sizer (APS, TSI APS3321) is used which detects particles in a size range of 370 nm to 20  $\mu\text{m}$ .

## Results

An exemplary signal is shown in fig.6.4. The sharp peaks in the signal are caused by 1  $\mu\text{m}$  PSL spheres passing the optical interaction volume and scattering light towards the photodiode. The width of the peaks is approximately 150  $\mu\text{s}$  which equals 5 to 6 data points. The variation in the signal height is caused by the variation in the particle positions and trajectories through the interaction volume as stated by Pribošek and Röhrer [70].

The number of peaks in the signal is proportional to the number of particles passing the optical interaction volume. The signal height relative to the stray light level and the integral over the single peaks is proportional to the particle size according to Mie theory.

Fig.6.5 shows a histogram of the size responses in terms of relative peak height of the particle sizes used in the experiments. Fig.6.6 shows a box-plot of the same data. The histogram is normalized and outliers greater than 2000 pA are not shown. There is clearly a dependence

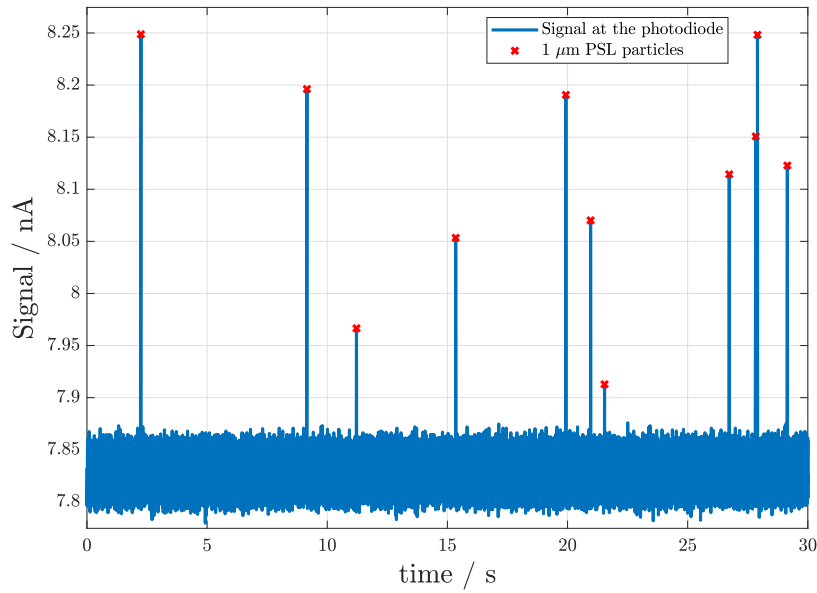


Fig. 6.4 Exemplary signal at the photodiode. The sharp peaks are due to 1  $\mu\text{m}$  particles passing through the optical interaction volume of the sensor.

of the signal height on the particle size. The populations of the investigated particle sizes can clearly be discriminated from another, although there is an overlap in terms of signal height, especially for 500 nm and 750 nm particles. Note that for 3  $\mu\text{m}$  signal below 840 pA have been excluded due to the occurrence of a particle mode centered at 1  $\mu\text{m}$  indicated by the APS. Signals below 840 pA clearly correlate to this mode for the experiments utilising 3  $\mu\text{m}$  PSL spheres. Outliers in terms of signal below 840 pA which would potentially result from 3  $\mu\text{m}$  can therefore not be seen in the signal directly.

This result marks a crucial milestone towards the final system and shows the great potential of the project.

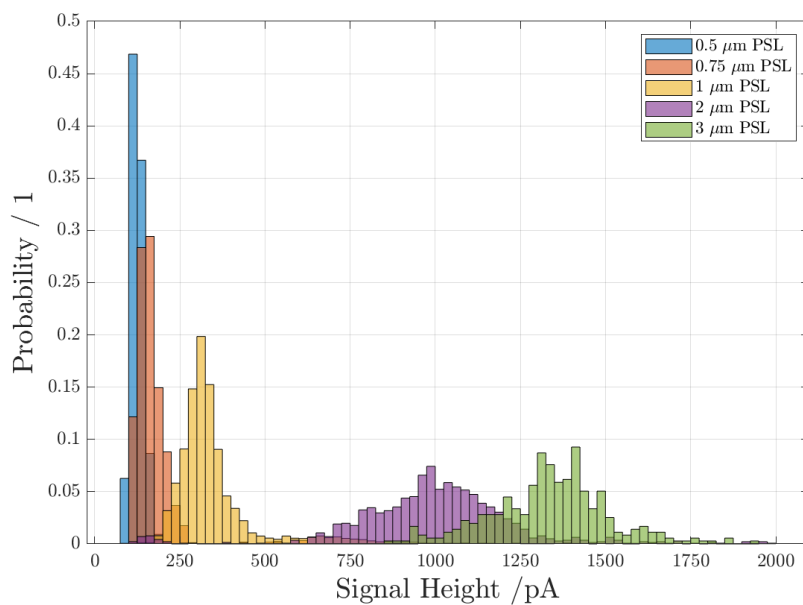


Fig. 6.5 The histogram shows the signal height relative to the stray light level for various particle sizes. Although the responses overlap partly, all populations can be discriminated.

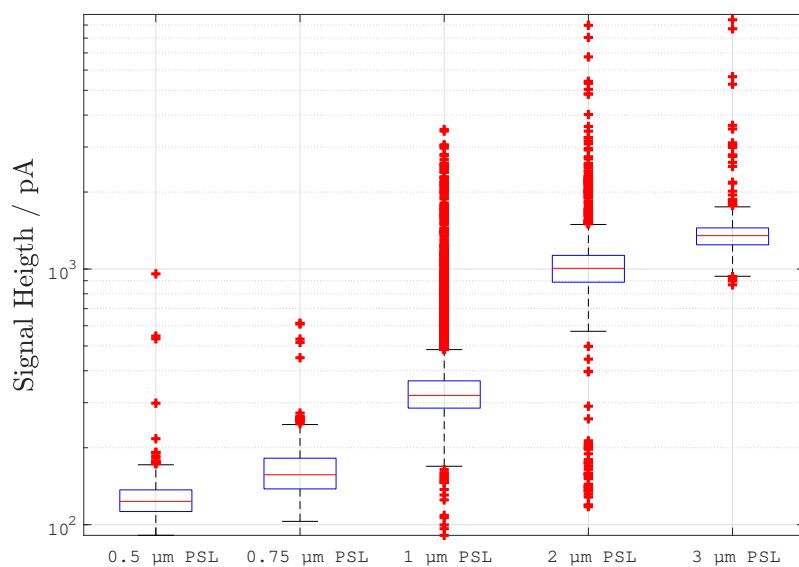


Fig. 6.6 The boxplot shows the signal height relative to the stray light level for various particle sizes. The responses can clearly be distinguished.

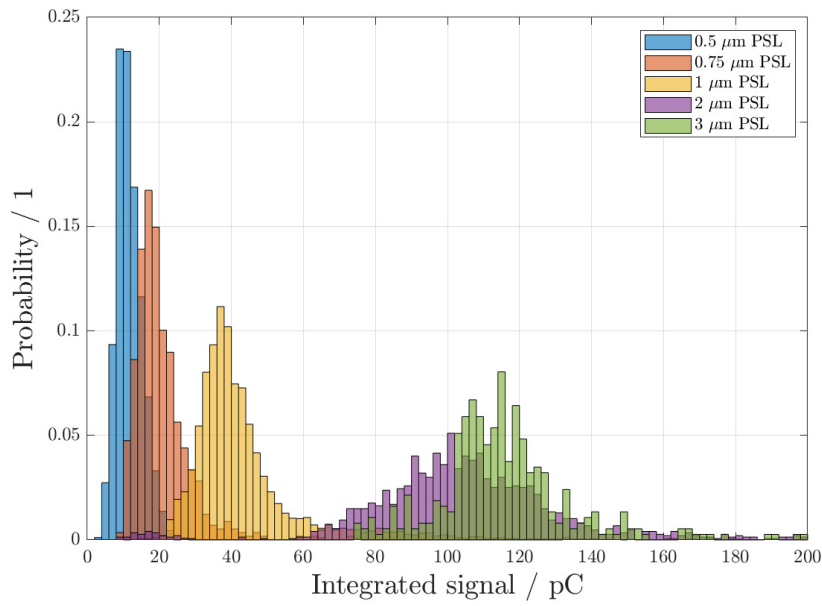


Fig. 6.7 The histogram shows the integrated signal for various particle sizes. The responses can clearly be distinguished.

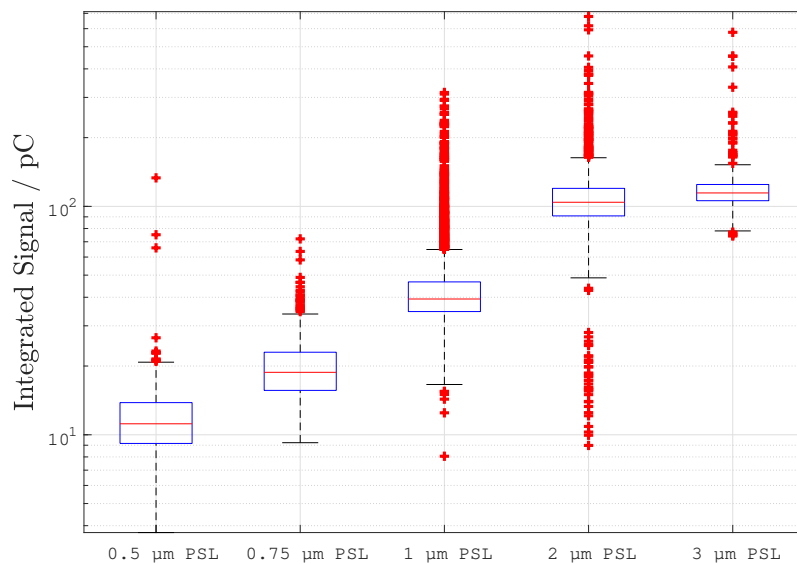


Fig. 6.8 The boxplot shows the integrated signal for various particle sizes. The responses can clearly be distinguished.

The peaks stemming from the particles can also be integrated. This might be the better option to look at the data since the peak height might be affected by the low number of data

points on the peaks. Fig.6.7 shows a histogram of the size responses in terms of integrated peaks of the particle sizes used in the experiments. The histogram is normalized and outliers greater than 200 pC are not shown. Fig.6.8 shows a boxplot of the same data as shown in fig.6.7.

Based on this data the 0.5  $\mu\text{m}$  and 0.75  $\mu\text{m}$  populations can be easier discriminated in terms of the integrated signal, whereas the particles with greater diameters are better separated in terms of the signal height. Since both information are available for each peak, both can be utilised in order to estimate the particle size for the estimation of PM2.5.

The counting efficiency for 500 nm, 750 nm, 1  $\mu\text{m}$  and 2  $\mu\text{m}$  particles can be specified to be as high as 80 to 100%. The counting efficiency can not be determined more precisely due to the uncertainty which we attribute to the aerosol setup. Note that the reference equipment requires flow rates on the order of hundreds of  $\text{mL min}^{-1}$  while the prototype is supplied with 3  $\text{mL min}^{-1}$ . This large difference in the flow rates implies severe difficulties for the setup leading to the estimated uncertainty in the counting efficiency.

Due to large particle losses for 3  $\mu\text{m}$  PSL particles, a counting efficiency has not been found experimentally. Nevertheless, the counting efficiency for 3  $\mu\text{m}$  can be assumed similar to the counting efficiency for 2  $\mu\text{m}$  particles. In summary the prototype is clearly able to correctly count and discriminate particles with various diameters in the size regime relevant for PM2.5.

### 6.3.2 Estimator for PN and PM2.5

The particle number concentration PN can simply be estimated from the signal by counting the total number of particles  $N$  in a finite time frame and dividing this value by the volume of aerosol sampled  $V_{\text{Sample}}$  as shown in eq.6.1

$$PN = \frac{N}{V_{\text{Sample}}} \quad (6.1)$$

$V_{\text{Sample}}$  is a function of the flow rate  $Q$  through the sensor and the measurement time  $\Delta t$  as shown in eq.6.2.

$$V_{\text{Sample}} = Q \cdot \Delta t \quad (6.2)$$

While the estimation of PN is straight forward, the estimation of PM2.5 is more delicate as more information on single particles is necessary. Eq.6.3 states PM2.5 in general.  $V_n$  is volume of each single individual particle measured,  $\rho_n$  is the mass density.

$$\text{PM2.5} = \frac{1}{V_{\text{Sample}}} \sum_{n=1}^N V_n \rho_n \quad (6.3)$$

As stated in sec.4 light scattering suffers from three drawbacks relevant for the estimation of PM2.5. One drawback is the occurrence of a lower limit of detection with respect to particle size, typically around 300 nm for commercial products. A second drawback is that the exact shape and volume of the particles cannot be measured and a spherical particle shape and a constant index of refraction has to be assumed. The third drawback is that the particles mass density  $\rho_n$  can not be measured and therefore has to be assumed constant. The results from sec.6.3.1 can be used to estimate the particle size of a particle passing the sensor system based on the signal. By assuming a spherical particle shape, the volume of the particles can be calculated. Since the response of the sensor in terms of signal partly overlaps for the PSL particle sizes used, the particle size distribution cannot be measured continuously but a finite number of bins is to be used.

Based on the results from sec. 6.3.1, we assume that the sensor is able to discriminate 5 size bins, one for 0.5  $\mu\text{m}$ , 0.75  $\mu\text{m}$ , 1  $\mu\text{m}$ , 2  $\mu\text{m}$  and 3  $\mu\text{m}$  each. As the integrated signal is better suited to discriminate particles below 1  $\mu\text{m}$ , for a first approximation only the integrated signal stemming from each individual particle event is considered for the particle sizing. The bin edges are stated in the following table.

Table 6.1 Bin edges for particle size estimation based on the experimental results with PSL spheres in sec.6.3.1

Particle diameter	Lower bin edge / pC	Upper bin edge / pC
0.5 $\mu\text{m}$	-	13.3
0.75 $\mu\text{m}$	13.3	29.8
1 $\mu\text{m}$	29.8	66.3
2 $\mu\text{m}$	66.3	102.8
3 $\mu\text{m}$	102.8	165.8

Further size bins might be introduced in future generations of prototypes and the signal height may be used as an additional information to find more precise and accurate size estimates. These complementary information can be included by using odds ratios based on Bayesian probability theory [71].

The estimator based on sec.6.3.1 and tab.6.1 reads as stated in eq.6.4.  $\rho$  denotes a mean mass density applicable to all particles which is assumed to be  $1650 \text{ kg m}^{-3}$  according to the OPC-N3.  $i$  is the index of the five bins defined in tab.6.1 whereas  $V_i$  is the volume of a particle in bin  $i$  and  $N_i$  is the number of particles counted in bin  $i$ . As stated before, the



particle shape is assumed to be spherical which yields the particles volume as a function of the diameter estimated based on the signal. Bin number five is not fully relevant for PM2.5 since 3  $\mu\text{m}$  particles are not part of PM2.5. Despite that, the bin is included in the evaluations in the following sections. Additional experiments using 2.5  $\mu\text{m}$  PSL particles are to be done in order to find the bin edges for 2.5  $\mu\text{m}$  particles. Additionally coefficients  $c_i$  are introduced which account for the counting efficiency in the respective bin. Due to the results obtained in sec.6.3.1 the counting efficiencies are assumed to be 100% which leads to  $c_i = 1$ . Note that  $c_i$  might be fitted according to PM2.5 reference data in order to find a robust estimator if necessary.

$$\text{PM2.5} = \frac{\rho}{V_{\text{Sample}}} \sum_{i=1}^5 V_i \cdot N_i \cdot c_i \quad (6.4)$$

### 6.3.3 Ambient Aerosol

The prototype has been challenged with ambient air in parallel to a Alphasense OPC-N3, a Sensirion SPS30 and TSI APS3321 for 24 hours. The setup is schematically shown in fig.6.9. For the PN measurements the TSI APS3321 is considered to be the best suited reference equipment out of the three. For PM2.5 we consider the Alphasense OPC-N3 as the most reliable reference out of the three as it is optimised for this specific task in contrary to the APS3321. Nevertheless, the comparison to the prototype as well as the correlations are shown for each reference sensor.

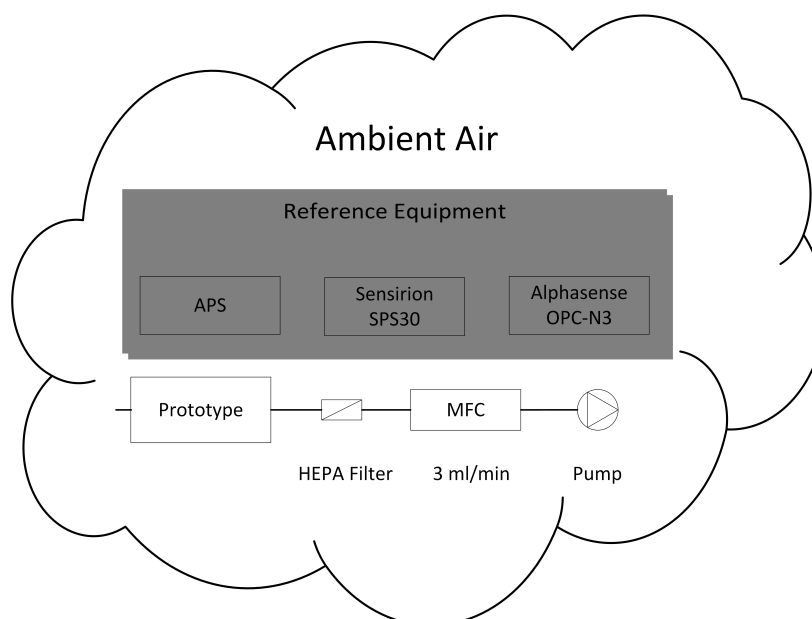


Fig. 6.9 Setup for tests with ambient aerosol. The prototype is tested against a TSI APS, Sensirion SPS30, and Alphasense OPC-N3.

## PN

As discussed in sec.6.3.2 the data obtained with the prototype can be used to estimate the particle number concentration PN. The full prototype data can be used to calculate one PN value per minute. The averaging time of the APS3321 is chosen to match the prototype and one value per minute is obtained. As the limit of detection of the APS3321 is  $0.37\ \mu\text{m}$  and the experimental results in sec.6.3.1 indicate that the limit of detection of the prototype is clearly above  $0.3\ \mu\text{m}$ , the instruments can be compared to each other rather conveniently. The results are shown in fig.6.10 and fig.6.11. The raw data obtained with the OPC-N3 and the SPS30 is smoothed by a moving average over 1 min. The SPS30 shows a size bin for particles below  $0.5\ \mu\text{m}$  which can be subtracted from the total PN reading in order to have a better comparison to the prototype. Similarly, the OPC-N3 shows a size bin for particles smaller than  $0.46\ \mu\text{m}$  which can also be disregarded for comparison. The comparison to the prototype as well as the correlations are shown in fig.6.12 and fig.6.13 in comparison to the OPC-N3 and in fig. 6.14 and fig.6.15 in comparison to the SPS30.

As can be seen in fig.6.10, the prototype agrees very well with the TSI APS3321 both for periods of constant PN and even for more distinct features. The higher noise on the prototype signal compared to the reference clearly stems from the lower flow rate and therefore the lower absolute particle count of the prototype. The high degree of correlation is also indicated by a correlation coefficient of 0.82. Fig.6.11 shows the correlation plot of the prototype

versus the APS3321. The plot clearly shows a linear relationship of both measurements indicated by a coefficient of determination of  $R^2$  of 0.67. The slope of 1.1 and the offset of 0.0 particle/cm<sup>3</sup> again shows the excellent agreement of both instruments. This excellent agreement together with the findings in sec.6.3.1 point towards a potentially good correlation of the prototype to the references in terms of PM2.5.

The results compared to the OPC-N3 and the SPS30 measurements further support the findings and are in good agreement with the previous results in general. The results show excellent agreement when the first size bin for particles below 0.5 µm and 0.46 µm in diameter of both reference sensors respectively is neglected for the calculation of PN. This is not surprising since the prototypes lower limit of detection is definitely above 0.3 µm as stated in sec.6.3.1.

The correlation statistics for PN are summarised in tab.6.2.

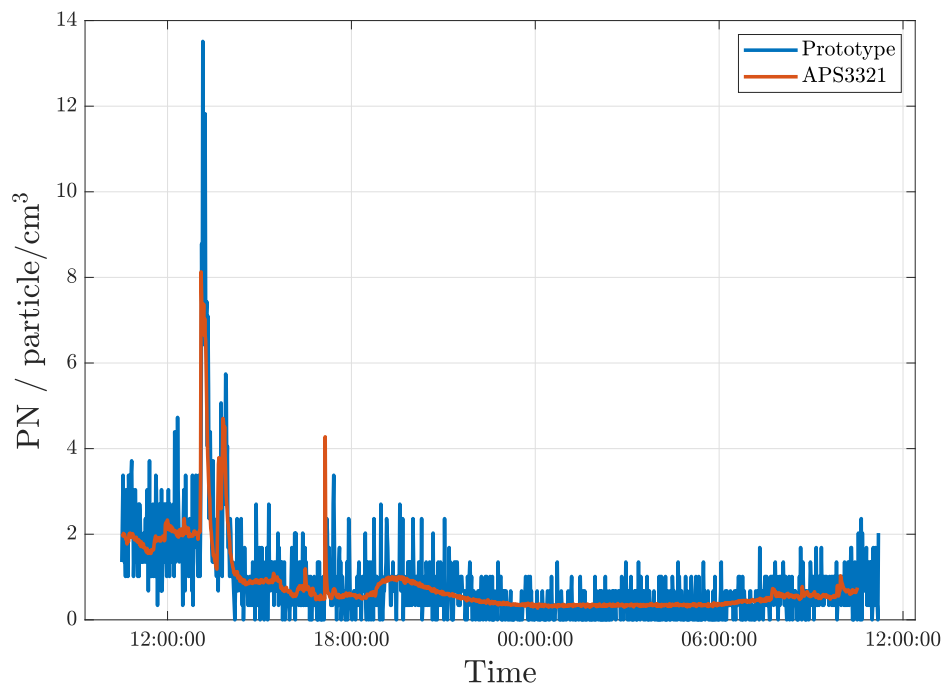


Fig. 6.10 The plot shows the PN measurement values from both the prototype and an TSI APS3321 as a reference. The correlation coefficient is 0.82, indicating a high degree of correlation as can be seen in the plot. In addition to the correlation also the absolute values and the range of PN values agree well.

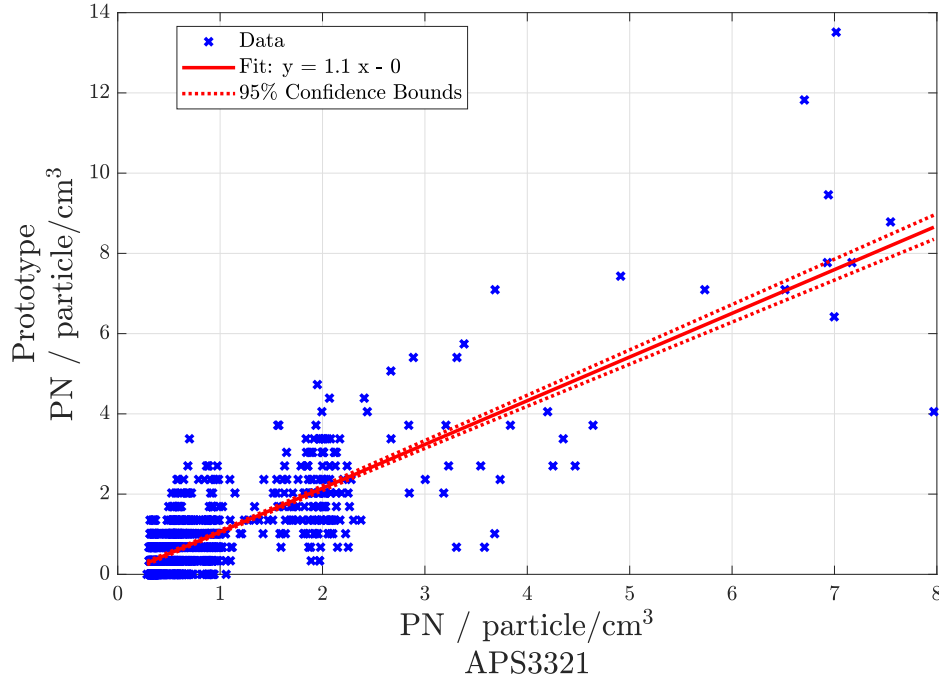
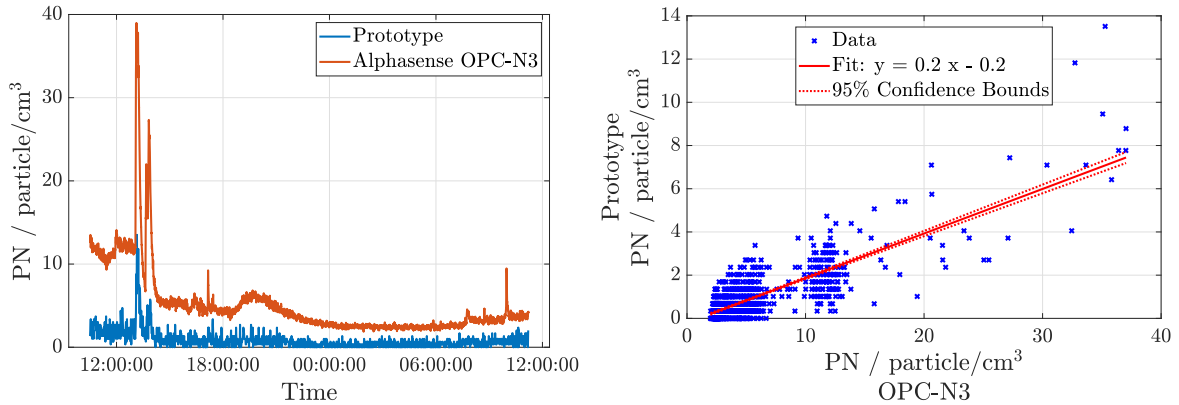


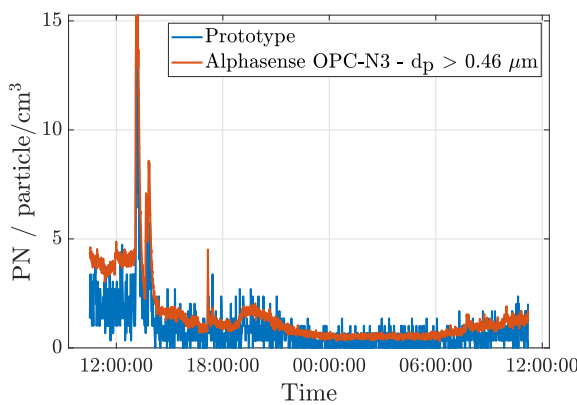
Fig. 6.11 The plot shows the PN measurement values from both the prototype and an TSI APS3321 as a reference. There is clearly a linear relationship visible. The linear fit shows a slope of 1.1 and an offset of 0.0 particle/cm<sup>3</sup>. The coefficient of determination  $R^2$  is 0.67 indicating a linear relationship of the prototype measurement and the OPC-N3 measurements.



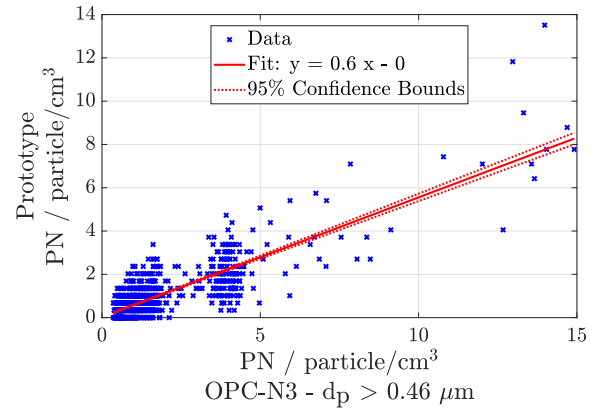
(a) As the OPC-N3 is able to detect particles with a minimum diameter of 0.35  $\mu\text{m}$  which the prototype is most certainly not capable of, the absolute values for PN differ substantially. Despite the disagreement over the absolute value, the correlation coefficient is 0.82, indicating a high degree of correlation as can be seen in the plot.

(b) The correlation plot clearly shows a linear dependency. The linear fit shows a slope of 0.2 and an offset of  $-0.2 \mu\text{g m}^{-3}$ . The coefficient of determination  $R^2$  is 0.64 indicating a linear relationship of the prototype measurement and the OPC-N3 measurements.

Fig. 6.12 The plots show the PN measurement values from both the prototype and the Alphasense OPC-N3 as a reference.

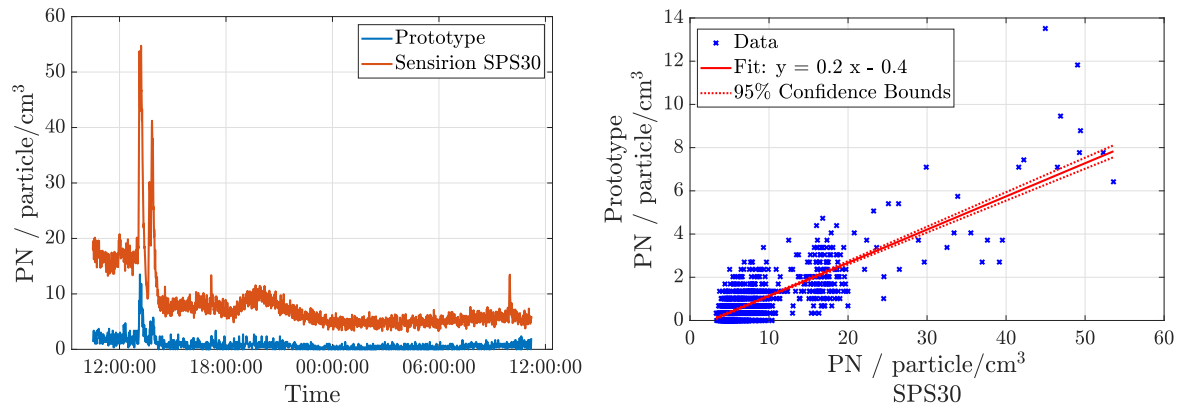


(a) The plot shows the PN values obtained with the OPC-N3 neglecting the first size bin, thus shifting the lower limit of particles considered for the PN value to 0.46 μm. This leads to an excellent agreement on the absolute PN concentrations. The correlation coefficient is 0.83, indicating a high degree of correlation as can be seen in the plot.



(b) The correlation plot clearly shows a linear dependency. The linear fit shows a slope of 0.6 and an offset of 0.0 μg m<sup>-3</sup>. The coefficient of determination  $R^2$  is 0.69 indicating a linear relationship of the prototype measurement and the OPC-N3 measurements.

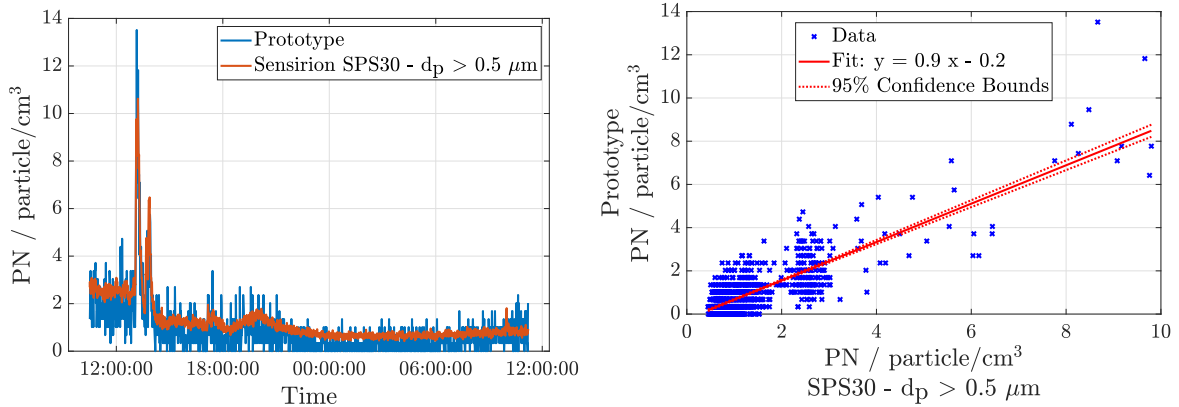
Fig. 6.13 The plot shows the PN measurement values from both the prototype and the Alphasense OPC-N3 as a reference. The first size bin of the OPC-N3 has been neglected for the calculation of PN. This shifts the lower limit of particles considered to 0.46 μm in order to better match the limit of detection with respect to size of the prototype



(a) As the SPS30 is able to detect particles with a minimum diameter of  $0.3 \mu\text{m}$  which the prototype is not capable of, the absolute values for PN differ substantially. Despite the disagreement over the absolute value, the correlation coefficient is 0.81, indicating a high degree of correlation as can be seen in the plot.

(b) The correlation plot clearly shows a linear dependency. The linear fit shows a slope of 0.2 and an offset of  $-0.4 \mu\text{g m}^{-3}$ . The coefficient of determination  $R^2$  is 0.65 indicating a linear relationship of the prototype measurement and the SPS30 measurements.

Fig. 6.14 The plots show the PN measurement values from both the prototype and the Sensirion SPS30 as a reference.



(a) The plot shows the PN values obtained with the SPS30 neglecting the first size bin, thus shifting the lower limit of particles considered for the PN value to  $0.5 \mu\text{m}$ . This leads to an excellent agreement on the absolute PN concentrations. The correlation coefficient is 0.83, indicating a high degree of correlation as can be seen in the plot.

(b) The correlation plot clearly shows a linear dependency. The linear fit shows a slope of 0.6 and an offset of  $0.0 \mu\text{g m}^{-3}$ . The coefficient of determination  $R^2$  is 0.69 indicating a linear relationship of the prototype measurement and the SPS30 measurements.

Fig. 6.15 The plot shows the PN measurement values from both the prototype and the Sensirion SPS30 as a reference. The first size bin of the SPS30 has been neglected for the calculation of PN. This shifts the lower limit of particles considered to  $0.5 \mu\text{m}$  in order to better match the limit of detection with respect to size of the prototype

Table 6.2 Correlation statistics for 24h PN measurements using ambient air as discussed earlier in this section 6.3.3. Prototype versus reference equipment.

Reference Sensor	Coefficient of Correlation	Linear Regression		
		Slope	Offset / $\mu\text{g m}^{-3}$	Coefficient of Determination $R^2$
APS3321	0.82	2.2	-0.4	0.78
OPC-N3	0.82	0.2	-0.2	0.64
OPC-N3 - $d_p > 0.46 \mu\text{m}$	0.83	0.6	-0.0	0.69
SPS30	0.81	0.2	-0.4	0.65
SPS30 - $d_p > 0.5 \mu\text{m}$	0.83	0.9	-0.2	0.69

## PM2.5

The estimator presented in sec.6.3.2 is used to calculate PM2.5 based on the data obtained with the prototype. The prototype data leads to one PM2.5 value per minute and has been smoothed using a ten minute moving average. The data from the Alphasense OPC-N3 and

the Sensirion SPS30 has been smoothed using a 1 min moving mean, whereas the APS3321 delivers average PM<sub>2.5</sub> values for fixed 1 min intervals. For the APS data a particle mass density of  $1650 \text{ kg m}^{-3}$  is used according to the OPC-N3. The mass density used by Sensirion SPS30 is not under disclosure and therefore unknown.

The results obtained with the prototype compared to the OPC-N3 are shown in fig.6.16 and fig.6.17. The plots clearly show a strong correlation of the measurements of both sensors. The coefficient of correlation is 0.89 which indicates a strong correlation of the measurements. The correlation plot shown in fig.6.17 shows that there is a linear relationship of the prototypes measurement values to the OPC-N3 with a coefficient of determination of 0.79. The linear fit shows a slope of 1.4 and an offset of  $-0.1 \text{ } \mu\text{g m}^{-3}$ . The slope and the offset can be tuned by the choice of the mass density assumed in the estimator discussed in sec.6.3.2, whereas the correlation is not influenced by this parameter. Note that the averaging over the period of 10 min is necessary mainly because of the relatively low values of PM<sub>2.5</sub> during the measurement. This low concentration leads to a low number of particles. The averaging is not necessary at elevated PM<sub>2.5</sub> concentrations. The results show an excellent agreement of the prototype and the reference OPC-N3.

The correlation with TSI APS3321 the Sensirion SPS30 are shown in fig.6.18 and fig.6.19 respectively. Also for those sensors there is clearly a strong correlation and a linear relationship of the prototype measurement and the respective reference. The correlation statistics are shown in tab.6.3.

Table 6.3 Correlation statistics for 24h PM<sub>2.5</sub> measurements using ambient air as discussed earlier in this section 6.3.3. Prototype versus reference equipment.

Reference Sensor	Coefficient of Correlation	Linear Regression		
		Slope	Offset / $\mu\text{g m}^{-3}$	Coefficient of Determination $R^2$
OPC-N3	0.89	1.4	-0.1	0.79
APS3321	0.88	2.2	-0.4	0.78
SPS30	0.86	2.7	-0.6	0.77

These results mark a crucial milestone as it is not only a proof of principle but a clear indication of the vast potential of the sensor in general.



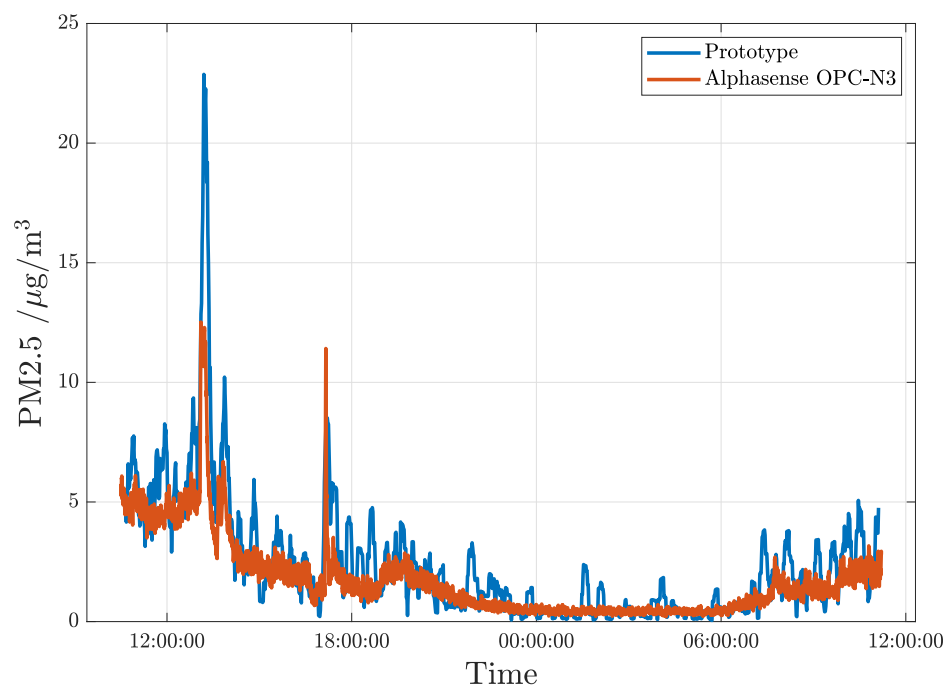


Fig. 6.16 The plot shows the PM2.5 measurement values from both the prototype and an Alphasense OPC-N3 as a reference. The prototype data is smoothed over a moving mean window of 10 min. The correlation coefficient is 0.89, indicating a high degree of correlation as can be seen in the plot. In addition to the correlation also the absolute values and the range of PM2.5 values agree well.

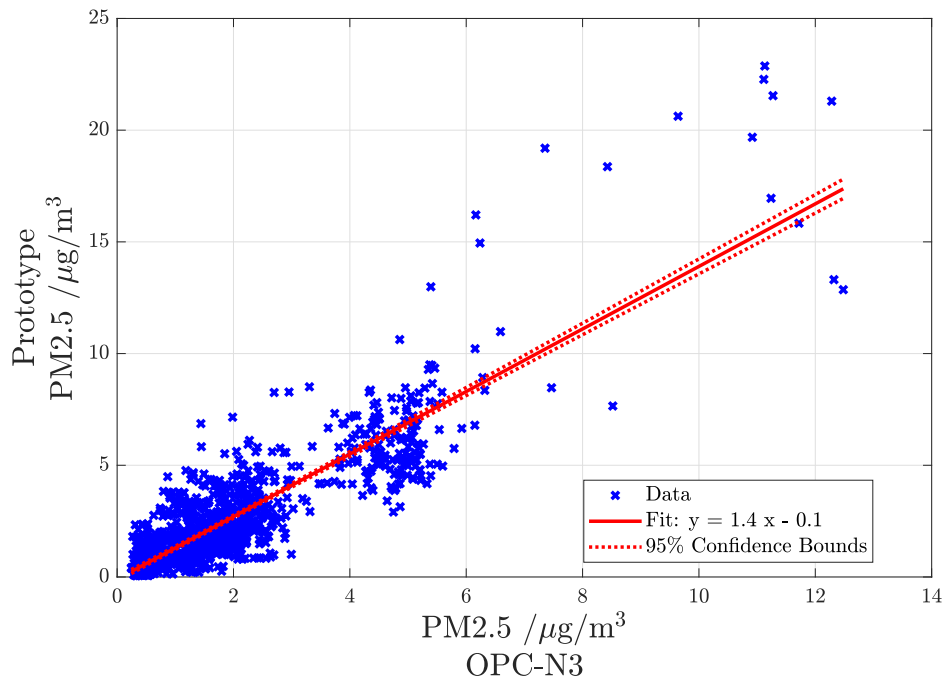
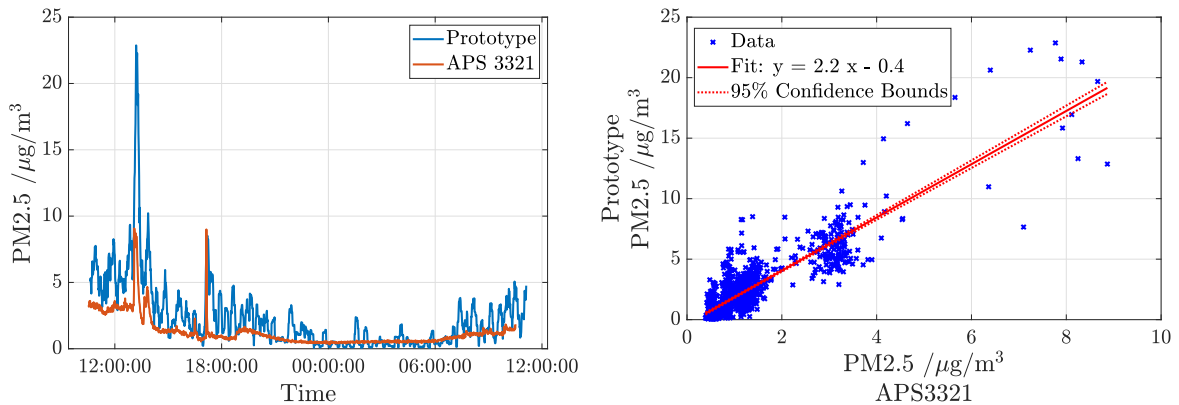


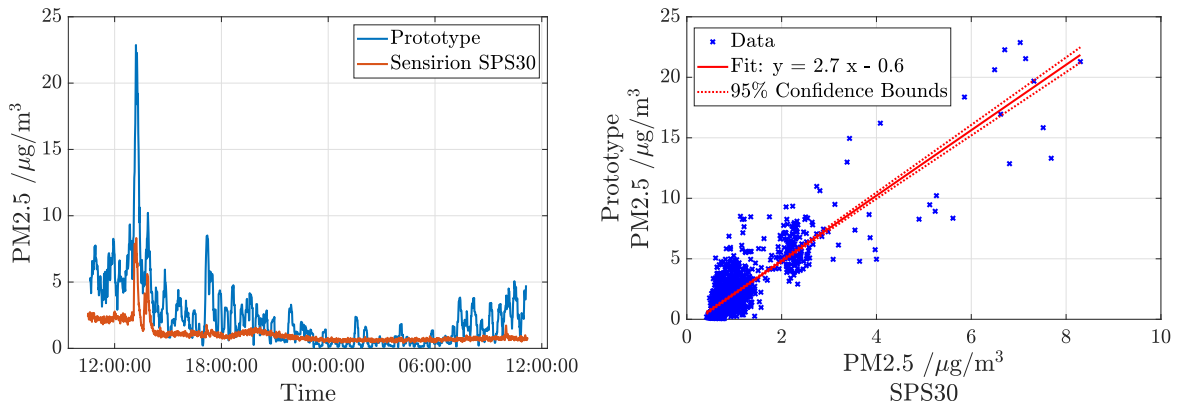
Fig. 6.17 The plot shows the PM2.5 measurement values from both the prototype and an Alphasense OPC-N3 as a reference. There is clearly a linear relationship visible. The linear fit shows a slope of 1.4 and an offset of  $-0.1 \mu\text{g m}^{-3}$ . The coefficient of determination  $R^2$  is 0.79 indicating a linear relationship of the prototype measurement and the OPC-N3 measurements.



(a) The prototype data is smoothed over a moving mean window of 10 min. The correlation coefficient is 0.88, indicating a high degree of correlation as can be seen in the plot. In addition to the correlation also the absolute values and the range of PM2.5 values agree well.

(b) There is clearly a linear relationship visible. The linear fit shows a slope of 2.2 and an offset of  $-0.4 \mu\text{g m}^{-3}$ . The coefficient of determination  $R^2$  is 0.78 indicating a linear relationship of the prototype measurement and the APS measurements.

Fig. 6.18 The plot shows the PM2.5 measurement values from both the prototype and the TSI APS3321 as a reference.



(a) The prototype data is smoothed over a moving mean window of 10 min. The correlation coefficient is 0.86, indicating a high degree of correlation as can be seen in the plot. In addition to the correlation also the absolute values and the range of PM2.5 values agree well.

(b) There is clearly a linear relationship visible. The linear fit shows a slope of 2.7 and an offset of  $-0.6 \mu\text{g}/\text{m}^3$ . The coefficient of determination  $R^2$  is 0.74 indicating a linear relationship of the prototype measurement and the APS measurements.

Fig. 6.19 The plot shows the PM2.5 measurement values from both the prototype and the Sensirion SPS30 as a reference.



# Chapter 7

## Summary and Outlook

During the course of the thesis, particulate matter metrics have been evaluated and PM<sub>2.5</sub> has been chosen as the target metric. Statistical implications of the small sample volume miniaturised particle sensors are capable of evaluating have been investigated and inherent limitations of miniaturisation have been identified. It has been shown that a total sampled mass of 100 pg at typical particle size distributions is necessary to estimate the ambient particle concentration in terms of PM<sub>2.5</sub> with an inherent uncertainty below 10%. This equals 4 mL of aerosol at a concentration of  $25 \mu\text{g m}^{-3}$ .

We have identified key components necessary for a functional particle sensor which include a particle size separator, a fluid path, a sensor component with a defined physical interaction and sensor effect, an active flow element and an outlet. Especially the statistical considerations have shown that an active flow through the sensor is necessary and therefore an active flow element like a pump cannot be left out.

Various sensor effects have been discussed in the context of miniaturisation. Novel concepts for optical particle detection have been proposed and experimentally validated.

It has been concluded that the well-established light scattering approach is suited for miniaturisation as there is no inherent penalty for the sensor effect with respect to miniaturisation, there is a correlation to PM<sub>2.5</sub>, and it is among the standard approaches for handheld sized devices, which makes it a logical next step towards mobile integration. The author considers the aethalometer approach to be very well suited in terms of technical feasibility because of a lower dependence on stray light, no interference with oscillating flows and no lower cut off with respect to particle size. One might also argue that the aethalometer is more sensitive to black carbon than to other constituents of ambient PM<sub>2.5</sub> and is therefore biased. Since there is evidence that BC poses a disproportionately high threat to human health, this might be considered a benefit, especially if legislation further tackles BC immissions.

A capacitive sensor has been tested experimentally, leading to the conclusion that the princi-

ple is not yet ready for mobile integration.

Two promising candidates for novel sensor effects which could also be exploited for sensor miniaturisation have been found: evanescent particle sensing and an interferometric approach which have both been filed as a patent application. The evanescent field particle sensing approach has mostly been split from the thesis and an additional research proposal has been submitted and approved. The interferometric approach has been evaluated using analytical methods and has been subject to a co-supervised master thesis which evaluated the principle experimentally. The promising results show a high potential for future activities.

A light-scattering based sensor design has been shown which incorporates the necessary complexity but is still on a scale which allows the integration in a mobile device. A solution for the active flow element has been identified and evaluated experimentally in a cooperation with Fraunhofer EMFT who provide the micro-pumps incorporated in the design of the sensor system.

Attention has been paid not only to end up with a functional device with respect to the sensor effect but also to have a design which can be assembled and can potentially be realised in volume production.

During the project, a prototype of the sensor was built in order to validate the design. The prototype relies on an external laser driver, an external read out for the photodiode, and an external pump which are to be incorporated into the next generation of prototypes beyond the scope of the thesis. The evaluated prototype is able to correctly count particles down to a size of 500 nm in diameter with a counting efficiency of 80-100%. The prototype is clearly able to discriminate particles based on the size in five bins relevant for PM<sub>2.5</sub>. This has been shown experimentally with monodisperse polystyrene latex spheres. Based on the results obtained with the polystyrene latex reference aerosol, an estimator for PM<sub>2.5</sub> has been found. The prototype has been tested with ambient aerosol in a 24h measurement in parallel to reference equipment for PM<sub>2.5</sub>. The measurement of the prototype matches the reference measurements extraordinarily well. A coefficient of correlation of 0.89 has been shown with respect to an Alphasense OPC-N3 as a reference.

Among the next steps will be the implementation of the micro-pump into the prototype as well as the laser driver. The prototypes will be tested in a range of environmental conditions and aerosols.

It should be mentioned that the final sensor system can not only be used as a particulate matter sensor but can in principle serve as a platform for various environmental sensors. Additional sensor units such as for example gas sensors for CO<sub>2</sub> or NO<sub>2</sub>, or a humidity sensor can be incorporated in the system design with reasonable effort and with the benefit of a shared integrated pump and the defined flow path. This potential synergy gives the project

a further perspective.

In the authors opinion, legislation concerning particulate matter will shift towards black carbon instead of PM<sub>2.5</sub> and PM<sub>10</sub>. This is reasonable, as there is increasing evidence that black carbon shows enhanced health effects compared to other particles and compared to PM<sub>2.5</sub>. Furthermore, black carbon can often be attributed to anthropogenic sources, so regulatory approaches are likely to succeed. Against this background, the author suggests to implement sensor effects which are able to detect black carbon concentrations. A shift in legislation and in public awareness towards black carbon might render light scattering devices obsolete. The author suggests to realise an integrated aethalometer approach that targets both PM<sub>2.5</sub> and black carbon.





# Chapter 8

## List of Publications

### Paper Publications

#### **On the Inherent Variability of Particulate Matter Concentrations on Small Scales and the Consequences for Miniaturized Particle Sensors [34]**

Paul Maierhofer, Georg Röhrer, Markus Bainschab and Alexander Bergmann: “On the Inherent Variability of Particulate Matter Concentrations on Small Scales and the Consequences for Miniaturized Particle Sensors”. In: Aerosol and Air Quality Research (2019). DOI: 10.4209/aaqr.2019.01.0048

#### **Author contributions**

All authors conceived of the presented ideas. Paul Maierhofer developed the analytical theory and performed the computations. Markus Bainschab, Alexander Bergmann and Georg Röhrer verified the analytical methods and supervised the findings of this work. All authors discussed the results. Paul Maierhofer is the main author of the publication and wrote the paper draft as well as the revised version. Alexander Bergmann and Paul Maierhofer have answered to the reviewers. All authors contributed to the final manuscript.

#### **Characterization of a Capacitive Sensor for Particulate Matter [72]**

Maierhofer, Paul, et al. "Characterization of a Capacitive Sensor for Particulate Matter." Multidisciplinary Digital Publishing Institute Proceedings. Vol. 2. No. 13. 2018.

### **Author contributions as stated in the publication**

Conceptualization: Georg Röhrer, Marco Sampietro and Alexander Bergmann

Methodology: Paul Maierhofer, Marco Carminati, Giorgio Ferrari, Georg Röhrer, Marco Sampietro and Alexander Bergmann

Software: Paul Maierhofer, Marco Carminati

Validation: Paul Maierhofer, Marco Carminati, Giorgio Ferrari, Georg Röhrer, Marco Sampietro and Alexander Bergmann

Formal Analysis: Paul Maierhofer

Investigation: Paul Maierhofer

Resources: Marco Sampietro and Alexander Bergmann

Writing — Original Draft Preparation: Paul Maierhofer

Writing—Review & Editing: Marco Carminati, Giorgio Ferrari, Georg Röhrer, Marco Sampietro and Alexander Bergmann

Visualization: Paul Maierhofer

Project Administration: Marco Sampietro and Alexander Bergmann

Funding Acquisition: Georg Röhrer, Marco Sampietro and Alexander Bergmann

## **Co-Authored Paper Publications**

### **Vacuum-assisted selective adhesive imprinting for heterogeneous system integration of MOEMS devices : Automated assembly of miniaturized PM sensor [68]**

Pribošek, J., Zauner, M., Bardong, J., Binder, A., Maierhofer, P., Bergmann, A., and Röhrer, G. (2019, October). Vacuum-assisted selective adhesive imprinting for heterogeneous system integration of MOEMS devices: Automated assembly of miniaturized PM sensor. In 2019 IEEE SENSORS (pp. 1-3). IEEE.

#### **Author contributions**

Major parts of the work have been done by Jaka Pribosek. The author has contributed to the conceptualisation and methodology, conducted the airtightness and leak tests mentioned in the publication, and helped in the review of the draft.

## **Single Particle Detector Using the Evanescent Field of a Silicon Nitride Waveguide [47]**

Buchberger, A. et al., "Single Particle Detector Using the Evanescent Field of a Silicon Nitride Waveguide," 2019 IEEE SENSORS, Montreal, QC, Canada, 2019, pp. 1-4.

### **Author contributions**

Major parts of the work have been done by Anton Buchberger. Paul Maierhofer contributed to the conceptualisation and methodology, to the logic of the software, and to the review of the paper draft. Due to the significant contribution to the project proposal which led to the funding of this work, Paul Maierhofer has contributed to the funding Acquisition.

## **Optical Aerosol Sensing – from Air Quality to Global Warming[73]**

Maierhofer, P., Buchberger, A., Breitegger, P., and Bergmann, A. (2019). Optical Aerosol Sensing – from Air Quality to Global Warming. Applied Industrial Optics 2019, M2A.2.

### **Author contributions**

All authors contributed to this work. Paul Maierhofer contributed to the conceptualisation and methodology and to the writing and reviewing of the draft.

## **Integrated Evanescent Field Detector for Ultrafine Particles - Theory and Concept**

Buchberger, A., Maierhofer, P., Baumgart, M., Kraft, J., and Bergmann, A.  
Under review in OSA Optics Express.

### **Author contributions**

Major parts of the work have been done by Anton Buchberger. Paul Maierhofer contributed to the conceptualisation and methodology, and to the review of the paper draft. Due to the significant contribution to the project proposal which led to the funding this work, Paul Maierhofer has contributed to the funding acquisition.

## Conference Contributions

### Talk Contribution

- P. Maierhofer, G. Röhrer and A. Bergmann. *On the inherent measurement uncertainty of miniaturized PM sensors*. 10th International Aerosol Conference. 2018. St. Louis, Missouri, USA.
- P. Maierhofer, A. Buchberger, B. Lang, and A. Bergmann. *Interferometric Particle Measurements*. 1st Winter School on Aerosol Technology. 2019. Gastein, Austria.

### Poster Contributions

- P. Maierhofer, M. Carminati, G. Ferrari, G. Röhrer, M. Sampietro and A. Bergmann. *Deposition of micrometric particles on a capacitive sensing area*. Aerosol Technology conference. 2018. Bilbao, Spain
- P. Maierhofer, M. Carminati, G. Ferrari, G. Röhrer, M. Sampietro and A. Bergmann. *Deposition of micrometric particles on a capacitive sensing area*. Cambridge Particle Meeting. 2018. Cambridge, UK.
- P. Maierhofer, M. Carminati, G. Ferrari, G. Röhrer, M. Sampietro and A. Bergmann. *Characterization of a Capacitive Sensor for Particulate Matter*. Eurosensors conference. 2018. Graz, Austria.
- P. Maierhofer, G. Röhrer, J. Pribošek, G. Fasching, A. Singulani, H. Etschmaier, M. Kraft, A. Bergmann. *Towards a Highly-Integrated Low-Cost PM Sensor*. 37th AAAR Annual Conference. 2019. Portland, Oregon, USA.

### Co-Authored Conference Contributions - Talks

- A. Buchberger, P. Maierhofer, M. Sagmeister, V. Sidorov, J. Kraft, and A. Bergmann. *Utilizing a Sub-Micron Silicon Nitride Waveguide as Single Particle Aerosol Detector*. 37th AAAR Annual Conference. 2019. Portland, Oregon, USA.
- A. Buchberger, P. Maierhofer, A. Bergmann, A. Singulani, M. Sagmeister, V. Sidorov, J. Kraft, M. Baumgart, A. Tortschanoff. *Single Particle Detector Using the Evanescent Field of a Silicon Nitride Waveguide*. IEEE Sensors. 2019. Montreal, Canada.

- J. Pribošek, M. Zauner, J. Bardong, A. Binder, P. Maierhofer, A. Bergmann, and G. Röhrer. *Vacuum-assisted selective adhesive imprinting for heterogeneous system integration of MOEMS devices: Automated assembly of miniaturized PM sensor*. IEEE Sensors. 2019. Montreal, Canada.
- P. Maierhofer, A. Buchberger, P. Breitegger, and A. Bergmann. *Optical Aerosol Sensing – from Air Quality to Global Warming*. Applied Industrial Optics: Spectroscopy, Imaging and Metrology. 2019. Washington DC.

## Co-Supervised Master Thesis

Within the present PhD thesis, a master thesis was co-supervised by Paul Maierhofer concerning the interferometric particle detection principle, see chap. 4. and A.3.

- Thomas Hofer. *Evaluierung eines Partikelsensors basierend auf Interferenz in optischen Resonatoren*. Master Thesis. Graz University of Technology, 2019.

## Patents Filed

### Integrated filter-based particulate matter sensors [53]

The application can be found in the appendix A.1.

### Particle density sensor using evanescent wave of waveguide [74]

The application can be found in the appendix A.2.

### Apparatus and method for detecting objects

The application can be found in the appendix A.3.



# References

- [1] F. M. Bulot, S. J. Johnston, P. J. Basford, et al. “Long-term field comparison of multiple low-cost particulate matter sensors in an outdoor urban environment”. In: *Scientific Reports* 9.1 (2019).
- [2] K. K. Johnson, M. H. Bergin, A. G. Russell, et al. “Field test of several low-cost particulate matter sensors in high and low concentration urban environments”. In: *Aerosol and Air Quality Research* 18.3 (Mar. 2018), pp. 565–578.
- [3] F. Karagulian, M. Gerboles, M. Barbieri, et al. *Review of sensors for air quality monitoring*. Tech. rep. 2019.
- [4] M. Dong, E. Iervolino, F. Santagata, et al. “Silicon microfabrication based particulate matter sensor”. In: *Sensors and Actuators, A: Physical* 247 (Aug. 2016), pp. 115–124.
- [5] M. Dong, E. Iervolino, F. Santagata, et al. “Integrated Virtual Impactor Enabled PM 2.5 Sensor”. In: *IEEE Sensors Journal* 17.9 (May 2017), pp. 2814–2821.
- [6] S. Thomas, F. H. Villa-Lopez, J. Theunis, et al. “Particle Sensor Using Solidly Mounted Resonators”. In: *IEEE Sensors Journal* 16.8 (Apr. 2016), pp. 2282–2289.
- [7] F. H. Villa-López, G. Rughoobur, S. Thomas, et al. “Design and modelling of solidly mounted resonators for low-cost particle sensing”. In: *Measurement Science and Technology* 27.2 (Feb. 2016), p. 025101.
- [8] I. Paprotny, F. Doering, P. A. Solomon, et al. “Microfabricated air-microfluidic sensor for personal monitoring of airborne particulate matter: Design, fabrication, and experimental results”. In: *Sensors and Actuators, A: Physical* 201 (Oct. 2013), pp. 506–516.
- [9] D. Fahimi, O. Mahdavi pour, J. Sabino, et al. “Vertically-stacked MEMS PM2.5 sensor for wearable applications”. In: *Sensors and Actuators, A: Physical* 299 (Nov. 2019).
- [10] M. Carminati, G. Ferrari, and M. Sampietro. “Emerging miniaturized technologies for airborne particulate matter pervasive monitoring”. In: *Measurement: Journal of the International Measurement Confederation* 101 (2017), pp. 250–256.
- [11] M. Carminati, L. Pedalà, E. Bianchi, et al. “Capacitive detection of micrometric airborne particulate matter for solid-state personal air quality monitors”. In: *Sensors and Actuators A: Physical* 219 (2014), pp. 80–87.
- [12] M. Carminati, L. Pedalà, E. Bianchi, et al. “Capacitive detection of micrometric airborne particulate matter for solid-state personal air quality monitors”. In: *Sensors and Actuators, A: Physical* 219 (Nov. 2014), pp. 80–87.

- [13] H. H. Lim, D. Park, J. Y. Maeng, et al. "MEMS based integrated particle detection chip for real time environmental monitoring". In: *Proceedings of the IEEE International Conference on Micro Electro Mechanical Systems (MEMS)*. Vol. 2006. 2006, pp. 62–65.
- [14] P. Kulkarni, P. A. Baron, and K. Willeke. *Aerosol Measurement: Principles, Techniques, and Applications: Third Edition*. John Wiley & Sons, 2011.
- [15] W. C. Hinds. *Aerosol technology: properties, behavior, and measurement of airborne particles*. John Wiley & Sons, 1999.
- [16] O. Schmid and T. Stoeger. "Surface area is the biologically most effective dose metric for acute nanoparticle toxicity in the lung". In: *Journal of Aerosol Science* 99 (Sept. 2016), pp. 133–143.
- [17] N. A. Janssen, G. Hoek, M. Simic-Lawson, et al. "Black carbon as an additional indicator of the adverse health effects of airborne particles compared with PM10 and PM2.5". In: *Environmental Health Perspectives* 119.12 (2011), pp. 1691–1699.
- [18] F. R. Cassee, M. E. Héroux, M. E. Gerlofs-Nijland, et al. "Particulate matter beyond mass: Recent health evidence on the role of fractions, chemical constituents and sources of emission". In: *Inhalation Toxicology* 25.14 (Dec. 2013), pp. 802–812.
- [19] T. C. Bond, S. J. Doherty, D. W. Fahey, et al. "Bounding the role of black carbon in the climate system: A scientific assessment". In: *Journal of Geophysical Research: Atmospheres* 118.11 (June 2013), pp. 5380–5552.
- [20] N. L. Mills, K. Donaldson, P. W. Hadoke, et al. "Adverse cardiovascular effects of air pollution". In: *Nature Clinical Practice Cardiovascular Medicine* 6.1 (2009), pp. 36–44.
- [21] G. Oberdörster, E. Oberdörster, and J. Oberdörster. "Nanotoxicology: An emerging discipline evolving from studies of ultrafine particles". In: *Environmental Health Perspectives* 113.7 (July 2005), pp. 823–839.
- [22] C. A. Pope, M. J. Thun, M. M. Namboodiri, et al. "Particulate air pollution as a predictor of mortality in a prospective study of U.S. Adults". In: *American Journal of Respiratory and Critical Care Medicine* 151.3 I (1995), pp. 669–674.
- [23] C. A. Pope, R. T. Burnett, M. J. Thun, et al. "Lung cancer, cardiopulmonary mortality, and long-term exposure to fine particulate air pollution". In: *Journal of the American Medical Association* 287.9 (Mar. 2002), pp. 1132–1141.
- [24] C. A. Pope, R. T. Burnett, G. D. Thurston, et al. "Cardiovascular Mortality and Long-Term Exposure to Particulate Air Pollution: Epidemiological Evidence of General Pathophysiological Pathways of Disease". In: *Circulation* 109.1 (2004), pp. 71–77.
- [25] C. A. Pope and D. W. Dockery. "Health effects of fine particulate air pollution: Lines that connect". In: *Journal of the Air and Waste Management Association* 56.6 (2006), pp. 709–742.
- [26] C. A. Pope, M. Ezzati, and D. W. Dockery. "Fine-particulate air pollution and life expectancy in the United States". In: *New England Journal of Medicine* 360.4 (Jan. 2009), pp. 376–386.
- [27] R. D. Brook, S. Rajagopalan, C. A. Pope, et al. "Particulate matter air pollution and cardiovascular disease: An update to the scientific statement from the american heart association". In: *Circulation* 121.21 (June 2010), pp. 2331–2378.



- [28] WHO European Centre for Environment and Health. *Review of evidence on health aspects of air pollution - REVIHAAP*. 2013.
- [29] C. A. Pope, M. Cropper, J. Coggins, et al. "Health benefits of air pollution abatement policy: Role of the shape of the concentration–response function". In: *Journal of the Air and Waste Management Association* 65.5 (2015), pp. 516–522.
- [30] Y. Shou, Y. Huang, X. Zhu, et al. "A review of the possible associations between ambient PM<sub>2.5</sub> exposures and the development of Alzheimer's disease". In: *Ecotoxicology and Environmental Safety* 174 (June 2019), pp. 344–352.
- [31] W. Tang, L. Du, W. Sun, et al. "Maternal exposure to fine particulate air pollution induces epithelial-to-mesenchymal transition resulting in postnatal pulmonary dysfunction mediated by transforming growth factor- $\beta$ /Smad3 signaling". In: *Toxicology Letters* 267 (Feb. 2017), pp. 11–20.
- [32] R. Basu, D. Pearson, K. Ebisu, et al. "Association between PM 2.5 and PM 2.5 Constituents and Preterm Delivery in California, 2000–2006". In: *Paediatric and Perinatal Epidemiology* 31.5 (Sept. 2017), pp. 424–434.
- [33] J. Sun, W. Birmili, M. Hermann, et al. "Variability of black carbon mass concentrations, sub-micrometer particle number concentrations and size distributions: results of the German Ultrafine Aerosol Network ranging from city street to High Alpine locations". In: *Atmospheric Environment* 202 (Apr. 2019), pp. 256–268.
- [34] P. Maierhofer, G. Röhrer, M. Bainschab, et al. "On the Inherent Variability of Particulate Matter Concentrations on Small Scales and the Consequences for Miniaturized Particle Sensors". In: *Aerosol and Air Quality Research* 20.2 (2020), pp. 271–280.
- [35] R. White, I. Paprotny, and F. Doering. "Microfabricated particulate matter monitor". US 8,806,915 B2. 2011.
- [36] P. H. McMurry. "A review of atmospheric aerosol measurements". In: *Atmospheric Environment* 34.12–14 (2000), pp. 1959–1999.
- [37] Z. Bozóki, A. Pogány, and G. Szabó. "Photoacoustic instruments for practical applications: Present, potentials, and future challenges". In: *Applied Spectroscopy Reviews* 46.1 (Jan. 2011), pp. 1–37.
- [38] P. Breitegger, M. A. Schriebl, R. T. Nishida, et al. "Soot mass concentration sensor using quartz-enhanced photoacoustic spectroscopy". In: *Aerosol Science and Technology* 53.9 (2019), pp. 971–975.
- [39] R. T. Nishida, N. M. Yamasaki, M. A. Schriebl, et al. "Modelling the effect of aerosol polydispersity on unipolar charging and measurement in low-cost sensors". In: *Journal of Aerosol Science* 130 (Apr. 2019), pp. 10–21.
- [40] M. Mohr, U. Lehmann, and J. Rutter. "Comparison of mass-based and non-mass-based particle measurement systems for ultra-low emissions from automotive sources". In: *Environmental Science and Technology* 39.7 (Apr. 2005), pp. 2229–2238.
- [41] P. Ciccarella, M. Carminati, M. Sampietro, et al. "Multichannel 65 zF rms Resolution CMOS Monolithic Capacitive Sensor for Counting Single Micrometer-Sized Airborne Particles on Chip". In: *IEEE Journal of Solid-State Circuits* 51.11 (2016), pp. 2545–2553.
- [42] C. F. Bohren. *Absorption and scattering of light by small particles*. Wiley, 1983, p. 530.

- [43] H. C. van de Hulst. *Light scattering by small particles*. New York: Dover Publication, Inc., 1981.
- [44] H. Axmann. “Verfahren zur Bestimmung der Partikelkonzentration in Abgasen von Verbrennungsmotoren”. PhD thesis. Graz University of Technology, 2015.
- [45] A. Cusano, F. Arregui, M. Giordano, et al., eds. *Optochemical nanosensors*. CRC PRESS, 2012.
- [46] A. Kulkarni, J. H. Lee, J. D. Nam, et al. “Thin film-coated plastic optical fiber probe for aerosol chemical sensing applications”. In: *Sensors and Actuators, B: Chemical* 150.1 (Oct. 2010), pp. 154–159.
- [47] A. Buchberger, P. Maierhofer, A. Bergmann, et al. “Single Particle Detector Using the Evanescent Field of a Silicon Nitride Waveguide”. In: *2019 IEEE SENSORS*. IEEE, Oct. 2019, pp. 1–4.
- [48] L. Drinovec, G. Močnik, P. Zotter, et al. “The “dual-spot” Aethalometer: An improved measurement of aerosol black carbon with real-time loading compensation”. In: *Atmospheric Measurement Techniques* 8.5 (May 2015), pp. 1965–1979.
- [49] H. Moosmüller, R. Chakrabarty, and W. Arnott. “Aerosol light absorption and its measurement: A review”. In: *Journal of Quantitative Spectroscopy and Radiative Transfer* 110.11 (July 2009), pp. 844–878.
- [50] E. Weingartner, H. Saathoff, M. Schnaiter, et al. “Absorption of light by soot particles: determination of the absorption coefficient by means of aethalometers”. In: *Journal of Aerosol Science* 34.10 (2003), pp. 1445–1463.
- [51] A. Virkkula, T. Mäkelä, R. Hillamo, et al. “A simple procedure for correcting loading effects of aethalometer data”. In: *Journal of the Air and Waste Management Association* 57.10 (Oct. 2007), pp. 1214–1222.
- [52] C. C.-K. Chou, W. N. Chen, S. Y. Chang, et al. “Specific absorption cross-section and elemental carbon content of urban aerosols”. In: *Geophysical Research Letters* 32.21 (2005), pp. 1–4.
- [53] H. Etschmaier, G. Röhrer, A. Singulani, et al. “Integrated Filter-Based Particulate Matter Sensors”. WO 2019/115690 A1. 2018.
- [54] J. S. Batchelder and M. A. Taubenblatt. “Interferometric detection of forward scattered light from small particles”. In: *Applied Physics Letters* 55.3 (1989), pp. 215–217.
- [55] M. Potenza and P. Milani. “Free nanoparticle characterization by optical scattered field analysis: opportunities and perspectives”. In: *Journal of Nanoparticle Research* 16.11 (Nov. 2014), p. 2680.
- [56] D. R. Pettit and T. W. Peterson. “Coherent detection of scattered light from submicron aerosols”. In: *Aerosol Science and Technology* 2.3 (1982), pp. 351–368.
- [57] E. Hecht. *Optics*. Pearson, 2015.
- [58] M. J. Berg and G. Videen. “Digital holographic imaging of aerosol particles in flight”. In: *Journal of Quantitative Spectroscopy and Radiative Transfer* 112.11 (July 2011), pp. 1776–1783.

- [59] G. Brunnhofer, A. Bergmann, and M. Kraft. “Concept for a holographic particle counter”. In: *30th Annual Conference of the IEEE Photonics Society, IPC 2017*. Vol. 2017-Janua. Institute of Electrical and Electronics Engineers Inc., Nov. 2017, pp. 581–582.
- [60] B. Fischer. “Optical microphone hears ultrasound”. In: *Nature Photonics* 10.6 (June 2016), pp. 356–358.
- [61] S. Preißer, B. Fischer, and N. Panzer. “Listening to Ultrasound with a Laser”. In: *Optik & Photonik* 12.5 (Dec. 2017), pp. 22–25.
- [62] W. Rohringer, S. Preißer, M. Liu, et al. “All-optical highly sensitive broadband ultrasound sensor without any deformable parts for photoacoustic imaging”. In: *Photons Plus Ultrasound: Imaging and Sensing 2016*. Vol. 9708. 2016, p. 970815.
- [63] T. Hofer. “Evaluierung eines Partikelsensors basierend auf Interferenz in optischen Resonatoren”. PhD thesis. Graz University of Technology, 2019.
- [64] P. P. Hairston, F. D. Dorman, G. J. Sem, et al. “Apparatus for measuring particle sizes and velocities”. US5561515A. 1994.
- [65] H. Etschmaier, G. Roehrer, A. Singulani, et al. “Integrated Particulate Matter Sensor Systems”. WO2019115689A1. 2019.
- [66] V. J. Novick, P. R. Monson, and P. E. Ellison. “The effect of solid particle mass loading on the pressure drop of HEPA filters”. In: *Journal of Aerosol Science* 23.6 (Sept. 1992), pp. 657–665.
- [67] M. Richter, M. Wackerle, Y. Congar, et al. “Miniaturisierung von Mikromembranpumpen für die Integration in Mobilfunkgeräte Zusammenfassung Einführung Miniaturisierung Reduktion des Totvolumens”. In: *MikroSystemTechnik Kongress*. Vol. 0. 2017, pp. 147–150.
- [68] J. Pribošek, M. Zauner, J. Bardong, et al. “Vacuum-assisted selective adhesive imprinting for heterogeneous system integration of MOEMS devices : Automated assembly of miniaturized PM sensor”. In: *2019 IEEE SENSORS*. IEEE, Oct. 2019, pp. 1–3.
- [69] J. Symonds, D. Walker, T. Johnson, et al. *Uniformity of Particle Concentration after Mixing Aerosol Flows*. 2018.
- [70] J. Pribošek and G. Röhrer. “Estimation of the Particle Sizing Error Due to Particle Position in an Integrated PM2.5 Optical Particle Counter”. In: *Proceedings* 2.13 (Dec. 2018), p. 850.
- [71] W. von der Linden, V. Dose, and U. von Toussaint. *Bayesian probability theory*. Vol. 9781107035. Cambridge University Press, Jan. 2010, pp. 1–637.
- [72] P. Maierhofer, M. Carminati, G. Ferrari, et al. “Characterization of a Capacitive Sensor for Particulate Matter”. In: *Proceedings* 2.13 (Dec. 2018), p. 995.
- [73] P. Maierhofer, A. Buchberger, P. Breitegger, et al. “Optical Aerosol Sensing – from Air Quality to Global Warming”. In: *Applied Industrial Optics 2019*. Washington, D.C.: OSA, July 2019, M2A.2.
- [74] J. Kraft, G. Röhrer, F. Castano, et al. “Particle density sensor using evanescent wave of waveguide”. WO2019115698A1. 2017.



# **Appendix A**

## **A.1 Patent Application WO 2019/115690 A1: INTEGRATED FILTER-BASED PARTICULATE MATTER SENSORS**



## (51) International Patent Classification:

G01N 1/22 (2006.01) G01N 15/14 (2006.01)  
G01N 15/06 (2006.01)

## (21) International Application Number:

PCT/EP20 18/084759

## (22) International Filing Date:

13 December 2018 (13.12.2018)

## (25) Filing Language:

English

## (26) Publication Language:

English

## (30) Priority Data:

62/599,138 15 December 2017 (15.12.2017) US

(71) Applicants: AMS INTERNATIONAL AG [CH/CH];  
Rietstrasse 4, 8640 Rapperswil (CH). TECHNISCHE  
UNIVERSITÄT GRAZ [AT/AT]; Rechbauerstrasse 12,  
8010 Graz (AT).

(72) Inventors: ETSCHMAIER, Harald; c/o ams International AG, Rietstrasse 4, 8640 Rapperswil (CH). ROEHRER,  
Georg; c/o ams International AG, Rietstrasse 4, 8640

Rapperswil (CH). SINGULANI, Anderson; c/o ams International AG, Rietstrasse 4, 8640 Rapperswil (CH). ENICHLMAIR, Hubert; c/o ams International AG, Rietstrasse 4, 8640 Rapperswil (CH). PARK, Jong-Mun; c/o ams International AG, Rietstrasse 4, 8640 Rapperswil (CH). BERGMANN, Alexander; c/o ams International AG, Rietstrasse 4, 8640 Rapperswil (CH). MAIERHOFER, Paul; c/o ams International AG, Rietstrasse 4, 8640 Rapperswil (CH).

(74) Agent: CONROY, John; Fish & Richardson P.C., Highlight Business Towers, Mies-van-der-Rohe-Strasse 8, 80807 Munchen (DE).

(81) Designated States (unless otherwise indicated, for every kind of national protection available): AE, AG, AL, AM, AO, AT, AU, AZ, BA, BB, BG, BH, BN, BR, BW, BY, BZ, CA, CH, CL, CN, CO, CR, CU, CZ, DE, DJ, DK, DM, DO, DZ, EC, EE, EG, ES, FI, GB, GD, GE, GH, GM, GT, HN, HR, HU, ID, IL, IN, IR, IS, JO, JP, KE, KG, KH, KN, KP, KR, KW, KZ, LA, LC, LK, LR, LS, LU, LY, MA, MD, ME, MG, MK, MN, MW, MX, MY, MZ, NA, NG, NI, NO, NZ, OM, PA, PE, PG, PH, PL, PT, QA, RO, RS, RU, RW, SA,

(54) Title: INTEGRATED FILTER-BASED PARTICULATE MATTER SENSORS

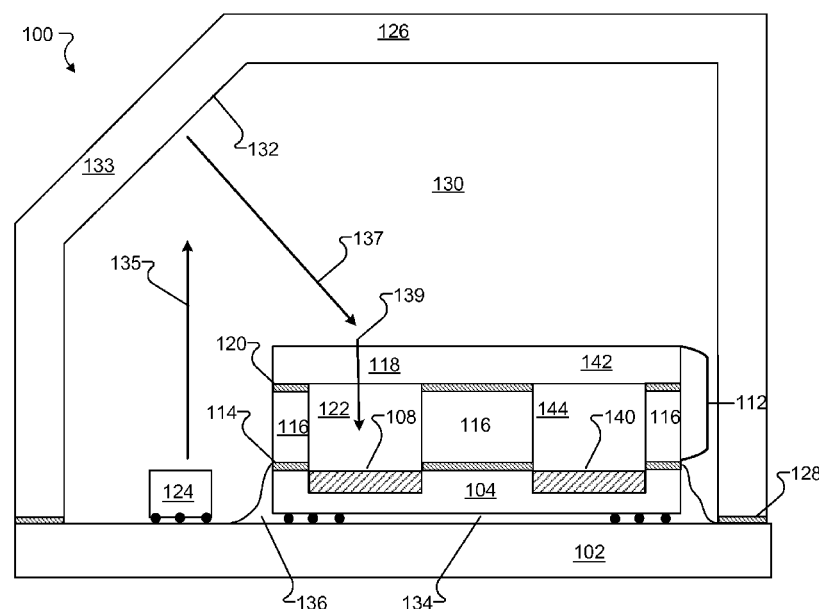


FIG. 1

(57) Abstract: An apparatus for sensing particulate matter in a fluid includes a substrate; and an integrated circuit electrically connected to the substrate, the integrated circuit including a photodetector. The apparatus includes a filter assembly including a particle filter aligned with the photodetector, and a filter housing for the particle filter, the filter housing defining a flow path for fluid through the particle filter. The apparatus includes a light source electrically connected to the substrate and positioned to illuminate the particle filter.



SC, SD, SE, SG, SK, SL, SM, ST, SV, SY, TH, TJ, TM, TN,  
TR, TT, TZ, UA, UG, US, UZ, VC, VN, ZA, ZM, ZW.

- (84) **Designated States** (*unless otherwise indicated, for every kind of regional protection available*): ARIPO (BW, GH, GM, KE, LR, LS, MW, MZ, NA, RW, SD, SL, ST, SZ, TZ, UG, ZM, ZW), Eurasian (AM, AZ, BY, KG, KZ, RU, TJ, TM), European (AL, AT, BE, BG, CH, CY, CZ, DE, DK, EE, ES, FI, FR, GB, GR, HR, HU, IE, IS, IT, LT, LU, LV, MC, MK, MT, NL, NO, PL, PT, RO, RS, SE, SI, SK, SM, TR), OAPI (BF, BJ, CF, CG, CI, CM, GA, GN, GQ, GW, KM, ML, MR, NE, SN, TD, TG).

**Published:**

— *with international search report (Art. 21(3))*

INTEGRATED FILTER-BASED PARTICULATE MATTER SENSORSClaim of Priority

[001] This application claims priority to U.S. Patent Application Serial No. 62/599,138, filed on December 15, 2017, the contents of which are incorporated here by reference in their entirety.

[002] This application incorporates by reference the entire contents of the following patent applications: U.S. Patent Application Serial No. 62/599,156, filed on December 15, 2017; U.S. Patent Application Serial No. 62/599,168, filed on December 15, 2017; and U.S. Patent Application Serial No. 62/720,492, filed on August 21, 2018.

Background

[003] There are various types of particulate matter sensors, including sensors based on optical scattering, sensors based on light absorption of filters, diffusion charging based sensors, sensors based on gravimetric filter analysis, beta attenuation sensors, tapered element oscillating microbalance sensors, and photoacoustic sensors.

Summary

[004] In an aspect, an apparatus for sensing particulate matter in a fluid includes a substrate; and an integrated circuit electrically connected to the substrate, the integrated circuit including a photodetector. The apparatus includes a filter assembly including a particle filter aligned with the photodetector, and a filter housing for the particle filter, the filter housing defining a flow path for fluid through the particle filter. The apparatus includes a light source electrically connected to the substrate and positioned to illuminate the particle filter.

[005] Embodiments can include one or more of the following features.

[006] The filter assembly is affixed to the integrated circuit.

[007] The filter assembly is affixed to the substrate.

[008] The substrate includes a printed circuit board.



[009] The light source is disposed on the substrate. The apparatus includes multiple light sources disposed on the substrate, a first light source disposed to a first side of the filter assembly and a second light source disposed to a second side of the filter assembly. The apparatus includes multiple light sources disposed on the substrate; and multiple photodetectors disposed on the substrate. Each of the multiple light sources is positioned to illuminate each photodetector with light of a substantially similar intensity.

[010] The apparatus includes multiple photodetectors disposed on the substrate, a first photodetector disposed to a first side of the filter assembly and a second photodetector disposed to a second side of the filter assembly.

[Oil] The apparatus includes a sensor housing affixed to the substrate. The sensor housing and the substrate define an interior space in which the integrated circuit, the filter assembly, and the light source are disposed. An interior surface of the sensor housing has a reflectivity of at least 30% to light emitted by the light source. The apparatus includes a layer of a reflective material disposed on an interior surface of the sensor housing. The light source is positioned to illuminate the sensor housing such that light reflected from the sensor housing illuminates the particle filter. The light source is disposed on an interior wall of the sensor housing. A cross section of the sensor housing has a curved profile.

[012] The integrated circuit includes a second photodetector. The filter assembly includes a reference particle filter aligned with the second photodetector. The filter housing does not define a flow path for fluid through the reference particle filter.

[013] The integrated circuit is electrically connected to the substrate by through silicon vias, a backside redistribution layer, and solder balls. The apparatus includes an underfill material disposed between the integrated circuit and the substrate. The apparatus includes a fillet disposed at one or more edges of the integrated circuit.

[014] The light source includes a broad spectrum light source. The photodetector includes a first region configured to detect a first wavelength emitted from the broad spectrum light source and a second region configured to detect a second wavelength emitted from the broad spectrum light source.

[015] The light source is a first light source configured to emit light at a first wavelength. The apparatus includes a second light source configured to emit light at a second wavelength. The photodetector is configured to detect the first wavelength and the second wavelength.

[016] In an aspect, a method for detecting particulate matter in a fluid includes flowing a fluid containing particulate matter through a flow path defined by a filter housing, including flowing the fluid through a particle filter disposed on the filter housing. The method includes illuminating the particle filter with light from a light source electrically connected to a substrate. The method includes detecting an optical characteristic of the particle filter by a photodetector formed in an integrated circuit electrically connected to the substrate, the photodetector being aligned with the particle filter.

[017] Embodiments can include one or more of the following features.

[018] Detecting an optical characteristic of the particle filter includes detecting an absorption of the particle filter.

[019] Detecting an optical characteristic of the particle filter includes detecting a rate of change in the optical characteristic.

[020] Illuminating the particle filter with light includes reflecting the light from the light source off of an interior wall of a sensor housing, the sensor housing and the substrate defining an interior space in which the integrated circuit, the filter housing, and the light source are disposed.

[021] The method includes stopping the flow of fluid when a threshold change in the optical characteristic of the particle filter is detected.

[022] In an aspect, a method for making an apparatus for sensing particulate matter in a fluid includes electrically connecting an integrated circuit including a photodetector to a printed circuit board substrate. The method includes disposing a filter housing on the printed circuit board substrate such that a particle filter disposed on the filter housing is aligned with the photodetector of the integrated circuit, the filter housing defining a flow path for fluid through the particle filter. The method includes electrically connecting a light source to the printed circuit board substrate such that the light source is positioned to illuminate the particle filter.

[023] Embodiments can include one or more of the following features.

[024] The method includes disposing an underfill material between the integrated circuit and the printed circuit board substrate.

[025] The method includes disposing the light source on the printed circuit board substrate.

[026] The method includes gluing the particle filter to the filter housing.

[027] Disposing the filter housing on the printed circuit board substrate includes affixing the filter housing to the integrated circuit including the photodetector. Affixing the filter housing to the integrated circuit includes gluing the filter housing to the integrated circuit.

[028] Disposing the filter housing on the printed circuit board substrate includes gluing the filter housing to the printed circuit board substrate.

[029] The method includes forming the filter housing by a molding process. Forming the filter housing includes forming multiple cavities in the filter housing.

[030] The method includes affixing a sensor housing to the printed circuit board substrate such that the sensor housing and the printed circuit board substrate define an interior space in which the integrated circuit, the filter housing, and the light source are disposed. The method includes forming the sensor housing by a molding process. The method includes disposing the light source on an interior wall of the sensor housing. The integrated circuit includes a second photodetector. The method includes affixing the filter housing to the integrated circuit such that a reference particle filter disposed on the filter housing is aligned with the second photodetector.

[031] The method includes affixing a molded cover piece onto the filter housing.

[032] Affixing a filter housing to an integrated circuit includes affixing a housing piece including multiple filter housings to a wafer including multiple integrated circuits such that each of one or more of the filter housings is aligned with a corresponding integrated circuit. The method includes singulating the wafer into multiple pieces, each piece including an integrated circuit with affixed filter housing. Electrically connecting the integrated circuit to a printed circuit board substrate includes electrically connecting the multiple pieces each including an integrated circuit to the printed circuit board substrate. The method includes singulating the printed circuit board substrate into multiple pieces.

[033] In an aspect, a sensing system for sensing particulate matter in a fluid includes an inlet microfluidic channel. The sensing system includes a particle sensing apparatus including a substrate; an integrated circuit electrically connected to the substrate, the

integrated circuit including a photodetector; a filter assembly including a particle filter aligned with the photodetector, and a filter housing for the particle filter, the filter housing defining a sensing microfluidic channel for fluid through the particle filter, the sensing microfluidic channel being fluidically connected to the inlet microfluidic channel; and a light source electrically connected to the substrate and positioned to illuminate the particle filter. The sensing system includes an outlet fluidically connected to the sensing microfluidic channel; and a fluid circulation component configured to induce fluid flow from the inlet microfluidic channel, through the sensing microfluidic channel, and out the outlet.

[034] Embodiments can include one or more of the following features.

[035] The fluid circulation component includes one or more of a pump, a fan, a heater, and an ultrasonic nozzle.

[036] The particulate matter sensors described here can have one or more of the following advantages. The particulate matter sensors are compact, and can be integrated into compact particulate matter sensing systems for use with mobile device based air quality sensing. The particulate matter sensors and sensing systems can be manufactured at low cost per sensor unit by using semiconductor manufacturing and packaging techniques.

#### Brief Description of Drawings

[037] Fig. 1 is a diagram of a particulate matter sensor.

[038] Fig. 2A is a top view of a particulate matter sensor.

[039] Figs. 2B-2D are cross sections of the particulate matter sensor of Fig. 2A.

[040] Figs 3A and 3B are diagrams of a particulate matter sensor.

[041] Fig. 4 is a diagram of a particulate matter sensor.

[042] Fig. 5 is a diagram of a particulate matter sensor.

[043] Figs. 6-8 are flow charts.

[044] Figs. 9A and 9B are exploded views of a particulate matter sensor.

[045] Figs. 10 and 11 are diagrams of particulate matter sensor systems.

[046] Figs. 12A and 12B are diagrams of a particulate matter sensor system.

[047] Fig. 13 is a diagram of a mobile computing device.

#### Detailed Description

[048] We describe here integrated particulate matter sensors that detect particulate matter present in a fluid by measuring an optical characteristic of a filter. Fluid flowing through the filter causes accumulation of particulate matter from the fluid onto the filter, changing an optical characteristic such as an absorption of light by the filter. The filter is illuminated by a light source, such as a light emitting diode, and light transmitted through the filter is measured by an integrated circuit photodiode affixed to the filter. The particulate matter sensors described here can be integrated into compact particulate matter sensing systems that can be used, e.g., to carry out mobile device based air quality sensing.

[049] Referring to Fig. 1, an example particulate matter sensor 100 includes a substrate 102, such as a printed circuit board. An integrated circuit 104, such as a silicon-based integrated circuit, e.g., a complementary metal-oxide-semiconductor (CMOS) integrated circuit, is electrically connected to the substrate 102. In some examples, the integrated circuit 104 can be connected to the substrate 102 by through silicon vias (TSVs), a backside redistribution layer, and solder balls. In some examples, the integrated circuit 104 can be connected to the substrate by wire bonding. Other types of connections can also be used. The integrated circuit 104 includes a photodetector 108, such as a photo diode, a pinned photo diode, a pin photodiode, an avalanche photo diode, a single photon avalanche photo diode, or another type of photo diode. In some examples, e.g., to reduce cross talk, the photodetector 108 can be a photodetector that has a low sensitivity to carriers generated within the semiconductor body of the integrated circuit 104, such as a substrate isolated photo diode (e.g., p+ in an n-well for a p-type integrated circuit body).

[050] A filter assembly 112 is affixed to the integrated circuit 104 by a connection layer 114, such as an adhesive or a weld. The filter assembly 112 includes a filter housing 116 that holds a particle filter 118, such as a hydrophobic fiber filter, a pore membrane filter, or another type of filter. For instance, the particle filter 118 can be affixed to the filter housing 116 by a layer of adhesive 120. The particle filter 118 can have openings sized such that particulate matter of a target size cannot pass through the particle filter 118. For instance, the particle filter can have openings with a diameter of less than about 100 nm. The filter housing 116 can be formed of a molded material, such as a molded

plastic. The filter housing 116 holds the particle filter 118 in alignment with the photodetector 108 such that a cavity 122 is defined between the particle filter 118 and the integrated circuit 104. The cavity 122 is fluidically connected to a laterally-oriented flow channel through the filter housing 116 such that the cavity 122 and the flow channel together form a flow path for fluid to flow through the particle filter 118, discussed further with respect to Figs. 2A-2D.

**[051]** A light source 124, such as a light-emitting diode (LED), a vertical cavity surface emitting laser (VCSEL), a laser diode, or another type of light source, is electrically connected to the substrate 102, e.g., by solder balls, wire bonding, or another type of connection. The light source 124 is positioned such that light emitted from the light source 124 illuminates the particle filter 118. In the particulate matter sensor 100, the light source 124 is disposed on the substrate 102 and electrically connected to the substrate 102, e.g., by solder balls, wire bonding, or another type of connection. In some examples, the light source 124 can be mounted on a molded interconnect device that is connected to the substrate 102.

**[052]** A sensor housing 126 is affixed to the substrate 102, e.g., by an adhesive 128. The sensor housing 126 can be formed of a molded material, such as a molded plastic. The sensor housing 126 and the substrate 102 define an interior space 130 within which the integrated circuit 104, the filter assembly 112, and the light source 124 are disposed.

**[053]** The material or color, or both, of the sensor housing 126 can be selected such that light emitted from the light source 124 and incident on an interior surface 132 of the sensor housing 126 (shown as an arrow 135) is reflected by the interior surface 132 onto the particle filter 118 (shown as an arrow 137). For instance, the interior surface 132 of the sensor housing 126 can be reflective to light emitted by the light source 124, e.g., having at least 30% reflectivity to the wavelength(s) of light emitted by the light source 124. In some examples, the interior surface 132 of the sensor housing 126 can be coated with a reflective material, such as an aluminum film. In some examples, the sensor housing 126 can be shaped such that a large amount of light incident from the light source 124 is reflected onto the particle filter 118. For instance, a wall 133 of the sensor housing 126 can be angled and/or curved relative to the substrate 102 to cause light reflection onto the particle filter 118.

**[054]** In some examples, the material or color, or both, of an exterior surface of the filter housing 116 can also be reflective to light emitted from the light source 124. In some examples, the exterior surface of the filter housing 116 can be coated with a

reflective material, such as an aluminum film. In some examples, the material or color, or both, of an interior surface of the filter housing 116 can also be reflective, e.g., coated with a reflective material, such as an aluminum film.

**[055]** In operation, light emitted from the light source 124 is incident on the particle filter 118 (e.g., via reflection from the interior surface 132 of the sensor housing 126). The photodetector 108 measures an amount of light transmitted through the particle filter 118 (shown as an arrow 139). As particle loaded fluid flows through the particle filter 118, particulate matter accumulates on or in the filter 118. The particulate matter on or within the particle filter 118 causes absorption, scattering, or both, of the light incident on the particle filter 118, reducing the amount of light transmitted through the particle filter 118. The change in intensity of the light transmitted through the particle filter 118 is an indication of the amount of particulate matter in the fluid.

**[056]** In some examples, the volume between the integrated circuit 104 and the substrate 102 is filled with an underfill material 134, e.g., to reduce or prevent fluid flow between the integrated circuit 104 and the substrate 102. In some examples, a fillet 136 can be formed at the lateral edges of the integrated circuit 104 to reduce cross talk between the light source 124 and the photo sensor 108.

**[057]** In the example particulate matter sensor 100 of Fig. 1, a second photodetector 140 is formed in the integrated circuit 104. The filter housing 116 holds a reference particle filter 142 in alignment with the second photodetector 140. A cavity 144 is defined between the reference particle filter 142 and the integrated circuit 104. However, the cavity 144 does not connect to a flow channel through the filter housing 116, so there is no flow path for fluid flow through the reference particle filter 142. In the example of Fig. 1, the reference particle filter 142 is the same piece of material as the particle filter 118. In some examples, the particle filter 118 and the reference particle filter 142 are formed of distinct pieces of material. In some examples, no reference particle filter is present. In the particulate matter sensor 100, the second photodetector 140 is formed in the same integrated circuit 104 as the photodetector 108. In some examples, the second photodetector 140 can be formed on a distinct integrated circuit from the integrated circuit 104 of the photodetector 108.

**[058]** The reference particle filter 142 allows for correction of measurement error due to variability in the intensity of the light source 124. As particle-loaded fluid flows through the particle filter 118, particulate matter accumulates in or on the particle filter 118. For instance, for a porous membrane filter, particulate matter can accumulate on the

surface of the filter; for a fibrous filter, particulate matter can accumulate on the surface and in the bulk of the filter. However, no fluid flows through the reference particle filter 142, so there is little to no particulate matter accumulation on the reference particle filter 142. In a system with no variability in the intensity of the light source, the amount of light transmitted through the reference particle filter 142 and detected by the photodetector 140 would be substantially constant over time. Variations in the amount of light detected by the photodetector 140 can indicate variability in the intensity of the light source and can be used to adjust the signal detected by the photodetector 108.

**[059]** In some examples, a particulate matter sensor can include multiple light sources, such as two, three, four, or more than four light sources. For instance, two light sources can be positioned on opposite sides of the filter assembly 112, e.g., along a lateral symmetry line between the two photo sensors 108, 140 or aligned perpendicular to the lateral symmetry line. Four light sources can be positioned one on each side of the filter assembly. In some examples, multiple light sources can be positioned on each of one or more of the sides of the filter assembly, e.g., to provide a greater signal to the photodetectors 108, 140. The multiple light sources can emit each with substantially the same spectral distribution to enhance the total optical power available in the particulate matter sensor 100.

**[060]** In some examples, multiple wavelengths can be used to enable the identification of different types of particulate matter (referred to as source apportionment). In some examples, each light source of multiple light sources can emit light of a different wavelength, e.g., light sources mounted symmetrically with respect to the photodetectors 108, 140, and the photodetectors 108, 140 can be configured to detect some or all of the wavelengths emitted by the multiple light sources. In some examples, one or more broad spectrum light sources, such as white LEDs, can be used to provided multiple wavelengths. For multiple wavelength sensing, the photodetectors 108, 140 can be divided into multiple regions, with each region covered with a wavelength filter to enable detection of specific wavelengths. For instance, the photodetectors 108, 140 can each be divided into a first region sensitive to infrared light (e.g., 880 nm wavelength light) and a second region sensitive to blue light (e.g., 470 nm light).

**[061]** Fig. 2A shows a top view of a particulate matter sensor 200 having two light sources 124a, 124b positioned on opposite sides of the filter assembly 112. Figs. 2B, 2C, and 2D show cross sections of the particulate matter sensor 200 along lines A-A', B-B', and C-C', respectively. These cross sections depict the presence of a flow path for fluid



flow through the particle filter 118 and the absence of a flow path such that fluid does not flow through the reference particle filter 142.

[062] Referring to Fig. 2B, the cross section along line A-A' shows the cavity 122 between the particle filter 118 and the integrated circuit 104 and the cavity 144 between the reference particle filter 142 and the integrated circuit 104. Referring to Fig. 2C, the cross section along line B-B' shows a cross section of a laterally-oriented flow channel 202 fluidically connected to the cavity 122. No such flow channel exists for the reference particle filter, and the cavity 144 is not fluidically connected to any flow channel. Referring to Fig. 2D, cross section along line C-C' shows that the flow channel 202 extends through the filter housing 116.

[063] The cavity 122 and the laterally-oriented flow channel 202 together define a flow path that enables fluid to flow through the particle filter 118. As fluid flows through the particle filter 118, particulate matter from the fluid accumulates on the particle filter 118. The absence of a flow channel connected to the cavity 144 means that there is no flow path that enables fluid to flow through the reference particle filter 142, which minimizes particulate deposition onto the reference particle filter 142.

[064] Referring to Figs. 3A and 3B, an example particulate matter sensor 300 includes a sensor housing 326 having a curved cross sectional profile, such as a spherical shape, an elliptical shape, or a parabolic mirror shape. The curved shape of the sensor housing 326 helps to reflect light from the light source 124 toward the particle filter 118, e.g., the sensor housing 326 acts as an integrating sphere. A fluid inlet 328 formed in the sensor housing 326 provides a flow pathway for fluid to enter into the particulate matter sensor 300.

[065] Referring to Fig. 4, an example particulate matter sensor 400 includes a sensor housing 426 having a wall 422 oriented substantially perpendicular to the substrate 102. A light source 424 is integrated into or affixed onto the wall 422, e.g., by an adhesive 430. To achieve this, the sensor housing 426 includes interconnect features (not shown), e.g., connected to the substrate 102 by a conductive adhesive 428. In areas of the sensor housing without interconnect features, a non-conductive adhesive is used. In this configuration, light emitted from the light source 424 (shown as arrows 435) is incident directly onto the particle filter 118 and the reference particle filter 142, which can increase the amount of light incident on the filter relative to configurations in which the light is reflected.

**[066]** Referring to Fig. 5, an example particulate matter sensor 500 includes multiple light sources 524a, 524b. Multiple photodetectors 542a, 542b are disposed on the substrate 102 external to the filter assembly 112, and electrically connected to the substrate 102. For instance, the photodetectors 542a, 542b can be disposed to opposite sides of the filter assembly 112. The external photodetectors 542a, 542b can be used to measure reflection of light from the filters 118, 142, e.g., by alternating illumination of the sides of the filter assembly 112. In the example of Fig. 5, the particulate matter sensor 500 is shown as having generally a similar structure as the particulate matter sensor 100 of Fig. 1; however, external photodetectors can also be used in other sensor configurations, such as those shown in Figs. 3 and 4. The configuration of Fig. 5, with multiple external photodetectors, can also be used without the use of a reference particulate filter (e.g., without the filter 142 and associated photodetector 140).

**[067]** Referring to Fig. 6, in an example process for detecting particulate matter in a fluid, a fluid is flowed along a flow path through a filter housing, including through a particle filter affixed to the filter housing (600). The filter housing is affixed to an integrated circuit that is electrically connected to a substrate, such as a printed circuit board. Particulate matter in the fluid accumulates on the particle filter as the fluid flows through the particle filter (602). The particle filter is illuminated with light from a light source that is electrically connected to the substrate (604). For instance, light emitted from the light source can be incident on an interior surface of a sensor housing and reflected from the interior surface of the sensor housing onto the particle filter.

**[068]** An optical characteristic of the particle filter is detected by a photodetector formed in the integrated circuit and aligned with the particle filter (606). The optical characteristic can include an amount of light transmitted through the particle filter or an absorption of the particle filter. The optical characteristic can include a rate of change of an optical characteristic, such as a rate of change in the amount of light transmitted through the particle filter or a rate of change in the absorption of the particle filter. The detected optical characteristic can be used to characterize a quality of the fluid (608), such as an air quality, e.g., an amount of particulate matter in the fluid (e.g., an amount of black carbon in the fluid).

**[069]** The particulate matter sensor can form part of a microfluidic sensor system, described below. Over time, the filter can become full of particulate matter such that little to no light is transmitted through the filter. To increase the useful lifetime of the particulate matter sensor, the sensor system can be operated in sessions. Operation of the

sensor system in a session can be stopped when a threshold is reached in measurement of the optical characteristic, such as a threshold noise level, a threshold change or percentage change in the absorption of the filter from the beginning of the session. If the fluid quality is poor (many particles in the fluid), the measurement time will be short. If the fluid is relatively clean (few particles in the fluid), the measurement time will be longer. With this approach, the number of measurement sessions the particulate matter sensor is capable of carrying out can be relatively independent of the particle concentration in the fluid.

**[070]** Referring to Fig. 7, in an example process for making a particulate matter sensor, a filter housing is formed, e.g., by a molding process, e.g., injection molding (700). The filter housing can be molded to include a cavity and a flow channel connected to the cavity and providing an outlet from the filter housing. In cases in which a reference particle filter is to be used, the filter housing can be molded to include a second cavity that is not connected to a flow channel. In some examples, the filter housing can be molded from a material that is reflective, e.g., greater than 30% reflective, to light of a wavelength to be used in the particulate matter sensor. In some examples, the filter housing is made such that an exterior surface of the housing, an interior surface of the housing, or both, are a reflective color, such as white. In some examples, the molded filter housing (e.g., the exterior surface, the interior surface, or both) is coated with a reflective layer, such as a layer of aluminum.

**[071]** The filter housing is affixed to an integrated circuit including a photodetector, e.g., by an adhesive (702), such that the cavity formed in the filter housing is aligned with the photodetector. In cases in which a reference particle filter is to be used, two cavities are formed in the filter housing, and each cavity is aligned with a corresponding one of the photodetectors.

**[072]** A particle filter is disposed on and affixed to the filter housing (704) in alignment with the cavity or cavities formed in the filter housing. In some examples, the filter housing is affixed to the integrated circuit prior to affixing the particle filter to the filter housing; in some examples, the particle filter is affixed to the filter housing prior to affixing the filter housing to the integrated circuit.

**[073]** The integrated circuit with the attached filter housing is electrically connected to a printed circuit board (PCB) substrate (706). In cases in which a reference particle filter is to be used, the integrated circuit can include a second photodetector. In some examples, two integrated circuits each including a photodetector can be electrically

connected to the PCB. In some examples, the integrated circuit(s) can be connected to the substrate by TSVs, a backside redistribution layer, and solder balls. In some examples, the integrated circuit(s) can be connected to the substrate by wire bonding.

[074] One or more light sources, such as LEDs or VCSELs, are positioned on and electrically connected to the PCB (708). For instance, the one or more light sources are disposed on the PCB and electrically connected to the PCB by TSVs, a backside redistribution layer, and solder balls, or by wire bonding. In some examples, the light sources can be electrically connected to the PCB substrate prior to connecting the integrated circuit.

[075] An underfill material is disposed between the integrated circuit(s) and the PCB and a fillet can be formed at the lateral edges of the integrated circuit(s) (710).

[076] A sensor housing is formed, e.g., by a molding process, e.g., injection molding (712). The sensor housing can be molded such that a wall of the sensor housing is angled, such that when assembled, the angled wall can help reflect light from the light source onto the particle filter. The sensor housing can be molded into a partial spherical shape.

[077] The sensor housing is affixed to the PCB (714), e.g., by an adhesive, such that the integrated circuit(s), the filter housing, and the light source are disposed within an interior space defined by the sensor housing and the PCB.

[078] In cases in which the one or more light sources are disposed on the sensor housing, the light sources can be affixed to the sensor housing, e.g., by an adhesive, and electrical connection features of the sensor housing can be electrically connected to the PCB.

[079] The particulate matter sensors described here can be fabricated in parallel, e.g., for efficient and low-cost manufacturing. For instance, multiple particulate matter sensors, e.g., hundreds of sensors, can be fabricated in parallel on a single PCB substrate, and the printed circuit board substrate with the multiple sensors formed thereon can then be singulated into individual dies.

[080] Referring to Fig. 8, in an example process for parallel manufacture of multiple particulate matter sensors, a wafer including multiple integrated circuits, each integrated circuit including a photodetector, is processed (800). The processing can include forming TSVs and a backside redistribution layer.

[081] A housing piece including multiple filter housings is formed (802), e.g., by injection molding, and attached to the wafer (804). The housing piece can be similarly sized to the wafer and the housing piece can be attached such that each filter housing is aligned with a corresponding integrated circuit of the wafer. Filters are attached to the filter housings in the molded piece (806). The wafer including the housing piece is singulated into individual integrated circuits (808), each integrated circuit having an attached filter housing.

[082] Multiple light sources are attached to a PCB substrate (810). The integrated circuits with attached filter housings are attached to the PCB substrate (812). An underfill material is disposed between each integrated circuit and the PCB substrate, and a fillet is formed at the lateral edges of each integrated circuit (814).

[083] A sensor housing piece including multiple sensor housings is formed (816), e.g., by injection molding, and attached to the PCB substrate (818). The PCB substrate is singulated into multiple individual particulate matter sensors (820).

[084] Figs. 9A and 9B are exploded views of an example particulate matter sensor 900. In this example, two integrated circuits 904a, 904b each including a photodetector are disposed on and electrically connected to a PCB substrate 902. Four light sources 926a-926d (referred to collectively as light sources 926) are also disposed on and electrically connected to the PCB substrate 902. For instance, two of the light sources 926a, 926c can emit light at a first wavelength (e.g., 900 nm) and the other two light sources can emit light at a second wavelength 926b, 926d (e.g., 500 nm), enabling source apportionment. The light sources 926 are positioned such that each light source can generate a similar light intensity on both photodetectors.

[085] A bottom molded piece 950 is disposed on and affixed to the PCB substrate 902, e.g., by an adhesive. The bottom molded layer 950 is molded to define cavities 922, 944 and two interior regions 954a, 954b. A lateral flow channel 952 connected to the cavity 922 is also defined in the bottom molded layer 950. The bottom molded layer 950 is disposed on the PCB substrate 902 such that the cavities 922, 944 are aligned with the photodetectors in the integrated circuits 904a, 904b. A filter 918 is disposed on and affixed to the bottom molded layer 950 to cover the top opening of both cavities 922, 944, forming a particle filter and a reference particle filter. The presence of walls 956 of the bottom molded layer 950 between the light sources 924 and the integrated circuits 904 with the photodetectors can help reduce cross-talk between the light sources and the photodetectors.

[086] A top molded piece 960 is disposed on and affixed to the top surface of the bottom molded piece 950. The top molded piece 960 defines an interior region 962. The interior regions 954a, 954b defined by the bottom molded piece 950 and the interior region 962 defined by the top molded piece 960 together form an interior space within which light from the light sources 924 can travel. A fluid inlet 964 is defined in the top molded piece to allow fluid to enter into the particulate matter sensor 900.

[087] The adhesive used in assembling the particulate matter sensor 900 can be applied in only two planes: the plane connecting the bottom molded piece 950 to the PCB substrate 902 and the plane connecting the top molded piece 960 to the bottom molded piece 950. Adhesive can also be applied to affix the filter 918 to the bottom molded layer 950.

[088] The particulate matter sensors described here can be incorporated into microfluidic particulate matter sensor systems. The integration of the filter with the integrated circuit including the photodetector, and the placement of the light source and the integrated circuit on the same PCB substrate enables the particulate matter sensors to be compact. For instance, particulate matter sensor systems incorporating the particulate matter sensors described here can have a height of less than about 3 mm, e.g., less than about 2 mm; and a footprint of less than about 10x10 mm<sup>2</sup>.

[089] Referring to Fig. 10, a particulate matter sensor 20 such as those described above is incorporated into a particulate matter sensor system 250. A microfluidic flow path is defined through the particulate matter sensor system 250 from an inlet 254, through the particulate matter sensor 20, and out through an outlet 256. The entire particulate matter sensor system 250, including the particulate matter sensor 20, is built on the same PCB substrate 252.

[090] The example particulate matter sensor 20, which includes a filter assembly 262, is structured similarly to the particulate matter sensor 100 of Fig. 1. Other configurations of the particulate matter sensor are also compatible with the particulate matter sensor system 250, such as the configurations shown in Figs. 2-4. A light source 274 of the particulate matter sensor 20 is controlled by a microcontroller 258 disposed on and electrically connected to the PCB substrate 252.

[091] A cover layer 270 is disposed over the PCB substrate 252 such that an interior space between the cover layer 270 and the PCB substrate 252 define the flow path through the sensor system 250. For instance, the cover layer 270 can be a molded piece,

e.g., a molded plastic piece. In the example of the particulate matter sensor system 250, the cover layer 270 serves both to define the flow path and as the sensor housing (e.g., the sensor housing 126 of Fig. 1) of the particulate matter sensor 20. For instance, the cover layer 270 can have an interior surface that is reflective to light emitted by the light source 274 of the particulate matter sensor 20.

**[092]** A fluid circulation device 260 is disposed on the PCB substrate 252 and drives fluid flow through the sensor system 250. The fluid circulation device can be, e.g., a pump, a fan, a heater, an ultrasonic nozzle, or another device capable of causing fluid flow through the sensor system 250. In the example of Fig. 9, the fluid circulation device 260 is a piezoelectric membrane pump. The fluid circulation device 260 is controlled by a controller 264, coupled to one or more capacitors and inductors 266, all of which are disposed on and electrically connected to the PCB substrate 252.

**[093]** The particulate matter sensor system 250 can include a heater 268 positioned at the inlet 254 of the microfluidic flow path. The heater 268, e.g., a resistive heater, can heat the fluid flowing into the sensor system 250, e.g., to reduce condensation of humidity in the air flowing through the system. In some examples, the heater 268 can function as a flow sensor to detect a mass flow rate of fluid in the sensor system 250. For instance, the mass flow rate of fluid can be determined based on a change in temperature of the fluid flowing through the heater 268.

**[094]** The particulate matter sensor system 250 can include a size separation feature 272, such as an impactor, for preventing particles above a threshold size from flowing through the rest of the microfluidic flow path. For instance, particles above a threshold size may not be of interest for air quality measurements, but would cause a significant change in optical characteristics of the filter of the particulate matter sensor 20 if allowed to flow through the rest of the microfluidic flow path. Separating out these larger particles can enable more precise measurements of particulate matter in a desired size range.

**[095]** In some particulate matter sensor systems, a filter is present upstream from an inlet to a chamber 280 of the fluid circulation device 260, e.g., in a region 282. Such a filter can prevent particulate matter from adversely affecting the operation of the fluid circulation device 260. In particulate matter sensor systems incorporating filter-based particulate matter sensors, such as the particulate matter sensor system 250 of Fig. 10, no filter is present in the region 282, e.g., because the filter of the filter-based particulate

matter sensor 20 serves to prevent particulate matter from progressing downstream through the microfluidic flow path in the sensor system.

[096] Referring to Fig. 11, a particulate matter sensor 30 such as those described above is incorporated into a particulate matter sensor system 350. In the particulate matter sensor system 350, a cover layer 370 disposed over the PCB substrate 252 defines a flow path through the sensor system 350. The cover layer 370 is distinct from a sensor housing 376 that defines an interior space 380 for the particulate matter sensor 30. In this configuration, an interior surface of the sensor housing 376 can be reflective to light emitted by a light source 374 of the particulate matter sensor 30. However, the light from the light source 374 does not reach the interior surface of the cover layer 370.

[097] The example particulate matter sensor 30 is structured similarly to the particulate matter sensor 400 of Fig. 4. Other configurations of the particulate matter sensor are also compatible with the particulate matter sensor system 350, such as the configurations shown in Figs. 1-3 and Fig. 5.

[098] Referring to Figs. 12A and 12B, a particulate matter sensor 40 such as those described above, including photodetectors 42, light sources 44, and a filter 46, is incorporated into a particulate matter sensor system 450. The sensor system 450 includes a PCB substrate 452 on which components 454 of the sensor system are disposed, such as controllers, capacitors, and inductors. A base part 456, e.g., a molded component, is formed to define portions of various components of the sensor system 450. For instance, the base part 456 can define the filter assembly of the particulate matter sensor 40. The base part 456 can also define an inlet 462 into a fluid circulation device 460 and an outlet 464 from the fluid circulation device. A cover layer 470 is disposed over the base part 456 and connected to the base part 456, e.g., by a form closure. The base part 456, the cover layer 470, or both define microfluidic channels of the flow path through the sensor system 450. In some examples, components of the sensor system 450, such as a size separation feature 458, can be defined by the structure of the base part 456, the cover layer 470, or both. For instance, in the example of Fig. 12A, the size separation feature 458 is formed between the base part 456 and the PCB substrate 452 and defined by the shape of the base part 456.

[099] In the configuration of the particulate matter sensor system 450, fluid passes first through a chamber of the sensor system 450 in which the photodetectors 42 are disposed, meaning that particulate matter in the fluid will not pass through a reference filter and also will not pass over the light sources 44. This configuration can help prevent



contamination of the reference filter and adverse effects that can result from particulate matter contamination of the light sources 44.

**[0100]** The fabrication of the particulate matter sensors and sensor systems described here is compatible with high-throughput, low-cost manufacturing techniques such as injection molding and microelectronics processing and packaging techniques, enabling rapid and economical manufacturing of these sensors and sensor systems.

**[0101]** Additional description of particulate matter sensor systems can be found in PCT Application No. [[Attorney Docket No. 45768-001 1WO1/120-17]], the contents of which are incorporated here by reference in their entirety.

**[0102]** Referring to Fig. 13, a particulate matter sensor system 50 such as those described above can be incorporated into a mobile computing device 52, such as a mobile phone (as shown), a tablet, or a wearable computing device. The particulate matter sensor system 50 can be operable by a user, e.g., under control of an application executing on the mobile computing device 52, to conduct air quality testing. A test result can be displayed on a display screen 54 of the mobile computing device 52, e.g., to provide substantially immediate feedback to the user about the quality of the air in the user's environment.

**[0103]** The particulate matter sensor systems described here can also be incorporated into other devices, such as air purifiers or air conditioning units; or used for other applications such as automotive applications or industrial applications.

**[0104]** A number of embodiments have been described. Nevertheless, it will be understood that various modifications may be made without departing from the spirit and scope of the invention. For example, some of the steps described above may be order independent, and thus can be performed in an order different from that described.

**[0105]** Other implementations are also within the scope of the following claims.

What is claimed is:

1. An apparatus for sensing particulate matter in a fluid, the apparatus comprising:
  - a substrate;
  - an integrated circuit electrically connected to the substrate, the integrated circuit including a photodetector;
  - a filter assembly comprising:
    - a particle filter aligned with the photodetector, and
    - a filter housing for the particle filter, the filter housing defining a flow path for fluid through the particle filter; and
  - a light source electrically connected to the substrate and positioned to illuminate the particle filter.
2. The apparatus of claim 1, in which the filter assembly is affixed to the integrated circuit.
3. The apparatus of claim 1 or 2, in which the filter assembly is affixed to the substrate.
4. The apparatus of any of the preceding claims, in which the substrate comprises a printed circuit board.
5. The apparatus of any of the preceding claims, in which the light source is disposed on the substrate.
6. The apparatus of claim 5, comprising multiple light sources disposed on the substrate, a first light source disposed to a first side of the filter assembly and a second light source disposed to a second side of the filter assembly.
7. The apparatus of claim 5 or 6, comprising:
  - multiple light sources disposed on the substrate; and
  - multiple photodetectors disposed on the substrate,

in which each of the multiple light sources is positioned to illuminate each photodetector with light of a substantially similar intensity.

8. The apparatus of any of the preceding claims, comprising multiple photodetectors disposed on the substrate, a first photodetector disposed to a first side of the filter assembly and a second photodetector disposed to a second side of the filter assembly.
9. The apparatus of any of the preceding claims, comprising a sensor housing affixed to the substrate, the sensor housing and the substrate defining an interior space in which the integrated circuit, the filter assembly, and the light source are disposed.
10. The apparatus of claim 9, in which an interior surface of the sensor housing has a reflectivity of at least 30% to light emitted by the light source.
11. The apparatus of claim 9 or 10, comprising a layer of a reflective material disposed on an interior surface of the sensor housing.
12. The apparatus of any of claims 9 to 11, in which the light source is positioned to illuminate the sensor housing such that light reflected from the sensor housing illuminates the particle filter.
13. The apparatus of any of claims 9 to 12, in which the light source is disposed on an interior wall of the sensor housing.
14. The apparatus of any of claims 9 to 13, in which a cross section of the sensor housing has a curved profile.
15. The apparatus of any of the preceding claims, in which the integrated circuit comprises a second photodetector, and in which the filter assembly comprises a reference particle filter aligned with the second photodetector.
16. The apparatus of claim 15, in which the filter housing does not define a flow path for fluid through the reference particle filter.

17. The apparatus of any of the preceding claims, in which the integrated circuit is electrically connected to the substrate by through silicon vias, a backside redistribution layer, and solder balls.
18. The apparatus of claim 17, comprising an underfill material disposed between the integrated circuit and the substrate.
19. The apparatus of claim 18, comprising a fillet disposed at one or more edges of the integrated circuit.
20. The apparatus of any of the preceding claims, in which the light source comprises a broad spectrum light source, and in which the photodetector includes a first region configured to detect a first wavelength emitted from the broad spectrum light source and a second region configured to detect a second wavelength emitted from the broad spectrum light source.
21. The apparatus of any of the preceding claims, in which the light source is a first light source configured to emit light a first wavelength, and comprising a second light source configured to emit light at a second wavelength; and
- in which the photodetector is configured to detect the first wavelength and the second wavelength.
22. A method for detecting particulate matter in a fluid, the method comprising:
- flowing a fluid containing particulate matter through a flow path defined by a filter housing, including flowing the fluid through a particle filter disposed on the filter housing;
- illuminating the particle filter with light from a light source electrically connected to a substrate; and
- detecting an optical characteristic of the particle filter by a photodetector formed in an integrated circuit electrically connected to the substrate, the photodetector being aligned with the particle filter.

23. The method of claim 22, in which detecting an optical characteristic of the particle filter comprises detecting an absorption of the particle filter.
24. The method of claim 22 or 23, in which detecting an optical characteristic of the particle filter comprises detecting a rate of change in the optical characteristic.
25. The method of any of claims 22 to 24, in which illuminating the particle filter with light comprises reflecting the light from the light source off of an interior wall of a sensor housing, the sensor housing and the substrate defining an interior space in which the integrated circuit, the filter housing, and the light source are disposed.
26. The method of any of claims 22 to 25, comprising stopping the flow of fluid when a threshold change in the optical characteristic of the particle filter is detected.
27. A method for making an apparatus for sensing particulate matter in a fluid, the method comprising:
- electrically connecting an integrated circuit including a photodetector to a printed circuit board substrate;
  - disposing a filter housing on the printed circuit board substrate such that a particle filter disposed on the filter housing is aligned with the photodetector of the integrated circuit, the filter housing defining a flow path for fluid through the particle filter; and
  - electrically connecting a light source to the printed circuit board substrate such that the light source is positioned to illuminate the particle filter.
28. The method of claim 27, comprising disposing an underfill material between the integrated circuit and the printed circuit board substrate.
29. The method of claim 27 or 28, comprising disposing the light source on the printed circuit board substrate.

30. The method of any of claims 27 to 29, comprising gluing the particle filter to the filter housing.
31. The method of any of claims 27 to 30, in which disposing the filter housing on the printed circuit board substrate comprises affixing the filter housing to the integrated circuit including the photodetector.
32. The method of claim 31, in which affixing the filter housing to the integrated circuit comprises gluing the filter housing to the integrated circuit.
33. The method of any of claims 27 to 32, in which disposing the filter housing on the printed circuit board substrate comprises gluing the filter housing to the printed circuit board substrate.
34. The method of any of claims 27 to 33, comprising forming the filter housing by a molding process.
35. The method of claim 34, in which forming the filter housing comprises forming multiple cavities in the filter housing.
36. The method of any of claims 27 to 35, comprising affixing a sensor housing to the printed circuit board substrate such that the sensor housing and the printed circuit board substrate define an interior space in which the integrated circuit, the filter housing, and the light source are disposed.
37. The method of claim 36, comprising forming the sensor housing by a molding process.
38. The method of claim 36 or 37, comprising disposing the light source on an interior wall of the sensor housing.
39. The method of any of claims 36 to 38, in which the integrated circuit comprises a second photodetector, and

in which the method comprises affixing the filter housing to the integrated circuit such that a reference particle filter disposed on the filter housing is aligned with the second photodetector.

40. The method of any of claims 27 to 39, comprising affixing a molded cover piece onto the filter housing.

41. The method of any of claims 27 to 40, in which affixing a filter housing to an integrated circuit includes affixing a housing piece including multiple filter housings to a wafer including multiple integrated circuits such that each of one or more of the filter housings is aligned with a corresponding integrated circuit.

42. The method of claim 41, comprising singulating the wafer into multiple pieces, each piece including an integrated circuit with affixed filter housing.

43. The method of claim 42, in which electrically connecting the integrated circuit to a printed circuit board substrate comprises electrically connecting the multiple pieces each including an integrated circuit to the printed circuit board substrate.

44. The method of claim 43, comprising singulating the printed circuit board substrate into multiple pieces.

45. A sensing system for sensing particulate matter in a fluid, the sensing system comprising:

an inlet microfluidic channel;

a particle sensing apparatus comprising:

a substrate;

an integrated circuit electrically connected to the substrate, the integrated circuit including a photodetector;

a filter assembly comprising:

a particle filter aligned with the photodetector, and

a filter housing for the particle filter, the filter housing defining a sensing microfluidic channel for fluid through the particle filter, the sensing microfluidic channel being fluidically connected to the inlet microfluidic channel; and

a light source electrically connected to the substrate and positioned to illuminate the particle filter;

an outlet fluidically connected to the sensing microfluidic channel; and

a fluid circulation component configured to induce fluid flow from the inlet microfluidic channel, through the sensing microfluidic channel, and out the outlet.

46. The sensing system of claim 45, in which the fluid circulation component comprises one or more of a pump, a fan, a heater, and an ultrasonic nozzle.



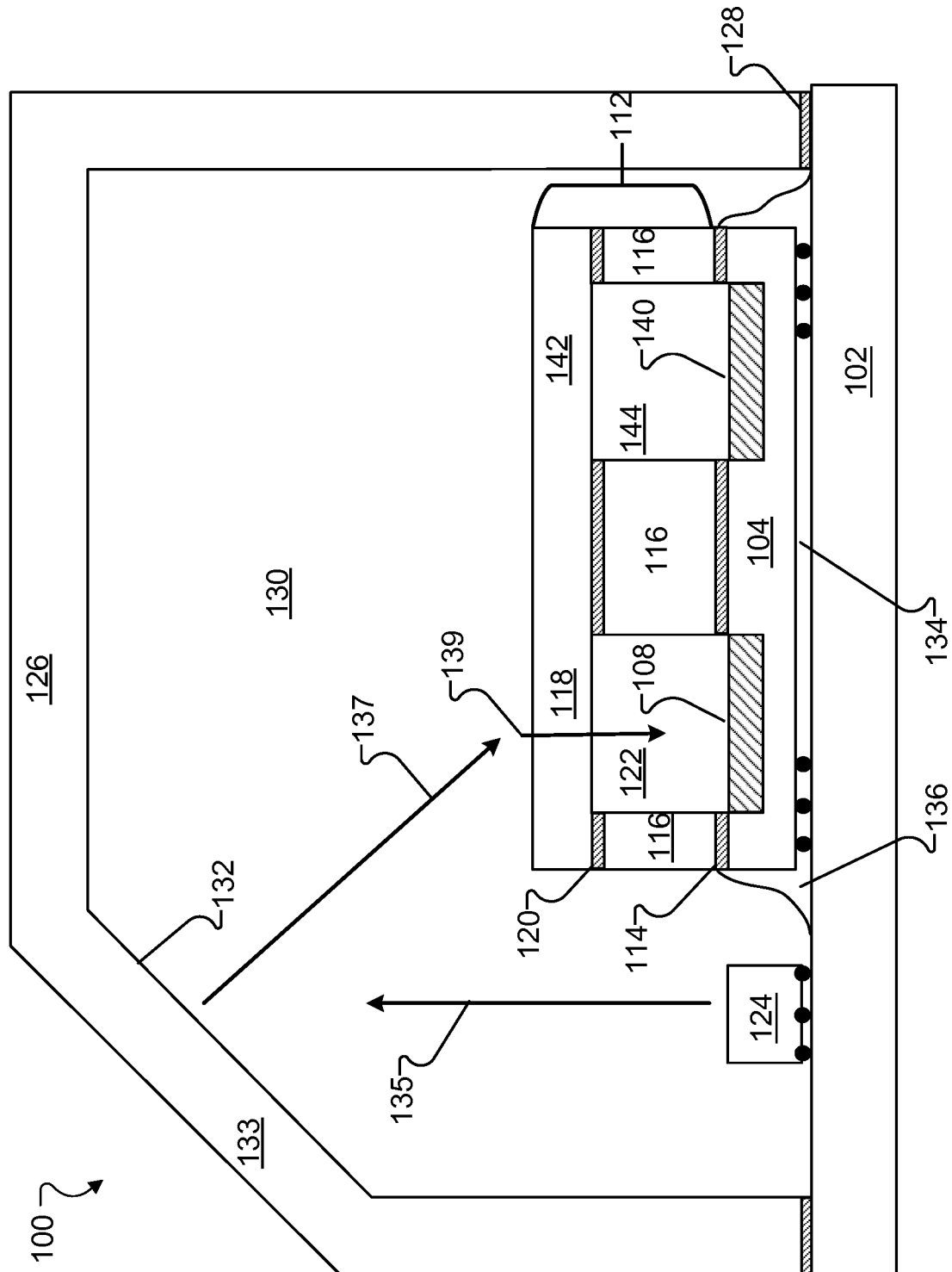


FIG. 1

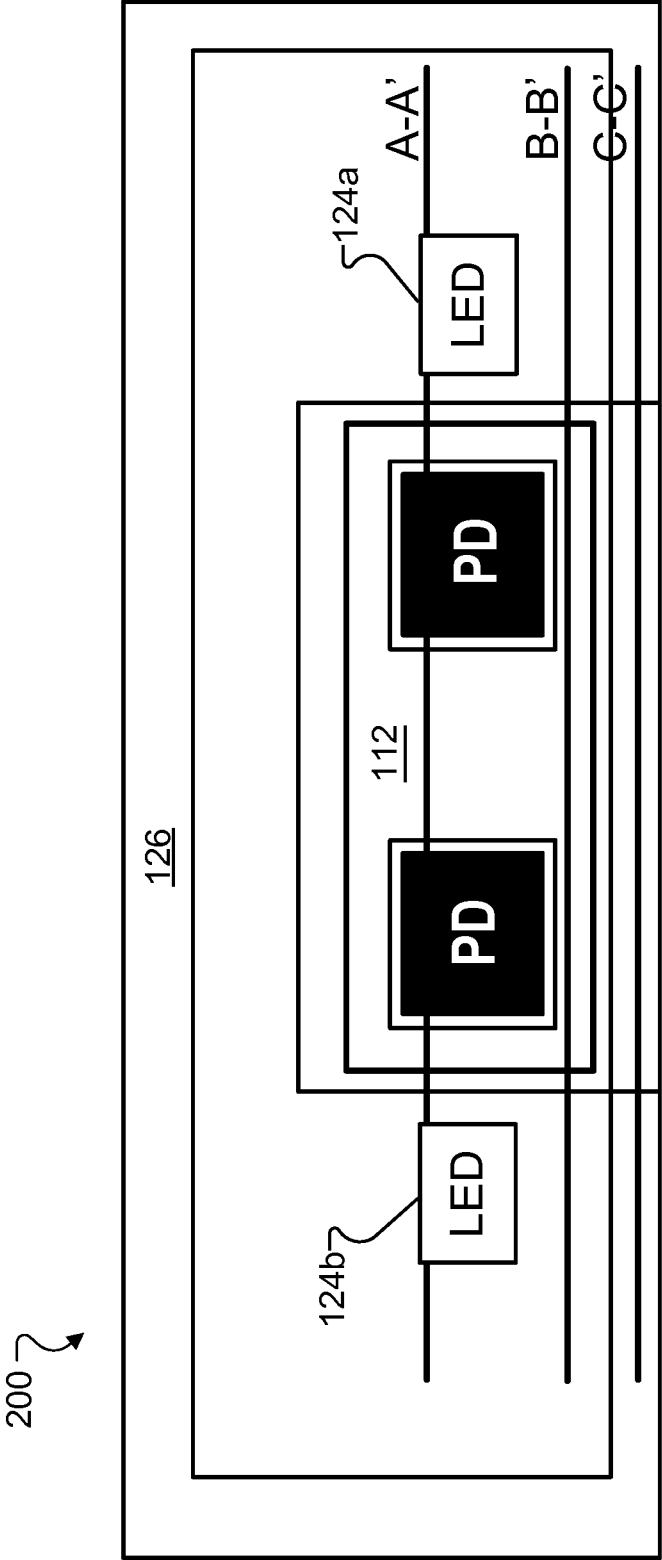


FIG. 2A

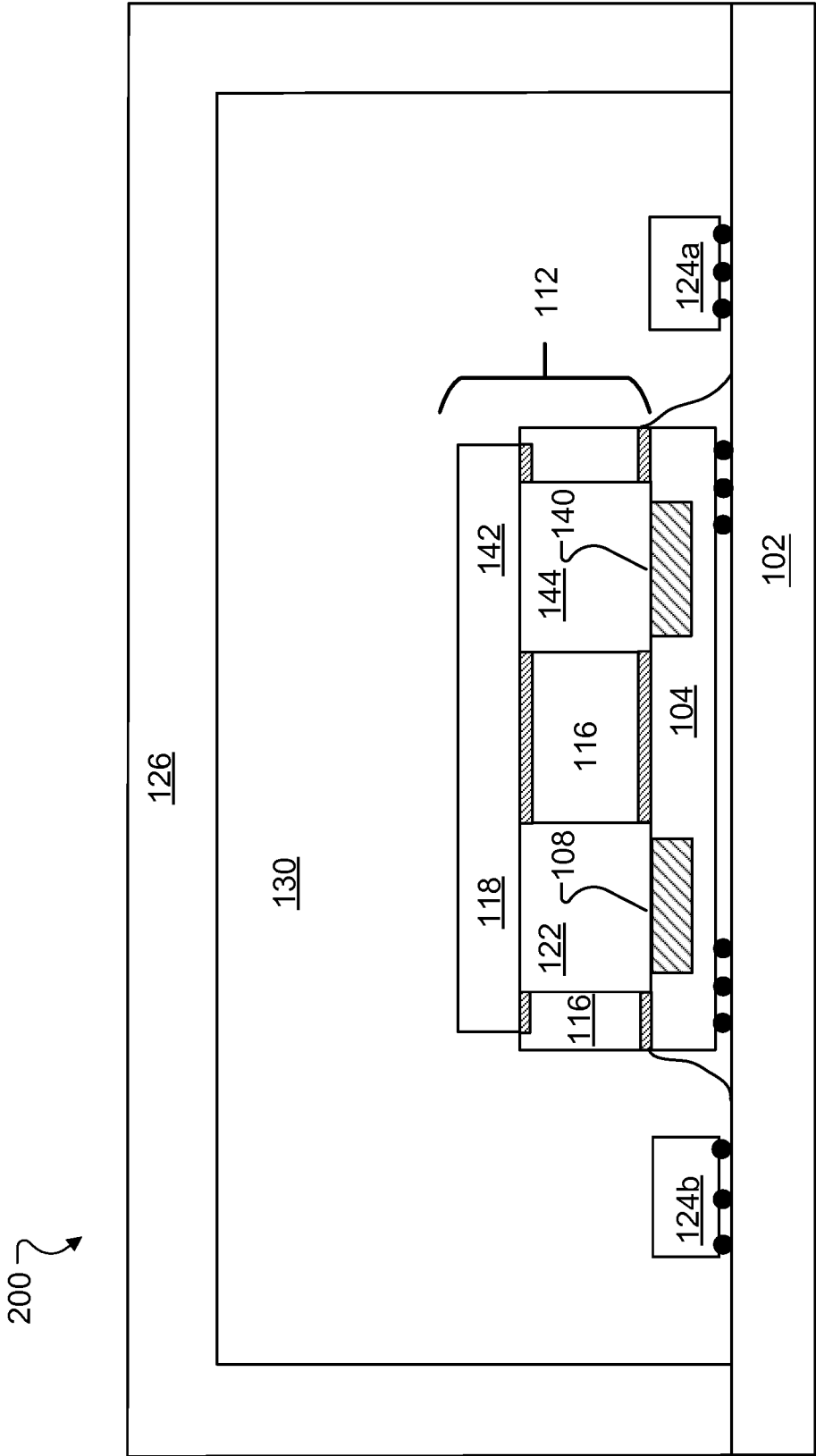


FIG. 2B

4/18

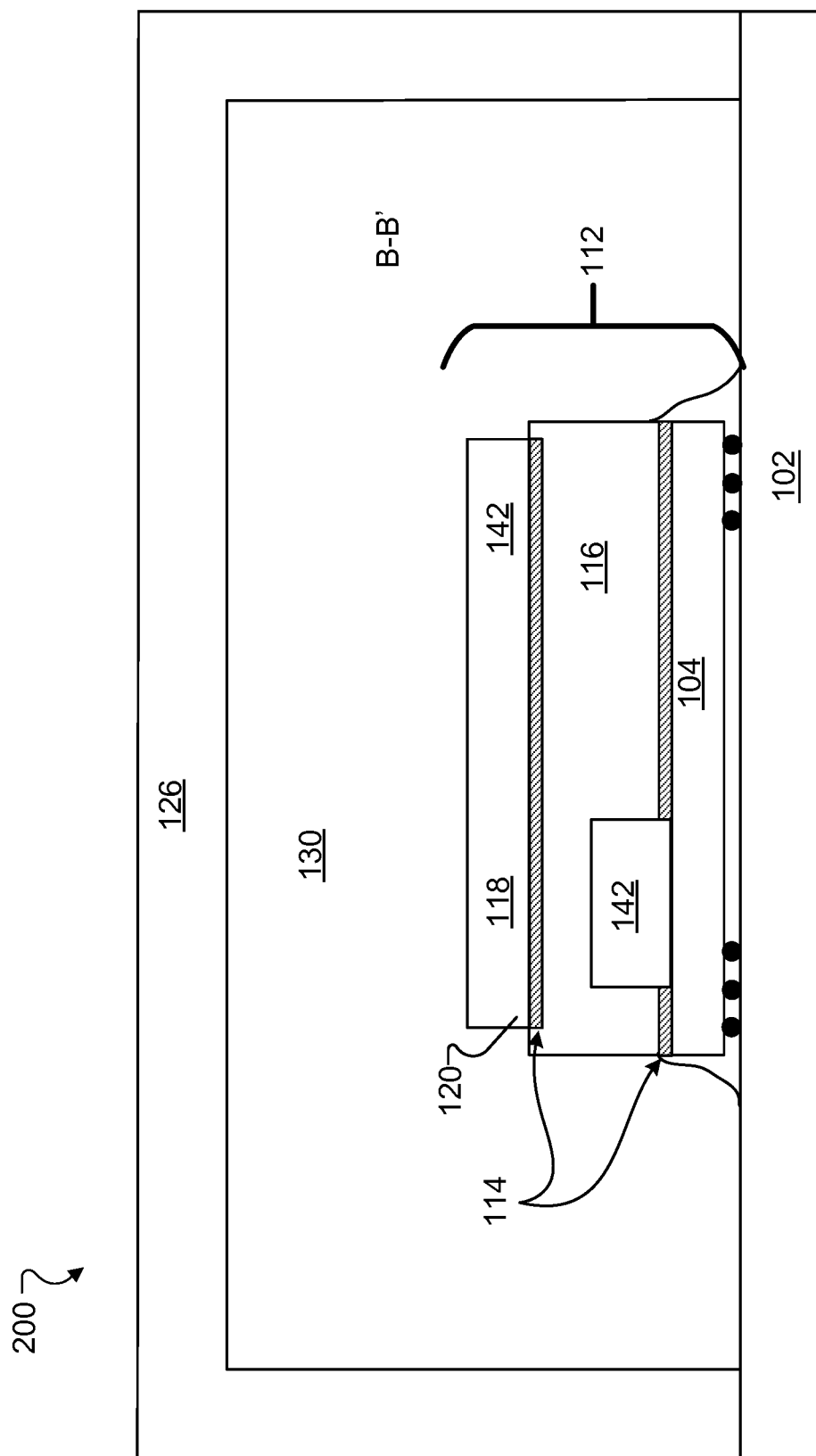


FIG. 2C

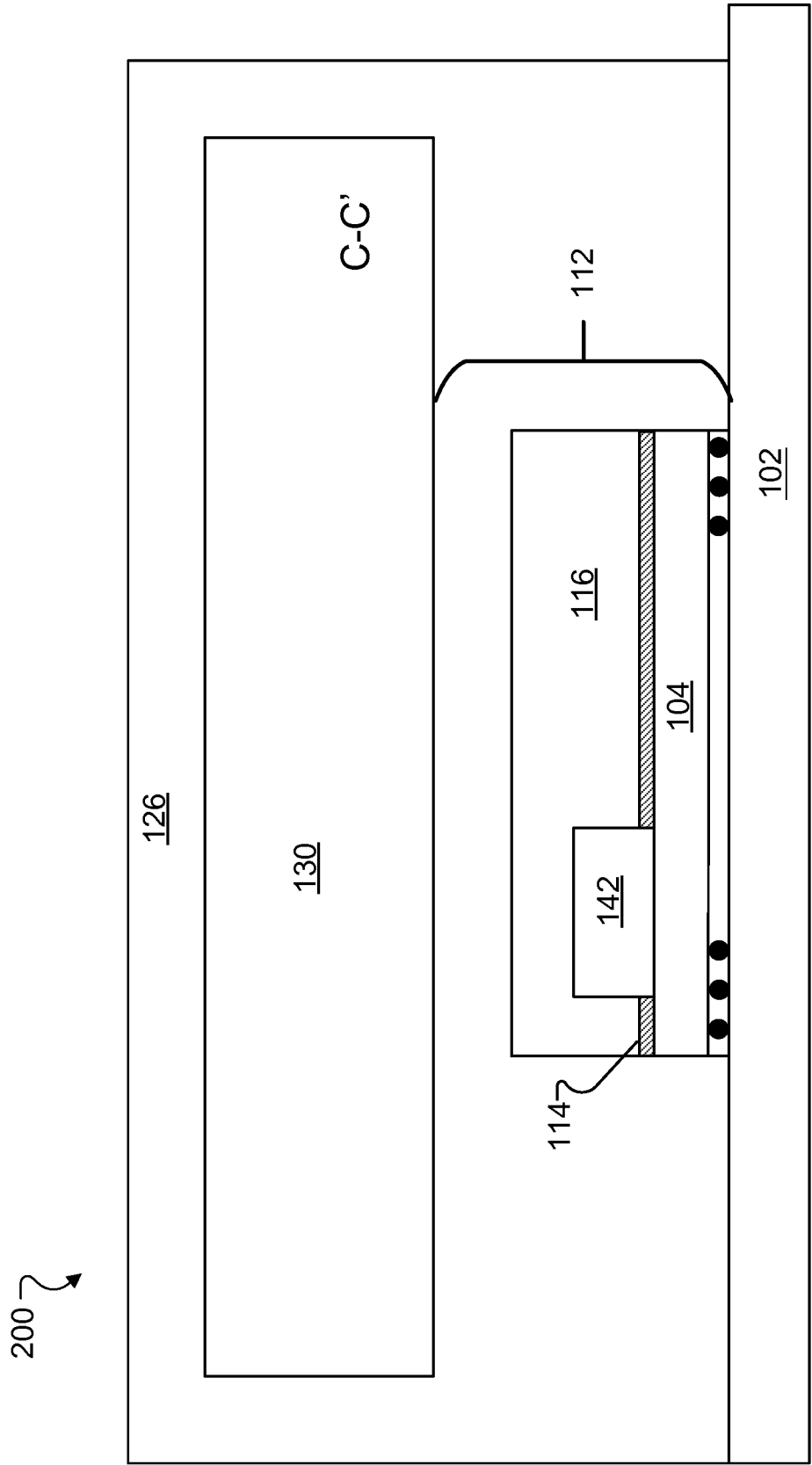


FIG. 2D

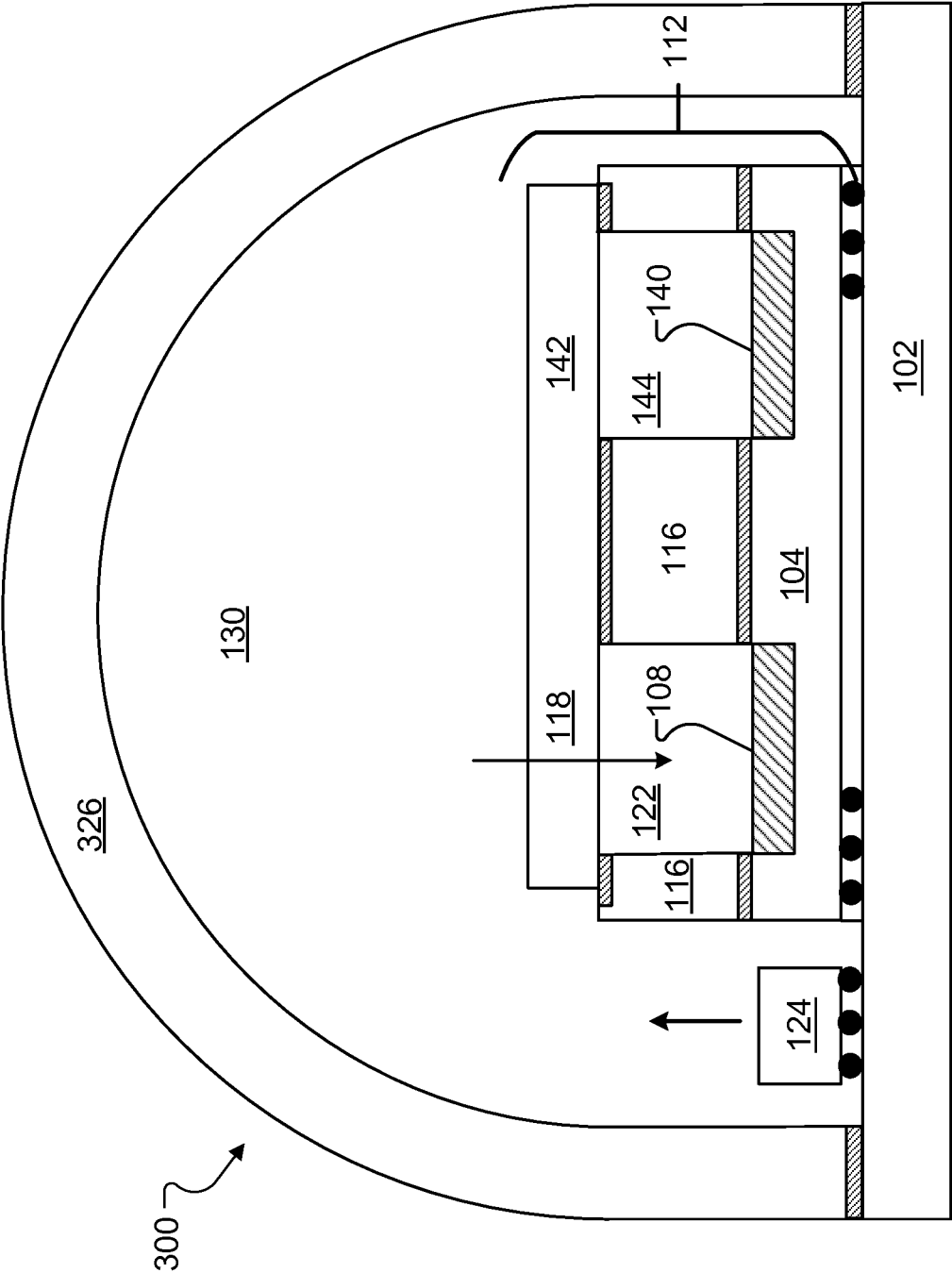


FIG. 3A

7/18

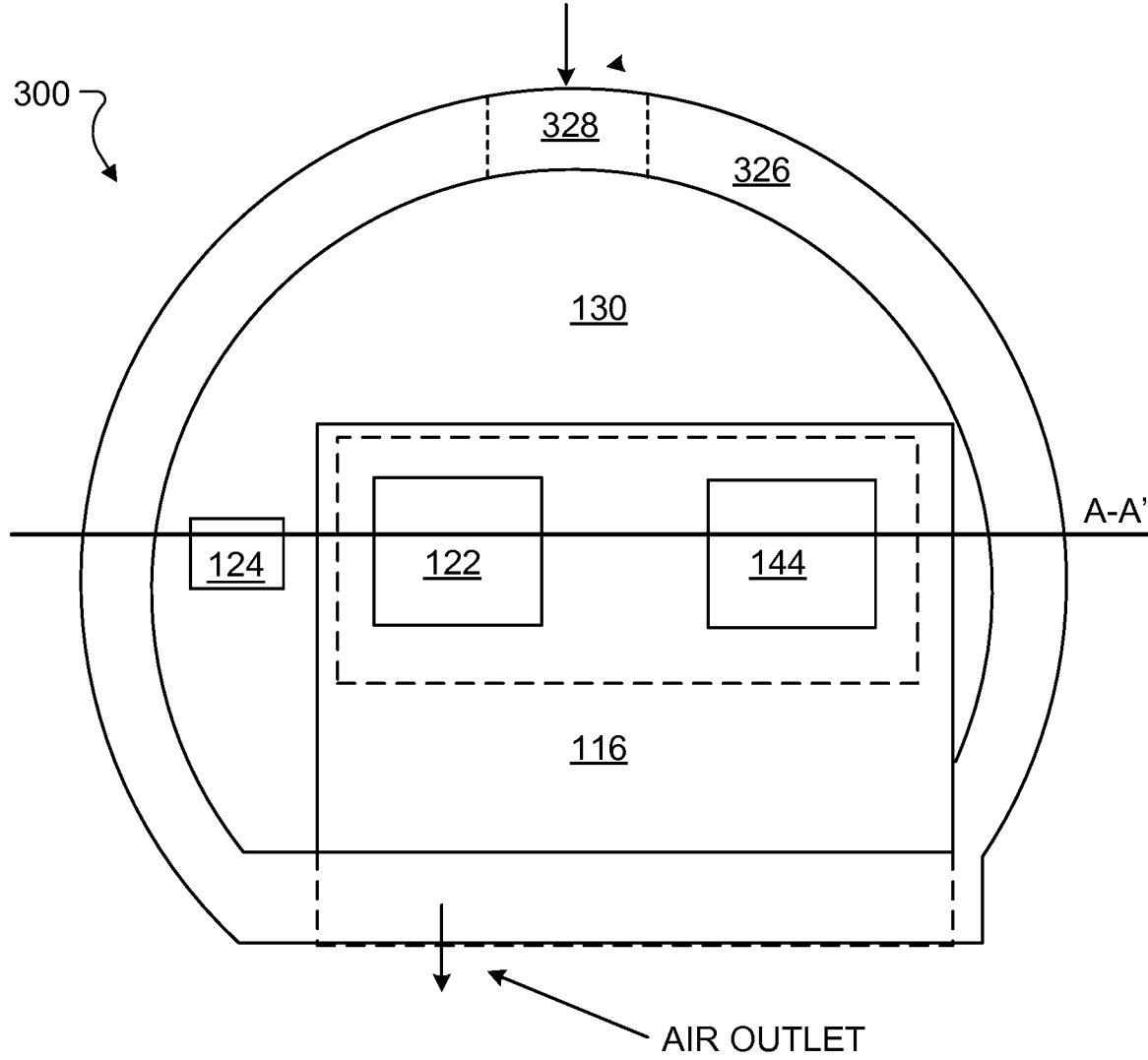


FIG. 3B

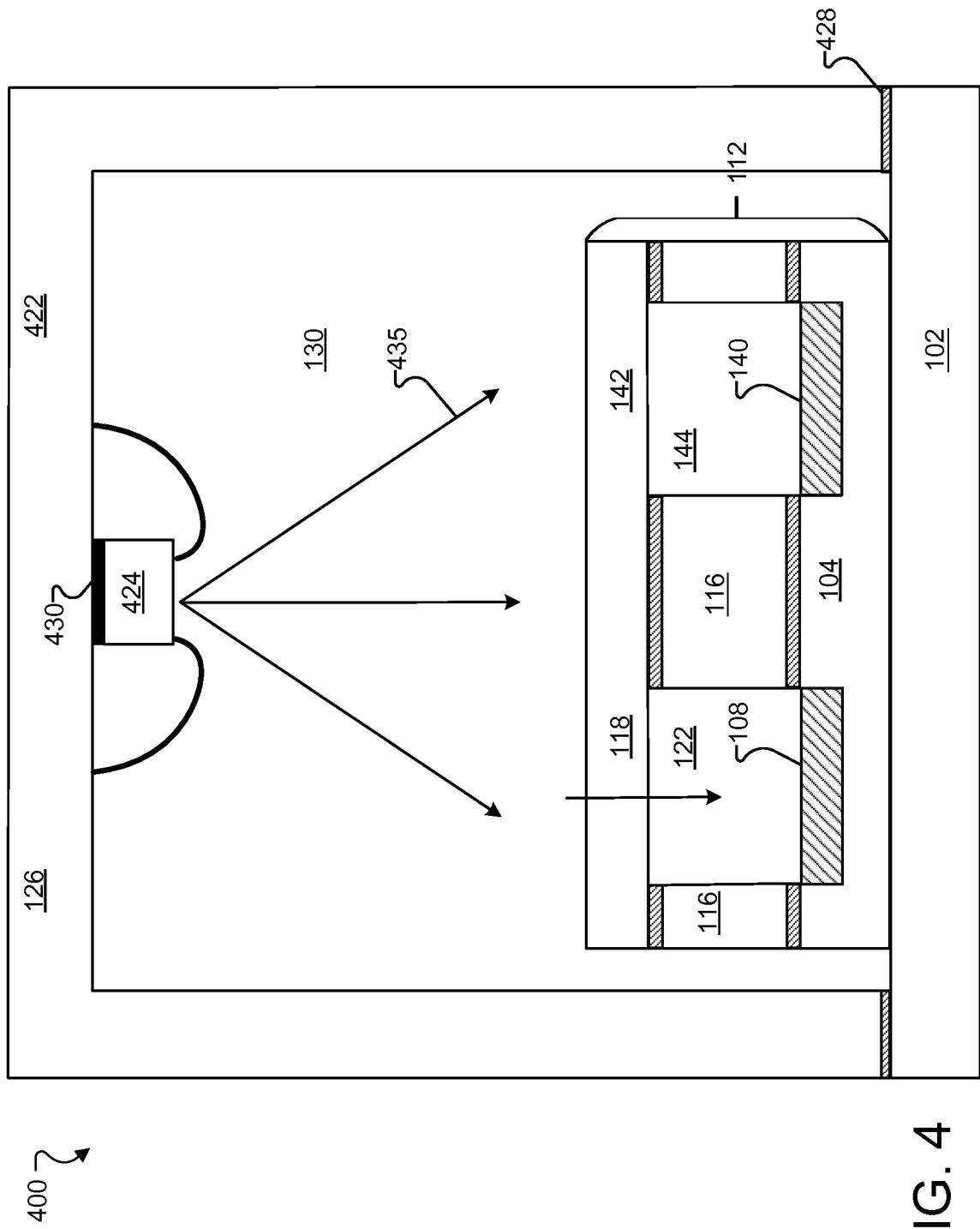


FIG. 4



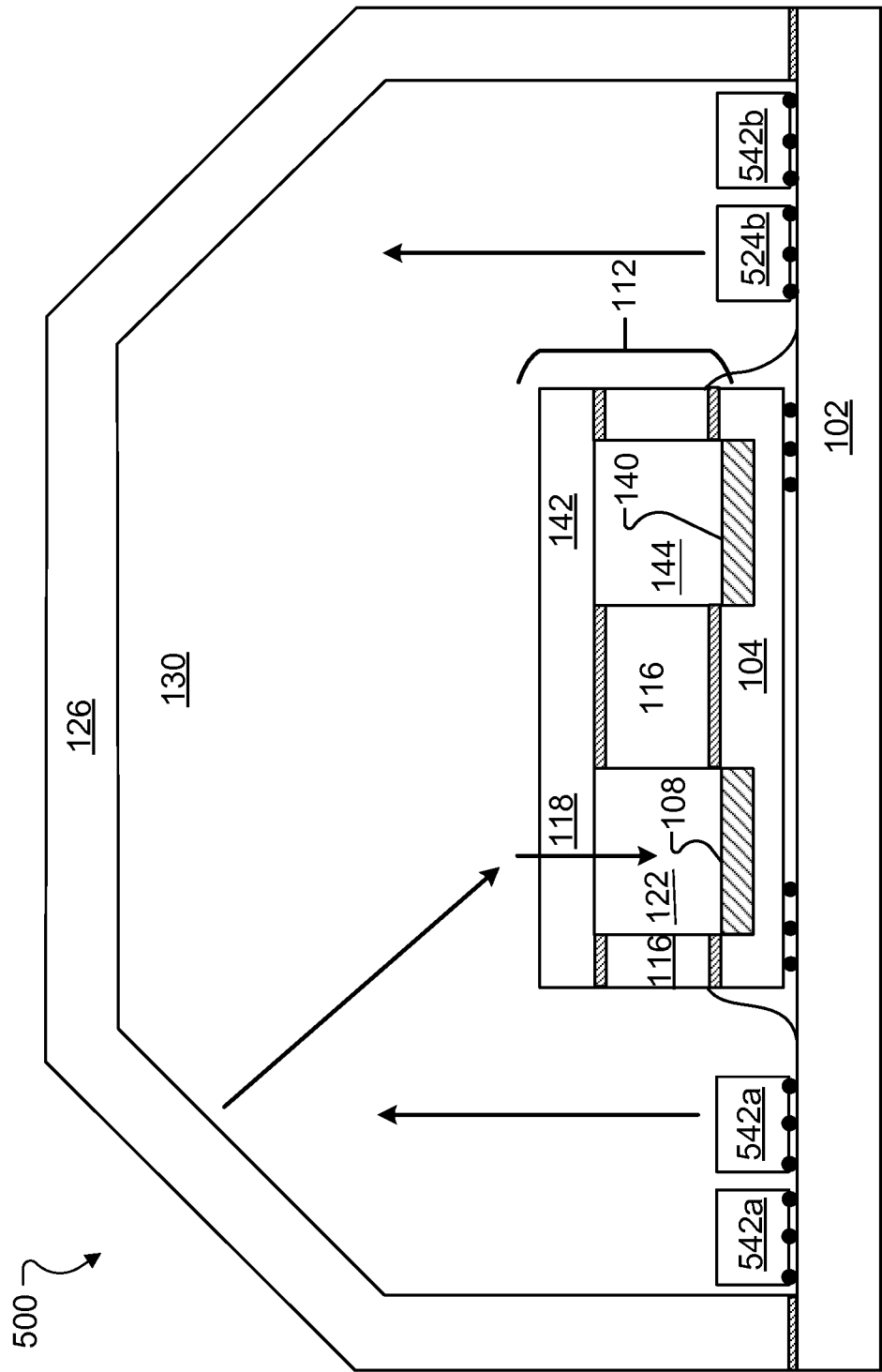


FIG. 5

10/18

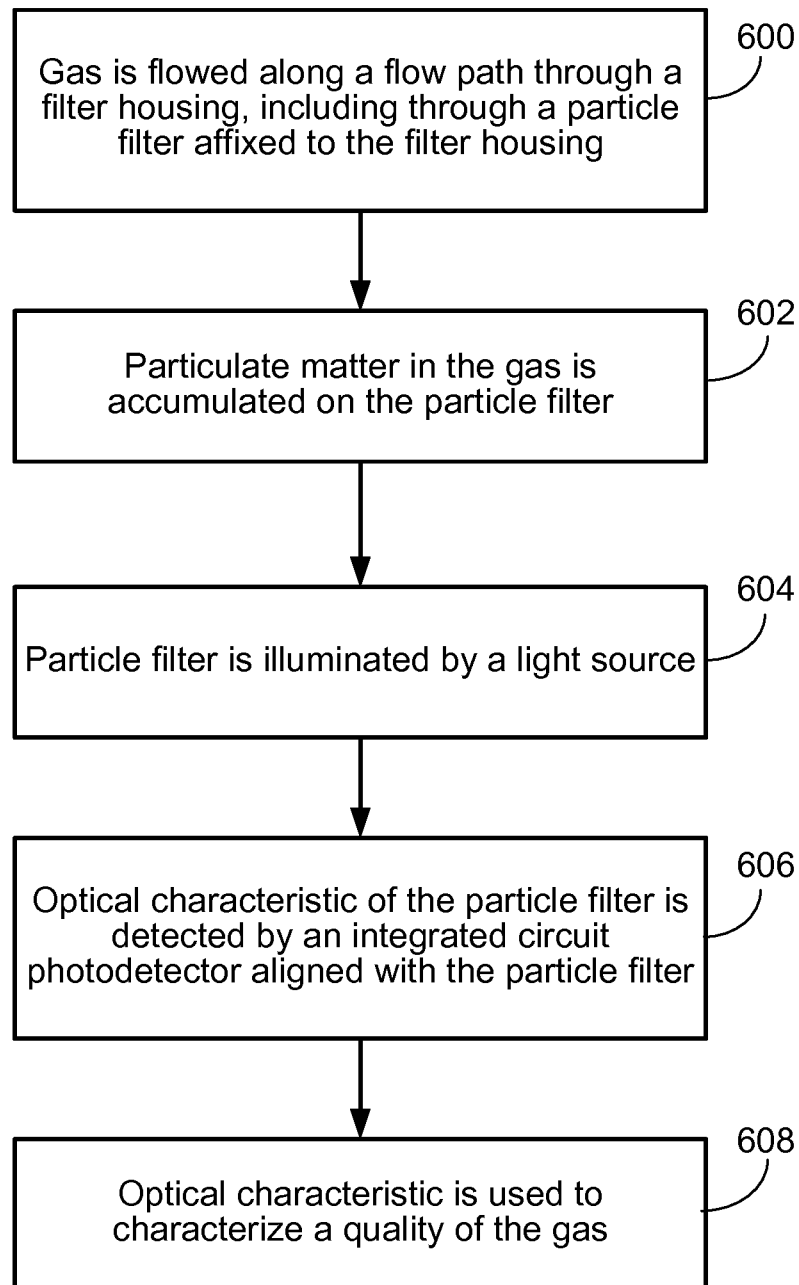


FIG. 6

11/18

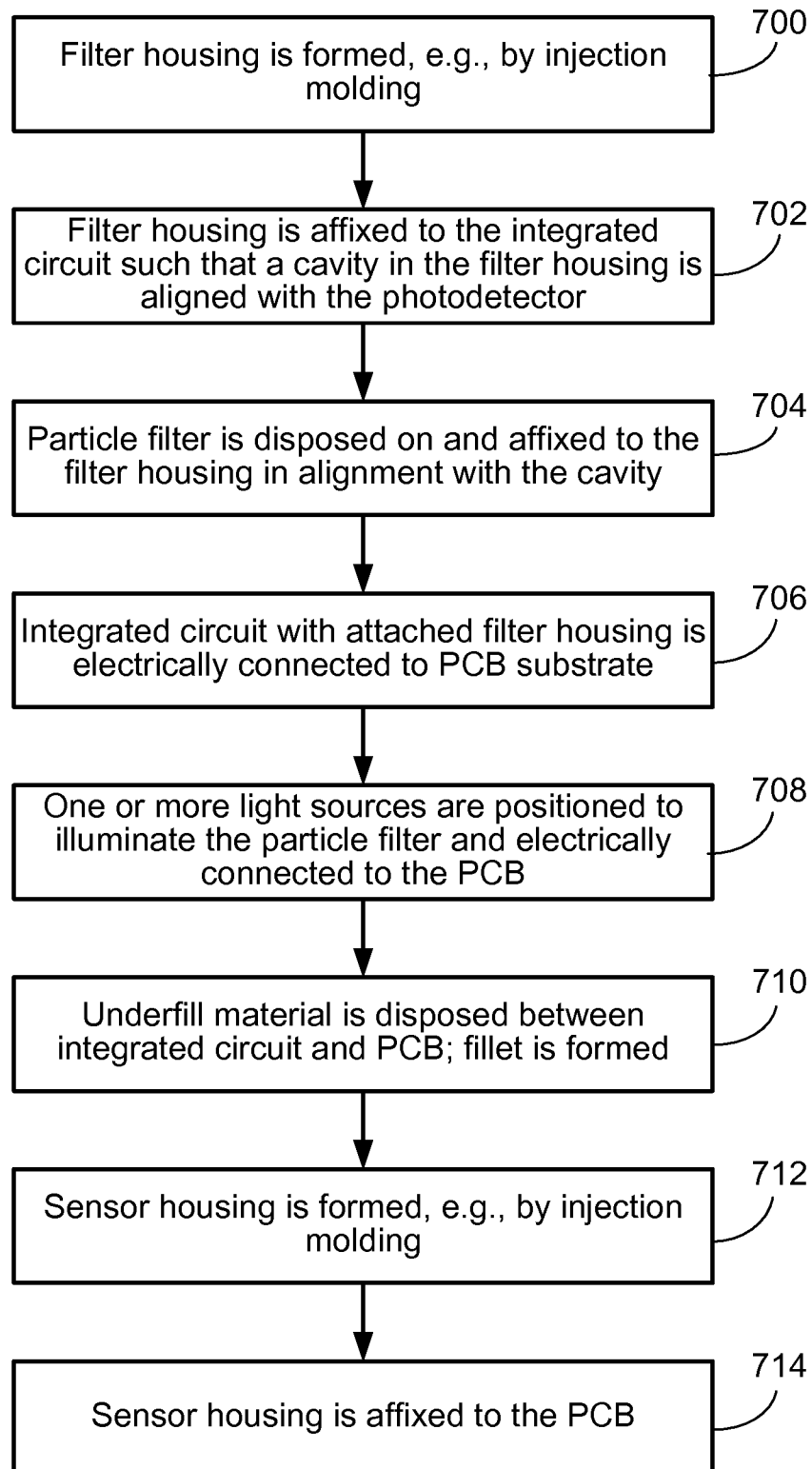


FIG. 7

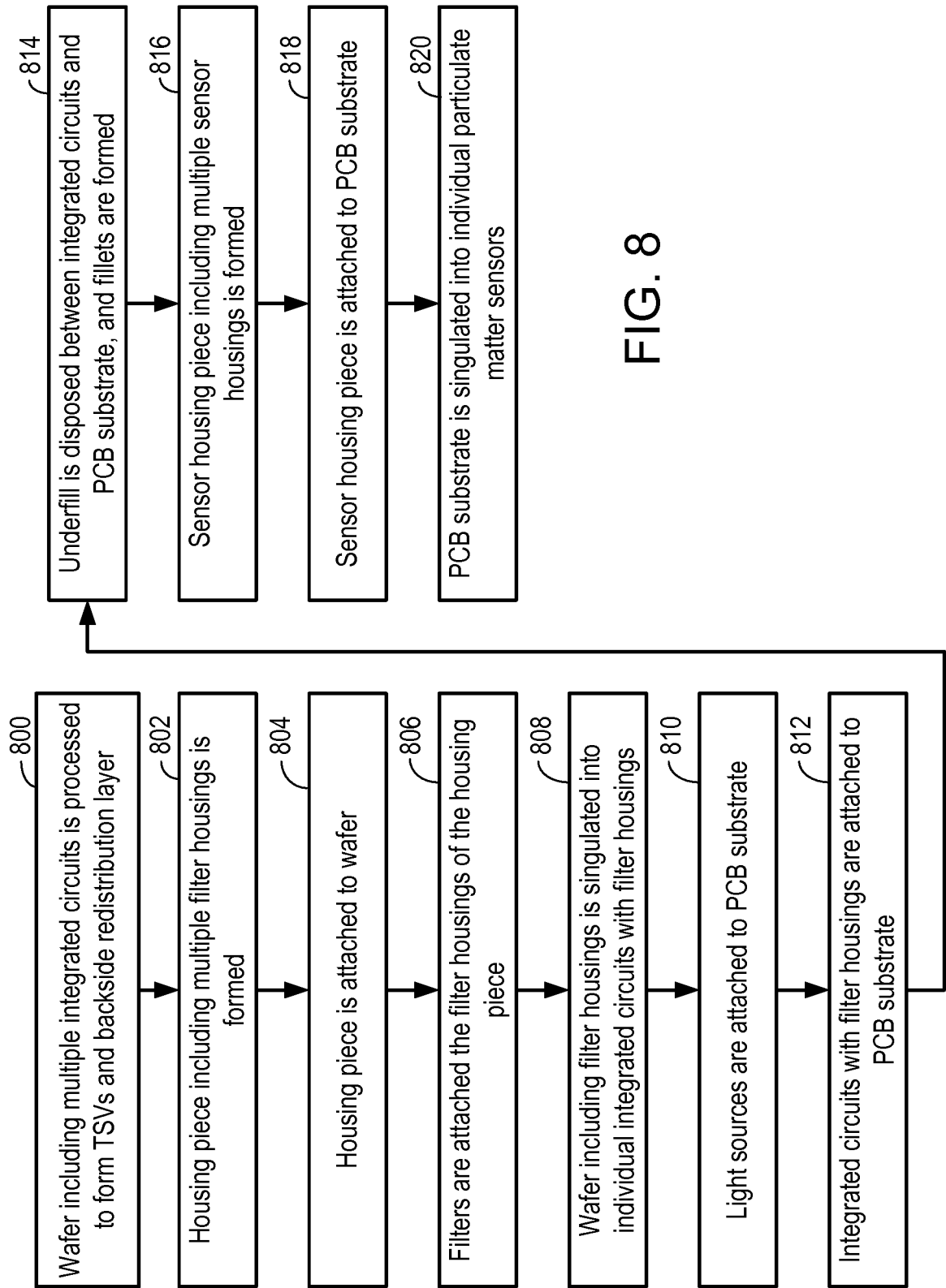


FIG. 8

13/18

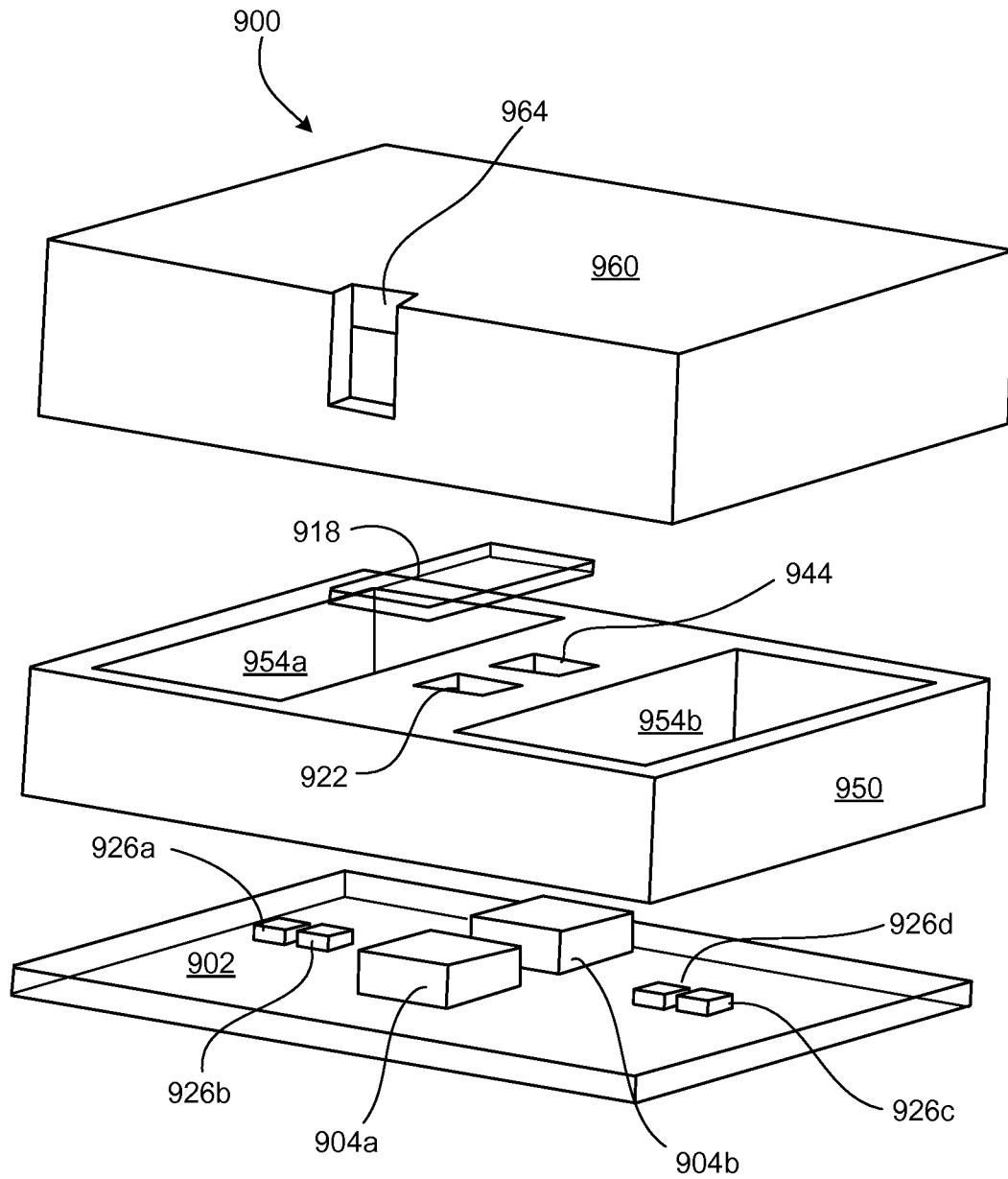


FIG. 9A

14/18

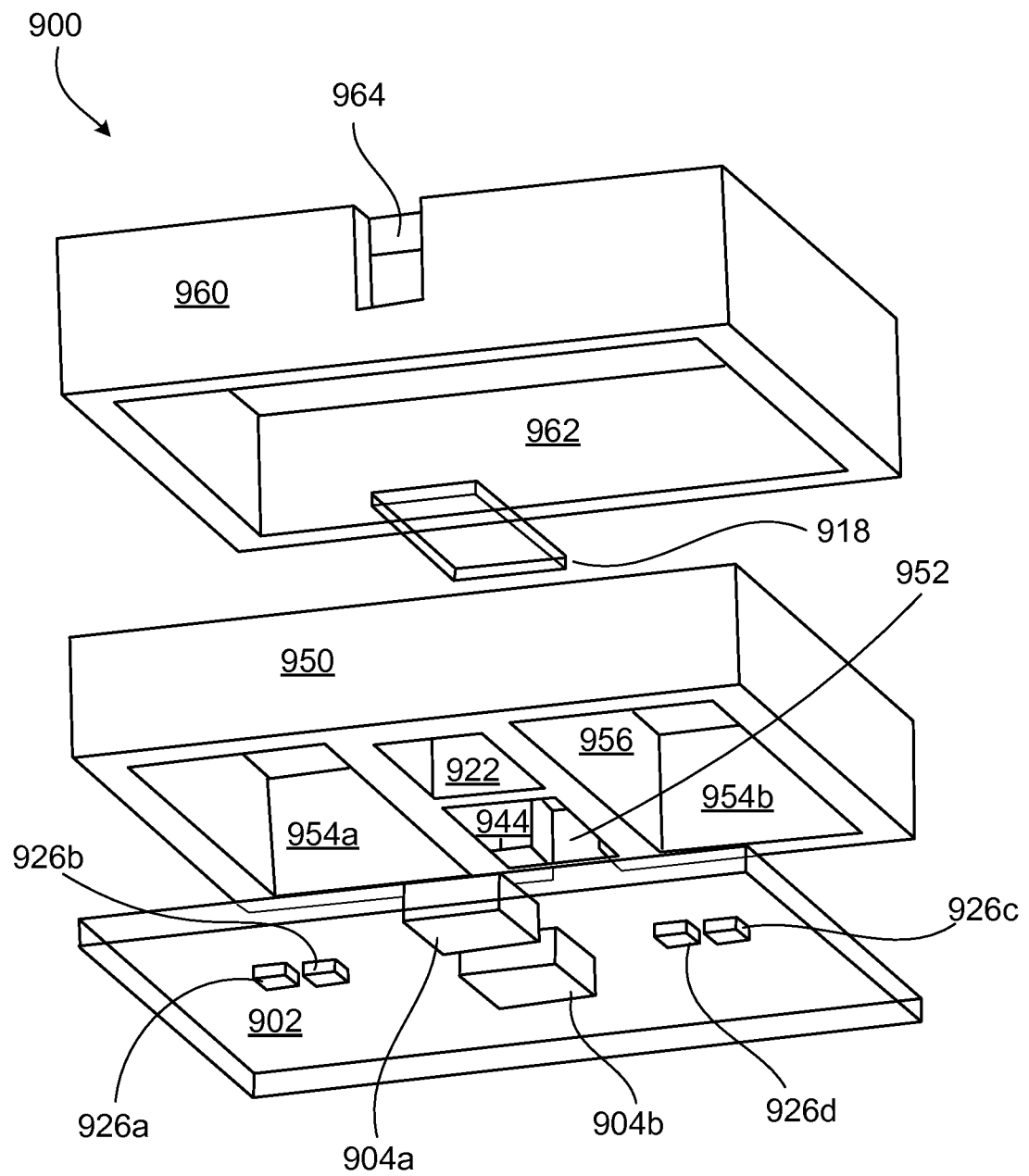


FIG. 9B

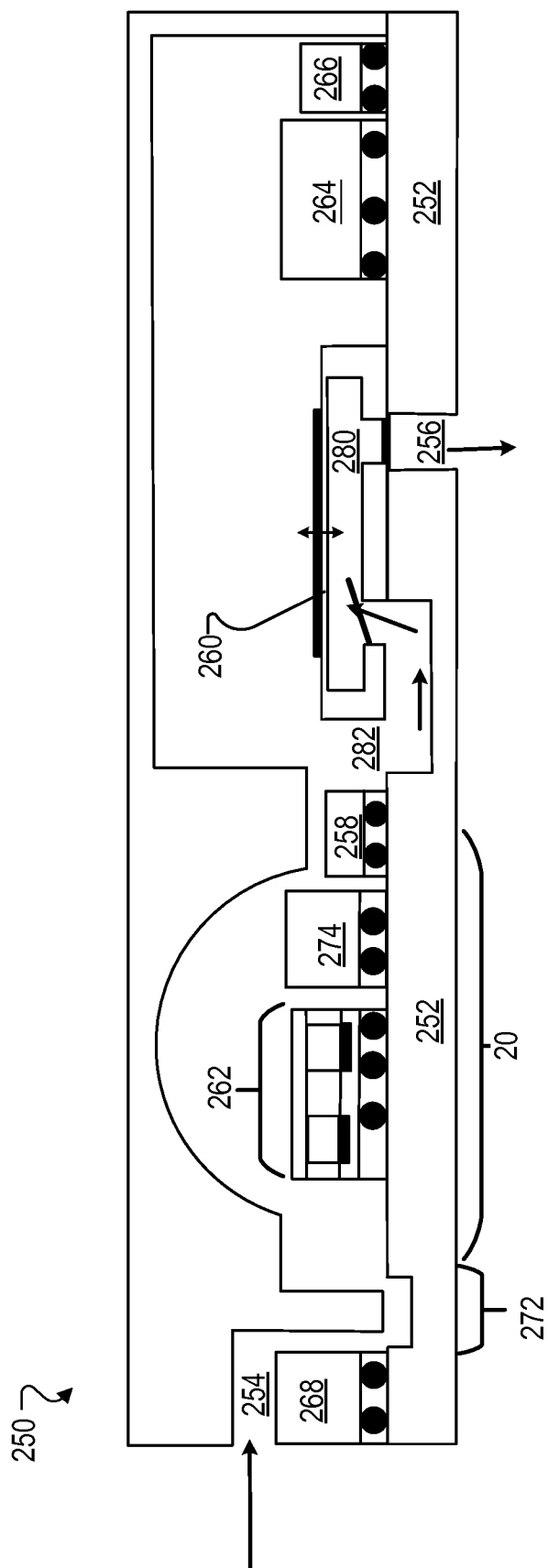


FIG. 10

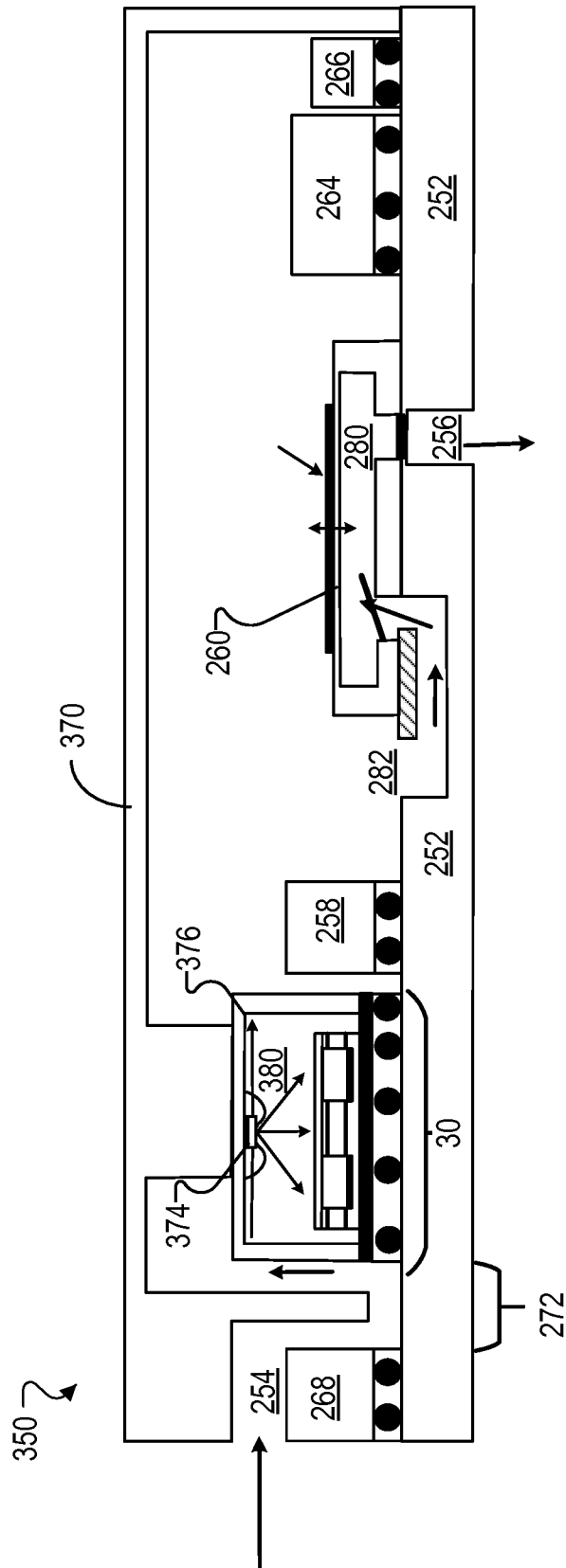


FIG. 11



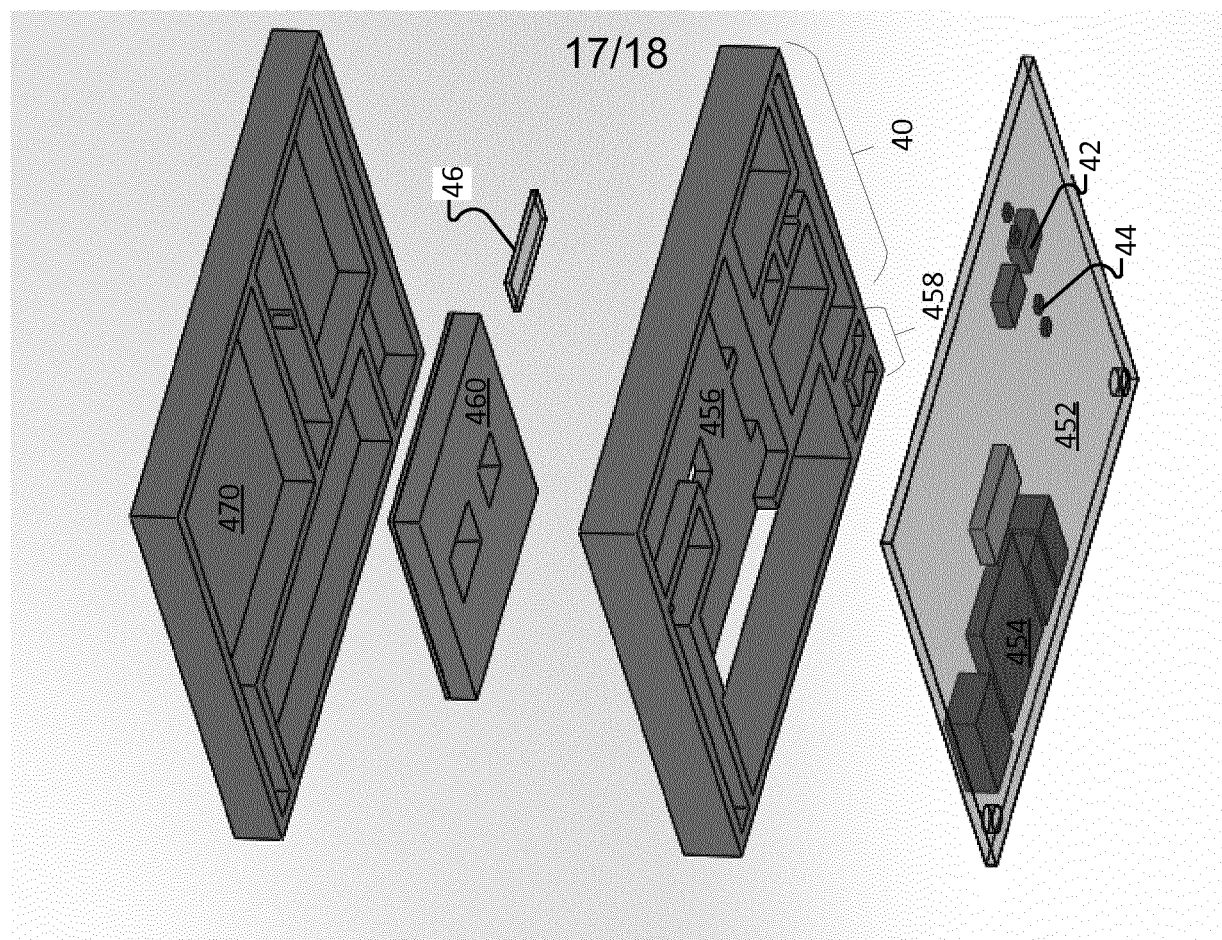


Fig. 12B

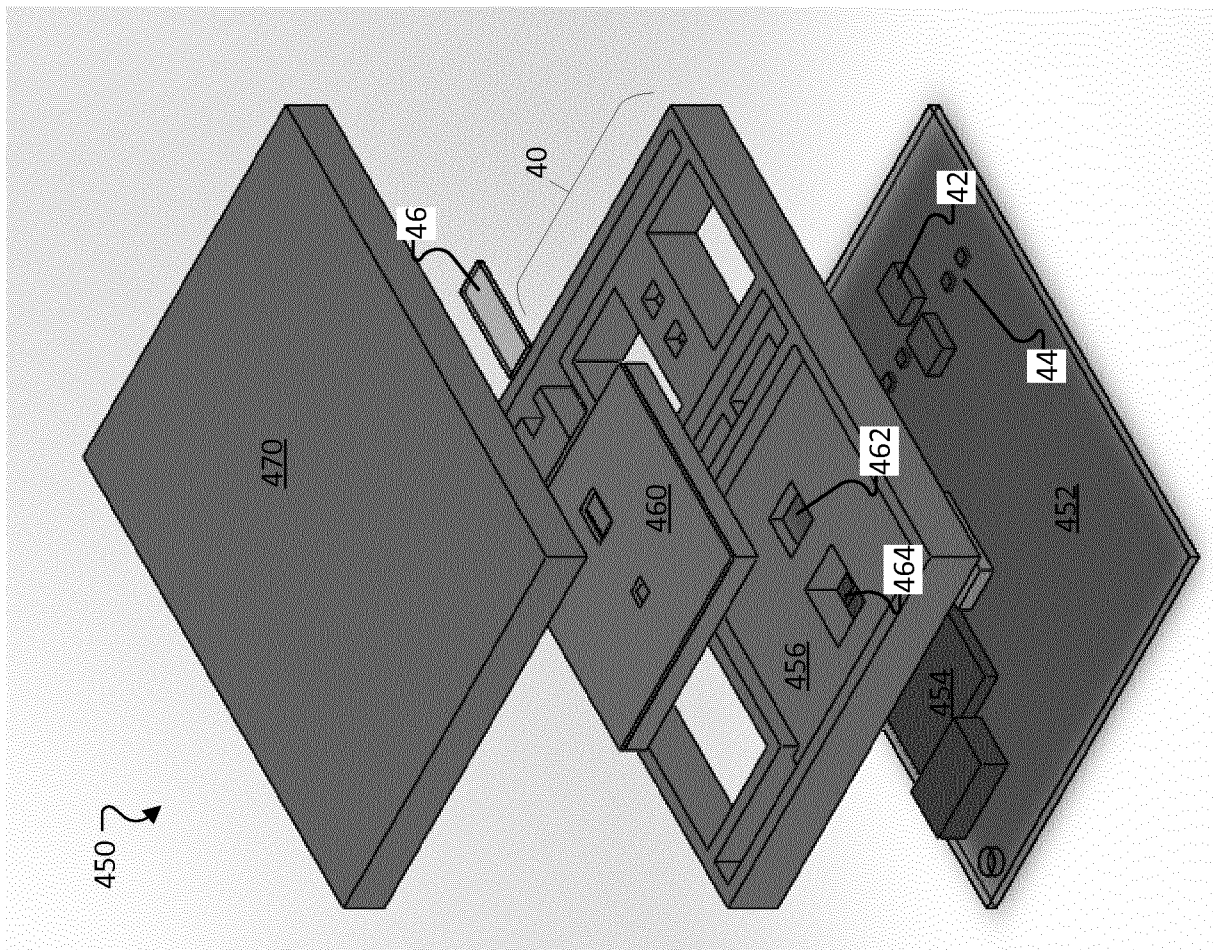


Fig. 12A

18/18

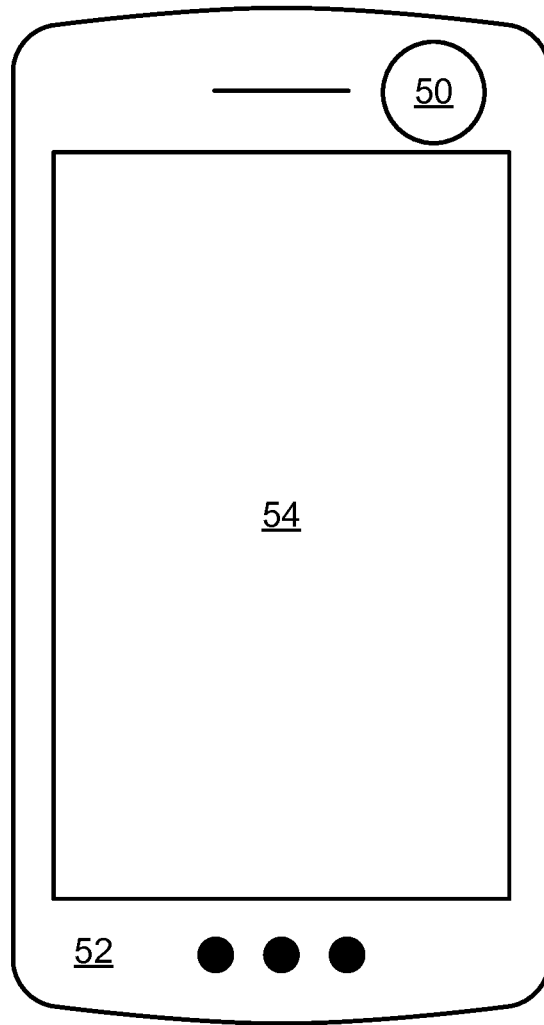


FIG. 13

## INTERNATIONAL SEARCH REPORT

International application No  
**PCT/EP2018/084759**

## A. CLASSIFICATION OF SUBJECT MATTER

**INV. G01N1/22 G01N15/06 G01N15/14**  
**ADD.**

According to International Patent Classification (IPC) or to both national classification and IPC

## B. FIELDS SEARCHED

Minimum documentation searched (classification system followed by classification symbols)

**G01N H05K**

Documentation searched other than minimum documentation to the extent that such documents are included in the fields searched

Electronic data base consulted during the international search (name of data base and, where practicable, search terms used)

**EPO-Internal , WPI Data**

## C. DOCUMENTS CONSIDERED TO BE RELEVANT

Category*	Citation of document, with indication, where appropriate, of the relevant passages	Relevant to claim No.
X	US 2012/229798 A1 (MOCNIK GRISA [SI] ET AL) 13 September 2012 (2012-09-13)	1,5, 8-26,45, 46
A	abstract figure 1 paragraph [0005] paragraph [0024] - paragraph [0048] -----	2-4,6,7, 27-44
A	DE 10 2015 114738 A1 (ST MICROELECTRONICS SRL [IT]) 17 March 2016 (2016-03-17) figures 1, 2, 6 paragraph [0052] - paragraph [0061] paragraph [0038] -----	27-44
A	US 2015/116710 A1 (NICOLETTI SERGIO [FR]) 30 April 2015 (2015-04-30) figures 1-4 ----- -/--	27-44



Further documents are listed in the continuation of Box C.



See patent family annex.

\* Special categories of cited documents :

"A" document defining the general state of the art which is not considered to be of particular relevance

"E" earlier application or patent but published on or after the international filing date

"L" document which may throw doubts on priority claim(s) or which is cited to establish the publication date of another citation or other special reason (as specified)

"O" document referring to an oral disclosure, use, exhibition or other means

"P" document published prior to the international filing date but later than the priority date claimed

"T" later document published after the international filing date or priority date and not in conflict with the application but cited to understand the principle or theory underlying the invention

"X" document of particular relevance; the claimed invention cannot be considered novel or cannot be considered to involve an inventive step when the document is taken alone

"Y" document of particular relevance; the claimed invention cannot be considered to involve an inventive step when the document is combined with one or more other such documents, such combination being obvious to a person skilled in the art

"&" document member of the same patent family

Date of the actual completion of the international search

28 March 2019

Date of mailing of the international search report

04/04/2019

Name and mailing address of the ISA/

European Patent Office, P.B. 5818 Patentlaan 2  
NL - 2280 HV Rijswijk  
Tel. (+31-70) 340-2040,  
Fax: (+31-70) 340-3016

Authorized officer

Schrauwen, Annel ore

## INTERNATIONAL SEARCH REPORT

International application No

PCT/EP2018/084759

C(Continuation). DOCUMENTS CONSIDERED TO BE RELEVANT

Category*	Citation of document, with indication, where appropriate, of the relevant passages	Relevant to claim No.
A	WO 2006/113070 A2 (SENSORS FOR MED & SCIENCE INC [US]; COLVIN ARTHUR E JR [US]; O'CONNOR) 26 October 2006 (2006-10-26) figure 1 paragraph [0037] -----	9-14,25

# INTERNATIONAL SEARCH REPORT

Information on patent family members

International application No

**PCT/EP2018/084759**

Patent document cited in search report	Publication date	Patent family member(s)	Publication date
US 2012229798 A1	13-09-2012	EP 2498079 A2	12-09-2012
		US 2012229798 A1	13-09-2012
		US 2016069787 A1	10-03-2016
-----			
DE 102015114738 A1	17-03-2016	CN 105466816 A	06-04-2016
		CN 205003048 U	27-01-2016
		DE 102015114738 A1	17-03-2016
		US 2016077218 A1	17-03-2016
		US 2019072676 A1	07-03-2019
-----			
US 2015116710 A1	30-04-2015	EP 2596329 A1	29-05-2013
		FR 2963101 A1	27-01-2012
		US 2013120749 A1	16-05-2013
		US 2015116710 A1	30-04-2015
		WO 2012011052 A1	26-01-2012
-----			
WO 2006113070 A2	26-10-2006	AU 2006237499 A1	26-10-2006
		BR PI0607554 A2	15-09-2009
		CA 2605164 A1	26-10-2006
		CN 101198857 A	11-06-2008
		CN 102608083 A	25-07-2012
		EP 1875213 A2	09-01-2008
		JP 5548220 B2	16-07-2014
		JP 2008535623 A	04-09-2008
		JP 2012118086 A	21-06-2012
		KR 20080011184 A	31-01-2008
		KR 20130023386 A	07-03-2013
		KR 20130103641 A	23-09-2013
		SG 161272 A1	27-05-2010
		TW 1338128 B	01-03-2011
		US 2006231749 A1	19-10-2006
		US 2008139904 A1	12-06-2008
		WO 2006113070 A2	26-10-2006
-----			

## **A.2 Patent Application EP 3 499 215 A1: PARTICLE DENSITY SENSOR USING EVANESCENT WAVE OF WAVEGUIDE**

(19)



(11)

**EP 3 499 215 A1**

(12)

**EUROPEAN PATENT APPLICATION**

(43) Date of publication:  
**19.06.2019 Bulletin 2019/25**

(51) Int Cl.:  
**G01N 15/06 (2006.01)** **G01N 21/53 (2006.01)**  
**G01N 15/00 (2006.01)**

(21) Application number: **17207761.2**

(22) Date of filing: **15.12.2017**

(84) Designated Contracting States:  
**AL AT BE BG CH CY CZ DE DK EE ES FI FR GB**  
**GR HR HU IE IS IT LI LT LU LV MC MK MT NL NO**  
**PL PT RO RS SE SI SK SM TR**  
 Designated Extension States:  
**BA ME**  
 Designated Validation States:  
**MA MD TN**

(71) Applicants:  
 • **ams AG**  
**8141 Premstätten (AT)**  
 • **Technische Universität Graz**  
**8010 Graz (AT)**

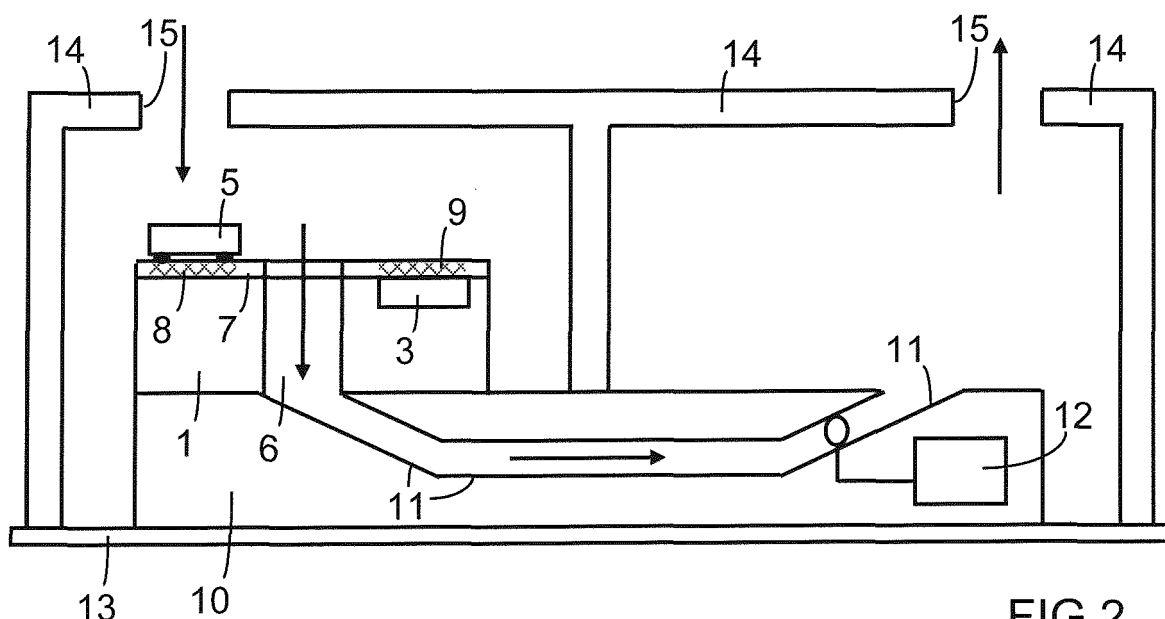
(72) Inventors:  
 • **Kraft, Jochen**  
**8600 Bruck an der Mur (AT)**  
 • **Röhler, Georg**  
**8403 Lebring - Sankt Margarethen (AT)**  
 • **Castano, Fernando**  
**46185 La Pobla de Vallbona (ES)**  
 • **Singulani, Anderson**  
**8047 Graz (AT)**  
 • **Maierhofer, Paul**  
**8010 Graz (AT)**

(74) Representative: **Epping - Hermann - Fischer**  
**Patentanwalts-gesellschaft mbH**  
**Schloßschmidstraße 5**  
**80639 München (DE)**

**(54) PARTICLE DENSITY SENSOR USING EVANESCENT WAVE OF WAVEGUIDE**

(57) The particle sensor device comprises a substrate (1), a photodetector (3), a dielectric (4) on or above the substrate (1), a source of electromagnetic radiation (5), and a through-substrate via (6) in the substrate (1). The through-substrate via is exposed to the environment, in particular to ambient air. A waveguide (7) is arranged in or above the dielectric so that the electromagnetic ra-

diation emitted by the source of electromagnetic radiation is coupled into a portion (7.1) of the waveguide. A further portion (7.2) of the waveguide is opposite the photodetector, so that said portions of the waveguide are on different sides of the through-substrate via, and the waveguide traverses the through-substrate via.

**FIG 2**

## Description

**[0001]** The present disclosure relates to the detection of small airborne particles.

**[0002]** A compact and readily available particle sensor device is desired to enable a quick and accessible check of airborne particles in the environment, especially particles having a diameter of 2.5  $\mu\text{m}$  or less. Such particles interfere with the propagation of light and can be detected by their scattering effect on electromagnetic radiation that is emitted by a light source provided in an optical sensor device.

**[0003]** It is an object of the present invention to provide a compact particle sensor device of improved sensitivity.

**[0004]** This object is achieved with the particle sensor device according to claim 1. Embodiments derive from the dependent claims.

**[0005]** The particle sensor device comprises a substrate, a photodetector, a dielectric on or above the substrate, a source of electromagnetic radiation, and a through-substrate via in the substrate. The through-substrate via is exposed to the environment, in particular to ambient air. A waveguide is arranged in or above the dielectric. Electromagnetic radiation emitted by the source of electromagnetic radiation is coupled into a portion of the waveguide on one side of the through-substrate via. A further portion of the waveguide is arranged on the other side of the through-substrate via at a location opposite the photodetector, so that said portions are on different sides of the through-substrate via. The waveguide traverses the through-substrate via in between.

**[0006]** In an embodiment of the particle sensor device, the waveguide comprises a plurality of individual waveguides arranged in parallel and laterally with respect to one another, each of the individual waveguides traversing the through-substrate via.

**[0007]** In a further embodiment, the waveguide comprises a plurality of individual waveguides arranged in parallel and on different levels above the substrate, each of the individual waveguides traversing the through-substrate via.

**[0008]** In a further embodiment, the source of electromagnetic radiation is integrated in the substrate or in the dielectric. The source of electromagnetic radiation may especially be a vertical-cavity surface-emitting laser.

**[0009]** In a further embodiment, the photodetector is integrated in the substrate.

**[0010]** In a further embodiment, an integrated circuit is formed in the substrate, especially if the substrate comprises semiconductor material, and configured for an operation of the photodetector, especially for an evaluation of a detection of electromagnetic radiation by the photodetector.

**[0011]** In a further embodiment, a grating is arranged in the waveguide at the source of electromagnetic radiation, and a further grating is arranged in the waveguide at a location opposite the photodetector.

**[0012]** A further embodiment comprises a further through-substrate via in the substrate, a conduit connecting the through-substrate via and the further through-substrate via, and a plurality of individual waveguides forming the waveguide. The individual waveguides traverse the through-substrate via, the further through-substrate via, or both the through-substrate via and the further through-substrate via.

**[0013]** In a further embodiment, the through-substrate via and the further through-substrate via have different dimensions along directions of the individual waveguides.

**[0014]** A further embodiment comprises a further substrate and a duct in the further substrate. The substrate is arranged on the further substrate, and the duct prolongs the through-substrate via of the substrate.

**[0015]** A further embodiment comprises a housing with at least two separate openings. The substrate and the further substrate are arranged in the housing, so that the openings communicate with one another via the through-substrate via and the duct.

**[0016]** In a further embodiment, the through-substrate via and the duct are the only connection between the openings that is provided inside the housing.

**[0017]** A further embodiment comprises a fan or pump in the further substrate, the fan or pump being configured to generate a gas flow through the through-substrate via and the duct. The gas flow can especially be modulated by a geometry of the through-substrate via and by an operation of the fan or pump.

**[0018]** The following is a detailed description of examples of the particle sensor device in conjunction with the appended figures.

Figure 1 is a cross section of a particle sensor device.

Figure 2 is a cross section of an arrangement of a particle sensor device in a housing.

Figure 3 is a schematic top view of an arrangement of through-substrate vias and waveguides.

Figure 4 is a cross section of a device comprising the arrangement according to Figure 3.

Figure 5 is a schematic top view of an arrangement of a plurality of through-substrate vias and waveguides.

**[0019]** The particle sensor device is configured to detect particles by the reduction of light intensity that is caused by an interaction with the particle. The interaction takes place between an adsorbed particle and the evanescent field of electromagnetic radiation conducted in a waveguide. The waveguide is arranged across one or several through-substrate vias (TSVs) of a substrate.

**[0020]** One way to tune the selectivity of the particle sensor device to the size of the particles that are to be



detected is to adapt the density and width of the waveguides. For this purpose, a plurality of waveguides of suitable sizes may be arranged in a gridlike manner over an array of through-substrate vias, which may comprise the same size or different dimensions. The gas carrying the particles can be introduced in some or all of the through-substrate vias in a predetermined sequence, according to the requirements of individual applications.

**[0021]** Figure 1 is a cross section of a particle sensor device. A substrate 1, which may comprise a glass or a semiconductor material, especially silicon, for instance, is provided with an open through-substrate via 6, which can be exposed to an environment, in particular to ambient air. If the substrate 1 comprises a semiconductor material, it may be provided with an integrated circuit 2, in particular a circuit that can be produced in a standard CMOS process, and the integrated circuit 2 can especially be configured to evaluate the measurements that are performed with the particle sensor device.

**[0022]** A photodetector 3 is provided. The photodetector 3 may especially be a photodiode, for instance. The photodetector 3 may be formed in the substrate 1, in particular as an integrated component, or it may be a separate component, which may be formed in or on a further substrate.

**[0023]** A dielectric 4, which may especially be an oxide of semiconductor material, is arranged on or above the substrate 1. Electric connections of the integrated circuit 2 and the photodetector 3 may be provided by a wiring embedded in the dielectric 4.

**[0024]** A source of electromagnetic radiation 5, which may be a vertical-cavity surface-emitting laser (VCSEL) or a light-emitting diode (LED), for example, is arranged in or near the dielectric 4. The source of electromagnetic radiation 5 may be a separate component, which may be formed in or on a further substrate, or it may be monolithically integrated in the substrate 1 or in the dielectric 4. The source of electromagnetic radiation 5 is provided for the emission of electromagnetic radiation, which may especially be visible light, for instance.

**[0025]** A waveguide 7 is arranged in or above the dielectric 4, so that the electromagnetic radiation from the source of electromagnetic radiation 5 is coupled into a portion of the waveguide 7. The coupling may be effected by butt coupling, for instance, or by a diffraction grating 8 arranged in the waveguide 7. A further portion of the waveguide 7 is arranged in a location opposite the photodetector 3. The portion and the further portion are on different sides of the through-substrate via 6, and the waveguide 7 traverses the through-substrate via 6.

**[0026]** The waveguide 7 may include a plurality of individual waveguides arranged in parallel, as indicated in Figure 1 by way of example. The individual waveguides may be arranged on different levels above the substrate 1 and/or laterally with respect to one another.

**[0027]** After traversing the through-substrate via 6, the electromagnetic radiation is directed from the waveguide 7 towards the photodetector 3. For this purpose a further

grating 9 may be arranged in the waveguide 7, but other means may also be applied to diffract or scatter the electromagnetic radiation out of the waveguide 7.

**[0028]** In each measurement by the particle sensor device, electromagnetic radiation from the source 5 is conducted by the waveguide 7 through the through-substrate via 6 and then detected by the photodetector 3. Thus a change of light intensity, which is due to an interaction between particles and the evanescent field around the waveguide 7, is detected and monitored. When a gas carrying particles is directed through the through-substrate via 6, one or more of the particles will be adsorbed on the waveguide 7 and thus change the intensity of the passing electromagnetic radiation. There are correlations between the change of light intensity and the adsorbed particles, as well as between the number of adsorbed particles and the density of particles in the gas.

**[0029]** Figure 2 is a cross section of an arrangement of a particle sensor device in a housing. Corresponding elements shown in Figures 1 and 2 are indicated with the same reference numerals. The arrangement according to Figure 2 comprises a further substrate 10, which may especially be a silicon substrate or wafer, for instance. The substrate 1 is mounted on the further substrate 10. A duct 11 in the further substrate 10 prolongs the through-substrate via 6 of the substrate 1.

**[0030]** The substrate 1 and the further substrate 10 are arranged on a carrier 13 and in a housing 14 forming a package of the particle sensor device. At least two openings 15 are formed in the housing 14, which comprises compartments in such a manner that the openings 15 communicate with one another only via the through-substrate via 6 and the duct 11. Thus a gas entering the first opening 15, which is on the left in Figure 2, passes the through-substrate via 6 and the duct 11 and leaves the inner volume of the housing 14 through the second opening 15, which is on the right in Figure 2.

**[0031]** An optional fan or pump 12, which is schematically represented in Figure 2, may be integrated in the further substrate 10 to generate and maintain a gas flow through the duct 11. The fan or pump 12 may instead be provided by a separate component. A suitable direction of the gas flow is indicated in Figure 2 with arrows. The gas may instead flow in the reverse direction. In any case, the gas is forced to pass the waveguide 7 inside the through-substrate via 6.

**[0032]** Figure 3 is a schematic top view of an arrangement of through-substrate vias and waveguides. The through-substrate vias 6, 16 are represented as cylindrical, but they may have any other suitable shape. In the example shown in Figure 3, a further through-substrate via 16 is provided, which has a diameter that is smaller than the diameter of the through-substrate via 6. The waveguide 7 comprises individual waveguides parallel and lateral relative to one another.

**[0033]** Figure 4 is a cross section of a device comprising the arrangement of through-substrate vias 6, 16 and waveguides 7 according to Figure 3. Corresponding el-

ements shown in Figures 2, 3 and 4 are indicated with the same reference numerals. A conduit 17 in the further substrate 10 forms a connection between the through-substrate via 6 and the further through-substrate via 16. When a gas has entered the through-substrate via 6, the conduit 17 allows the gas to flow to the further through-substrate via 16 and leave the substrate 1 according to the arrows inserted in Figure 4. The gas may instead flow in the opposite direction.

**[0034]** Owing to the different dimensions of the vias, the velocity of the gas in the further through-substrate via 16 is greater than the velocity of the gas in the through-substrate via 6.

**[0035]** The velocity of the gas determines the relation between the amount of larger and smaller particles that are trapped by the waveguide 7. Small particles are primarily trapped by the waveguide 7 inside the larger through-substrate via 6, while larger particles are primarily trapped inside the smaller further through-substrate via 16. This concept can be extended to particle sensor devices comprising a plurality of through-substrate vias of the same or different dimensions.

**[0036]** The density of the arrangement of individual waveguides and the size of the gaps between them also have an influence on the velocity of the gas. The individual waveguides may typically have a width of about 1  $\mu\text{m}$  and a spacing between them that is in the range from 2.5  $\mu\text{m}$  to 10  $\mu\text{m}$ , for example.

**[0037]** Figure 5 shows a top view of an example of an arrangement of several through-substrate vias 6, 16 and individual waveguides 7. Every individual waveguide 7 is provided with a photodetector 3 for an increased signal-to-noise ratio. The required light intensity is reduced when the waveguide 7 crosses two or more through-substrate vias 6, 16, as in the example shown in Figure 5.

**[0038]** The probability of adsorption is a function of the particle size, the velocity of the gas flow, and the pitch and width of the waveguide 7. The gas flow can especially be modulated by the geometry of the through-substrate via 6 and by the operation of the fan or pump 12. A smaller velocity of the gas assists the detection of smaller particles, whereas larger particles are mainly detected at a greater velocity.

**[0039]** Advantages of the describe particle sensor device are an enhanced integrability and a reduction of the required light intensity. As small airborne particles are prone to being adsorbed on the waveguide, only a comparatively small number of holes is required for the adsorption of a sufficient number of particles in order to achieve a high sensitivity. Hence the device can be realized on a chip of standard size.

**[0040]** The use of a waveguide enhances the scattering effect of particles that are small in relation to the wavelength of the electromagnetic radiation. The confinement of the waveguide reduces the probability of undesired scattering, which might otherwise increase the noise level, and increases the effect of the presence of particles on the radiation that is received by the photodetector.

## List of reference numerals

### [0041]

5	1	substrate
	2	integrated circuit
	3	photodetector
	4	dielectric
	5	source of electromagnetic radiation
10	6	through-substrate via
	7	waveguide
	7.1	portion of the waveguide
	7.2	further portion of the waveguide
	8	grating
15	9	further grating
	10	further substrate
	11	duct
	12	fan or pump
	13	carrier
20	14	housing
	15	opening
	16	further through-substrate via
	17	conduit

25

### Claims

1. A particle sensor device, comprising:

30

a substrate (1),  
a photodetector (3),  
a dielectric (4) on or above the substrate (1),  
a source of electromagnetic radiation (5), and  
a through-substrate via (6) in the substrate (1),

35

**characterized in that**  
the through-substrate via (6) is exposed to an environment,

40

a waveguide (7) is arranged in or above the dielectric (4),  
electromagnetic radiation from the source of electromagnetic radiation (5) being coupled into a portion (7.1) of the waveguide (7),

45

a further portion (7.2) of the waveguide (7) is arranged at the photodetector (3), and  
the waveguide (7) traverses the through-substrate via (6) at a location between the portion (7.1) and the further portion (7.2) .

50

2. The particle sensor device according to claim 1, wherein the waveguide (7) comprises a plurality of individual waveguides arranged in parallel and laterally with respect to one another, each of the individual waveguides traversing the through-substrate via (6).

55

3. The particle sensor device according to claim 1 or 2, wherein the waveguide (7) comprises a plurality of individual waveguides arranged in parallel and on

different levels above the substrate (1), each of the individual waveguides traversing the through-substrate via (6).

4. The particle sensor device according to one of claims 1 to 3, wherein the source of electromagnetic radiation (5) is integrated in the substrate (1) or in the dielectric (4).

5. The particle sensor device according to one of claims 1 to 4, wherein the source of electromagnetic radiation (5) is a vertical-cavity surface-emitting laser.

6. The particle sensor device according to one of claims 1 to 5, wherein the photodetector (3) is integrated in the substrate (1).

7. The particle sensor device according to one of claims 1 to 6, further comprising:

an integrated circuit (2) formed in the substrate (1), the integrated circuit (2) being configured for an operation of the photodetector (3).

8. The particle sensor device according to one of claims 1 to 7, further comprising:

a grating (8) in the portion (7.1) of the waveguide (7) where the electromagnetic radiation is coupled into the waveguide (7), and  
a further grating (9) in the further portion (7.2) of the waveguide (7) opposite the photodetector (3).

9. The particle sensor device according to one of claims 1 to 8, further comprising:

a further through-substrate via (16) in the substrate (1),  
a conduit (17) connecting the through-substrate via (6) and the further through-substrate via (16), and  
a plurality of individual waveguides forming the waveguide (7), the individual waveguides traversing the through-substrate via (6), the further through-substrate via (16), or both the through-substrate via (6) and the further through-substrate via (16).

10. The particle sensor device according to claim 9, wherein the through-substrate via (6) and the further through-substrate via (16) have different dimensions along directions of the individual waveguides.

11. The particle sensor device according to one of claims 1 to 10, further comprising:

a further substrate (10), the substrate (1) being

arranged on the further substrate (10), and a duct (11) in the further substrate (10), the duct (11) prolonging the through-substrate via (6).

12. The particle sensor device according to claim 11, further comprising:

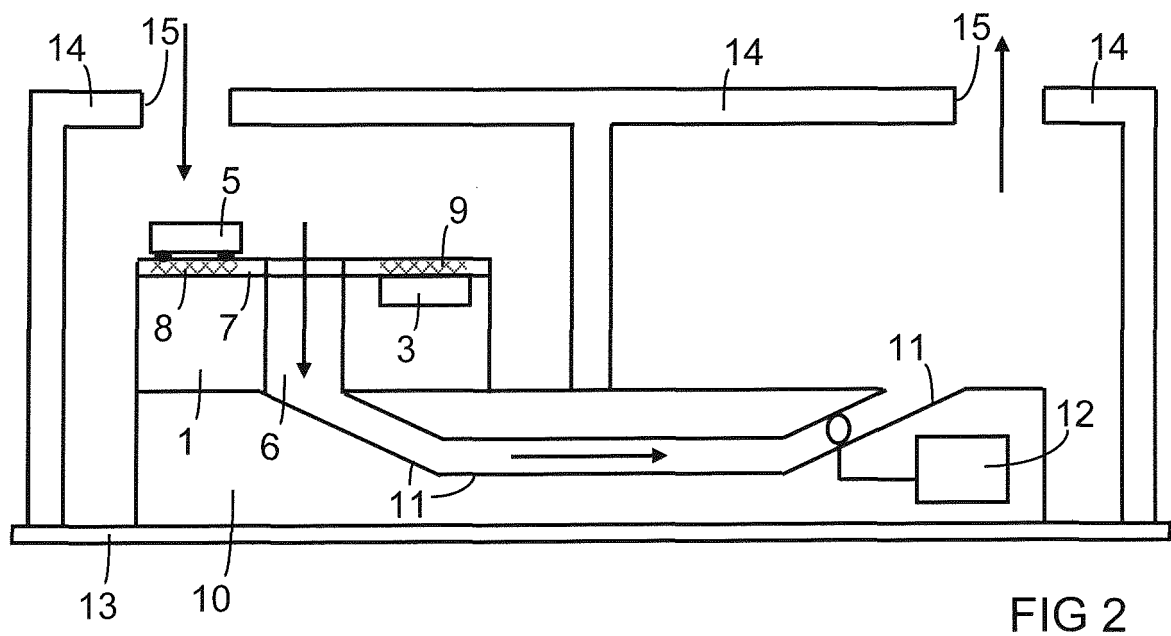
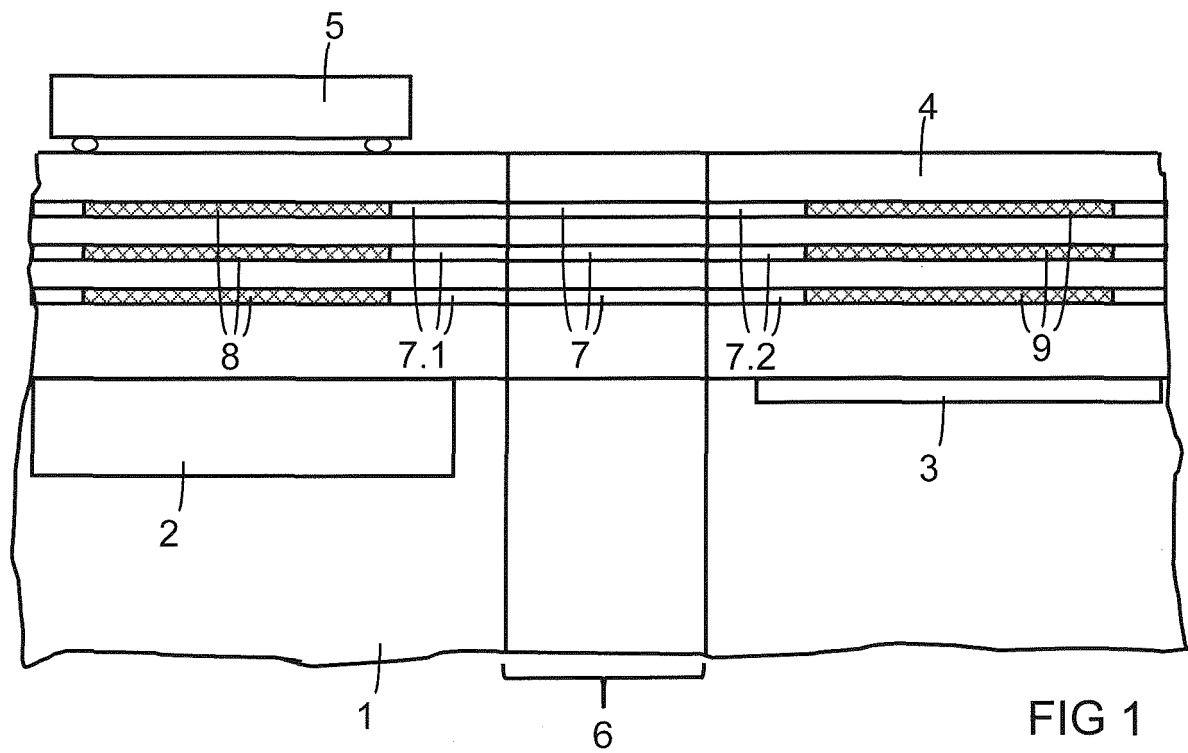
a housing (14) with at least two separate openings (15), the substrate (1) and the further substrate (10) being arranged in the housing (14), the openings (15) communicating with one another via the through-substrate via (6) and the duct (11).

13. The particle sensor device according to claim 12, wherein the through-substrate via (6) and the duct (11) are the only connection between the openings (15) inside the housing (14).

14. The particle sensor device according to one of claims 11 to 13, further comprising:

a fan or pump (12) in the further substrate (10), the fan or pump (12) being configured to generate a gas flow through the through-substrate via (6) and the duct (11).

15. The particle sensor device according to claim 14, wherein the gas flow is modulated by a geometry of the through-substrate via (6) and by an operation of the fan or pump (12).



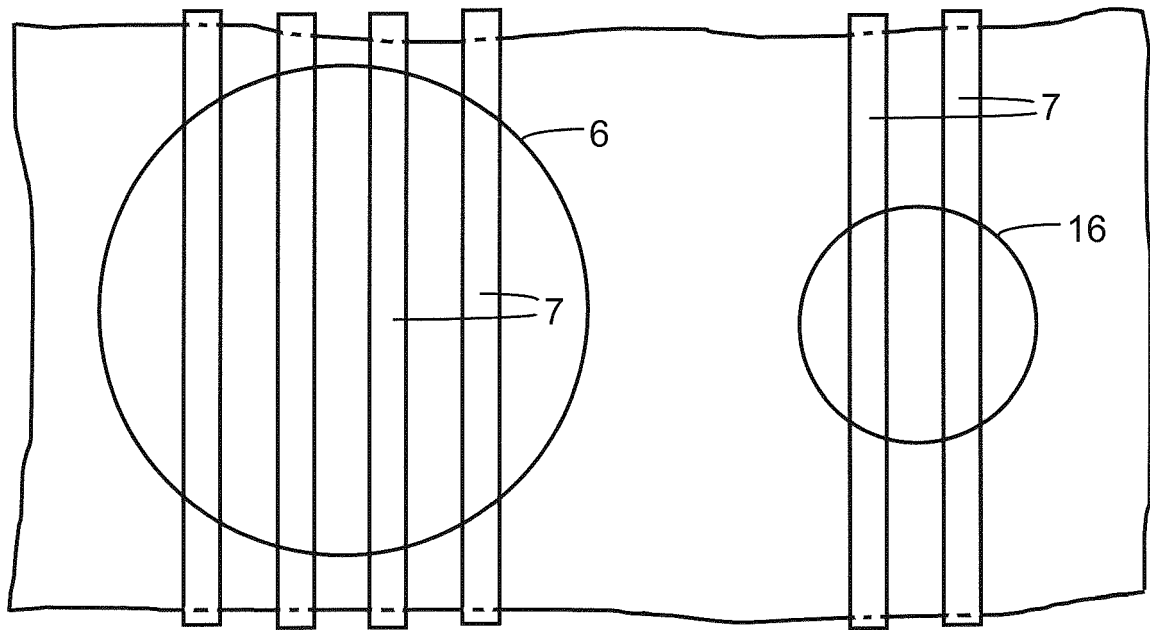


FIG 3

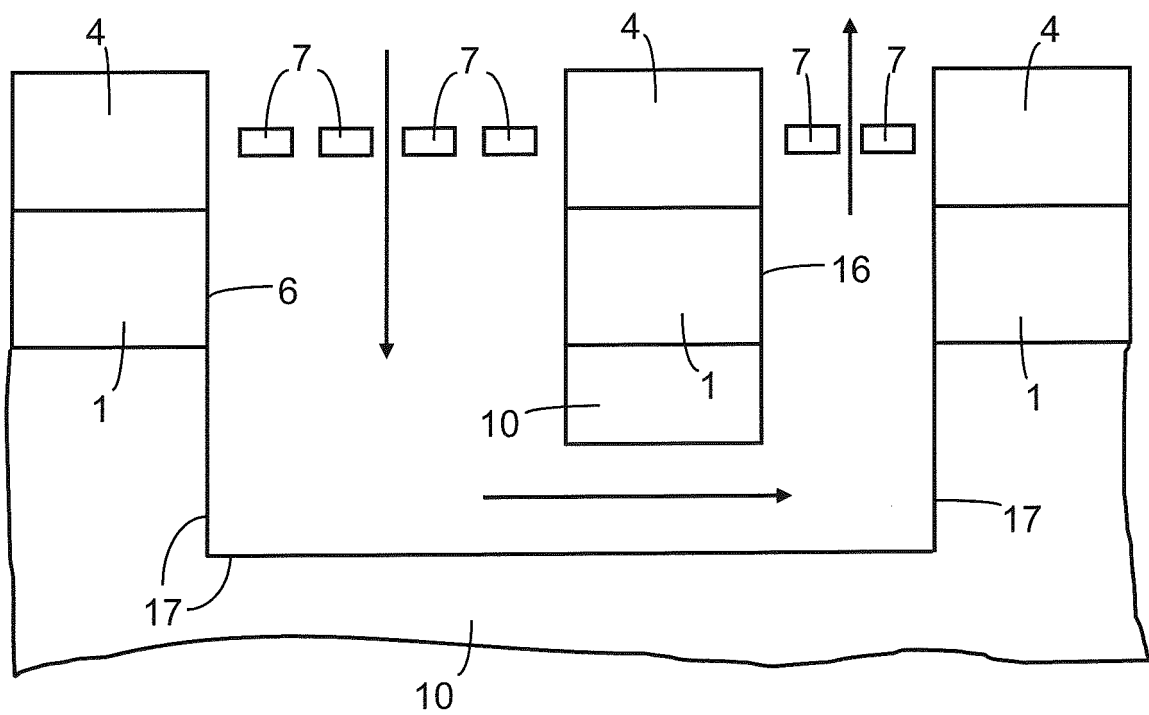


FIG 4

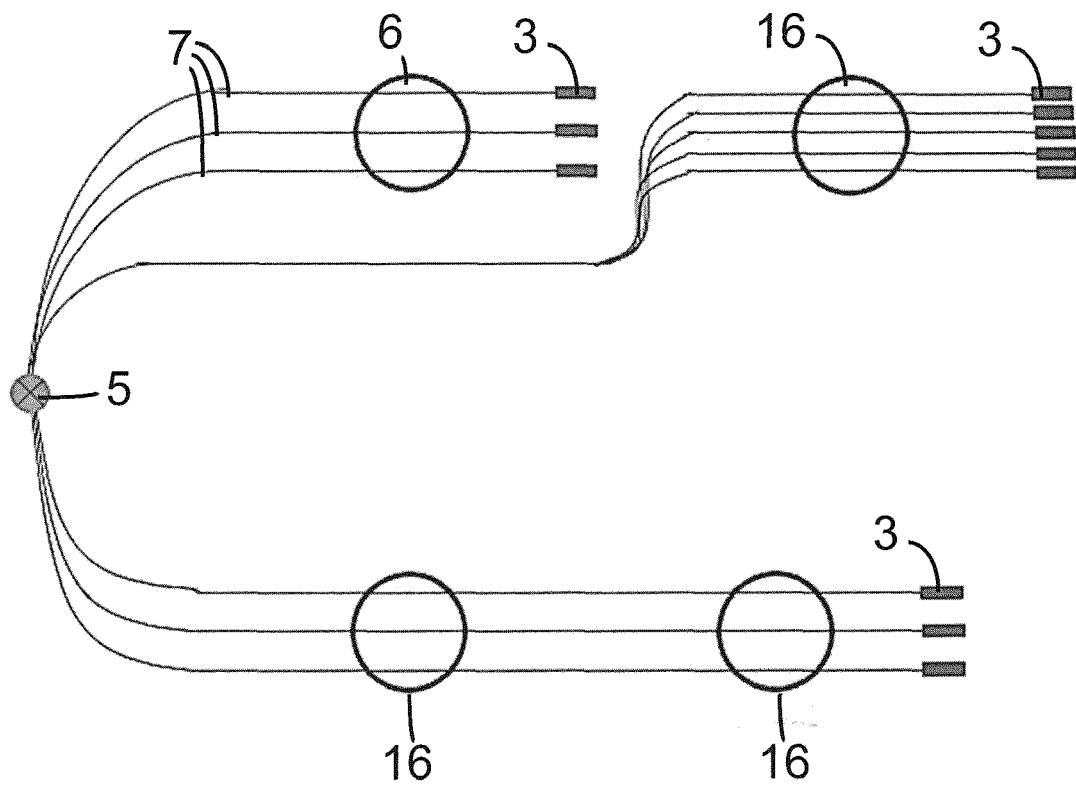


FIG 5



## EUROPEAN SEARCH REPORT

Application Number  
EP 17 20 7761

5

10

15

20

25

30

35

40

45

50

55

DOCUMENTS CONSIDERED TO BE RELEVANT			
Category	Citation of document with indication, where appropriate, of relevant passages	Relevant to claim	CLASSIFICATION OF THE APPLICATION (IPC)
X	US 2012/170044 A1 (PRABHAKAR AMIT [IN] ET AL) 5 July 2012 (2012-07-05) * abstract * * paragraph [0060]; figure 3F * * figure 13B * * paragraph [0061]; figure 3F * * paragraph [0087] * * figure 13E * * paragraph [0054] *	1-15	INV. G01N15/06 G01N21/53  ADD. G01N15/00
A	----- CN 103 630 466 A (CHINESE ACAD INST ELECTRONICS; FOURTH RES INST OF THE CHINESE PEOPLE S) 12 March 2014 (2014-03-12) * figure 1 * * figure 4 * -----	1-15	
			TECHNICAL FIELDS SEARCHED (IPC)
			G01N
The present search report has been drawn up for all claims			
Place of search <b>The Hague</b>		Date of completion of the search <b>29 May 2018</b>	Examiner <b>Mensink, Rob</b>
CATEGORY OF CITED DOCUMENTS X : particularly relevant if taken alone Y : particularly relevant if combined with another document of the same category A : technological background O : non-written disclosure P : intermediate document T : theory or principle underlying the invention E : earlier patent document, but published on, or after the filing date D : document cited in the application L : document cited for other reasons & : member of the same patent family, corresponding document			

EPO FORM 1503 03.82 (F04C01)

**ANNEX TO THE EUROPEAN SEARCH REPORT  
ON EUROPEAN PATENT APPLICATION NO.**

EP 17 20 7761

5

This annex lists the patent family members relating to the patent documents cited in the above-mentioned European search report.  
The members are as contained in the European Patent Office EDP file on  
The European Patent Office is in no way liable for these particulars which are merely given for the purpose of information.

29-05-2018

10

15

20

25

30

35

40

45

50

55

Patent document cited in search report	Publication date	Patent family member(s)	Publication date
US 2012170044 A1	05-07-2012	NONE	
CN 103630466 A	12-03-2014	NONE	

EPO FORM P0459

For more details about this annex : see Official Journal of the European Patent Office, No. 12/82



## **A.3 Patent Application EP19211018.7: APPARATUS AND METHOD FOR DETECTING OBJECTS**

## Description

### Apparatus and method for detecting objects

- 5 The present disclosure relates to an apparatus for detecting objects and to a method for detecting objects. Specifically, the disclosure employs an optical interferometer with an interaction volume.
- 10 Most low-cost state of the art optical particle detectors rely on detecting light that is scattered from objects or particles that are located in a sampling volume. Such particle detectors typically employ a light source, such as a laser, for illuminating the objects or particles in the
- 15 sampling volume and a photodetector arranged at a certain scattering angle with respect to optical axis defined by the path between a light source and the sampling region. The photodetector is thus configured to detect the amount of light that is scattered from the objects or particles in the
- 20 sampling volume at said scattering angle. The resulting signal is proportional to the particle number concentration within the sampling volume and contains information on the size of the particles.
- 25 The state of the art particle detectors have a number of disadvantages. Firstly, most of the scattered light is lost and does not contribute to the signal as the photodetector is only configured to measure scattered light at a single certain scattering angle. Moreover, in typical scattering the
- 30 bulk of the light is scattered in a forward direction, i.e. further along the optical axis, and typically cannot be discriminated from the incident light beam. In addition,

light that is absorbed by the particles is also lost and does not contribute to the signal.

Furthermore, for actual particle detection, the index of refraction has to be known or assumed for every particle in the sampling region. Also, conventional particle detectors require a minimum particle size in the order of 200 to 300 nm, which is larger than many types of particles of interest for such detectors, such as soot particles that have a diameter of around 20 nm to 100 nm and are thus not detectable by conventional detectors.

An object to be solved is to provide an improved concept of an apparatus for detecting objects and/or particles and of a method for detecting such objects and/or particles.

This object is achieved with the subject-matter of the independent claims. Embodiments and developments of the improved concept are the subject-matter of the dependent claims.

The improved concept is based on the idea of introducing objects or particles that are to be detected into an interaction volume of an optical interferometer and subsequently detecting the change in the interference signal caused by a change in the effective path length of the optical interferometer and extinction of light. As such a change of the effective path length in an optical interferometer can be detected with tremendous sensitivity, even objects as small as nanoparticles can be potentially detected with an apparatus according to the improved concept. Specifically, the improved concept can be applied to free space as well as to waveguide-based interferometers.

An apparatus for detecting objects according to the improved concept comprises an optical interferometer that is configured to receive electromagnetic radiation from a light source, and emit electromagnetic radiation to a detector.

5    Therein, the optical interferometer is coupled to an environment and further configured to respond to objects in the environment intruding into an interaction volume of the optical interferometer by varying an intensity of the electromagnetic radiation emitted to the detector based on a  
10   property of the objects in the interaction volume. The apparatus further comprises a signal processor that is configured to generate an output signal based on the intensity of the electromagnetic radiation emitted to the detector.

15

The electromagnetic radiation is light from a light source that is provided to the optical interferometer, for instance. For example, the light source is comprised by the apparatus. Alternatively, the light source is an external light source.

20   The electromagnetic radiation can be monochromatic, e.g. a laser beam, or is broadband, e.g. light from an LED.

Analogous to the light source, the detector can either be comprised by the apparatus or be an external detector.

25   Depending on the type of optical interferometer employed, the detector can be a single detector or a detector array having multiple detector channels, such as a balanced detector. For monochromatic light sources, the detector can be a photodetector such as a photodiode. For broadband  
30   electromagnetic radiation, the detector can be a spectrometer.

The optical interferometer serves the purpose of emitting the electromagnetic radiation to the detector with an intensity that depends on a property of objects that intrude into an interaction volume of the interferometer. The interaction  
5 volume is a part of the interferometer at which objects can interact with the electromagnetic radiation that is coupled into the interferometer. For example, the intensity emitted to the detector deviates from a standard intensity, e.g. a predefined intensity which may be zero, if objects are  
10 located in or traverse the interaction volume, whereas the standard intensity is emitted to the detector in the case that no object is present in or traverses the interaction volume. The property of the objects can be a number and/or a size of the objects. In other words, an effective path length  
15 of the interaction volume can depend on a number and/or on a size of the objects intruding into the interaction volume.

The signal processor, for example, comprises an evaluation circuit that is configured to generate the output signal  
20 based on a signal generated by the detector based on the detected intensity of the electromagnetic radiation emitted to the detector. The output signal can be provided to a further processor for generating an output value indicating a presence of objects in the interaction volume and/or a  
25 measurement of the property of the objects, for instance. The further processor can be comprised by the apparatus or be an external processor.

In some embodiments, the apparatus further comprises an  
30 instrument for generating a fluid flow through the interaction volume.

The apparatus in these embodiments further features an instrument for deliberately directing objects towards and through the interaction volume. For example, a pump or a fan structure generates a fluid stream that is directed from the instrument towards the interaction volume. Optionally, the instrument further comprises a particle transfer unit for directing a specific species of objects towards the interaction volume. Furthermore, for a well-defined flow, the instrument can comprise a nozzle for ejecting objects from the instrument towards the interaction volume in a well-defined manner, e.g. with a constant velocity. With a laminar flow, turbulences can be avoided in the interaction volume, for instance.

15 In some embodiments, the optical interferometer is further configured to operate at a predetermined operating point if the interaction volume is free of objects.

The operating point of the interferometer can be set such that in the absence of objects in the interaction volume, a predefined intensity of electromagnetic radiation is emitted from the interferometer to the detector. To this end, the interferometer can be tuned, e.g. by means of adjusting a cavity length in relation to the wavelength of the light source, such that a specific operating point is achieved. For example, the operating point can be set such that minimum, near minimum or zero intensity is emitted to the detector if no objects are present in the interaction volume by realizing destructive interference of the interferometer.

30 Alternatively, said operating point can be set such that maximum or near maximum intensity is emitted to the detector if no objects are present in the interaction volume by realizing constructive interference of the interferometer.

For instance, the destructive interference condition for a Fabry-Pérot interferometer with a detector arranged in transmission is given by:  $2*n*d = (m+1/2)*\lambda$ , whereas for a detector arranged in reflection it is given by:  $2*n*d = m*\lambda$ . Therein,  $n$  is the index of refraction of a medium in the cavity,  $d$  is the distance between mirrors,  $\lambda$  denotes the wavelength of the electromagnetic radiation, and  $m$  is a positive integer.

10 As the operating point of an interferometer generally depends on the refractive index of the medium in a cavity of the interferometer, slight changes in temperature, absolute pressure and/or the surrounding gas can significantly influence the operating point.

15

In order to compensate for such drifts, countermeasures such as a tunable or a broadband light source can be employed for providing the electromagnetic radiation to the interferometer. For broadband radiation, a spectrometer can be used as the detector, realized by using a photodiode array with thin film wavelength selective filters on top of each single photodiode, for instance. Hence, the transmission or reflection of an interferometer can be monitored as a function of the wavelength with such a spectrometer. Other solutions include standard realizations of spectrometers, e.g. by utilizing a diffraction grating or a prism. Alternatively, differential measurements with no fixed operating point can be performed.

30 In some embodiments, the interferometer is one of the following types of interferometers: Mach-Zehnder interferometer, Michelson interferometer, Sagnac interferometer, Twyman-Green interferometer, and Fabry-Pérot

interferometer. The interferometer can be a Fabry-Pérot-based interferometer comprising two mirrors facing each other and thus forming a cavity. The mirrors can be any combination of plane parallel, concentric focal, hemispherical, concave and  
5 convex. The cavity mirrors can be made of any standard material for optics, such as fused silica or  $\text{CaF}_2$ . Moreover, the mirrors can comprise a thin film coating, e.g. a gold or silver coating, for tuning the reflectivity of the mirrors. The reflectivity of each mirror can be in the range of 30% to  
10 over 99%, for instance. The size of the mirrors of the cavity can be approximately  $300 \times 300 \mu\text{m}^2$  to 500 by 500  $\mu\text{m}^2$ , thus having a relatively high ratio of particle cross-section to light beam cross-section in the interaction volume which is the cavity volume between the mirrors, for instance. The  
15 cavity length in these cases can be accordingly in the order of 0.3 mm to a few tens of millimeters.

For Fabry-Pérot-type interferometers operating in reflection mode, the interferometer can further comprise a beam-  
20 splitting element, such as a thin-film beam splitter or a prism with approximately 50/50 reflection and transmission.

Alternative solutions are interferometers that comprise multiple arms such as Michelson and Mach-Zehnder  
25 interferometers. In these interferometer types, the interaction volume can be located in one of the arms. The realizations of the interferometric setup are analogous to a Fabry-Pérot-type interferometer.

30 In some embodiments, the interaction volume is a free space volume of the interferometer.



For example, in a Fabry-Pérot, Michelson or Mach-Zehnder type free space interferometer, the propagation of the electromagnetic radiation occurs at least partially in free space, i.e. through a gaseous or through a vacuum volume. For  
5 example, the interaction volume is located in a free space cavity of a Fabry-Pérot-type interferometer or in a free space path in one of the arms of a Michelson or Mach-Zehnder type interferometer.

10 Objects or particles intruding into the free space interaction volume alter the effective optical path length due to their refractive index being different from that of the medium in the interaction volume or alter the operating point of the interferometer through absorption of  
15 electromagnetic radiation. Thus, the presence of a particle can be detected due to a varying transmission and/or reflection of the interferometer.

In some embodiments, the interaction volume is an evanescent  
20 field region of a waveguide structure of the interferometer.

In these embodiments, the interferometer can be of one of the types described above and comprise a dielectric waveguide structure in which the electromagnetic radiation propagates  
25 through total internal reflection. To this end, a waveguide core with a higher refractive index than that of surrounding materials is employed. For such waveguide structures, the electromagnetic field at and outside the core interfaces does not vanish but decays exponentially in the surrounding  
30 material as an evanescent field. The evanescent field strength around the core can be tuned by altering the dimensions of the core and hence altering the ratio of electromagnetic field inside and outside the core. The core

dimensions in a cross-section of the waveguide structure can be in the order of the wave length of the electromagnetic radiation, e.g. in the order of a few hundreds of nanometers.

- 5 Objects entering the evanescent field region interact with the electromagnetic field which influences the transmission of the waveguide structure through scattering and/or absorption processes, for instance. Also, a refractive index of the objects being different than that of the medium  
10 surrounding the waveguide structure induces a phase change, therefore also in this case altering the effective path length of the electromagnetic radiation through the waveguide.
- 15 In some embodiments, the optical interferometer operates in transmission or reflection.

Depending on the application and/or on the type of interferometer employed in the apparatus, the detector can be  
20 arranged for a measurement in transmission or in reflection. For a Fabry-Pérot-type interferometer, for example, in transmission the operating point can be set to a low level transmission but close to maximum transmission. In other words, the operating point can be near the flank of the the  
25 transmission function of the interferometer, e.g the Airy distribution function. If the reflected power is monitored, the operating point can be set to the maximum of the transmission function. Monitoring of the reflected power can be preferable for some interferometer types as the ground  
30 level signal at the detector can be achieved arbitrarily low in reflection while the maximum normalized transmission can in principle reach unity regardless of the finesse.

In some embodiments, the optical interferometer is configured to respond to objects with a minimum diameter of about 10 nm.

Due to the high sensitivity of optical interferometers, the  
5 detection of nanoparticles as small as 10 nm is possible with  
an apparatus according to the improved concept. This is an  
order of magnitude smaller than what can be achieved with  
conventional particle detectors that are based on light-  
scattering, for instance. Hence, an apparatus according to  
10 the improved concept can be employed for detecting objects  
such as anthropogenic and bio-aerosol particles, e.g. soot,  
fine dust, salt and pollen particles.

In some embodiments, the intensity of the electromagnetic  
15 radiation emitted to the detector is a function of size  
and/or refractive index of the objects intruding into the  
interaction volume.

The interferometer can be designed such that the emitted  
20 intensity is, for example, proportional or inversely  
proportional to the refractive index and/or the size of the  
objects. For example, this can be realized by providing an  
interferometer with an interaction volume that is  
characterized by a medium with a refractive index  
25 substantially different than that of the objects intruding  
into the interaction volume. For example, the interaction  
volume is an empty cavity or a cavity filled with air.

In some embodiments, the apparatus according to the improved  
30 concept further comprises a further interaction volume that  
is oriented parallel, or basically parallel, to the  
interaction volume, and a particle source emitting objects  
with a velocity that depends on a size of the objects. The

objects emitted from the particle source intrude into the interaction volume and the further interaction volume.

As described above, the signal at the detector can be a  
5 function of particle size and the refractive index. If the size of the objects is known, the signal at the detector can be used to calculate the refractive index of the particle and vice versa.

10 In some further embodiments, the further interaction volume is comprised by a further optical interferometer that is coupled to the environment and configured to respond to objects in the environment intruding into the further interaction volume by varying in intensity of electromagnetic  
15 radiation emitted, by means of the further optical interferometer, to a further detector based on a property of the objects in the further interaction volume.

The object is further solved by a particle detector, in  
20 particular designed as an integrated device, comprising an apparatus for detecting objects according to one of the embodiments described above.

In order to have a maximum of stability with respect to  
25 vibrations and to have a smallest possible sensor e.g. for mobile applications, the sensor can be realized as follows: The particle detector device can comprise a substrate, a photodetector, a dielectric on, above or within the substrate, a source of electromagnetic radiation, and a  
30 through-substrate via in the substrate. The through-substrate via is exposed to the environment, in particular to ambient air. A waveguide is arranged in, above or within the dielectric so that the electromagnetic radiation emitted by

the source of electromagnetic radiation is coupled into a portion of the waveguide. A further portion of the waveguide is opposite the photodetector, so that said portions of the waveguide are on different sides of the through-substrate  
5 via. By having the via also extending through the waveguide, the optical cavity is formed. A material such as gold can be sputtered onto the surfaces of the optical cavity formed by the waveguide and the via to increase the reflectivity.

10 If used in reflection, the system needs to have a beam splitter integrated in the waveguide. The beam splitter has to be situated after the source of radiation and before the optical cavity. The cavity can be etched into an optical fiber, similar to the via in the substrate. In fiber optics  
15 there are standard elements such as beam splitters and coupled light sources and detectors available which are used for example in telecommunication. Furthermore, the cavity can be formed by discrete elements which have to be fixed in a stable way.

20 The object is further solved by a method for detecting objects. The method comprises coupling an optical interferometer to an environment, receiving by means of the optical interferometer electromagnetic radiation from a light  
25 source, and emitting by means of the optical interferometer electromagnetic radiation to a detector. The method further comprises varying in intensity of the electromagnetic radiation emitted to the detector based on a property of objects intruding from the environment into an interaction  
30 volume of the optical interferometer. The method further comprises generating an output signal based on the intensity of the electromagnetic radiation emitted to the detector.

Further embodiments of the method for detecting objects become apparent to a person skilled in the art from the embodiments of the apparatus described above.

5 The improved concept will be described in more detail in the following with the aid of drawings. Elements having the same or similar function bear the same reference symbols throughout the drawings. Hence, the description is not necessarily repeated in the description of the following  
10 drawings.

In the drawings:

15 Figures 1 and 2 show an exemplary embodiment of an apparatus for detecting objects according to the improved concept;  
Figure 3 shows a further exemplary embodiment of an apparatus for detecting objects;  
20 Figure 4 shows various cavity configurations of an interferometer employed in an exemplary embodiment of an apparatus for detecting objects;  
Figures 5 to 9 show further exemplary embodiments of an apparatus for detecting objects;  
25 Figure 10 illustrates the working principle of an exemplary embodiment of an apparatus for detecting objects comprising a waveguide based interferometer; and  
Figure 11 illustrates suitable choices of operating  
30 points of an interferometer employed in an apparatus according to the improved concept.

Figure 1 shows an exemplary embodiment of an apparatus 1 for detecting objects according to the improved concept. In this embodiment, the apparatus 1 comprises a Fabry-Pérot type interferometer 2 having two mirrors 2a, 2b that form a Fabry-Pérot cavity enclosing a free space interaction volume 5. The mirrors 2a, 2b are thus optical cavity mirrors and can be made of any standard material for optics, such as fused silica or CaF<sub>2</sub>. Optionally, the mirrors 2a, 2b can comprise a thin film coating, such as a gold or a silver coating, for tuning the reflectivity.

The apparatus 1 further comprises a light source 3, e.g. a monochromatic light source such as a laser light source, and a detector 4. For example, the light source 3 is a VCSEL, a NdYAG, a HeNe laser, a diode laser, a distributed feedback laser. Alternatively, the light source 3 can be an LED. In alternative embodiments, the light source 3 can be a broadband light source. The detector can be realized as a photo diode or as a single photon avalanche diode, for instance.

The light source 3 emits electromagnetic radiation, e.g. visible light, towards the first mirror 2a of the interferometer 2. The mirrors 2a, 2b are characterized by a reflectivity that is less than 1. In other words, a certain amount of electromagnetic radiation is transmitted by the mirrors 2a, 2b. For example, the reflectivity of the mirrors 2a, 2b are between 30% and above 99%. The reflectivities of the mirrors 2a, 2b can be the same or be different from each other. Due to this, electromagnetic radiation is coupled into the cavity and circulates between the mirrors 2a, 2b of the interferometer 2. Behind the second mirror 2b the detector 4 is arranged and configured to detect the electromagnetic

radiation that is emitted from the interferometer 2 through the second mirror 2b. Hence, the embodiment shown features an optical interferometer 2 that operates in transmission.

5 The interferometer 2 is aligned such that in the absence of objects in the interaction volume 5, the electromagnetic radiation within the cavity interacts destructively such that no or nearly no electromagnetic radiation is coupled out through the second mirror 2b towards the detector 4. This is  
10 also often referred to as a dark-field configuration of the interferometer 2.

The embodiment further features an instrument 6 for generating a fluid flow through the interaction volume 5. For  
15 example, the instrument 6 creates an airstream of objects 10 using a pump and/or a nozzle such that the objects 10 traverse the interaction volume 5. In the drawing, the airstream is directed into or out of the plane of the drawing. The fluid flow can aid in directing wanted objects  
20 10 intentionally towards the interaction volume 5 for enhancing the efficiency of the apparatus 1. Also, in some embodiments, depending on the interferometer type and readout scheme, the sensitivity to moving objects 10 can be larger compared to that of stationary objects 10.

25

The apparatus 1 further comprises a signal processor for generating an output signal based on the signal detected by the detector 4. For illustration purposes, the signal processor is not shown in the figure.

30

Figure 2 shows the exemplary embodiment of the apparatus 1 shown in Figure 1 with objects 10 inside the interaction volume 5, i.e. within the cavity of the interferometer 2. For



example, the objects 10 are introduced via an airstream created by the instrument 6. The objects 10 influences the operation of the interferometer 2 in multiple manners. Firstly, due to scattering and/or absorption effects, light within the cavity is lost, hence disturbing the balance of the destructive interference. Secondly, due to the refractive index of the objects 10 being substantially different from that of a medium in the cavity, e.g. air, the effective optical path length is altered, i.e. increased, thus changing the operating point of the interferometer 2.

As a result, the intensity emitted from the interferometer 2 towards the detector 4 changes, e.g. increases. A signal at the detector 4 being different from that of an empty cavity thus indicates the presence of objects 10. It is apparent that the larger the number of objects 10 and/or the larger the size of the objects 10, the higher is the disturbance and hence the larger is the signal at the detector 4. In other words, the signal at the detector 4 in this embodiment of the apparatus is a function of, e.g. proportional to, object size and/or number.

Figure 3 shows a further exemplary embodiment of an apparatus 1 that is based on that shown in Figure 1. In contrast to the latter, in this embodiment the interferometer 2 operates in reflection. In other words, the detector 4 is arranged on the same side of the Fabry-Pérot cavity as the light source 3. In order to distinguish between input and output radiation, a beam splitter 2c is employed such that no input radiation is detected by the detector 4. For example, the beam splitter is a thin film beam splitter or a prism with for example 50-50 reflection and transmission.

In contrast to the embodiment shown in Figures 1 and 2, the preferred dark-field configuration in this embodiment means that the cavity of the interferometer 2 is aligned such that in case of an empty cavity, i.e. in the absence of objects 10 in the interaction volume 5, the transmission at the second mirror 2b is maximum. This way, no or substantially no radiation exits the cavity via the first mirror 2a and reaches the detector 4. Apart from this, the working principle of this embodiment is similar to that shown in the previous figures.

Figure 4 shows various cavity configurations of a Fabry-Pérot type interferometer 2 employed in an apparatus 1 according to the improved concept. As shown in the Figure from top to bottom, the cavity mirrors 2a, 2b can be chosen to be plane-parallel, concentric, spherical, of different types such as concave convex, or confocal. Typical cavity parameters include the cavity length  $L$  and the radius of curvature  $R$  of the cavity mirrors 2a, 2b. Depending on the choices, different beam wastes can be achieved at different locations within the cavity as illustrated. For example, a small beam waste is suitable for rendering the interferometer 2 sensitive to extremely small objects few tens of nanometers in diameter, such as soot particles.

Figure 5 shows a further exemplary embodiment of an apparatus 1 according to the improved concept. In this embodiment, the apparatus 1 comprises a Michelson type interferometer 2 comprising a beam splitter 2c and to end mirrors 2a, 2b forming two interferometer arms. The interaction volume 5 is located in one of the arms, the sensing arm SA, while the other arm, the reference arm RA, is free of any objects 10 at all times. Also in this embodiment, the detector 4 is

arranged with respect to the beam splitter 2c such that no radiation is detected directly from the light source 3.

In a Michelson type interferometer, the distances of the  
5 mirrors 2a, 2b from the beam splitter 2c can be tuned to achieve a certain operating point of the interferometer 2. For example, the distances are tuned such that destructive interference occurs at the location of the beam splitter 2c, hence also in this case realizing a dark-field configuration  
10 wherein no or substantially no radiation reaches the detector 4 in case no objects 10 are located in or traverse the interaction volume 5. Analogous to the embodiments of Figures 1 to 3, this embodiment also features an instrument 6 for generating a fluid flow through the interaction volume 5.

15 Figure 6 shows a further exemplary embodiment of an apparatus 1 according to the improved concept. In this embodiment, the apparatus 1 comprises a Mach-Zehnder type interferometer 2 comprising two beam splitters 2c, 2d. The Mach-Zehnder  
20 interferometer 2 further comprises a phase shifting element 2e in the reference arm RA for shifting the phase in order to achieve a certain operating point. The embodiment further features two detectors 4 that each are arranged on one of the output sides of the second beam splitter 2d. However, either  
25 one of the detectors 4 is sufficient for efficient operation of the apparatus 1.

Analogous to the Michelson interferometer shown in the previous drawing, the interaction volume 5 is located in the  
30 sensing arm SA. Also in this case, the apparatus one can feature an instrument 6 for generating a fluid flow through the interaction volume 5 as mentioned before.

Figure 7 shows a further exemplary embodiment of an apparatus 1 for detecting objects. In this embodiment, the apparatus 1 comprises a particle source 7 that is configured to emit objects 10 with a velocity that depends on a size of the objects 10. For example, this is realized via a nozzle on the output of the particle source 7. The aforementioned instrument 6 can be the nozzle, for instance.

The apparatus 1 further comprises a further interaction volume 5a that is oriented basically parallel to the interaction volume 5 of the interferometer 2. Therein, the interferometer 2 can be any interferometer type, such as those described in illustrated in the previous figures. The further interaction volume 5a is for example a light barrier realized by a further light source 3a and a further detector 4a arranged opposite of each other.

The particle source 7 is configured to emit the objects 10 such that the objects 10 traverse both the interaction volume 5 and the further interaction volume 5a. The order with which the interaction volumes 5, 5a are arranged with respect to the particle source 7 can be chosen arbitrarily.

As the final velocity of a particle after leaving a nozzle is a function of the aerodynamic particle size, the measured time difference between each object 10 traversing the interaction volume 5 and traversing the interaction volume 5a gives information of the particle size. Furthermore, as mentioned before, the signal at the detector 4 is a function of object size and refractive index of the object 10. Hence, if the object size is determined, e.g. via the time difference, the signal at the detector 4 can be used to calculate the refractive index of the object 10. Thus,

different particle classes, such as soot, dust, salt or pollen, can be discriminated by size and refractive index using an apparatus 1 as shown.

- 5 In an alternative embodiment not shown, the further interaction volume 5a can be realized inside a further interferometer. This can further enhance the sensitivity of the object detection mechanism.
- 10 Figure 8 shows an exemplary embodiment of an apparatus 1 comprising a waveguide based interferometer 2. The interferometer 2 is a Mach-Zehnder type interferometer. However, all interferometer types are possible. Also in this case, the interferometer 2 comprises two arms, a sensing arm
- 15 SA and a reference arm RA, and two beam splitters 2c, 2d. For example, the beam splitter is a waveguide beam splitter or a directional coupler e.g. with 50-50 reflection and transmission. The interferometer 2 further comprises a phase shifting element 2e in the reference arm RA for shifting the
- 20 phase in order to tune the system to a certain operating point.

- The sensing arm SA features the interaction volume 5, e.g. realized by an uncladded waveguide core with cross-sectional
- 25 dimensions that are in the order of the wavelength of electromagnetic radiation, e.g. in the order of 1  $\mu\text{m}$ . Guiding light through such a waveguide means that a significant amount of light propagates as evanescent field, i.e. outside the waveguide. Also, for waveguide based interferometers, an
- 30 instrument 6 can be employed to direct objects 10 towards the interaction volume 5.

Objects 10 that are located within this evanescent region, which is the interaction volume 5, alter the amount of light that is transmitted via scattering and/or absorption processes. Furthermore, due to a local change of the refractive index, also in this case the effective optical path length is altered, hence leading to a path length difference between the two interferometer arms. Due to these effects, the signal at the detector 4 changes from the operating point in case no objects 10 are located within the interaction volume 5.

Figure 9 shows a three-dimensional scheme of a further exemplary embodiment of an apparatus 1. In this embodiment, a free space cavity analogous to that illustrated in Figures 1 and 2 is formed via a gap between two waveguides. The cavity mirrors 2a, 2b therein are formed by end facets of the waveguides. A first waveguide directs light from the light source 3 towards the first mirror 2a, i.e. towards the cavity, while a second waveguide directs light from the second mirror 2b, i.e. from the cavity, towards the detector 4. The instrument 6 is arranged with respect to the interaction volume 5 such that objects 10 are directed towards and/or through the interaction volume 5.

Figure 10 illustrates the near-field around a waveguide and shows the electromagnetic field strength in cross-section. If an object 10 is located in the evanescent region of the waveguide, e.g. if an object 10 is adsorbed, the evanescent field is disturbed at the location of the object 10 leading to the effects mentioned above. In particular, the transmission in z-direction is influenced.

Figure 11 shows exemplary transmission functions of a Fabry-Pérot type interferometer for different reflectivities of the mirrors 2a, 2b indicated as the percentage numbers in the figure. In the graph, the normalized transmission intensity is plotted versus phase angle  $\alpha$ . For a detector configuration in transmission, a suitable operating point for the dark-field configuration is indicated as T in the figure for mirror reflectivities of 98%. The transmission operating point T is set to a low level transmission but close to maximum transmission. In other words, the operating point is chosen to be near the flank of the transmission function of the Fabry-Pérot cavity.

In contrast, for a detector configuration in reflection, the reflection operating point R is preferably chosen to be the point of maximum transmission independent of the mirror reflectivities. In both cases, the presence of even small objects can lead to a significant change of the interferometer's operating point and hence of the signal detected at the detector 4.

## Reference numerals

	1	apparatus
	2	interferometer
5	2a, 2b	mirror
	2c, 2d	beam splitters
	2e	phase shifting element
	3, 3a	source
	4, 4a	detector
10	5, 5a	interaction volume
	6	instrument
	7	particle source
	10	object
	R	reflection operating point
15	T	transmission operating point
	RA	reference arm
	SA	sensing arm



## Claims

1. An apparatus (1) for detecting objects (10), comprising
  - an optical interferometer (2) that is configured to
  - 5 - receive electromagnetic radiation from a light source (3);
  - and
  - emit electromagnetic radiation to a detector (4); wherein
  - the optical interferometer (2) is coupled to an
  - environment and further configured to respond to objects
  - 10 (10) in the environment intruding into an interaction
  - volume (5) of the optical interferometer (2) by varying an
  - intensity of the electromagnetic radiation emitted to the
  - detector (4) based on a property of the objects (10) in
  - the interaction volume (5); and
  - 15 - a signal processor configured to generate an output signal
  - based on the intensity of the electromagnetic radiation
  - emitted to the detector (4).
2. The apparatus (1) according to claim 1, further comprising
- 20 an instrument (6) for generating a fluid flow through the
- interaction volume (5).
3. The apparatus (1) according to claim 1 or 2, wherein the
- optical interferometer (2) is further configured to operate
- 25 at a predetermined operating point if the interaction volume
- (5) is free of objects (10).
4. The apparatus (1) according to one of claims 1 to 3,
- wherein the interferometer (2) is of one of the following
- 30 types of interferometers: Mach-Zehnder interferometer,
- Michelson interferometer, and Fabry-Pérot interferometer.

5. The apparatus (1) according to one of claims 1 to 4,  
wherein an effective path length of the interaction volume  
(5) depends on a number and/or on a size of the objects (10)  
intruding into the interaction volume (5).

5

6. The apparatus (1) according to one of claims 1 to 5,  
wherein the interaction volume (5) is a free space volume of  
the interferometer (2).

10 7. The apparatus (1) according to one of claims 1 to 5,  
wherein the interaction volume (5) is an evanescent field  
region of a waveguide structure of the interferometer (2).

8. The apparatus (1) according to one of claims 1 to 7,  
15 wherein the optical interferometer (2) operates in  
transmission or reflection.

9. The apparatus (1) according to one of claims 1 to 8,  
wherein the optical interferometer (2) is configured to  
20 respond to objects (10) with a minimum diameter of about 10  
nm.

10. The apparatus (1) according to one of claims 1 to 9,  
wherein  
25 - the electromagnetic radiation is monochromatic; or  
- the electromagnetic radiation is broadband and the  
detector (4) is a spectrometer.

11. The apparatus (1) according to one of claims 1 to 10,  
30 wherein the intensity of the electromagnetic radiation  
emitted to the detector (4) is a function of size and/or  
refractive index of the objects (10) intruding the  
interaction volume (5).

12. The apparatus (1) according to one of claims 1 to 11, further comprising

- a further interaction volume (5a) that is oriented basically parallel to the interaction volume (5); and
- 5 - a particle source (7) emitting objects (10) with a velocity that depends on a size of the objects (10); wherein
- the objects (10) emitted from the particle source (3) intrude the interaction volume (5) and the further
- 10 interaction volume (5a).

13. The apparatus (1) according to claim 12, wherein the further interaction volume (5a) is comprised by a further optical interferometer that is coupled to the environment and

15 configured to respond to objects (10) in the environment intruding into the further interaction volume (5a) by varying an intensity of electromagnetic radiation emitted, by means of the further optical interferometer, to a further detector (4a) based on a property of the objects (10) in the further

20 interaction volume (5a).

14. A particle detector, in particular designed as an integrated device, comprising an apparatus (1) for detecting objects (10) according to one of claims 1 to 13.

25

15. A method for detecting objects (10), the method comprising

- coupling an optical interferometer (2) to an environment;
- receiving by means of the optical interferometer (2)
- 30 electromagnetic radiation from a light source (3);
- emitting by means of the optical interferometer (2) electromagnetic radiation to a detector (4);

- 27 -

- varying an intensity of the electromagnetic radiation emitted to the detector (4) based on a property of objects (10) intruding from the environment into an interaction volume (5) of the optical interferometer (2); and
- 5 - generating an output signal based on the intensity of the electromagnetic radiation emitted to the detector (4).

## Abstract

### Apparatus and method for detecting objects

5 An apparatus (1) for detecting objects comprises an optical interferometer (2) that is configured to receive electromagnetic radiation from a light source (3), and emit electromagnetic radiation to a detector (4). The optical interferometer (2) is coupled to an environment and further  
10 configured to respond to objects (10) in the environment intruding into an interaction volume (5) of the optical interferometer (2) by varying an intensity of the electromagnetic radiation emitted to the detector (4) based on a property of the objects (10) in the interaction volume  
15 (5). A signal processor is configured to generate an output signal based on the intensity of the electromagnetic radiation emitted to the detector (4).

Significant Figure: Fig. 2

FIG 1

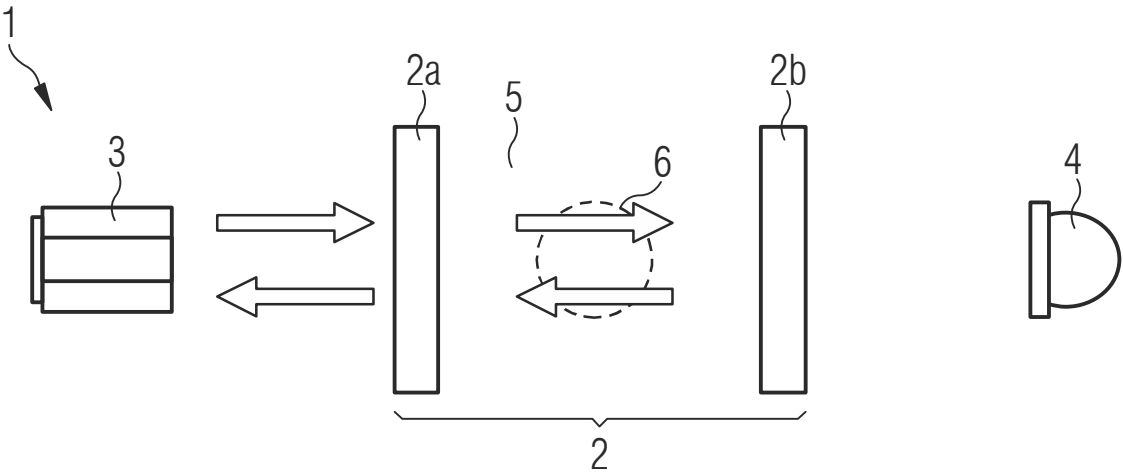


FIG 2

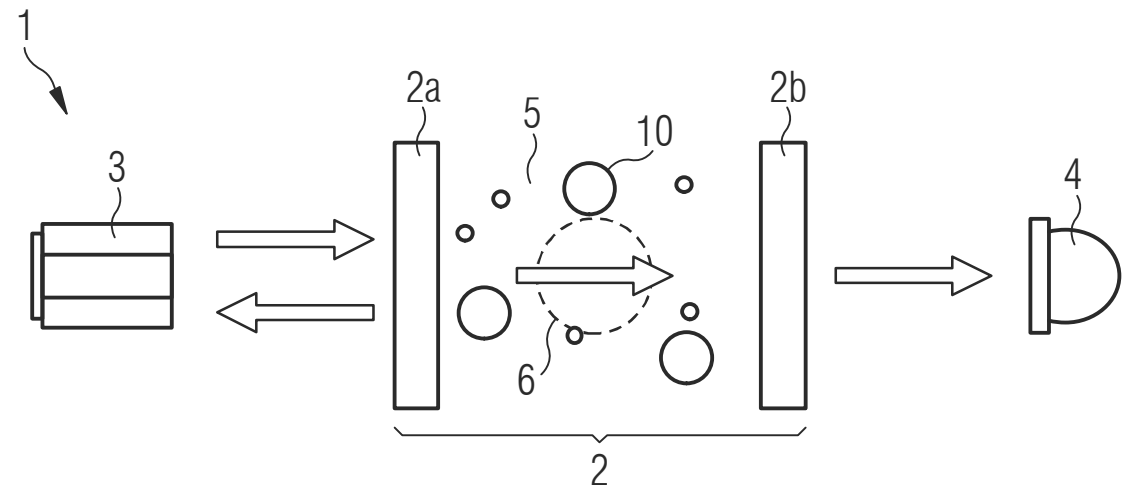


FIG 3

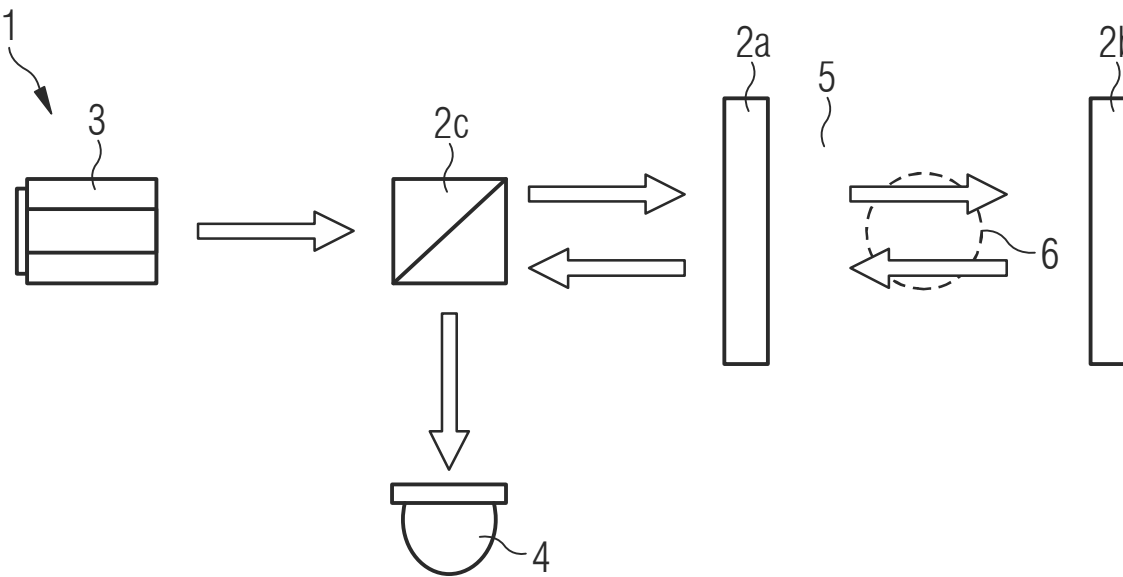


FIG 4

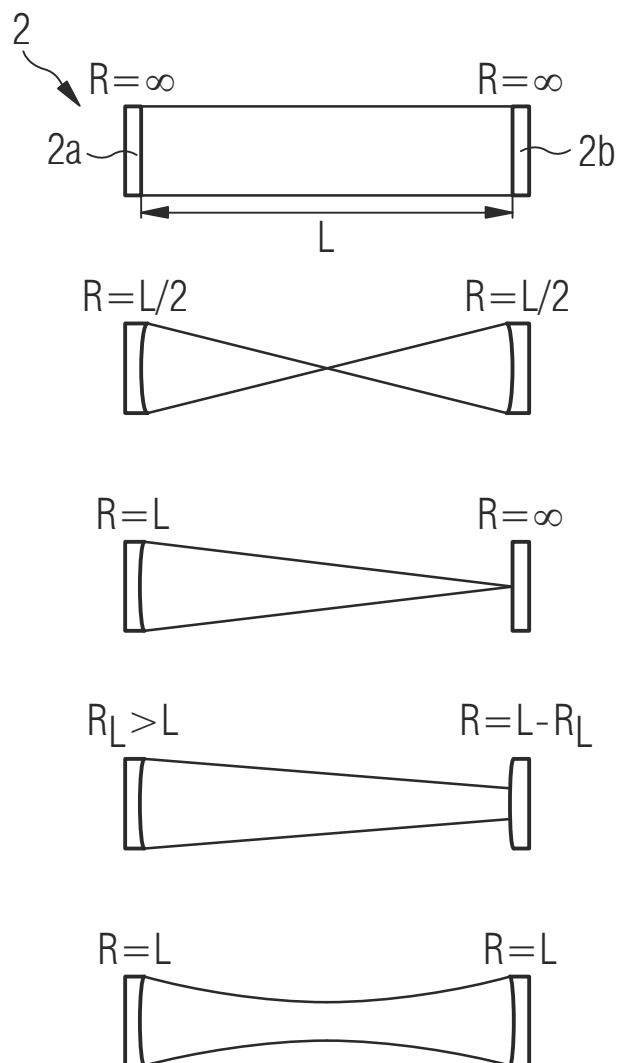


FIG 5

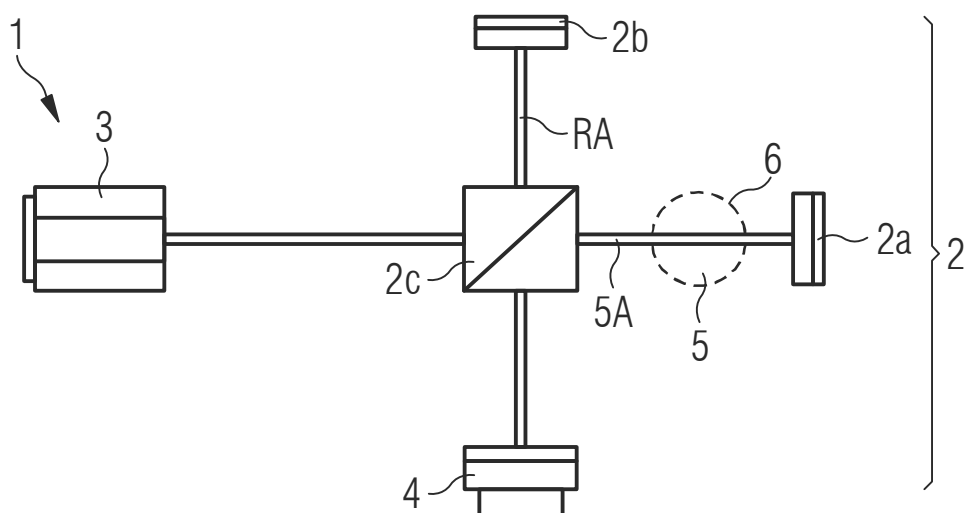


FIG 6

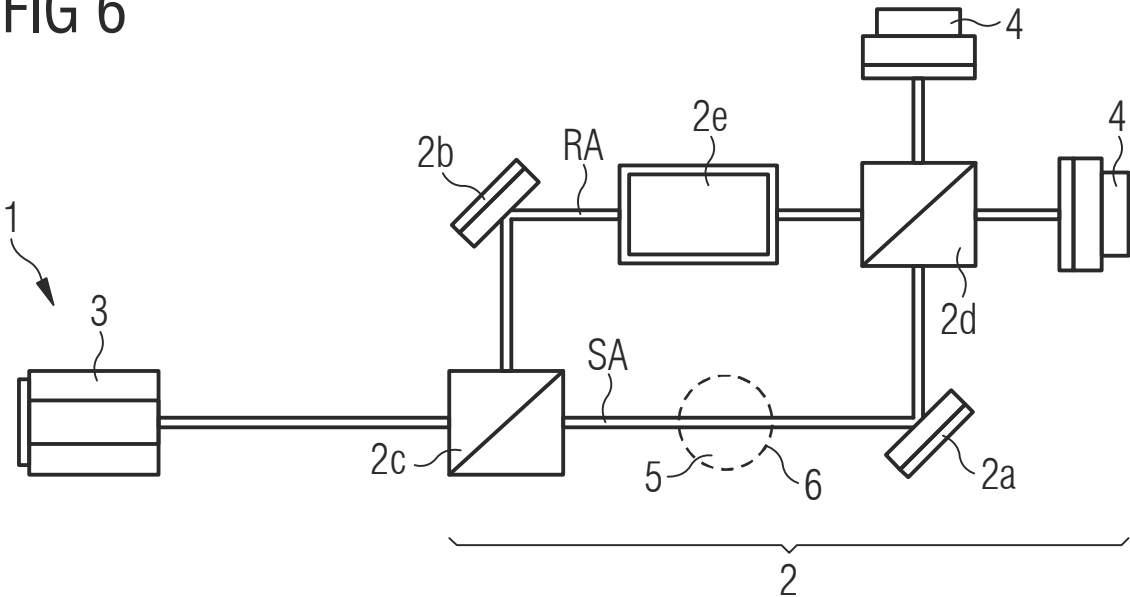


FIG 7

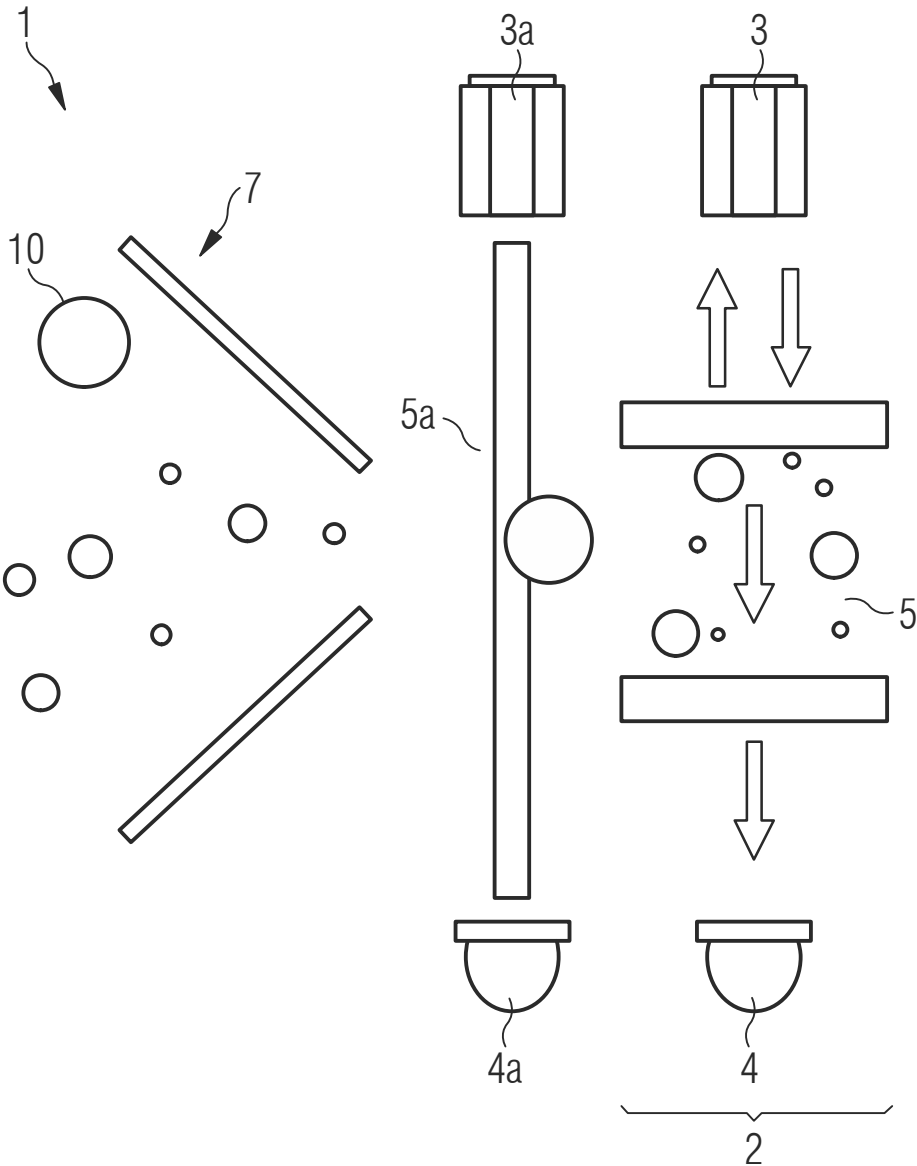




FIG 8

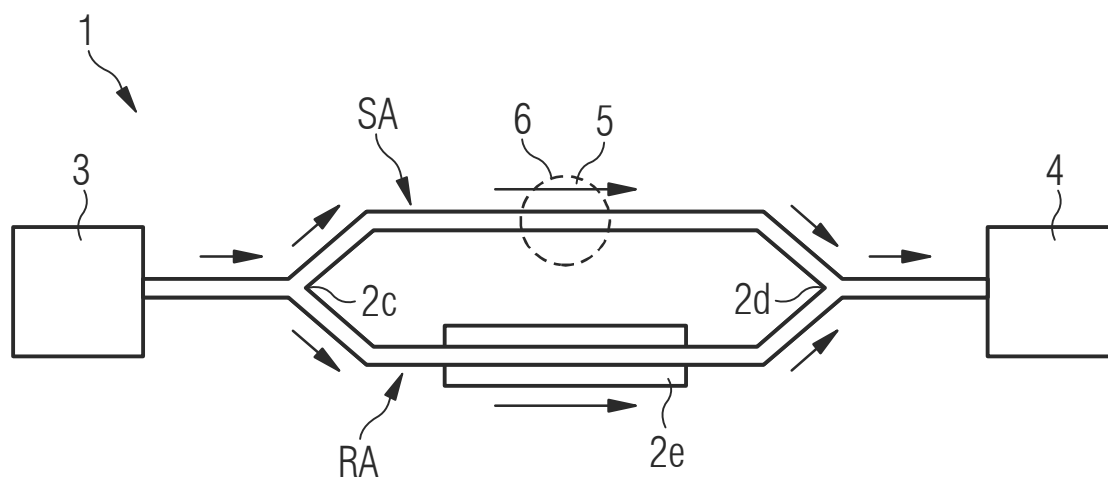


FIG 9

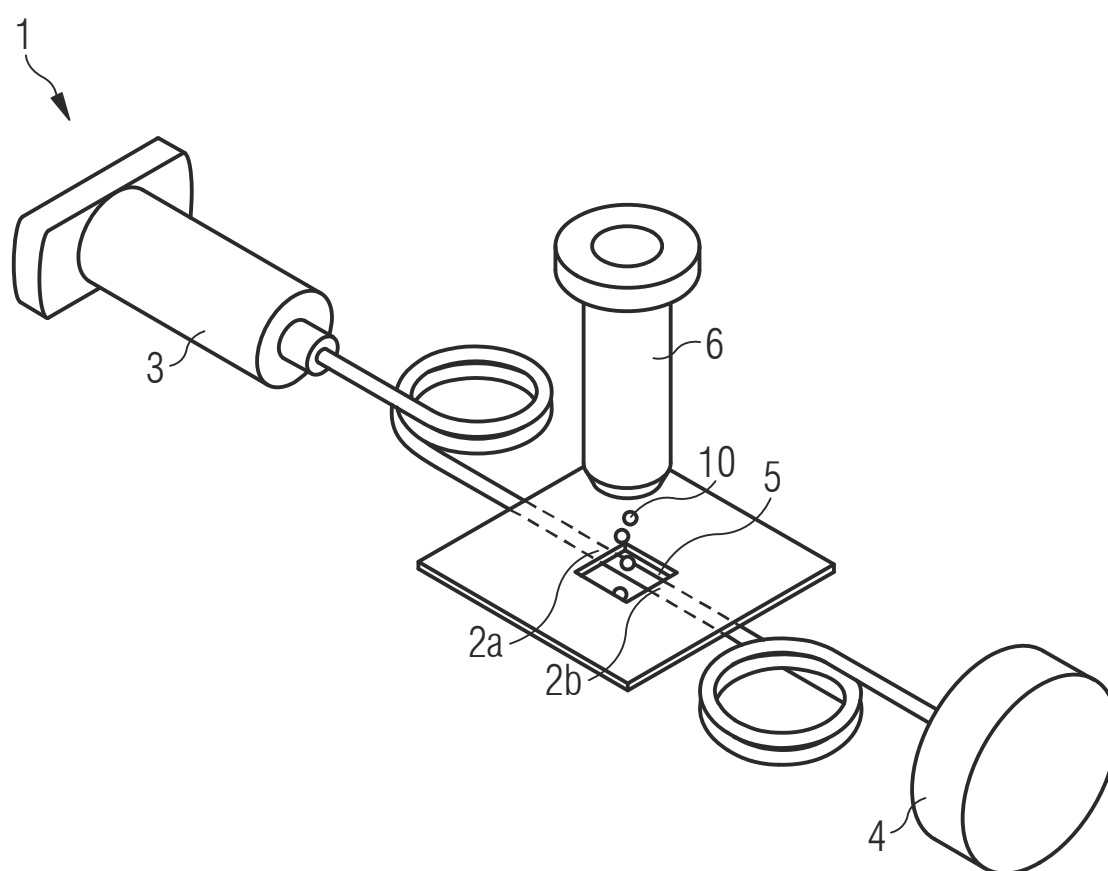


FIG 10

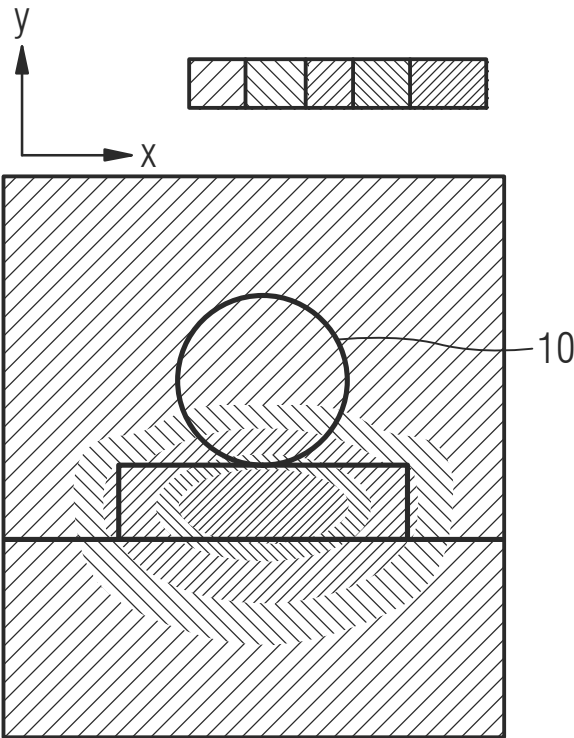


FIG 11

